Universitat Politècnica de Catalunya
Escola Tècnica Superior d'Enginyers de Camins, Canals i Ports de Barcelona
Departament d'Enginyeria del Terreny, Cartogràfica i Geofísica

Seismic vulnerability analysis of mid-height steel buildings in Bogotá

Miguel Ángel Montaña Peña

5 PUSH-OVER ANALYSES

5.1 Introductory remarks

This chapter describes and discusses the results of the 2-D nonlinear static (push-over) analyses (subsection 2.1.6.1 and Figure 2-15) of the prototype buildings described in the previous chapter. In the push-over analyses, only the contribution of the first mode is considered, since, in most of the analyzed situations, more than 75% of the total mass participates in the fundamental mode in the direction under consideration [FEMA 356 2000], see Table 4-31. As discussed previously, the variation of the lateral pushing forces along the height of the buildings is defined in two ways: uniform (corresponding to constant acceleration, e.g. approximately proportional to the mass of each floor) and modal (as the first modal shape, Figure 4-7) [EN-1998 2004]. Figure 5-1 displays the main features of both cases. Figure 5-1.a and Figure 5-1.d present the modal and uniform distributions of pushing forces, respectively. In order to derive global and simple conclusions, several simplifications have been considered in Figure 5-1.a and Figure 5-1.d: (i) the force distributions are continuous, despite the actual distributions are discrete (a pushing force per floor), (ii) the modal shape is assumed to be linear, Figure 4-7 shows that this supposition is close to reality. In Figure 5-1.a and Figure 5-1.d, $q\ H$ accounts for the base shear force, where is the height of the building. Figure 5-1.b and Figure 5-1.e present the shear force laws for modal and uniform distributions of pushing forces, respectively. Figure 5-1.c and Figure 5-1.f present the bending moment laws for modal and uniform distributions of pushing forces, respectively.

The observation of Figure 5-1 provides the following general conclusions:

- For the same base shear force, the shear forces, the bending moments, and the lateral displacements are higher for the modal distribution than for the uniform one. Therefore, the damage for the modal distribution should be higher; particularly in terms of plastic hinges formation and development. Moreover, the second-order effects are bigger for the modal distribution.
- Since the distribution of plastic hinges along the height of the building is strongly correlated to the shear forces in each floor, the faster variation of the shear forces law in the bottom levels of the building for the uniform distribution (Figure 5-1.e) shows that, in that case, the plastic hinges tend to concentrate in the lowest stories, thus generating more fragile collapse mechanisms.

To determine the target drifts (performance points), the demanding spectra are obtained from the former and current Colombian design codes [NSR-98 1998; Decreto 196 2006] and from the previous and the recently issued microzonation for Bogotá [Decreto 523 2010; Montaña, López Almansa 2012], Figure 3-6 and Figure 3-8, respectively. For LS (Life Safety) such spectra are intended to correspond to 475 years return period, and for IO (Immediate Occupancy) and CP (Collapse Prevention) they correspond to 225 and 2475 years, respectively [Priestley et al. 2007, FEMA 356 2000], see Figure 2-14. The demanding spectra for IO and CP are obtained by multiplying the ordinates of the LS spectrum by $(225 / 475)^{0.4}$ (= 0.742) and $(2475 / 475)^{0.4}$ (= 1.935), respectively [EN-1998-2 2005]. The Target Drifts are determined by intersecting the

capacity curves and the demand spectra, according the iterative process indicated in [ATC-40 1996], see Figure 2-18. Given the rather lateral flexibility of these buildings, the soil-structure interaction is not accounted for. Second-order analyses are performed; however, in most of the cases the differences with the first-order analyses are rather small.

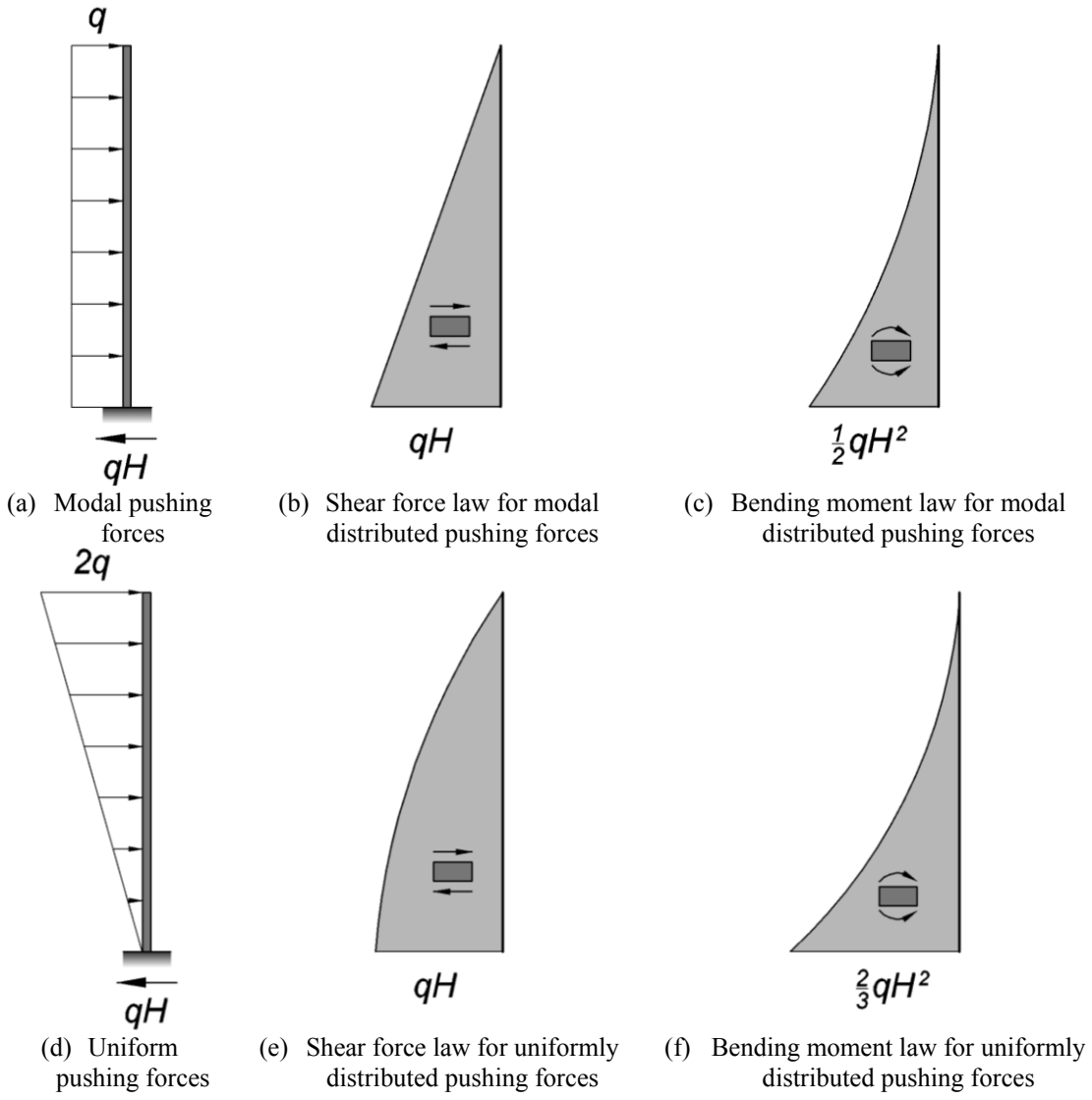

(a) Modal pushing forces

(b) Shear force law for modal distributed pushing forces

(c) Bending moment law for modal distributed pushing forces

(d) Uniform pushing forces

(e) Shear force law for uniformly distributed pushing forces

(f) Bending moment law for uniformly distributed pushing forces

Figure 5-1. Shear force and bending moment laws for uniform and modal distributed pushing forces

5.2 Software code

The numerical modelling described in section 4.5 is implemented in the multipurpose structural analysis simulation software package STAAD.Pro Version 8 [STAAD.Pro 2010]. This program was chosen because of its adequacy to the problems to be analyzed, its availability, and the previous experience of this author. STAAD.Pro is well suited for the objectives of the research and constitutes an user-friendly software with big reliability and accuracy.

STAAD.Pro is a structural analysis and design computer program originally developed by Research Engineers International in Yorba Linda, CA. In late 2005, Research Engineer International was bought by Bentley Systems. STAAD.Pro is one of the most widely used structural analysis and design software; it supports several steel, concrete and timber design codes. STAAD.Pro can perform various forms of analysis from the traditional 1st order static analysis to 2nd order P-delta analysis (nonlinear geometric analysis or buckling analysis) accounting for several types of mechanical nonlinearities. It can also carry out response spectrum analysis and

various forms of dynamic analysis from modal extraction to time-history. In the push-over analysis, the pushing forces acting on each floor are not concentrated on the left nodes but are distributed to every node (in the corresponding level) proportionally to their associated masses.

The accuracy and reliability of the calculations with STAAD.Pro are checked by comparison with other widely used software packages. In particular, a number of analyses using SAP 2000 Version 16.0 [CSI 2010] has been carried out. Figure 5-2 displays capacity curves (subsection 2.1.6.1 and Figure 2-15) of a prototype building (5 – 6 × 6 – MRF in *x* direction designed for the "Lacustre-500" zone according to the new microzonation, Figure 3-7) obtained with STAAD.Pro and SAP 2000. In Figure 5-2, "Modal distribution" and "Uniform distribution" account for the variation pattern for the pushing forces along the height of the building (subsection 2.1.6.1, Table 2-4 and section 5.1). Comparison among the corresponding pairs of plots in Figure 5-2 shows a satisfactory agreement, both in the linear and nonlinear ranges. The same conclusion has been obtained from other representative and similar comparisons. This confirms the correctness of the main analyses discussed in this study.

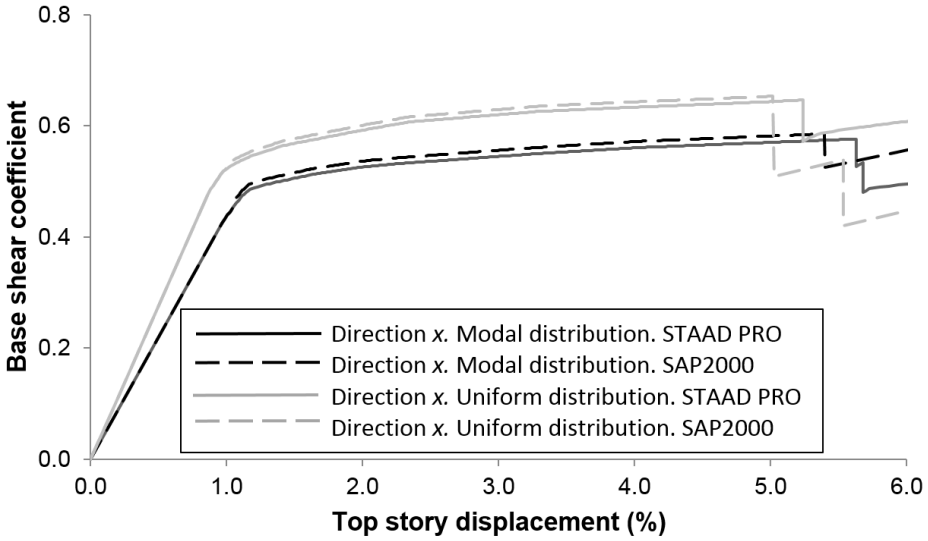

Figure 5-2. Capacity curves obtained with STAAD.Pro and SAP 2000. Building 5 – 6 × 6 – MRF in *x* direction. Zone "Lacustre-500" (new microzonation, Figure 3-7)

5.3 Numerical results

5.3.1 Overall considerations

Next ten subsections describe the numerical results for the prototype buildings (Table 4-1 through Table 4-10), grouped according to the ten considered zones (Figure 3-5 for the former microzonation and Figure 3-7 for the new microzonation), respectively. Each subsection contains four types of results: figures displaying the capacity curves of the prototype buildings, figures describing the progression of the damage in a number of prototype buildings, tables listing the seismic performance in each prototype building, and tables showing the obtained values of the response reduction factor *R* (equations (2-9), (4-4) and (4-5)). Next four paragraphs describe the presentation of the capacity curves, the damage progression, the seismic performance, and the response reduction factor, respectively.

Capacity curves. For each seismic zone, this information is provided in three Figures; they correspond to MRF, CBF and EBF buildings, respectively. In a given building, the capacity curves corresponding to the *x* and *y* directions (Figure 4-3 and Figure 4-4) are plotted together. Point "•" ("First yielding") indicates the onset of the first plastic hinge (corner point B in Figure 4-9), which is coincident with the end of the linear initial branch of the capacity curve; points

"○", "△" and "◇" correspond to Target Drifts IO, LS and CP, respectively. In the Figures that display the capacity curves, the vertical axis depicts the base shear coefficient, i.e. the base shear force normalized with respect to the weight of the building, and the horizontal axis represents the relative displacement of the top floor in terms of percentage of the height of the building (drift angle or drift ratio). Noticeably, all the capacity curves correspond to forces pushing in the right direction.

Damage progression. For each seismic zone, this information is provided in three pairs of Figures; each Figure corresponds to a building. These data are only delivered in a number of relevant selected cases; the selection criteria aims to clarify the most controversial or unexpected situations. The progression of damage is depicted by showing the combinations of plastic hinges (MRF and EBF buildings) and other types of failures (mainly for CBF buildings) for eight growing values of the drift angle (ratio between the top floor displacement and the building height), where the highest considered value of the drift angle corresponds to collapse conditions. For MRF and EBF, symbols ○, ◌, ◍ and ● are utilized, for any plastic hinge (or other type of failure), as indicated in [FEMA 356 2000]: ○ corresponds to the onset of yielding (corner point B in Figure 4-9) and ◌, ◍ and ● correspond to local acceptance criteria IO, LS and CP, respectively [FEMA 356 2000]. For CBF, a similar criterion is also considered for the tensioned braces while the compressed braces, because of their fragile behavior, have only the code ● in virtually all the cases; noticeably, in the tensioned braces, point ● corresponds to the final segment of the yielding branch (near the corner point C in Figure 4-9).

Seismic performance. For each seismic zone, this information is provided in a single Table. For each capacity curve, the damage intervals suggested by the research project RISK-UE [Milutinovic, Trendafiloski 2003] are adopted. "ND" (No Damage) corresponds to drift displacements lower than 0.7 Δ_y, "SD" (Slight Damage) corresponds to drift displacements between 0.7 Δ_y and Δ_y, "MD" (Moderate Damage) corresponds to drift displacements between Δ_y and $\Delta_y + 0.25\ (\Delta_u - \Delta_y)$, "ED" (Extensive Damage) corresponds to drift displacements between $\Delta_y + 0.25\ (\Delta_u - \Delta_y)$ and Δ_u, and "HD" (Heavy Damage, that meaning collapse) corresponds to drift displacements higher than Δ_u. Symbols Δ_y and Δ_u refer to the yielding and ultimate (collapse) displacements, respectively. For a proper seismic behavior, Target Drifts for IO, LS and CP should correspond to SD, MD and ED, respectively [Pujades et al. 2012]. According to this criterion, the adequacy of the levels of damage corresponding to each of the three considered Target Drifts is displayed. In the Table, "YES" indicates satisfactory performance, i.e. Target Drift corresponding either to the assigned damage level or to a smaller one, and "NO" specifies unsatisfactory performance, i.e. Target Drift corresponding to a damage level higher than the assigned one. In the Table, "-" means that the corresponding performance point does not exist because the capacity curve and the demand spectrum have no intersection; certainly, this can be understood as highly unsatisfactory performance.

Response reduction factor. For each seismic zone, this information is provided in a single Table. Following the classical equal-displacement approach [Priestley et al. 2007], the response reduction factor R is determined from the capacity curves [Miranda 1997; Cuesta et al. 2003; Kang, Choi 2011]. Since Table 4-21 through Table 4-30 show that the fundamental periods of the buildings are clearly out of the short period range [Nassar, Krawinkler 1991], the correction for short periods is not deemed necessary. As discussed in subsection 2.1.6.3 (Figure 2-22 and equation (2-16)), the R factor is determined as the ratio between the collapse and the yielding displacements; $R = \Omega\ R_d$ where Ω is the over-strength factor (the ratio between the actual and the design strength) and R_d is the ductility factor (the ratio between the elastic and the actual –plastic– strength).

Next ten subsections present the results of the 2-D nonlinear static (push-over) analyses of the prototype buildings designed for the ten seismic zones, respectively. Subsection 5.3.12 discusses globally the results for the previous ten subsections and overall conclusions are formulated.

5.3.2 *"Piedemonte" Zone (former microzonation)*

Figure 5-3, Figure 5-6 and Figure 5-9 display the capacity curves of the prototype buildings (Table 4-1) designed for the "Piedemonte" Zone (former microzonation, Figure 3-5); Figure 5-3, Figure 5-6 and Figure 5-9 refer to the MRF, CBF and EBF buildings, respectively.

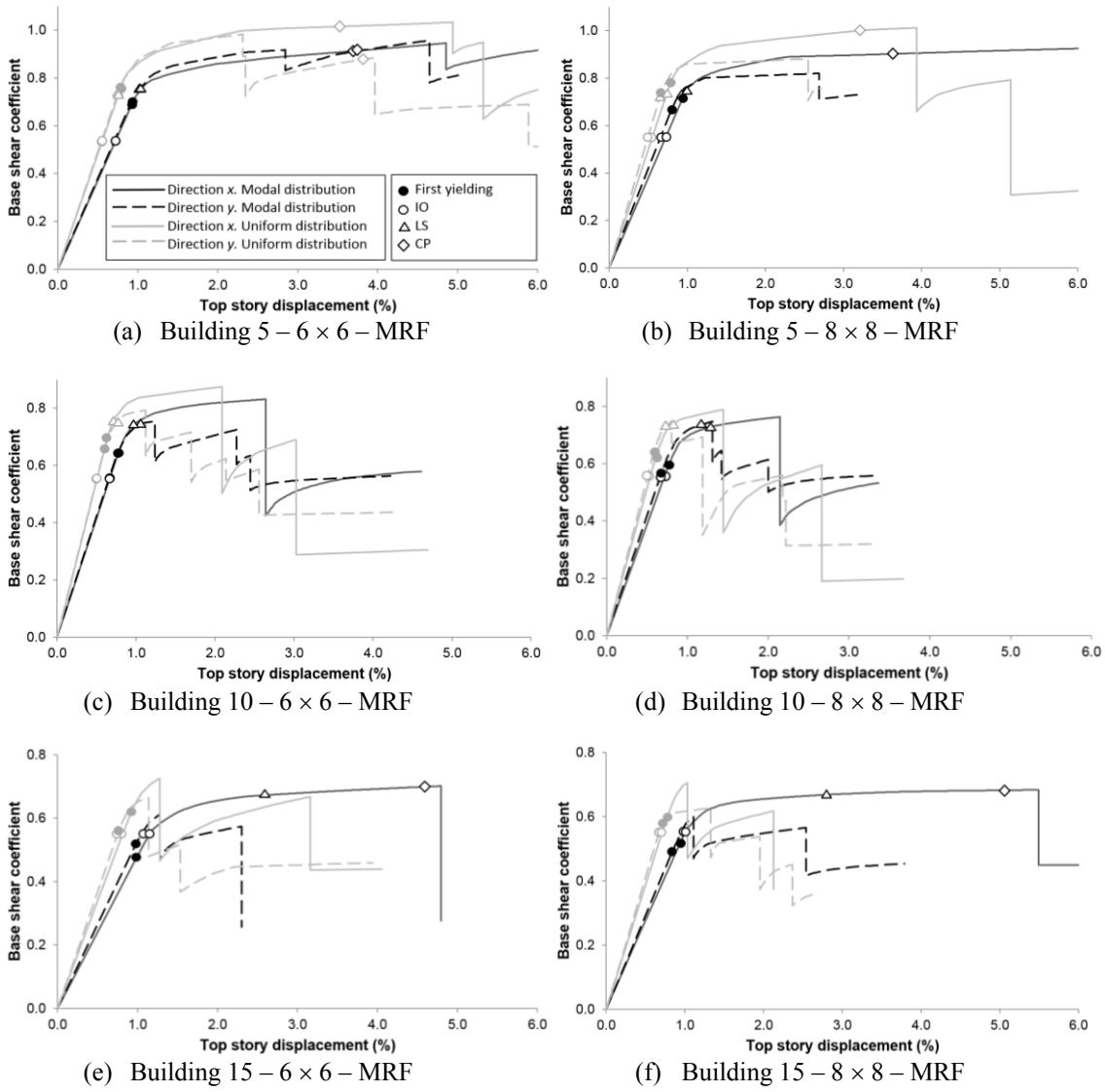

(a) Building 5 – 6 × 6 – MRF (b) Building 5 – 8 × 8 – MRF

(c) Building 10 – 6 × 6 – MRF (d) Building 10 – 8 × 8 – MRF

(e) Building 15 – 6 × 6 – MRF (f) Building 15 – 8 × 8 – MRF

Figure 5-3. Capacity curves and Target Drifts of buildings with Moment-Resisting Frames. Zone "Piedemonte" (former microzonation, Figure 3-5)

Most of the results in Figure 5-3 are regular and expected; subsection 5.3.12 holds deeper conclusions issued globally for all the cases. However, Figure 5-3.e shows that, for the 15 – 6 × 6 – MRF prototype building (Table 4-1) in *x* direction, the push-over analysis under modal force distribution predicts less initial stiffness and force strength, whereas that analysis predicts a significantly higher displacement ductility than the analysis under constant force distribution. To further investigate this issue, Figure 5-4 and Figure 5-5 display the damage progression of the 15 – 6 × 6 – MRF prototype building in *x* direction designed for the "Piedemonte" Zone (former microzonation, Figure 3-5). Figure 5-4 and Figure 5-5 correspond to push-over analyses under modal and uniform force distribution, respectively.

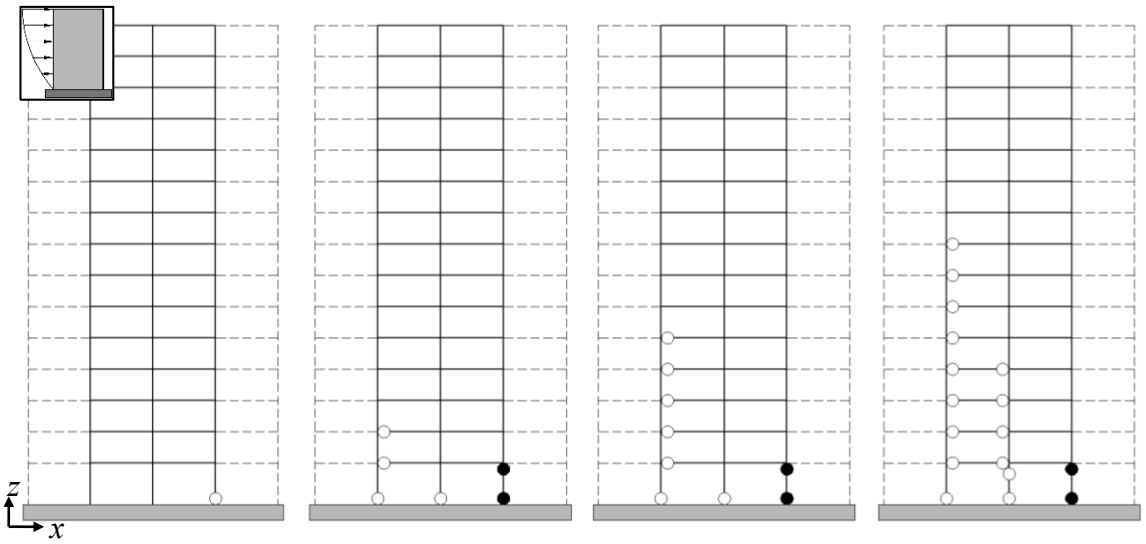

(a) Drift angle 1.17% (b) Drift angle 1.40% (c) Drift angle 1.55% (d) Drift angle 1.79%

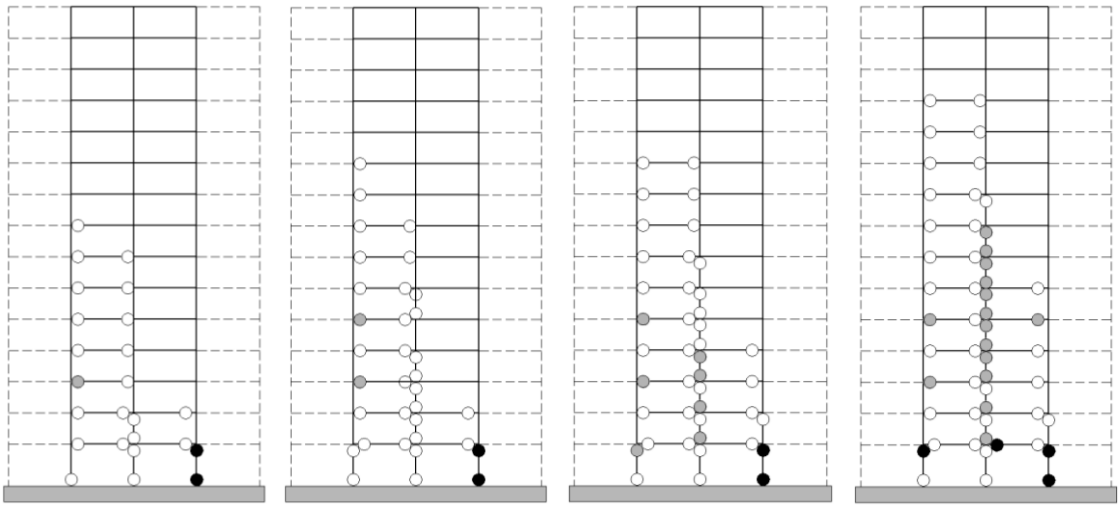

(e) Drift angle 2.12% (f) Drift angle 2.43% (g) Drift angle 2.85% (h) Drift angle 4.76%

Figure 5-4. Hinge progression sequence for the 15 – 6 × 6 – MRF building, modal distribution and *x* direction (right displacement). Zone "Piedemonte" (former microzonation, Figure 3-5). ○: yielding, ◎: IO, ◉: LS, ●: CP [FEMA 356 2000]

In Figure 5-4, each frame has four bays; the two inner bays (seismic) are represented with solid lines because they contribute to the lateral strength while the cooperation of the outer bays (non-seismic) is negelected (Figure 4-3) and they are depicted with dashed lines. Figure 5-4 represents the damage, in terms of the progression of plastic hinges at the ends of the members (beams and columns), for eight selected states corresponding to growing values of the drift angle. These values of the drift displacement have been chosen to highlight a number of characteristic points of the corresponding capacity curve (Figure 5-3.e), namely: onset of yielding (Figure 5-4.a), failure of the right bottom column (Figure 5-4.b), formation of plastic hinges in the beams of the left seismic (inner) bay (Figure 5-4.c and Figure 5-4.g) and near collapse (Figure 5-4.h). Figure 5-4.h shows that the collapse mechanism is mainly concentrated in the bottom floor but it involves an important number of floors (both beams and columns). The observation of Figure 5-4 shows that the early failure of the right bottom column causes that most of the plastic hinges concentrate on the left bay because the failed column does not transmit any additional moment to the upper members.

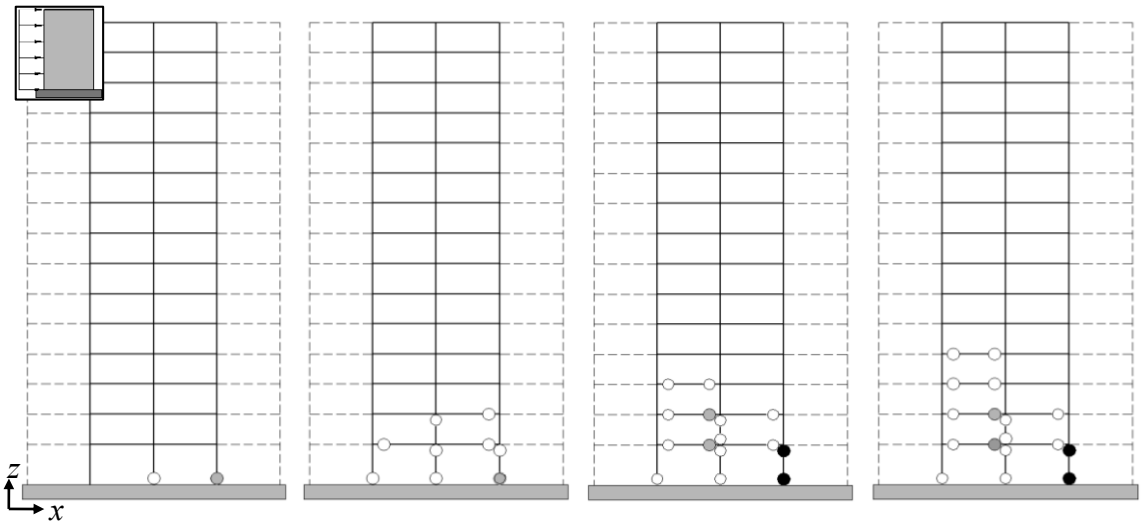

(a) Drift angle 0.96% (b) Drift angle 1.20% (c) Drift angle 1.61% (d) Drift angle 1.79%

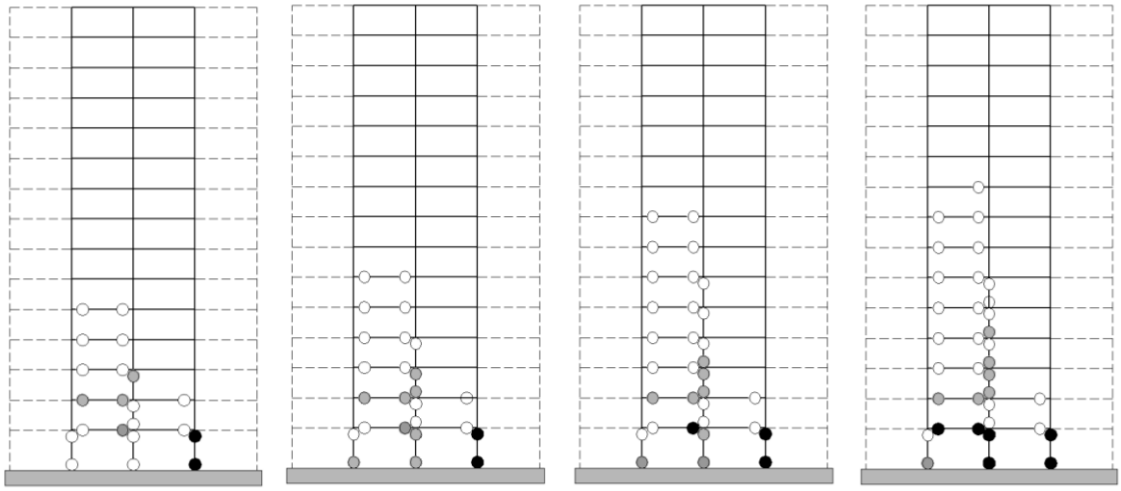

(e) Drift angle 2.15% (f) Drift angle 2.47% (g) Drift angle 3.01% (h) Drift angle 4.14%

Figure 5-5. Hinge progression sequence for the 15 – 6 × 6 – MRF building, uniform distribution and *x* direction (right displacement). Zone "Piedemonte" (former microzonation, Figure 3-5). ○: yielding, ◎: IO, ◉: LS, ●: CP [FEMA 356 2000]

Comparison between Figure 5-4 and Figure 5-5 shows that under modal force distribution, the collapse mechanism involves hinges in many levels of the building (up to the twelfth level), while for uniform distribution, the hinges concentrate more in the lower levels, mainly in the bottom one (although in the collapse, there is a plastic hinge in a beam in the 9th story). This difference between modal and uniform pushing forces is consistent with the shear forces and bending moments distribution along the height of the building (Figure 5-1). Noticeably, Figure 5-4 and Figure 5-5 show that in many joints, hinges occur earlier in columns than in beams. This undesired brittle behavior arises from the lack of enforced requirements of the Colombian design codes [NSR-98 1998, NSR-10 2010] for guaranteeing the "strong column-weak beam" behavior for the intermediate seismicity zones, such as Bogotá (Figure 3-3). The observed collapse mechanisms show that this circumstance, seriously reduces the structural ductility.

As previously announced, Figure 5-6 displays the capacity curves of the prototype CBF buildings

(Table 4-1) designed for the "Piedemonte" Zone (former microzonation, Figure 3-5).

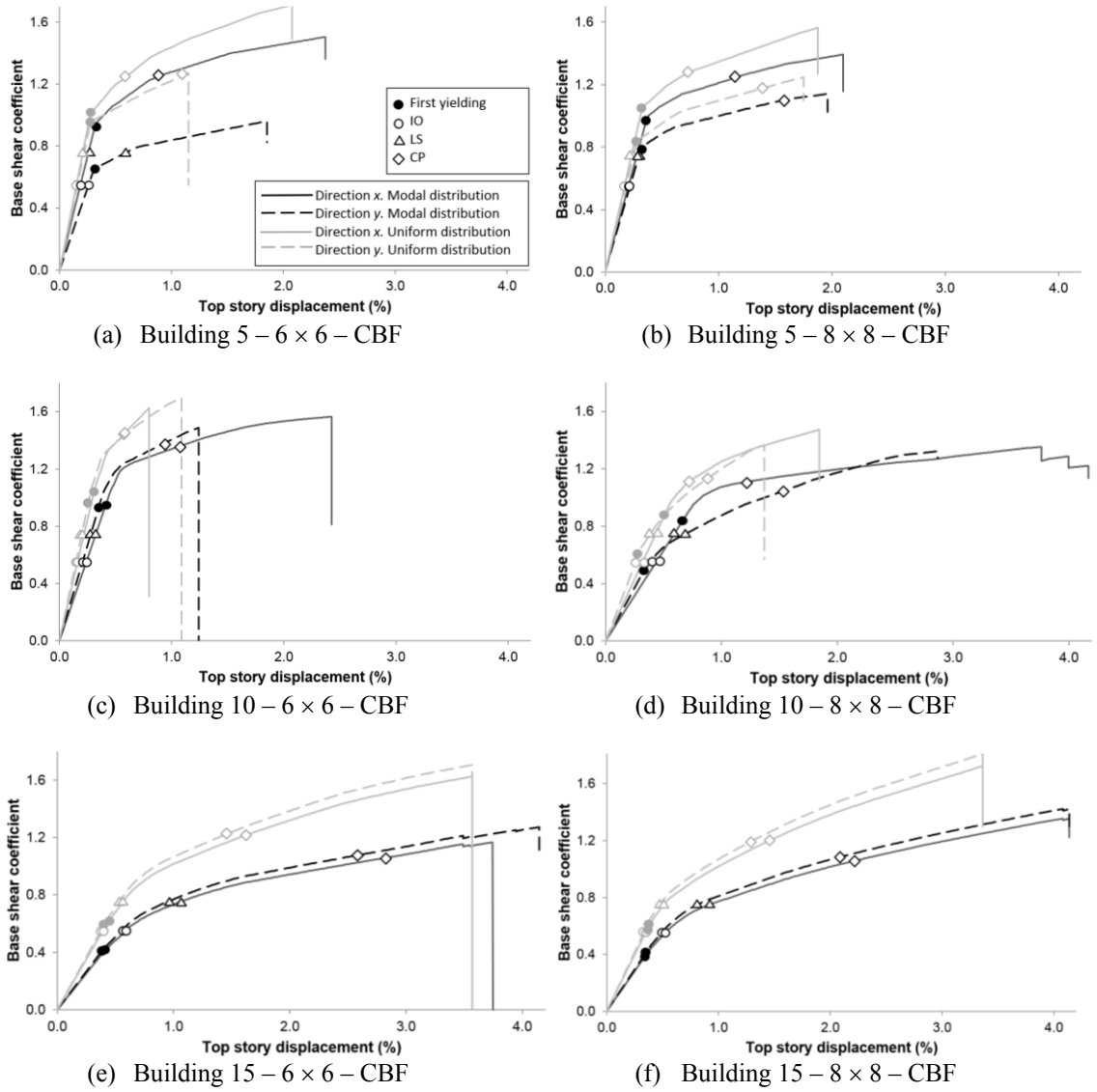

(a) Building 5 – 6 × 6 – CBF (b) Building 5 – 8 × 8 – CBF

(c) Building 10 – 6 × 6 – CBF (d) Building 10 – 8 × 8 – CBF

(e) Building 15 – 6 × 6 – CBF (f) Building 15 – 8 × 8 – CBF

Figure 5-6. Capacity curves and Target Drifts of buildings with Concentric-Braced Frames. Zone "Piedemonte" (former microzonation, Figure 3-5)

Most of the results in Figure 5-6 are regular and expected; subsection 5.3.12 holds deeper conclusions issued globally for all the cases. However, Figure 5-6.c shows that, for the 10 – 6 × 6 – CBF prototype building (Table 4-1) in *x* direction, the push-over analysis under modal force distribution predicts less initial stiffness and force strength, whereas that analysis predicts a significantly higher displacement ductility than the analysis under constant force distribution. To further investigate this issue, Figure 5-7 and Figure 5-8 display the damage progression of the 10 – 6 × 6 – CBF prototype building in *x* direction designed for the "Piedemonte" Zone (former microzonation, Figure 3-5). Figure 5-7 and Figure 5-8 correspond to push-over analyses under modal and uniform force distribution, respectively. Comparison between Figure 5-7 and Figure 5-8 shows that under modal force distribution, the collapse mechanism involves hinges in many levels of the building (even in the top one), while for uniform distribution the hinges concentrate in the three lowest levels, mainly in the bottom one. This difference between modal and uniform pushing forces is consistent with the corresponding shear forces and bending moments distribution along the height of the building (Figure 5-1).

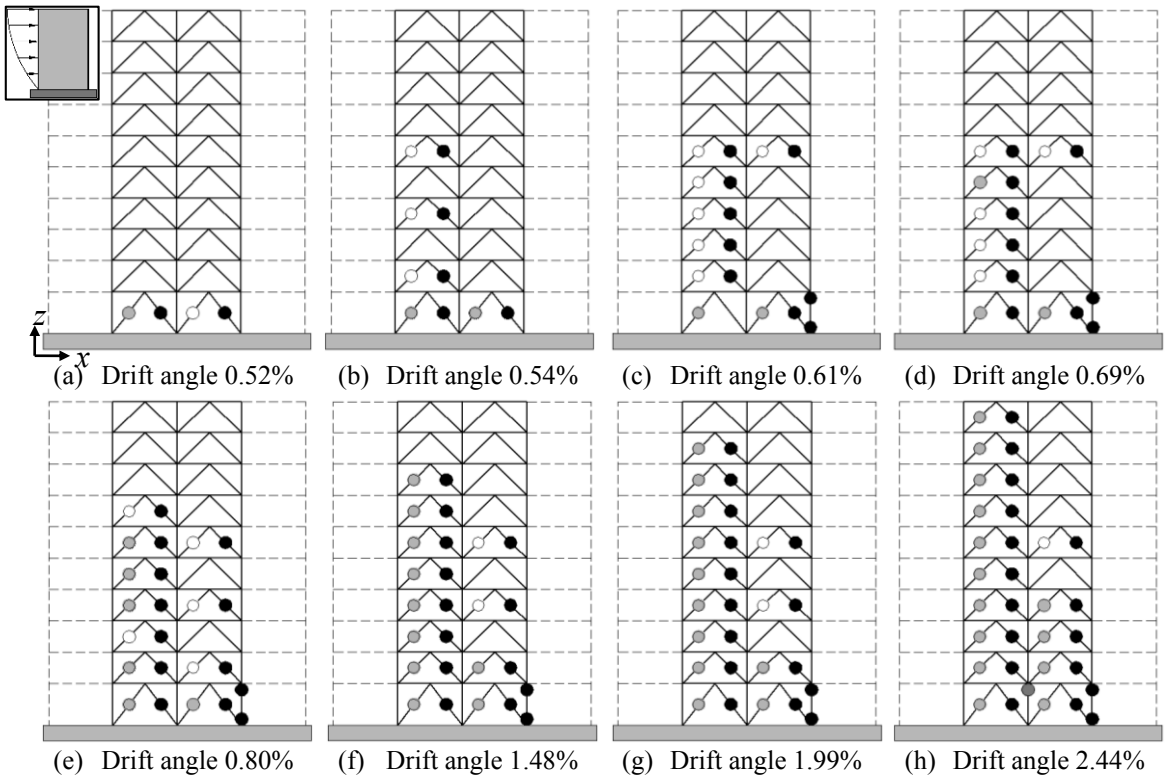

Figure 5-7. Hinge progression sequence for the 10 – 6 × 6 – CBF building, modal distribution and *x* direction (right displacement). Zone "Piedemonte" (former microzonation, Figure 3-5). ○: yielding, ○: IO, ●: LS, ●: CP [FEMA 356 2000]

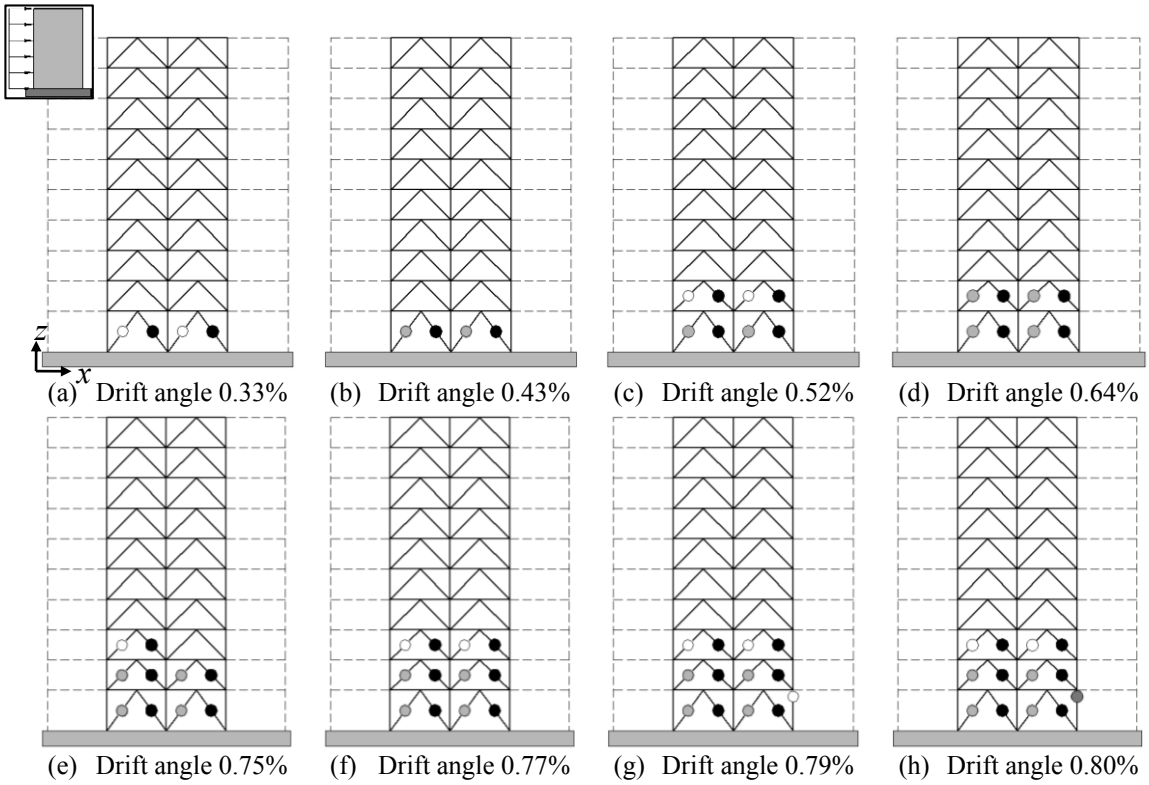

Figure 5-8. Hinge progression sequence for the 10 – 6 × 6 – CBF building, uniform distribution and *x* direction (right displacement). Zone "Piedemonte" (former microzonation, Figure 3-5). ○: yielding, ○: IO, ●: LS, ●: CP [FEMA 356 2000]

As previously announced, Figure 5-9 displays the capacity curves of the prototype EBF buildings

(Table 4-1) designed for the "Piedemonte" Zone (former microzonation, Figure 3-5).

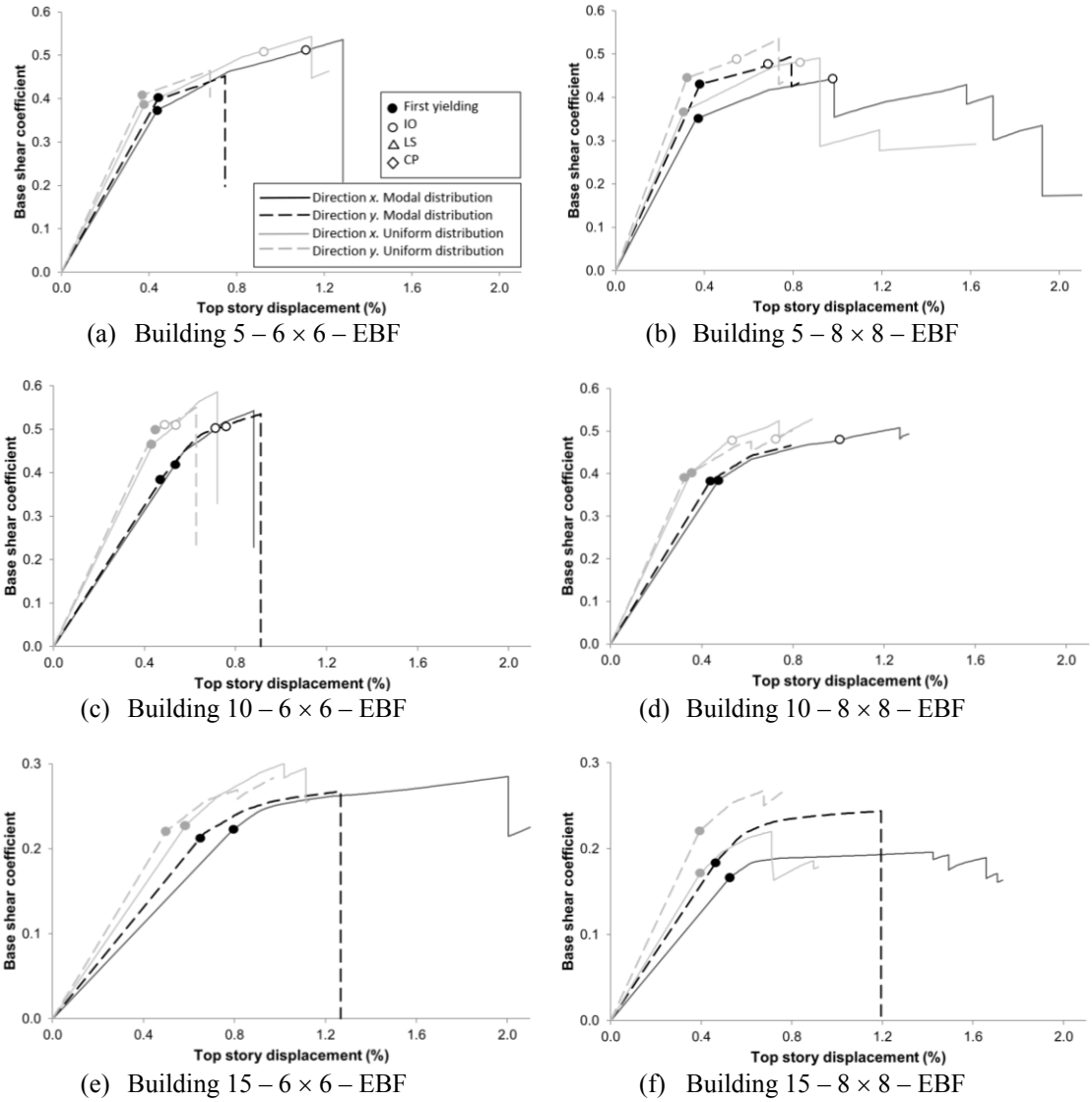

(a) Building 5 – 6 × 6 – EBF (b) Building 5 – 8 × 8 – EBF

(c) Building 10 – 6 × 6 – EBF (d) Building 10 – 8 × 8 – EBF

(e) Building 15 – 6 × 6 – EBF (f) Building 15 – 8 × 8 – EBF

Figure 5-9. Capacity curves and Target Drifts of buildings with Eccentric-Braced Frames. Zone "Piedemonte" (former microzonation, Figure 3-5)

Most of the results in Figure 5-9 are regular and expected; subsection 5.3.12 holds deeper conclusions issued globally for all the cases. However, Figure 5-9.f shows that, for the 15 – 8 × 8 – EBF prototype building (Table 4-1) in *y* direction, the push-over analysis under modal force distribution predicts less initial stiffness and force strength, whereas that analysis predicts a significantly higher displacement ductility than the analysis under constant force distribution. To further investigate this issue, Figure 5-10 and Figure 5-11 display the damage progression of the 15 – 8 × 8 – EBF prototype building in *y* direction designed for the "Piedemonte" Zone (former microzonation, Figure 3-5). Figure 5-10 and Figure 5-11 correspond to push-over analyses under modal and uniform force distribution, respectively (Figure 5-1).

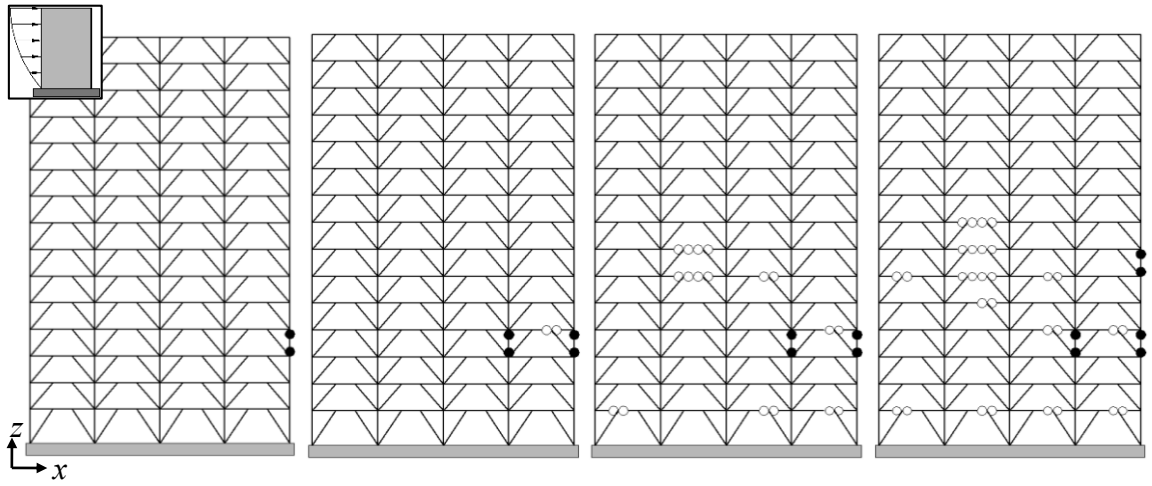

(a) Drift angle 0.49% (b) Drift angle 0.81% (c) Drift angle 0.86% (d) Drift angle 0.90%

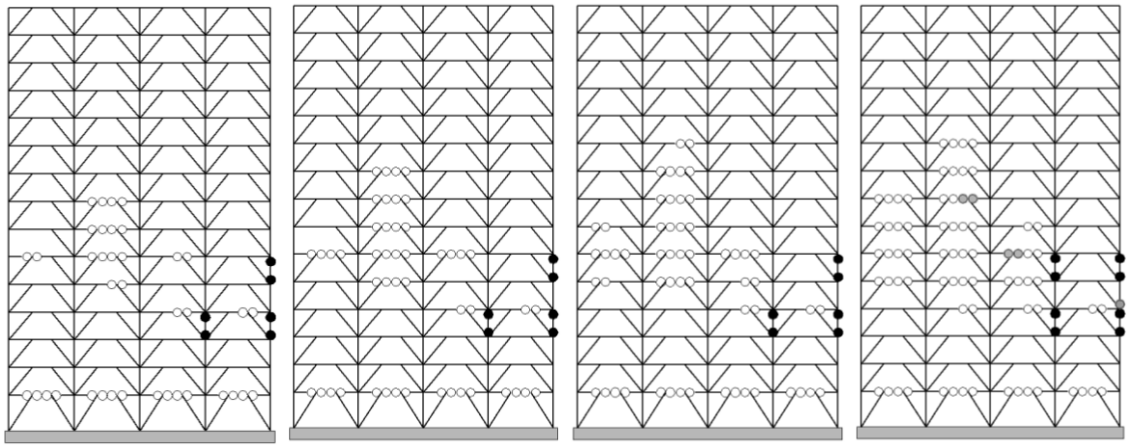

(e) Drift angle 0.94% (f) Drift angle 1.01% (g) Drift angle 1.07% (h) Drift angle 1.19%

Figure 5-10. Hinge progression sequence for the 15 – 8 × 8 – EBF building, modal distribution and *y* direction (right displacement). Zone "Piedemonte" (former microzonation, Figure 3-5). ○: yielding, ◎: IO, ◉: LS, ●: CP [FEMA 356 2000]

In Figure 5-10, each frame has four bays; all of them are seismic, since they have (eccentric) chevron braces (see Figure 4-3 and Figure 4-4.f). Figure 5-10 represents the damage, in terms of the progression of plastic hinges at the ends of links and columns, for eight selected states corresponding to growing values of the drift angle. These values of the drift displacement have been chosen to highlight a number of characteristic points of the corresponding capacity curve (Figure 5-9.f), namely: onset of yielding (Figure 5-10.a), formation of the full set of plastic hinges (yielding) in the bottom floor link segments (Figure 5-10.e), and near collapse (Figure 5-10.h). Figure 5-10.h shows that the collapse mechanism is mainly concentrated in the right columns of the 4th and 6th floors. This differential behavior (compared to the left side columns) is due to the interaction between the compressive axial forces and the bending moments.

Figure 5-10 shows that most of the plastic hinges start and develop in the columns; in fact, all the hinges that reach the CP level, belong to columns. Since the columns form, together with the braces and a segment of the upper beam, a rigid triangle, this behavior must be due to the bending moments generated by the rigid connections with the adjoining members. Noticeably, this should not happen in the CBF buildings because they are composed by triangles; this result might point towards a less satisfactory seismic performance of the EBF buildings. More precisely, the early formation of plastic hinges in the columns might lead to brittle collapse mechanisms.

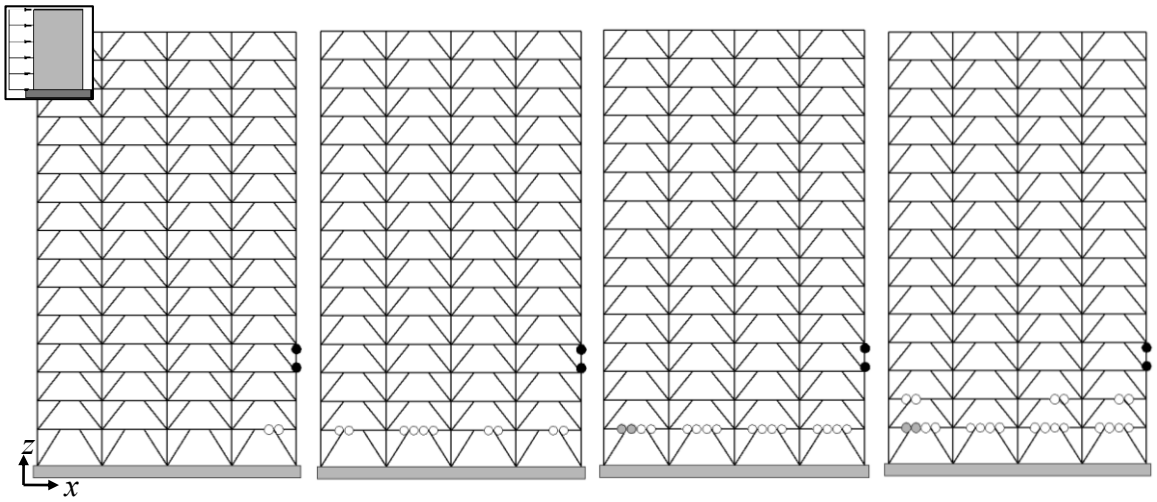

(a) Drift angle 0.41% (b) Drift angle 0.43% (c) Drift angle 0.47% (d) Drift angle 0.58%

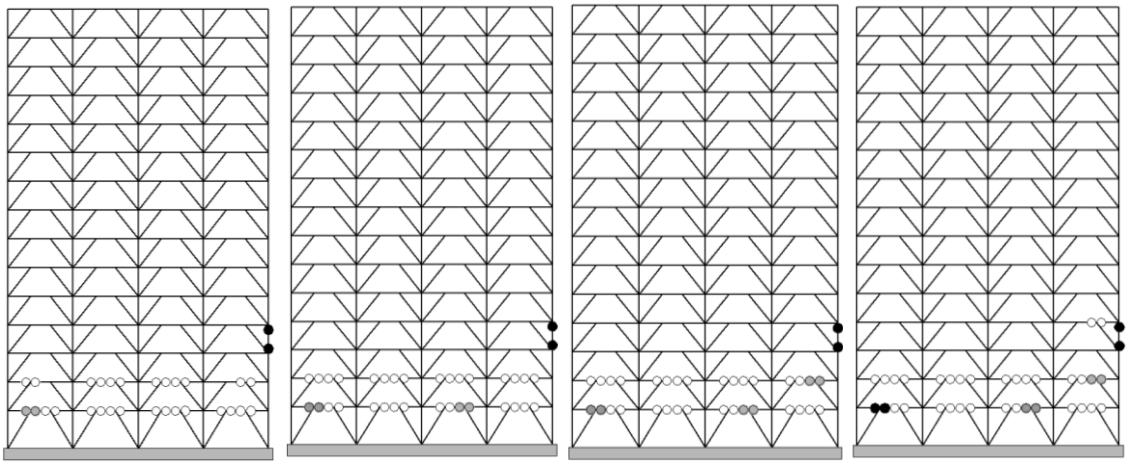

(e) Drift angle 0.59% (f) Drift angle 0.62% (g) Drift angle 0.64% (h) Drift angle 0.69%

Figure 5-11. Hinge progression sequence for the 15 – 8 × 8 – EBF building, uniform distribution and *y* direction (right displacement). Zone "Piedemonte" (former microzonation, Figure 3-5). ○: yielding, ◎: IO, ◉: LS, ●: CP [FEMA 356 2000]

Comparison between Figure 5-10 and Figure 5-11 shows that under modal force distribution, the collapse mechanism involves hinges in many levels of the building (reaching the tenth story and concentrating in the columns of the fourth and sixth ones), while for uniform distribution the hinges concentrate mainly in the link segments of the two lowest levels, although there are also hinges in the right columns of the fourth story. This difference between modal and uniform pushing forces is consistent with the corresponding shear forces and bending moments distribution along the height of the building (Figure 5-1). Figure 5-11.h shows that the collapse mechanism is similar to the one described by Figure 4-8.c; noticeably, the full collapse mechanism would involve (apart from the progression of the hinges in the link segments of the first floor beams) also the development of plastic hinges in the bottom sections of the second floor columns and braces.

Table 5-1 and Table 5-2 show, respectively, the seismic performance and the obtained values of the response reduction factor (R, Ω and R_d) of the prototype buildings (Table 4-1) designed for the "Piedemonte" Zone (former microzonation, Figure 3-5).

Table 5-1. Seismic performance. "Piedemonte" zone (former microzonation)

Building	Target Drift IO(*)		Target Drift LS(*)		Target Drift CP(*)	
	Direction *x*	Direction *y*	Direction *x*	Direction *y*	Direction *x*	Direction *y*
5 – 6 × 6 – MRF	YES / YES	YES / YES	YES / YES	YES / YES	YES / YES	YES / YES
5 – 8 × 8 – MRF	YES / YES	YES / YES	YES / YES	YES / YES	YES / -	YES / -
5 – 6 × 6 – CBF	YES / YES	YES / YES	YES / YES	YES / YES	YES / YES	- / YES
5 – 8 × 8 – CBF	YES / YES	YES / YES	YES / YES	YES / YES	YES / YES	YES / YES
5 – 6 × 6 – EBF	**NO** / **NO**	- / -	- / -	- / -	- / -	- / -
5 – 8 × 8 – EBF	**NO** / **NO**	**NO** / **NO**	- / -	- / -	- / -	- / -
10 – 6 × 6 – MRF	YES / YES	YES / YES	YES / YES	YES / YES	- / -	- / -
10 – 8 × 8 – MRF	YES / YES	YES / YES	**NO** / YES	**NO** / YES	- / -	- / -
10 – 6 × 6 – CBF	YES / YES	YES / YES	YES / YES	YES / YES	YES / YES	YES / YES
10 – 8 × 8 – CBF	YES / YES	YES / YES	YES / YES	YES / YES	YES / YES	YES / YES
10 – 6 × 6 – EBF	**NO** / **NO**	**NO** / **NO**	- / -	- / -	- / -	- / -
10 – 8 × 8 – EBF	**NO** / **NO**	- / **NO**	- / -	- / -	YES / -	- / -
15 – 6 × 6 – MRF	YES / YES	YES / YES	**NO** / -	- / -	YES / -	- / -
15 – 8 × 8 – MRF	YES / YES	YES / YES	**NO** / -	- / -	YES / -	- / -
15 – 6 × 6 – CBF	YES / YES	YES / YES	YES / YES	YES / YES	YES / YES	YES / YES
15 – 8 × 8 – CBF	YES / YES	YES / YES	YES / YES	YES / YES	YES / YES	YES / YES
15 – 6 × 6 – EBF	- / -	- / -	- / -	- / -	- / -	- / -
15 – 8 × 8 – EBF	- / -	- / -	- / -	- / -	- / -	- / -

(*) First / second values correspond to modal and uniform distributions, respectively

Table 5-1 reveals that in 54% of the cases, performance is satisfactory (YES), in 8% unsatisfactory (NO) and in 38% highly unsatisfactory (-). In the MRF/CBF/EBF buildings such percentages are 63/99/0%, 6/0/18% and 31/1/82%. In the 5/10/15-story buildings such percentages are 63/52/47%, 8/13/3% and 29/35/50%. For the IO/LS/CP limit states, the percentages are 72/52/44%, 18/6/0% and 10/42/56%. For the Modal/Uniform distributions, the percentages are 56/54%, 9/6% and 35/40%. No relevant differences have been observed for *x/y* directions.

Table 5-2**.** Response reduction factor *R* in the *x* and *y* directions. "Piedemonte" zone (former microzonation)

Building	Over-strength factor (Ω)(*)		Ductility factor R_d(*)		*R* factor ($R = \Omega R_d$)(*)	
	Direction *x*	Direction *y*	Direction *x*	Direction *y*	Direction *x*	Direction *y*
5 – 6 × 6 – MRF	1.37 / 1.38	1.35 / 1.30	3.77 / 4.49	3.71 / 2.29	5.16 / 6.19	5.01 / 2.98
5 – 8 × 8 – MRF	1.29 / 1.30	1.22 / 1.20	4.91 / 3.85	2.75 / 3.21	6.34 / 5.00	3.36 / 3.85
5 – 6 × 6 – CBF	1.63 / 1.67	1.46 / 1.32	4.33 / 4.41	4.02 / 3.20	7.06 / 7.36	5.87 / 4.22
5 – 8 × 8 – CBF	1.44 / 1.49	1.47 / 1.47	4.10 / 3.89	4.11 / 4.31	5.91 / 5.79	6.04 / 6.34
5 – 6 × 6 – EBF	1.46 / 1.41	1.13 / 1.12	1.98 / 2.12	1.50 / 1.64	2.89 / 2.99	1.69 / 1.84
5 – 8 × 8 – EBF	1.34 / 1.34	1.15 / 1.20	2.25 / 2.24	1.82 / 1.92	3.02 / 3.00	2.10 / 2.30
10 – 6 × 6 – MRF	1.31 / 1.26	1.20 / 1.21	2.56 / 2.63	1.34 / 1.55	3.35 / 3.31	1.61 / 1.88
10 – 8 × 8 – MRF	1.29 / 1.26	1.33 / 1.16	2.16 / 1.79	1.47 / 1.16	2.78 / 2.26	1.96 / 1.34
10 – 6 × 6 – CBF	1.66 / 1.56	1.60 / 1.79	3.40 / 1.69	2.23 / 2.32	5.64 / 2.64	3.56 / 4.15
10 – 8 × 8 – CBF	1.54 / 1.52	2.62 / 2.22	3.54 / 1.95	3.25 / 2.30	5.45 / 2.97	8.52 / 5.10
10 – 6 × 6 – EBF	1.29 / 1.26	1.39 / 1.11	1.28 / 1.33	1.39 / 1.27	1.65 / 1.67	1.93 / 1.41
10 – 8 × 8 – EBF	1.34 / 1.36	1.22 / 1.29	2.00 / 2.01	1.49 / 1.93	2.68 / 2.74	1.82 / 2.49
15 – 6 × 6 – MRF	1.47 / 1.17	1.16 / 1.17	3.28 / 1.20	1.13 / 1.27	4.82 / 1.40	1.31 / 1.49
15 – 8 × 8 – MRF	1.33 / 1.18	1.22 / 1.08	4.33 / 1.13	1.09 / 1.73	5.76 / 1.33	1.33 / 1.87
15 – 6 × 6 – CBF	2.89 / 2.64	3.06 / 2.85	3.04 / 3.03	3.52 / 3.14	8.80 / 8.00	10.76 / 8.95
15 – 8 × 8 – CBF	3.60 / 3.00	3.51 / 2.95	3.34 / 2.98	3.44 / 3.03	12.04 / 8.95	12.06 / 8.93
15 – 6 × 6 – EBF	1.27 / 1.30	1.26 / 1.28	1.98 / 1.47	1.53 / 1.53	2.52 / 1.91	1.94 / 1.96
15 – 8 × 8 – EBF	1.19 / 1.28	1.35 / 1.21	2.28 / 1.39	1.91 / 1.60	2.71 / 1.78	2.58 / 1.93

(*) First / second values correspond to modal and uniform distributions, respectively

Comparison among the values of *R* in Table 5-2 with the assumed factors in Table 4-21 shows that, in 67% of the cases, the analyzed buildings do not possess the required ductility. In the MRF/CBF/EBF buildings, such percentage is 71/29/100%. In the 5/10/15-story buildings such percentage is 50/83/67%. For the Modal/Uniform distributions, the percentages are 58/75%. No relevant differences have been observed for *x/y* directions.

5.3.3 "Lacustre A" Zone (former microzonation)

Figure 5-12, Figure 5-15 and Figure 5-18 display the capacity curves of the prototype buildings (Table 4-1) designed for the "Lacustre A" Zone (former microzonation, Figure 3-5); Figure 5-12, Figure 5-15 and Figure 5-18 refer to the MRF, CBF and EBF buildings, respectively.

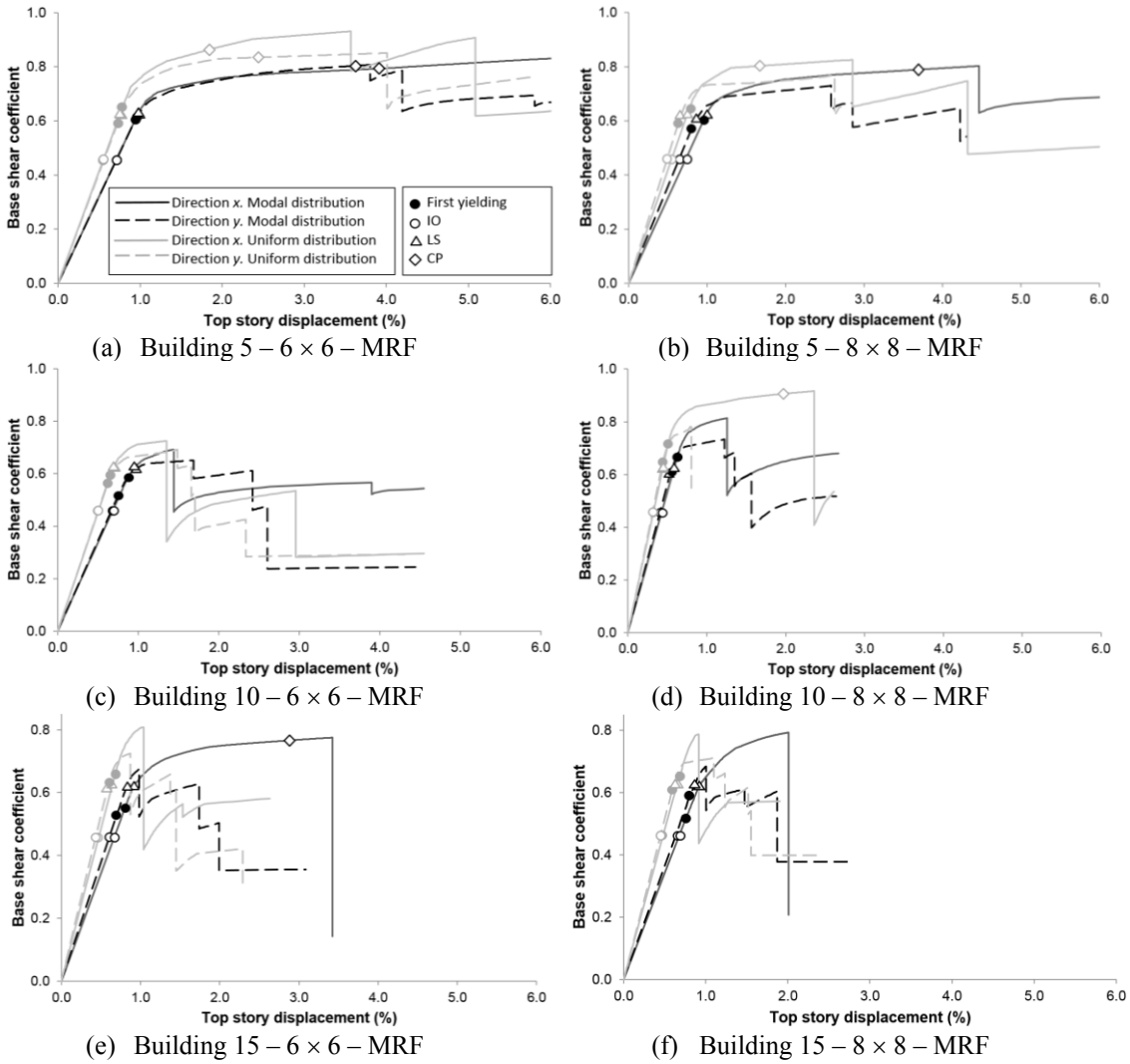

(a) Building 5 – 6 × 6 – MRF (b) Building 5 – 8 × 8 – MRF

(c) Building 10 – 6 × 6 – MRF (d) Building 10 – 8 × 8 – MRF

(e) Building 15 – 6 × 6 – MRF (f) Building 15 – 8 × 8 – MRF

Figure 5-12. Capacity curves and Target Drifts of buildings with Moment-Resisting Frames. Zone "Lacustre A" (former microzonation, Figure 3-5)

Most of the results in Figure 5-12 are regular and expected; subsection 5.3.12 holds global conclusions. However, Figure 5-12.d shows that, for the 10 – 8 × 8 – MRF building (Table 4-1) in *y* direction, the push-over analysis under modal force distribution predicts less initial stiffness, less force strength, and significantly higher displacement ductility than the analysis under constant force distribution. To further investigate this issue, Figure 5-13 and Figure 5-14 display the damage progression of the 10 – 8 × 8 – MRF building in *y* direction designed for the "Lacustre A" Zone (former microzonation, Figure 3-5). Figure 5-13 and Figure 5-14 correspond to push-over analyses under modal and uniform force distribution, respectively (Figure 5-1).

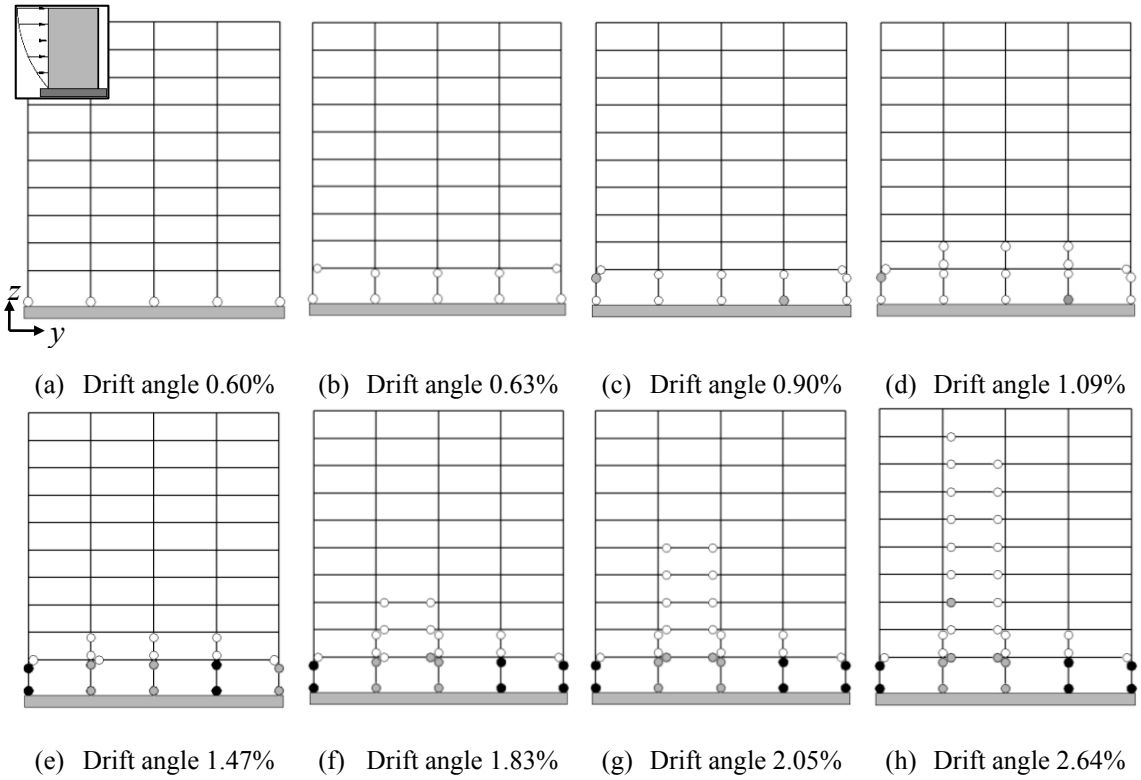

(a) Drift angle 0.60% (b) Drift angle 0.63% (c) Drift angle 0.90% (d) Drift angle 1.09%

(e) Drift angle 1.47% (f) Drift angle 1.83% (g) Drift angle 2.05% (h) Drift angle 2.64%

Figure 5-13. Hinge progression sequence for the 10 – 8 × 8 – MRF building, modal distribution and *y* direction (right displacement). Zone "Lacustre A" (former microzonation, Figure 3-5). ○: yielding, ○: IO, ●: LS, ●: CP [FEMA 356 2000]

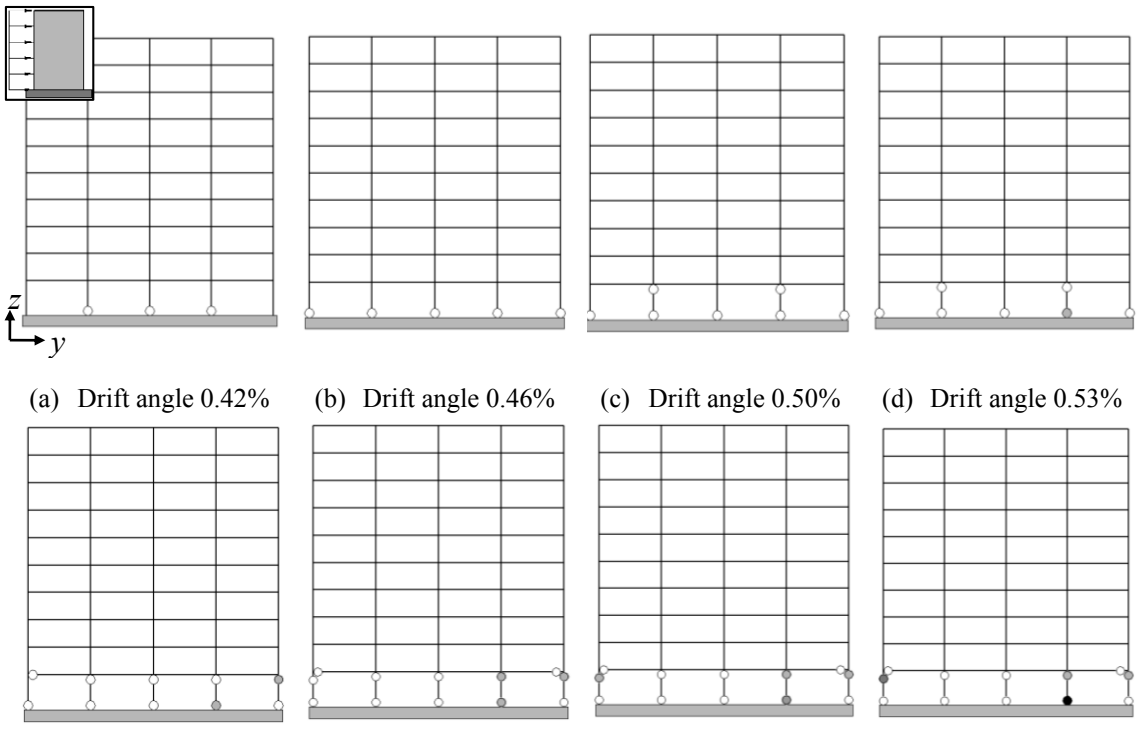

(a) Drift angle 0.42% (b) Drift angle 0.46% (c) Drift angle 0.50% (d) Drift angle 0.53%

(e) Drift angle 0.59% (f) Drift angle 0.61% (g) Drift angle 0.71% (h) Drift angle 0.81%

Figure 5-14. Hinge progression sequence for the 10 – 8 × 8 – MRF building, uniform distribution and *y* direction (right displacement). Zone "Lacustre A" (former microzonation, Figure 3-5). ○: yielding, ○: IO, ●: LS, ●: CP [FEMA 356 2000]

Figure 5-13 and Figure 5-14 show that under modal force distribution the collapse mechanism involves hinges in virtually all the levels of the building, while for uniform distribution the hinges concentrate in the bottom level, thus generating an extremely brittle collapse mechanism. This is consistent with the shear forces and bending moments distribution along the height of the building (Figure 5-1).

As previously announced, Figure 5-15 displays the capacity curves of the prototype CBF buildings (Table 4-1) designed for the "Lacustre A" Zone (former microzonation, Figure 3-5).

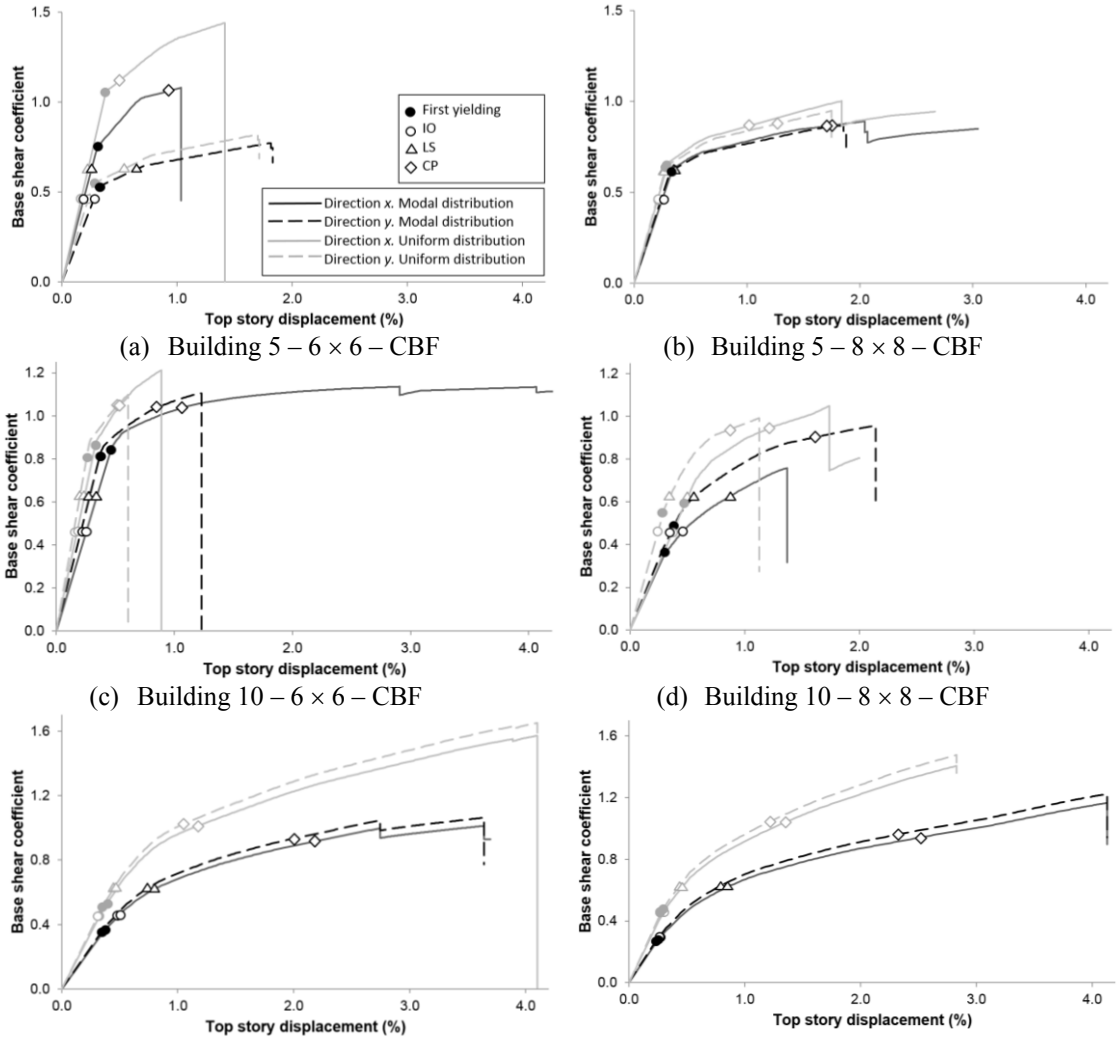

(a) Building 5 – 6 × 6 – CBF (b) Building 5 – 8 × 8 – CBF

(c) Building 10 – 6 × 6 – CBF (d) Building 10 – 8 × 8 – CBF

(e) Building 15 – 6 × 6 – CBF (f) Building 15 – 8 × 8 – CBF

Figure 5-15. Capacity curves and Target Drifts of buildings with Concentric-Braced Frames. Zone "Lacustre A" (former microzonation, Figure 3-5)

Most of the results in Figure 5-15 are regular and expected; subsection 5.3.12 holds deeper conclusions issued globally for all the cases. However, Figure 5-15.c shows that, for the 10 – 6 × 6 – CBF prototype building (Table 4-1) in *x* direction, the push-over analysis under modal force distribution predicts less initial stiffness, less force strength, and significantly higher displacement ductility than the analysis under constant force distribution (this failure is extremely premature). To further investigate this issue, Figure 5-16 and Figure 5-17 display the damage progression of the 10 – 6 × 6 – CBF prototype building in *x* direction designed for the "Lacustre A" Zone (former microzonation, Figure 3-5). Figure 5-16 and Figure 5-17 correspond to push-over analyses under modal and uniform force distribution, respectively (Figure 5-1).

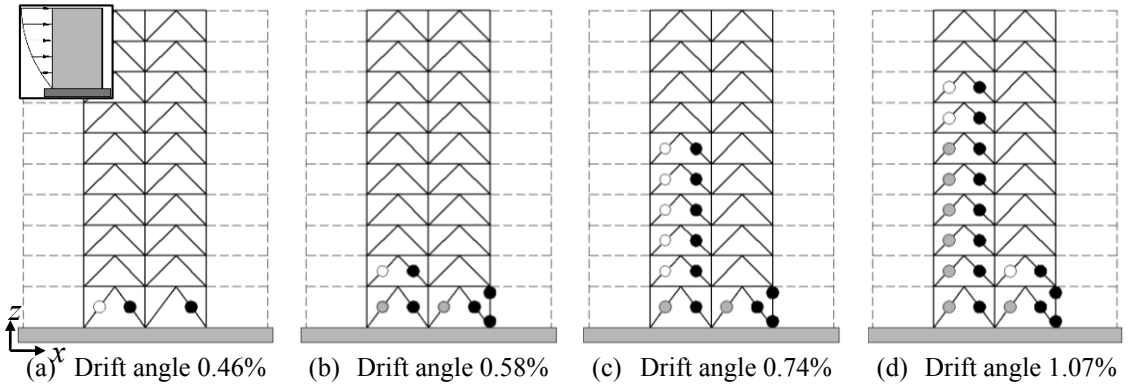

Figure 5-16. Hinge progression sequence for the 10 – 6 × 6 – CBF building, modal distribution and *x* direction (right displacement). Zone "Lacustre A" (former microzonation, Figure 3-5). ○: yielding, ◎: IO, ◍: LS, ●: CP [FEMA 356 2000]

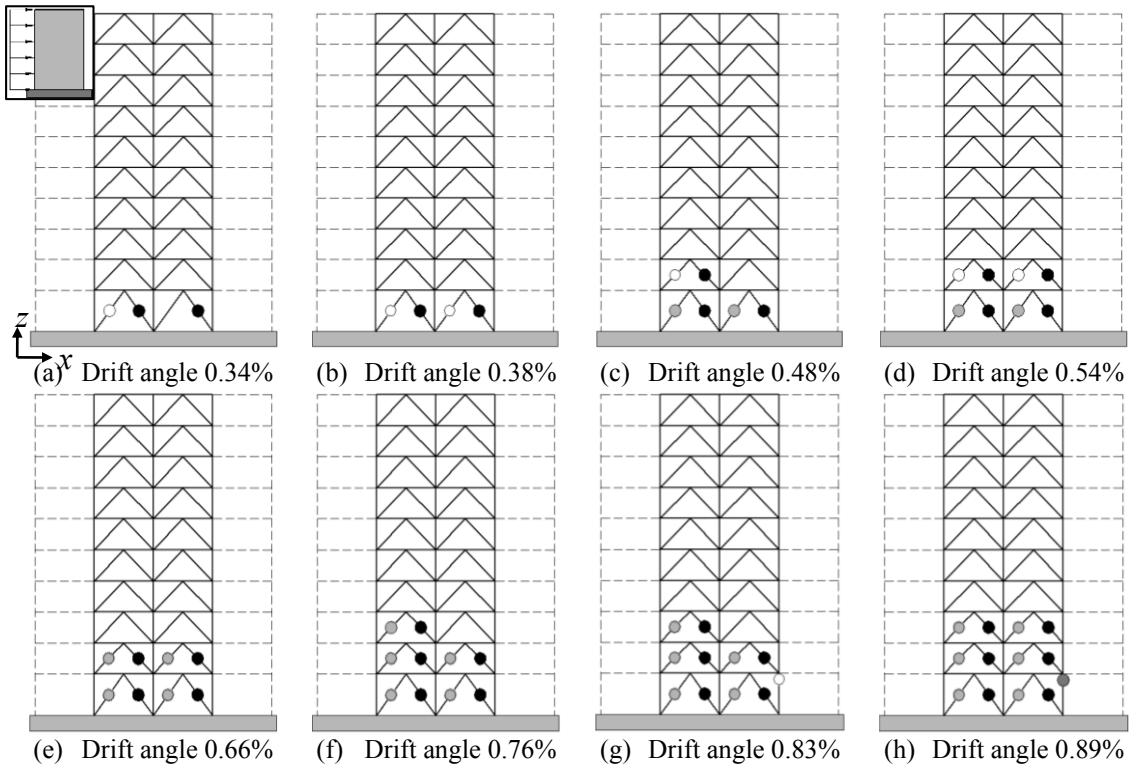

Figure 5-17. Hinge progression sequence for the 10 – 6 × 6 – CBF building, uniform distribution and *x* direction (right displacement). Zone "Lacustre A" (former microzonation, Figure 3-5). ○: yielding, ◎: IO, ◍: LS, ●: CP [FEMA 356 2000]

Figure 5-16 and Figure 5-17 show that under modal force distribution the collapse mechanism

involves hinges in all the levels of the building, while for uniform distribution the hinges concentrate in the three lowest levels, mainly in the bottom one, thus generating a brittle collapse mechanism. This is consistent with the shear forces and bending moments distribution along the height of the building (Figure 5-1).

As previously announced, Figure 5-18 displays the capacity curves of the prototype EBF buildings (Table 4-1) designed for the "Lacustre A" Zone (former microzonation, Figure 3-5).

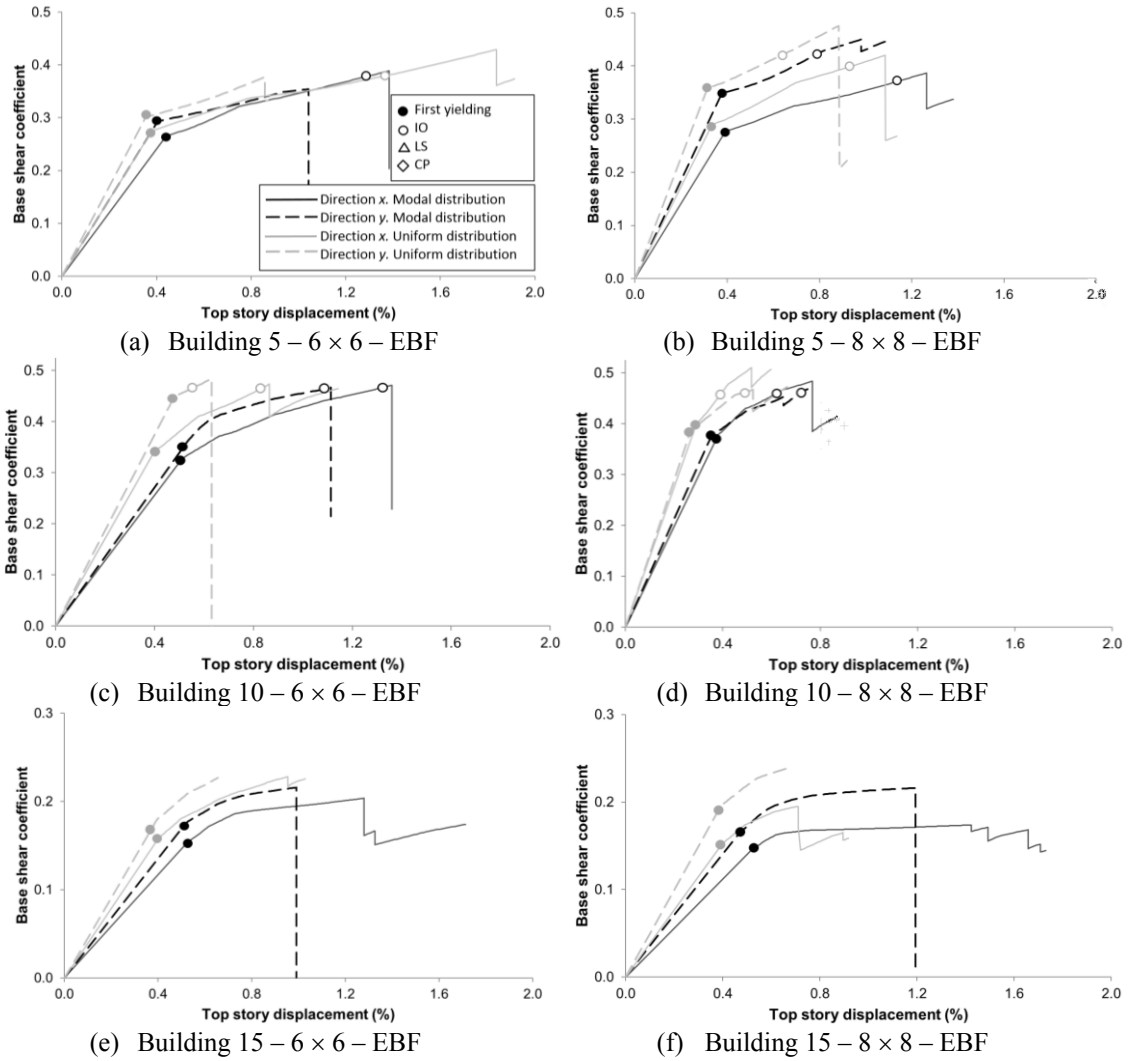

(a) Building 5 – 6 × 6 – EBF (b) Building 5 – 8 × 8 – EBF

(c) Building 10 – 6 × 6 – EBF (d) Building 10 – 8 × 8 – EBF

(e) Building 15 – 6 × 6 – EBF (f) Building 15 – 8 × 8 – EBF

Figure 5-18. Capacity curves and Target Drifts of buildings with Eccentric-Braced Frames. Zone "Lacustre A" (former microzonation, Figure 3-5)

Most of the results in Figure 5-18 are regular and expected; subsection 5.3.12 holds deeper conclusions issued globally for all the cases. However, Figure 5-18.c shows that, for the 10 – 6 × 6 – EBF prototype building (Table 4-1) in *y* direction, the push-over analysis under modal force distribution predicts less initial stiffness, similar force strength, and significantly higher displacement ductility than the analysis under constant force distribution (this failure is extremely premature). To further investigate this issue, Figure 5-19 and Figure 5-20 display the damage progression of the 10 – 6 × 6 – EBF prototype building in *y* direction designed for the "Lacustre A" Zone (former microzonation, Figure 3-5). Figure 5-19 and Figure 5-20 correspond to push-over analyses under modal and uniform force distribution, respectively (Figure 5-1).

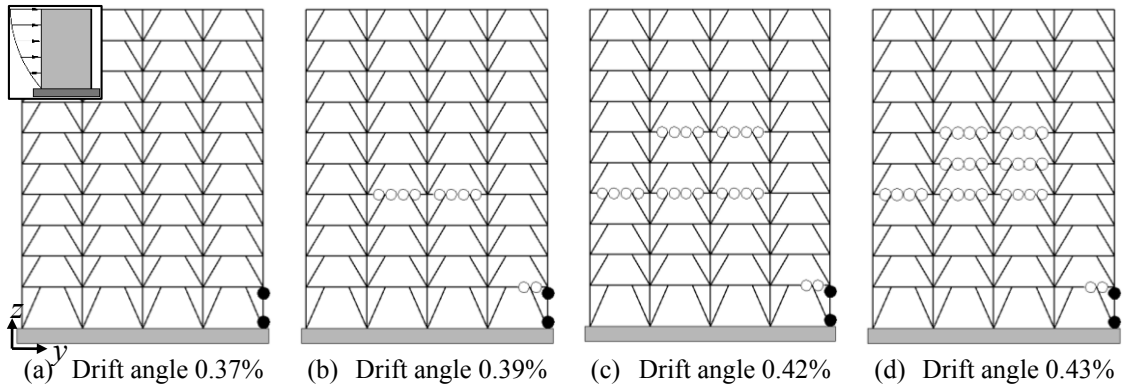

(a) Drift angle 0.37% (b) Drift angle 0.39% (c) Drift angle 0.42% (d) Drift angle 0.43%

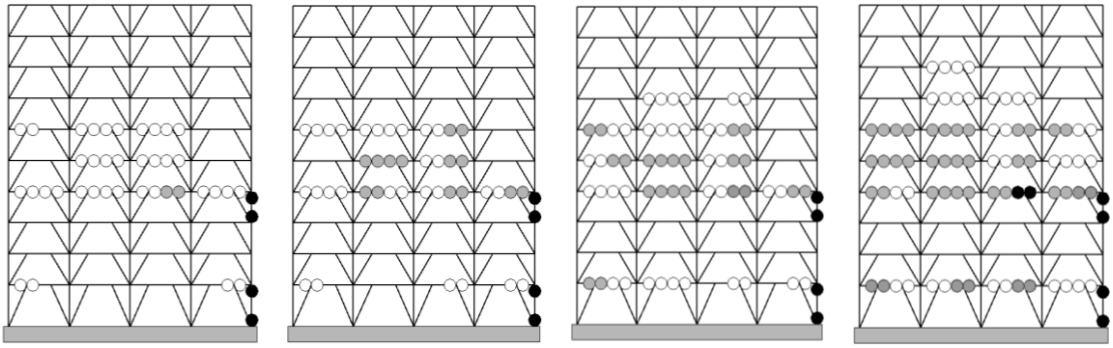

(e) Drift angle 0.47% (f) Drift angle 0.53% (g) Drift angle 0.57% (h) Drift angle 0.75%

Figure 5-19. Hinge progression sequence for the 10 – 6 × 6 – EBF building, modal distribution and *y* direction (right displacement). Zone "Lacustre A" (former microzonation, Figure 3-5). ○: yielding, ◎: IO, ◉: LS, ●: CP [FEMA 356 2000]

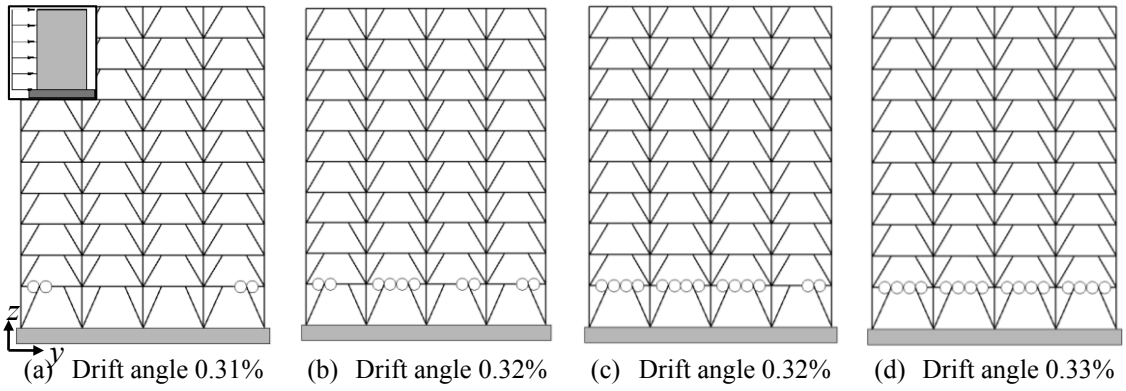

(a) Drift angle 0.31% (b) Drift angle 0.32% (c) Drift angle 0.32% (d) Drift angle 0.33%

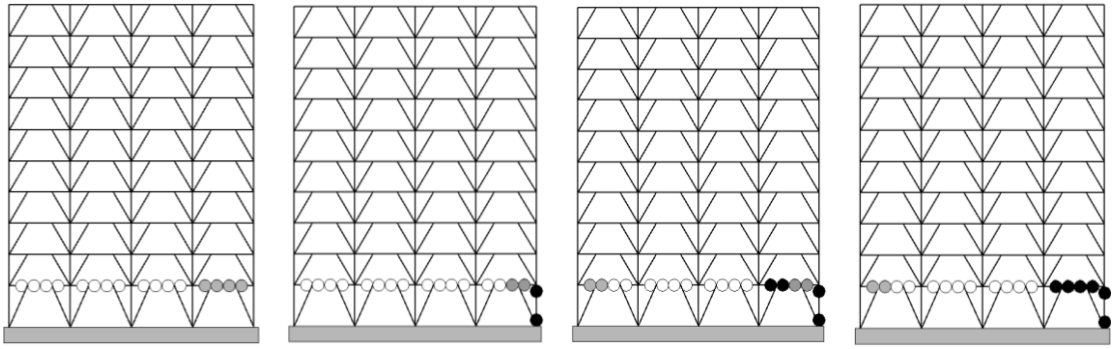

(e) Drift angle 0.36% (f) Drift angle 0.39% (g) Drift angle 0.40% (h) Drift angle 0.42%

Figure 5-20. Hinge progression sequence for the 10 – 6 × 6 – EBF building, uniform distribution and *y* direction (right displacement). Zone "Lacustre A" (former microzonation, Figure 3-5). ○: yielding, ◎: IO, ◉: LS, ●: CP [FEMA 356 2000]

Figure 5-19 and Figure 5-20 show that under modal force distribution, the collapse mechanism involves hinges in many levels (reaching the eighth story and concentrating mainly in the first and fourth stories), while for uniform distribution, the hinges concentrate in the link segments of the bottom floor. This difference between modal and uniform pushing forces is consistent with the corresponding shear forces and bending moments distribution along the height of the building (Figure 5-1).

Table 5-3 and Table 5-4 show, respectively, the seismic performance and the response reduction factor (R, Ω and R_d) of the prototype buildings (Table 4-1) designed for the "Lacustre A" Zone (former microzonation, Figure 3-5).

Table 5-3 reveals that 56% of the cases exhibit a satisfactory performance (YES), 9% unsatisfactory (NO) and 35% highly unsatisfactory (-). In the MRF/CBF/EBF buildings, such percentages are 79/89/0%, 0/8/19% and 21/3/81%. In the 5/10/15-story buildings such percentages are 61/54/52%, 10/13/6% and 29/33/42%. For the IO/LS/CP limit states, the percentages are 67/66/42%, 19/1/1% and 14/33/57%. For the Modal/Uniform distributions, the percentages are 56/60%, 9/7% and 35/33%. No relevant differences have been observed for *x/y* directions.

Comparison among the values of R in Table 5-4 with the assumed factors in Table 4-22 shows that, in 71% of the cases, the analyzed buildings do not possess the required ductility. In the MRF/CBF/EBF buildings, such percentage is 79/33/100%. In the 5/10/15-story buildings such percentage is 58/88/67%. For the Modal/Uniform distributions, the percentages are 69/72%. No relevant differences have been observed for *x/y* directions.

Table 5-3. Seismic performance. "Lacustre A" zone (former microzonation)

Building	Target Drift IO(*)		Target Drift LS(*)		Target Drift CP(*)	
	Direction *x*	Direction *y*	Direction *x*	Direction *y*	Direction *x*	Direction *y*
5 – 6 × 6 – MRF	YES / YES	YES / YES	YES / YES	YES / YES	YES / YES	YES / YES
5 – 8 × 8 – MRF	YES / YES	YES / YES	YES / YES	YES / YES	YES / YES	- / -
5 – 6 × 6 – CBF	YES / YES	YES / YES	YES / YES	YES / YES	YES / YES	- / **NO**
5 – 8 × 8 – CBF	YES / YES	YES / YES	YES / YES	YES / YES	YES / YES	YES / **NO**
5 – 6 × 6 – EBF	**NO** / **NO**	- / -	- / -	- / -	- / -	- / -
5 – 8 × 8 – EBF	**NO** / **NO**	**NO** / **NO**	- / -	- / -	- / -	- / -
10 – 6 × 6 – MRF	YES / YES	YES / YES	YES / YES	YES / YES	- / -	- / -
10 – 8 × 8 – MRF	YES / YES	YES / YES	YES / YES	YES / YES	YES / YES	- / -
10 – 6 × 6 – CBF	YES / YES	YES / YES	YES / YES	YES / YES	YES / YES	YES / YES
10 – 8 × 8 – CBF	YES / YES	YES / YES	**NO** / YES	YES / YES	- / YES	YES / YES
10 – 6 × 6 – EBF	**NO** / **NO**	**NO** / **NO**	- / -	- / -	- / -	- / -
10 – 8 × 8 – EBF	**NO** / **NO**	**NO** / **NO**	- / -	- / -	- / -	- / -
15 – 6 × 6 – MRF	YES / YES	YES / YES	YES / YES	YES / YES	YES / YES	- / -
15 – 8 × 8 – MRF	YES / YES	YES / YES	YES / YES	YES / YES	YES / -	- / -
15 – 6 × 6 – CBF	**NO** / YES	**NO** / YES	YES / YES	YES / YES	YES / YES	YES / YES
15 – 8 × 8 – CBF	**NO** / YES	**NO** / YES	YES / YES	YES / YES	YES / YES	YES / YES
15 – 6 × 6 – EBF	- / -	- / -	- / -	- / -	- / -	- / -
15 – 8 × 8 – EBF	- / -	- / -	- / -	- / -	- / -	- / -

(*) First / second values correspond to modal and uniform distributions, respectively

Table 5-4**.** Response reduction factor R in the x / y directions. "Lacustre A" zone (former microzonation)

Building	Over-strength factor (Ω)(*)		Ductility factor R_d(*)		R factor ($R = \Omega R_d$) (*)	
	Direction x	Direction y	Direction x	Direction y	Direction x	Direction y
5 – 6 × 6 – MRF	1.37 / 1.30	1.32 / 1.32	4.56 / 3.97	3.00 / 3.87	6.25 / 5.16	3.96 / 5.11
5 – 8 × 8 – MRF	1.34 / 1.28	1.28 / 1.30	3.45 / 2.81	2.52 / 3.22	4.62 / 3.60	3.22 / 4.18
5 – 6 × 6 – CBF	1.44 / 1.35	1.45 / 1.50	2.26 / 2.74	3.81 / 4.06	3.26 / 3.73	5.52 / 6.09
5 – 8 × 8 – CBF	1.48 / 1.55	1.41 / 1.43	4.11 / 4.06	4.01 / 4.32	6.08 / 6.30	5.65 / 6.18
5 – 6 × 6 – EBF	1.48 / 1.58	1.20 / 1.22	2.11 / 3.14	2.17 / 1.98	3.12 / 4.96	2.60 / 2.41
5 – 8 × 8 – EBF	1.38 / 1.47	1.30 / 1.32	2.35 / 2.24	1.99 / 2.14	3.24 / 3.30	2.59 / 2.83
10 – 6 × 6 – MRF	1.20 / 1.22	1.27 / 1.24	1.36 / 1.69	1.74 / 1.91	1.63 / 2.06	2.22 / 2.37
10 – 8 × 8 – MRF	1.22 / 1.28	1.21 / 1.20	1.66 / 3.62	1.83 / 1.48	2.03 / 4.63	2.22 / 1.78
10 – 6 × 6 – CBF	1.34 / 1.40	1.37 / 1.37	6.53 / 1.89	2.47 / 1.69	8.75 / 2.64	3.38 / 2.31
10 – 8 × 8 – CBF	2.09 / 1.79	1.99 / 1.81	2.07 / 2.03	2.78 / 2.20	4.32 / 3.63	5.54 / 3.99
10 – 6 × 6 – EBF	1.46 / 1.40	1.33 / 1.09	1.84 / 1.54	1.64 / 1.23	2.68 / 2.15	2.18 / 1.34
10 – 8 × 8 – EBF	1.31 / 1.28	1.25 / 1.23	1.56 / 1.41	1.71 / 2.06	2.05 / 1.80	2.14 / 2.53
15 – 6 × 6 – MRF	1.41 / 1.23	1.28 / 1.16	2.99 / 1.24	1.10 / 1.23	4.22 / 1.52	1.41 / 1.43
15 – 8 × 8 – MRF	1.55 / 1.19	1.15 / 1.17	1.70 / 1.10	1.10 / 1.56	2.63 / 1.31	1.27 / 1.83
15 – 6 × 6 – CBF	2.68 / 2.98	2.97 / 3.25	3.57 / 3.47	3.56 / 3.61	9.56 / 10.4	10.6 / 11.7
15 – 8 × 8 – CBF	4.30 / 2.97	4.56 / 3.15	3.78 / 3.08	3.98 / 3.06	16.3 / 9.15	18.2 / 9.64
15 – 6 × 6 – EBF	1.35 / 1.46	1.25 / 1.36	1.80 / 1.64	1.56 / 1.32	2.43 / 2.39	1.95 / 1.80
15 – 8 × 8 – EBF	1.17 / 1.28	1.31 / 1.24	2.31 / 1.41	1.93 / 1.39	2.70 / 1.81	2.53 / 1.72

(*) First / second values correspond to modal and uniform distributions, respectively

5.3.4 "Piedemonte-A" Zone (new microzonation)

Figure 5-21, Figure 5-24 and Figure 5-27 display the capacity curves of the prototype buildings (Table 4-1) designed for the "Piedemonte-A" (new microzonation, Figure 3-7); Figure 5-21, Figure 5-24 and Figure 5-27 refer to the MRF, CBF and EBF buildings, respectively.

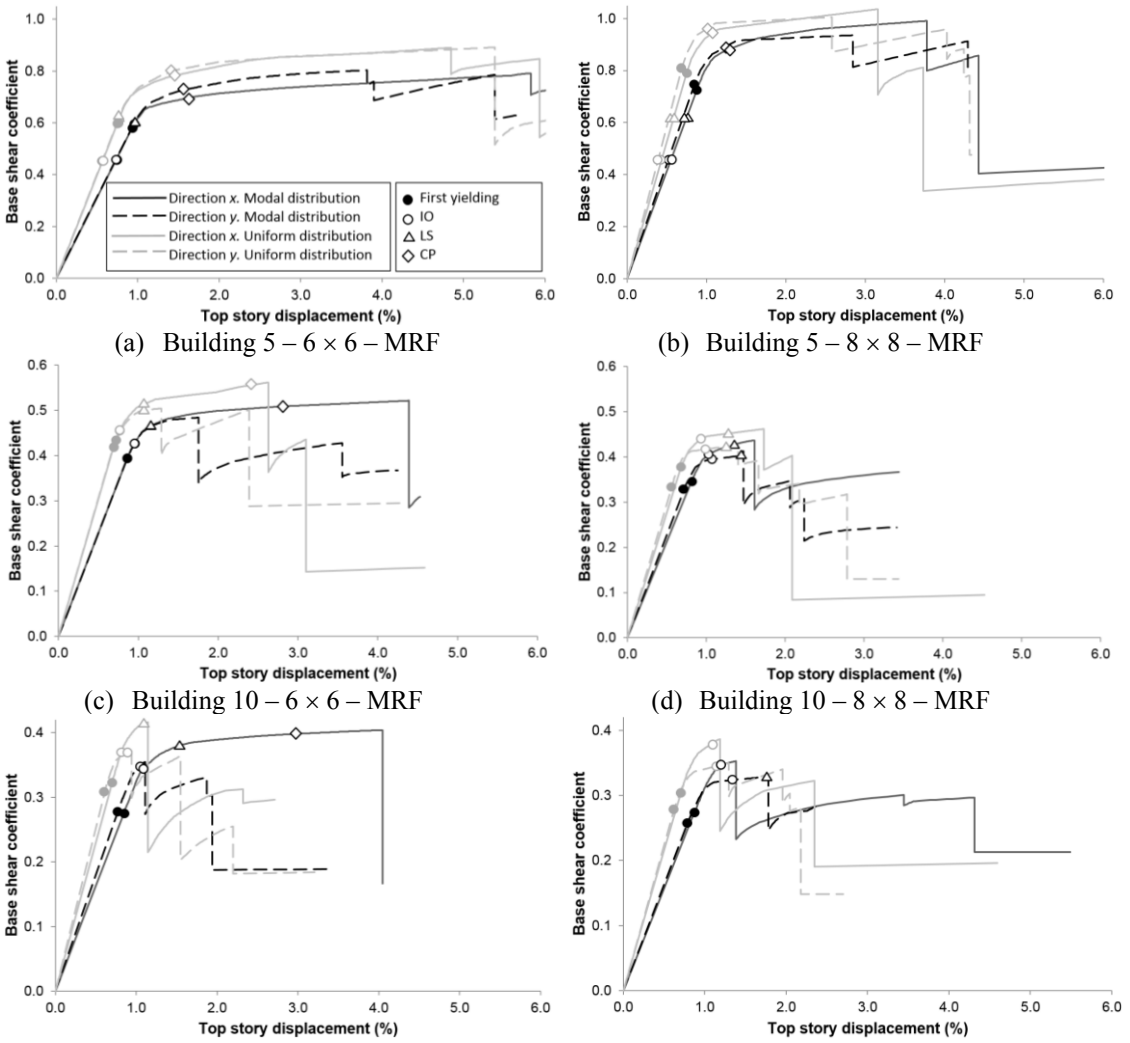

(a) Building 5 – 6 × 6 – MRF

(b) Building 5 – 8 × 8 – MRF

(c) Building 10 – 6 × 6 – MRF

(d) Building 10 – 8 × 8 – MRF

(e) Building 15 – 6 × 6 – MRF

(f) Building 15 – 8 × 8 – MRF

Figure 5-21. Capacity curves and Target Drifts of buildings with Moment-Resisting Frames. Zone "Piedemonte-A" (new microzonation, Figure 3-7)

Most of the results in Figure 5-21 are regular and expected; subsection 5.3.12 holds deeper conclusions issued globally for all the cases. However, Figure 5-21.e shows that, for the 15 – 6 × 6 – MRF prototype building (Table 4-1) in *x* direction, the push-over analysis under modal force distribution predicts less initial stiffness, slightly less force strength, and significantly higher displacement ductility than the analysis under constant force distribution. To further investigate this issue, Figure 5-22 and Figure 5-23 display the damage progression of the 15 – 6 × 6 – MRF prototype building in *x* direction designed for the "Piedemonte A" Zone (new microzonation, Figure 3-7). Figure 5-22 and Figure 5-23 correspond to push-over analyses under modal and uniform force distribution, respectively (Figure 5-1).

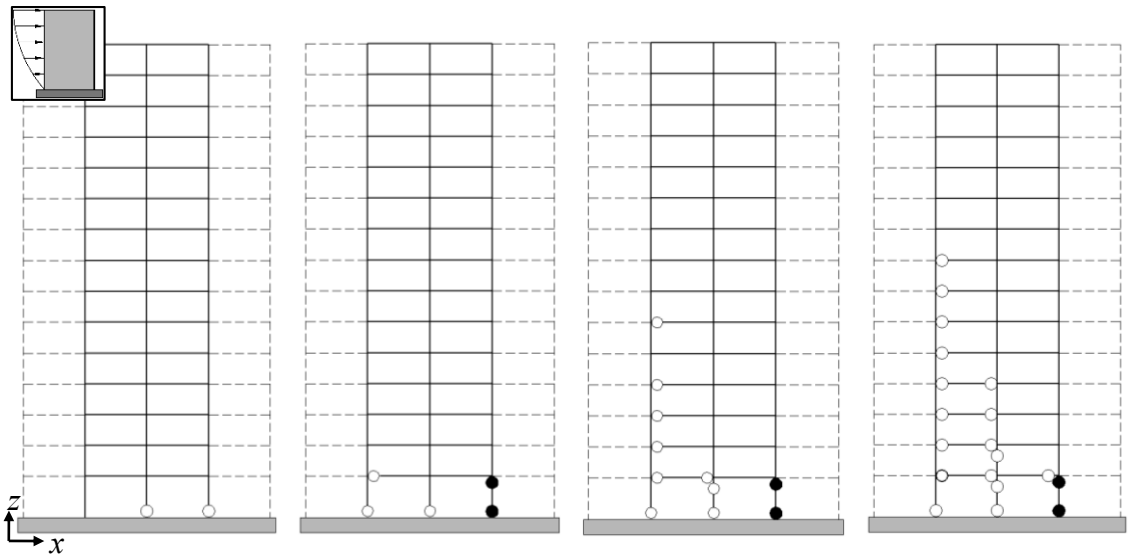

(a) Drift angle 1.04% (b) Drift angle 1.24% (c) Drift angle 1.32% (d) Drift angle 1.52%

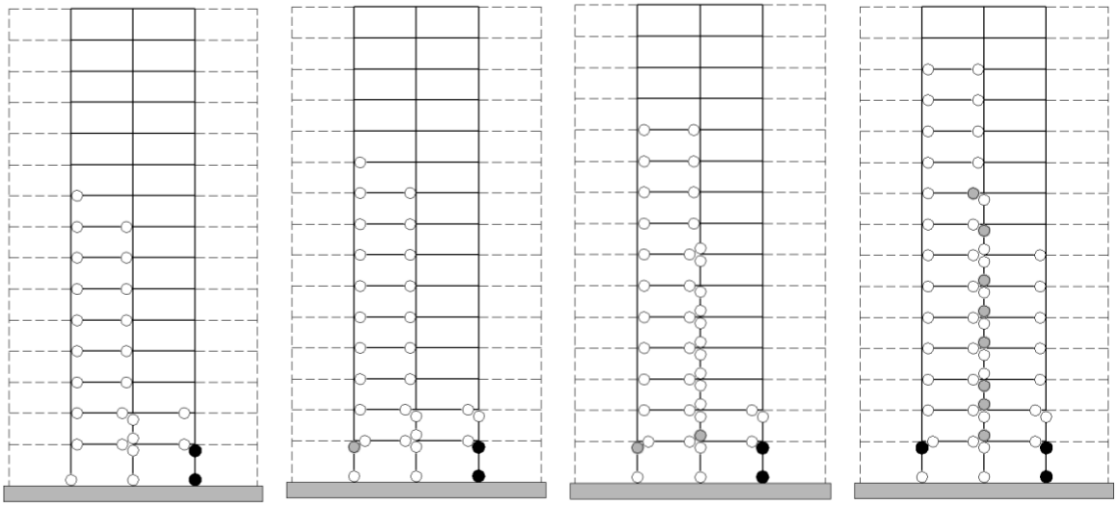

(e) Drift angle 1.71% (f) Drift angle 2.00% (g) Drift angle 2.79% (h) Drift angle 4.05%

Figure 5-22. Hinge progression sequence for the 15 – 6 × 6 – MRF building, modal distribution and *x* direction (right displacement). Zone "Piedemonte-A" (new microzonation, Figure 3-7). ○: yielding, ◎: IO, ◉: LS, ●: CP [FEMA 356 2000]

In Figure 5-22, each frame has two seismic bays. Figure 5-22 represents the damage, in terms of the progression of plastic hinges at the ends of beams and columns, for eight selected states corresponding to growing values of the drift angle. These values of the drift displacement have been chosen to highlight a number of characteristic points of the corresponding capacity curve (Figure 5-21.e), namely: onset of yielding (Figure 5-22.a), and near collapse (Figure 5-22.h). Figure 5-22.h shows that the collapse mechanism involves virtually all the floors although it is mainly concentrated in the first floor columns.

As in Figure 5-22, in Figure 5-23 each frame has two seismic bays. The growing values of the drift displacement have been chosen to highlight a number of characteristic points of the corresponding capacity curve (Figure 5-21.e), namely: onset of yielding (Figure 5-23.a), first sudden drop (Figure 5-23.d), and near collapse (Figure 5-23.h). Figure 5-23.h shows that the collapse mechanism involves the seven bottom floors being mainly concentrated in the first floor columns.

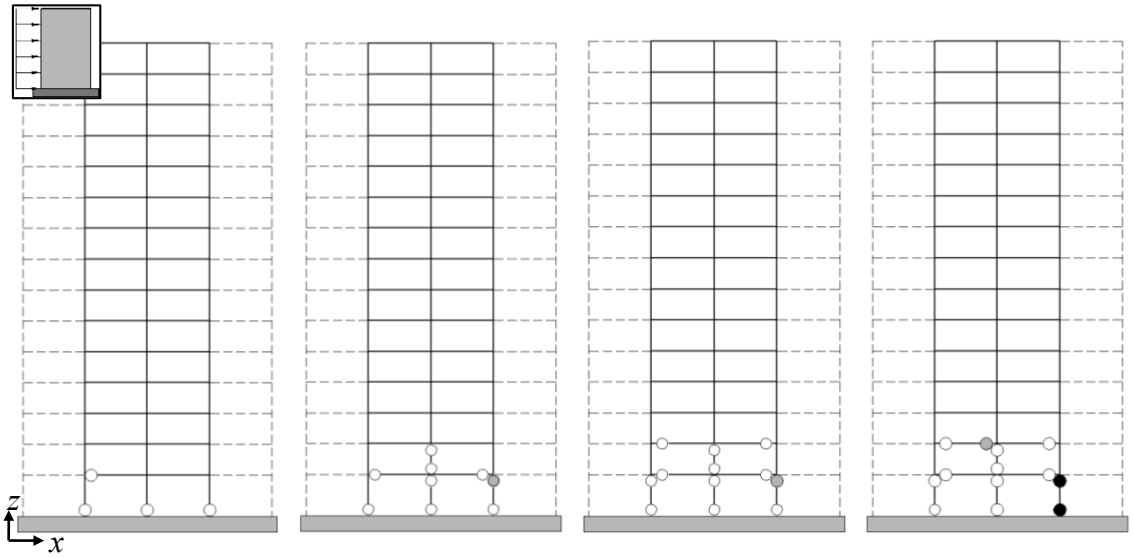

(a) Drift angle 0.82% (b) Drift angle 1.00% (c) Drift angle 1.07% (d) Drift angle 1.26%

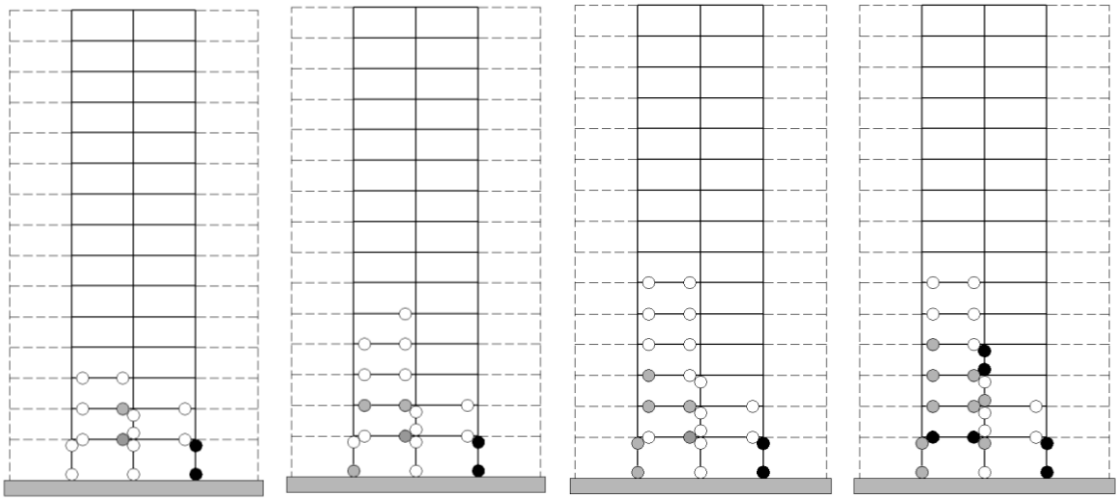

(e) Drift angle 1.46% (f) Drift angle 1.68% (g) Drift angle 1.84% (h) Drift angle 2.80%

Figure 5-23. Hinge progression sequence for the 10 – 6 × 6 – MRF building, uniform distribution and *x* direction (right displacement). Zone "Piedemonte-A" (new microzonation, Figure 3-7). ○: yielding, ◎: IO, ◉: LS, ●: CP [FEMA 356 2000]

Figure 5-22 and Figure 5-23 show that under modal force distribution, the collapse mechanism involves hinges in almost all the levels (reaching the thirteenth story although concentrating mainly in the first story), while for uniform distribution, the hinges concentrate in the columns of the bottom floor. This difference between modal and uniform pushing forces is consistent with the corresponding shear forces and bending moments distribution along the height of the building (Figure 5-1). Noticeably, Figure 5-22 and Figure 5-23 show that in a number of joints, hinges occur earlier in columns than in beams. This undesired brittle behavior arises from the lack of enforced requirements of the Colombian design codes [NSR-98 1998, NSR-10 2010] for guaranteeing the "strong column-weak beam" behavior for the intermediate seismicity zones, such as Bogotá (Figure 3-3). The observed collapse mechanisms show that this circumstance seriously reduces the structural ductility.

As previously announced, Figure 5-24 displays the capacity curves of the prototype CBF buildings (Table 4-1) designed for the "Piedemonte-A" Zone (new microzonation, Figure 3-7).

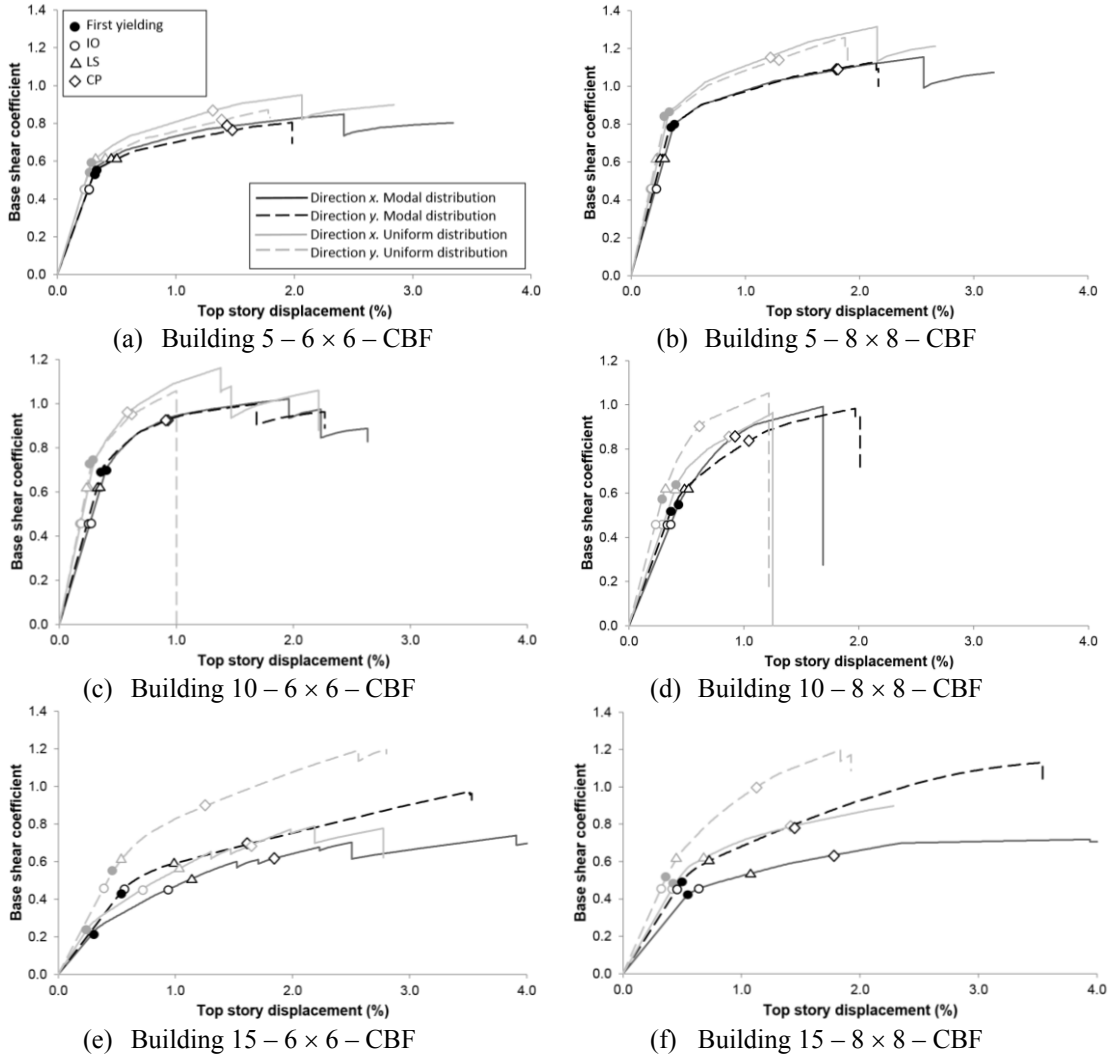

(a) Building 5 – 6 × 6 – CBF

(b) Building 5 – 8 × 8 – CBF

(c) Building 10 – 6 × 6 – CBF

(d) Building 10 – 8 × 8 – CBF

(e) Building 15 – 6 × 6 – CBF

(f) Building 15 – 8 × 8 – CBF

Figure 5-24. Capacity curves and Target Drifts of buildings with Concentric-Braced Frames. Zone "Piedemonte-A" (new microzonation, Figure 3-7)

Most of the results in Figure 5-24 are regular and expected; subsection 5.3.12 holds deeper conclusions issued globally for all the cases. However, Figure 5-24.c shows that, for the 10 – 6 × 6 – CBF prototype building (Table 4-1) in *y* direction, the push-over analysis under modal force distribution predicts less initial stiffness, slightly less force strength, whereas that analysis predicts a significantly higher displacement ductility than the analysis under constant force distribution. To further investigate this issue, Figure 5-25 and Figure 5-26 display the damage progression of the 10 – 6 × 6 – CBF prototype building in *y* direction designed for the "Piedemonte A" Zone (new microzonation, Figure 3-7). Figure 5-25 and Figure 5-26 correspond to push-over analyses under modal and uniform force distribution, respectively. Comparison between Figure 5-25 and Figure 5-26 shows that under modal force distribution, the collapse mechanism involves hinges in many levels of the building (except in upper two ones), while for uniform distribution the hinges concentrate in the four lowest levels, mainly in the bottom one. Comparison between Figure 5-25.h and Figure 5-26.h shows that the collapse mechanism for uniform distribution is initially less severe, although progresses rapidly, as shown by the vertically descendant branch in Figure 5-24.c. These differences between modal and uniform pushing forces are consistent with the corresponding shear forces and bending moments distribution along the height of the building (Figure 5-1).

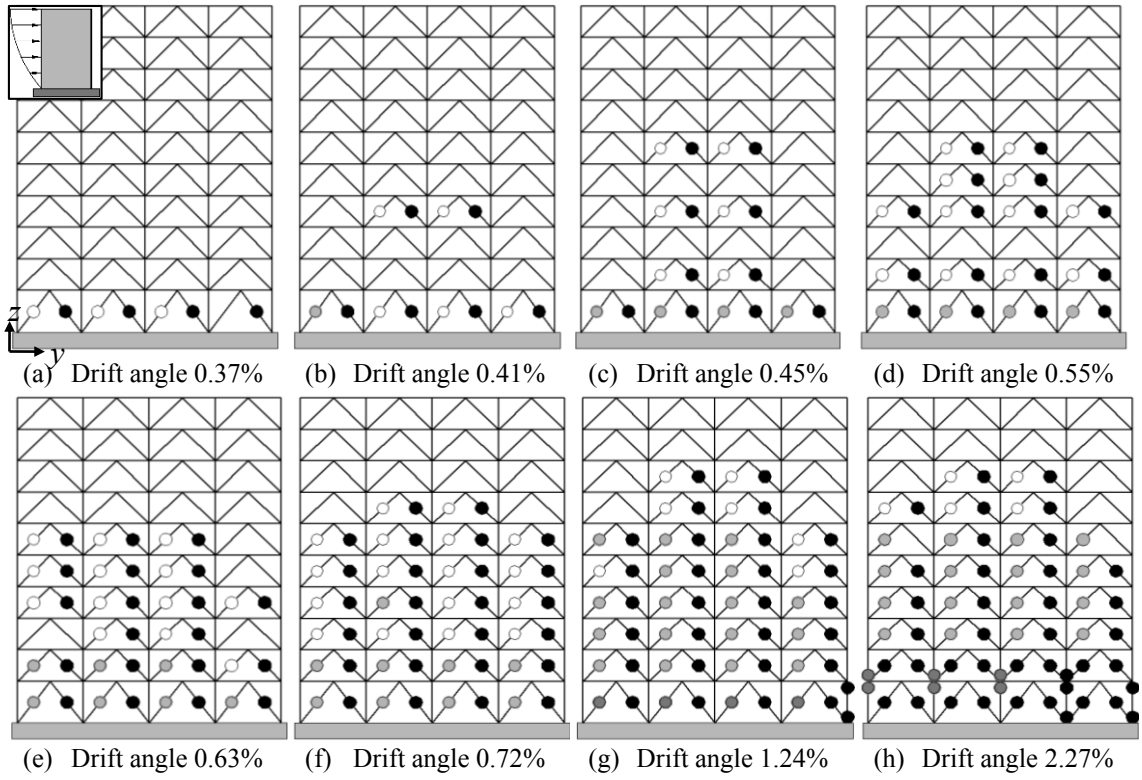

(a) Drift angle 0.37% (b) Drift angle 0.41% (c) Drift angle 0.45% (d) Drift angle 0.55%

(e) Drift angle 0.63% (f) Drift angle 0.72% (g) Drift angle 1.24% (h) Drift angle 2.27%

Figure 5-25. Hinge progression sequence for the 10 – 6 × 6 – CBF building, modal distribution and *y* direction (right displacement). Zone "Piedemonte-A" (new microzonation, Figure 3-7). ○: yielding, ◎: IO, ◉: LS, ●: CP [FEMA 356 2000]

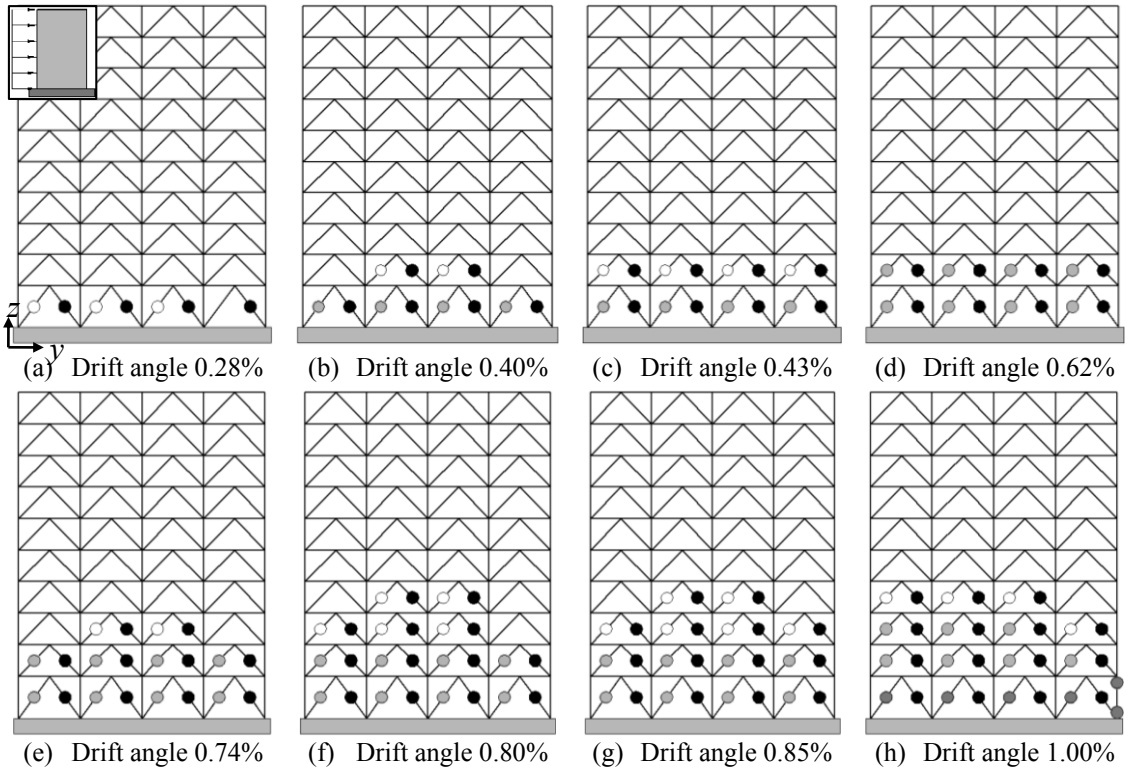

(a) Drift angle 0.28% (b) Drift angle 0.40% (c) Drift angle 0.43% (d) Drift angle 0.62%

(e) Drift angle 0.74% (f) Drift angle 0.80% (g) Drift angle 0.85% (h) Drift angle 1.00%

Figure 5-26. Hinge progression sequence for the 10 – 6 × 6 – CBF building, uniform distribution and *y* direction (right displacement). Zone "Piedemonte-A" (new microzonation, Figure 3-7). ○: yielding, ◎: IO, ◉: LS, ●: CP [FEMA 356 2000]

As previously announced, Figure 5-27 displays the capacity curves of the prototype EBF buildings (Table 4-1) designed for the "Piedemonte-A" Zone (new microzonation, Figure 3-7).

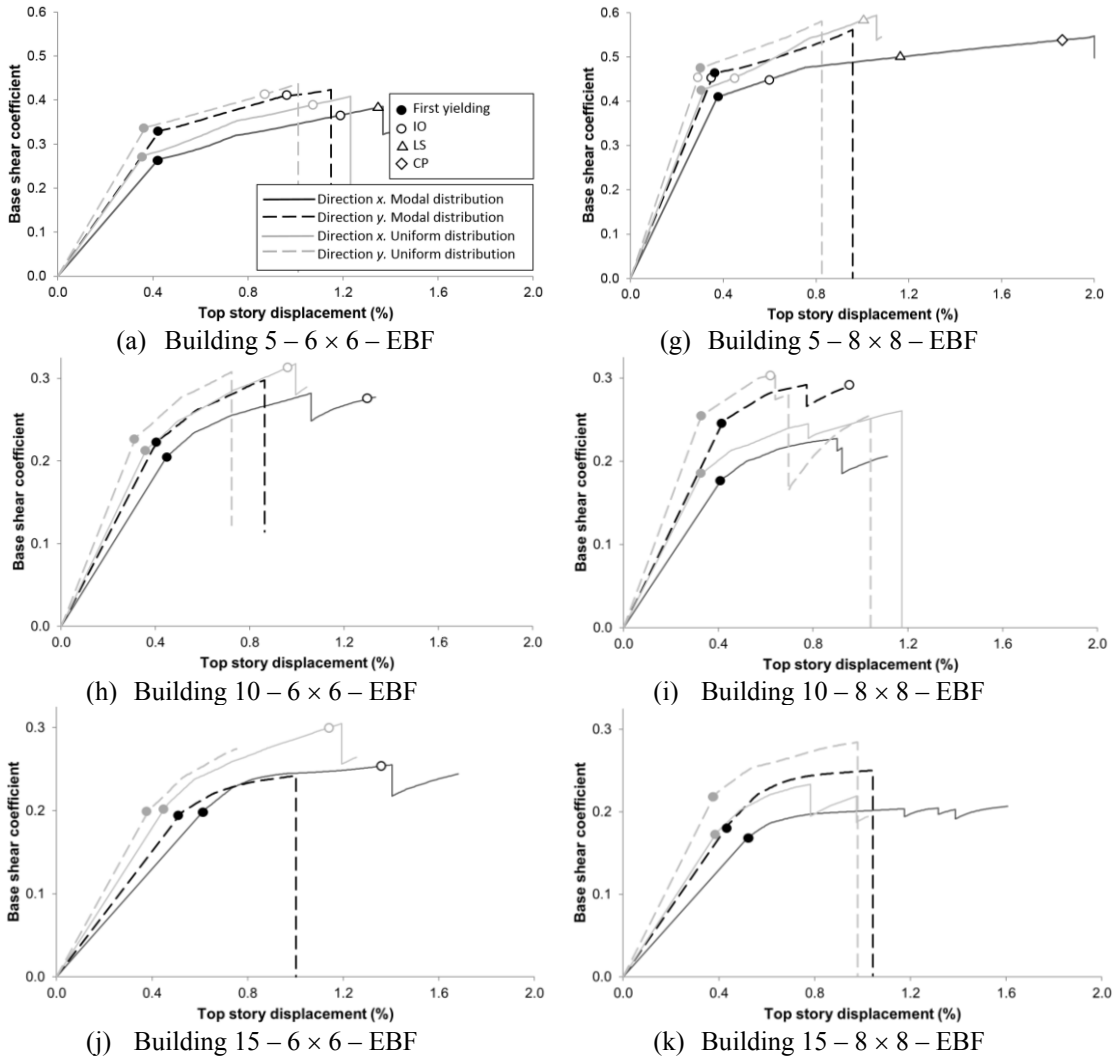

(a) Building 5 – 6 × 6 – EBF (g) Building 5 – 8 × 8 – EBF

(h) Building 10 – 6 × 6 – EBF (i) Building 10 – 8 × 8 – EBF

(j) Building 15 – 6 × 6 – EBF (k) Building 15 – 8 × 8 – EBF

Figure 5-27. Capacity curves and Target Drifts of buildings with Eccentric-Braced Frames. Zone "Piedemonte-A" (new microzonation, Figure 3-7)

Most of the results in Figure 5-27 are regular and expected; subsection 5.3.12 holds deeper conclusions issued globally for all the cases. However, Figure 5-27.b shows that, for the 5 – 8 × 8 – EBF prototype building (Table 4-1) in *x* direction, the push-over analysis under modal force distribution predicts less initial stiffness and force strength, whereas that analysis predicts a significantly higher displacement ductility than the analysis under constant force distribution. To further investigate this issue, Figure 5-28 and Figure 5-29 display the damage progression of the 5 – 8 × 8 – EBF prototype building in *x* direction designed for the "Piedemonte A" Zone (new microzonation, Figure 3-7). Figure 5-28 and Figure 5-29 correspond to push-over analyses under modal and uniform force distribution, respectively (Figure 5-1).

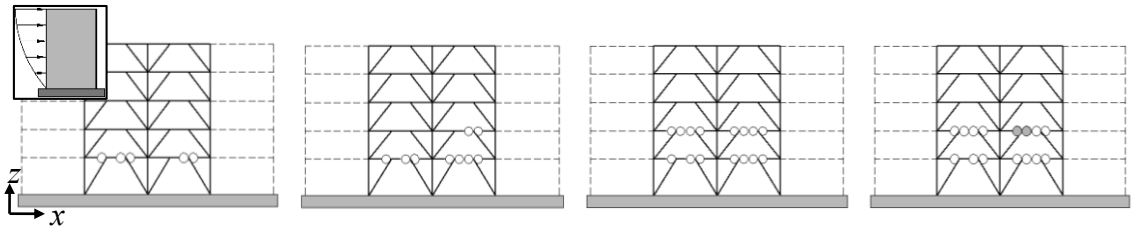

(a) Drift angle 0.43% (b) Drift angle 0.87% (c) Drift angle 0.92% (d) Drift angle 1.75%

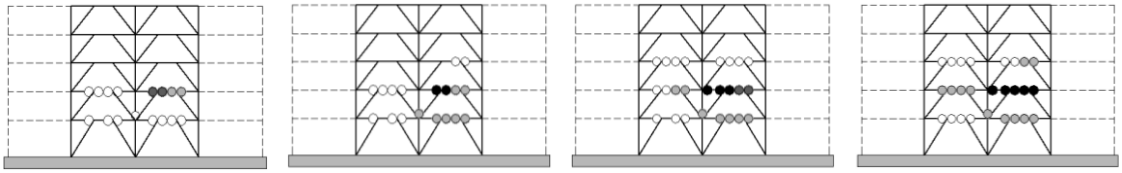

(e) Drift angle 2.05% (f) Drift angle 2.25% (g) Drift angle 2.33% (h) Drift angle 2.50%

Figure 5-28. Hinge progression sequence for the 5 – 8 × 8 – EBF building, modal distribution and *x* direction (right displacement). Zone "Piedemonte-A" (new microzonation, Figure 3-7). ○: yielding, ◎: IO, ◉: LS, ●: CP [FEMA 356 2000]

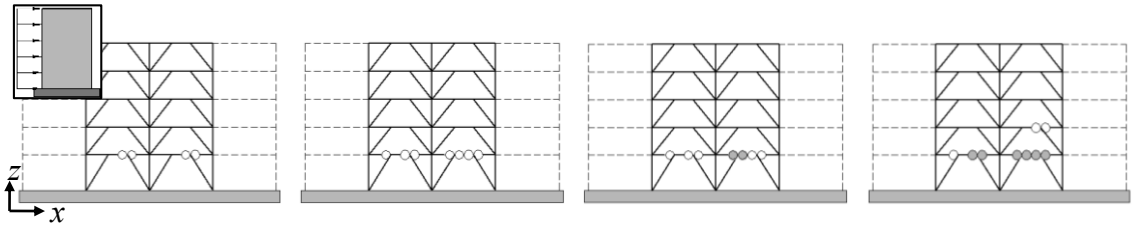

(a) Drift angle 0.37% (b) Drift angle 0.49% (c) Drift angle 0.63% (d) Drift angle 0.88%

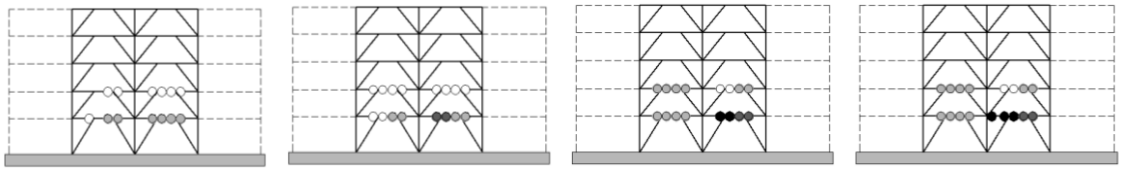

(e) Drift angle 0.89% (f) Drift angle 0.98% (g) Drift angle 1.19% (h) Drift angle 1.25%

Figure 5-29. Hinge progression sequence for the 5 – 8 × 8 – EBF building, uniform distribution and *x* direction (right displacement). Zone "Piedemonte-A" (new microzonation, Figure 3-7). ○: yielding, ◎: IO, ◉: LS, ●: CP [FEMA 356 2000]

Comparison between Figure 5-28 and Figure 5-29 shows that under modal force distribution, the collapse mechanism involves hinges in the bottom three levels of the building, although for uniform distribution, the hinges concentrate only in the link segments of the two lowest levels. This difference between modal and uniform pushing forces is consistent with the corresponding shear forces and bending moments distribution along the height of the building (Figure 5-1). Figure 5-28.h and Figure 5-29.h show that the collapse mechanism is similar to the one described by Figure 4-8.c; noticeably, the full collapse mechanism would involve (apart from the progression of the hinges in the link segments of the first floor beams) also the development of plastic hinges in columns and braces.

Table 5-5 and Table 5-6 show, respectively, the seismic performance and the response reduction factor (R, Ω and R_d) of the prototype buildings (Table 4-1) designed for the "Piedemonte A" Zone (new microzonation, Figure 3-7).

Table 5-5. Seismic performance. "Piedemonte A" zone (new microzonation)

Building	Target Drift IO(*)		Target Drift LS(*)		Target Drift CP(*)	
	Direction *x*	Direction *y*	Direction *x*	Direction *y*	Direction *x*	Direction *y*
5 – 6 × 6 – MRF	YES / YES	YES / YES	YES / YES	YES / YES	YES / YES	YES / YES
5 – 8 × 8 – MRF	YES / YES	YES / YES	YES / YES	YES / YES	YES / YES	YES / YES
5 – 6 × 6 – CBF	YES / YES	YES / YES	YES / YES	YES / YES	YES / YES	YES / YES
5 – 8 × 8 – CBF	YES / YES	YES / YES	YES / YES	YES / YES	YES / YES	YES / YES
5 – 6 × 6 – EBF	**NO** / **NO**	**NO** / **NO**	**NO** / -	- / -	- / -	- / -
5 – 8 × 8 – EBF	**NO** / **NO**	YES / YES	**NO** / -	- / -	YES / -	- / -
10 – 6 × 6 – MRF	YES / YES	YES / YES	YES / YES	YES / YES	YES / YES	YES / -
10 – 8 × 8 – MRF	YES / YES	YES / YES	**NO** / **NO**	YES / **NO**	YES / YES	YES / -
10 – 6 × 6 – CBF	YES / YES	YES / YES	YES / YES	YES / YES	YES / YES	YES / YES
10 – 8 × 8 – CBF	YES / YES	YES / YES	YES / YES	YES / YES	YES / YES	YES / YES
10 – 6 × 6 – EBF	**NO** / **NO**	**NO** / -	- / -	- / -	- / -	- / -
10 – 8 × 8 – EBF	- / -	**NO** / **NO**	- / -	- / -	- / -	- / -
15 – 6 × 6 – MRF	**NO** / **NO**	**NO** / **NO**	YES / **NO**	**NO** / -	YES / -	- / -
15 – 8 × 8 – MRF	**NO** / **NO**	**NO** / **NO**	- / -	YES / -	- / -	YES / -
15 – 6 × 6 – CBF	**NO** / **NO**	**NO** / YES	YES / YES	YES / **NO**	YES / YES	YES / YES
15 – 8 × 8 – CBF	**NO** / YES	YES / YES	YES / YES	YES / YES	YES / YES	YES / YES
15 – 6 × 6 – EBF	**NO** / **NO**	- / -	- / -	- / -	- / -	- / -
15 – 8 × 8 – EBF	- / -	- / -	- / -	- / -	- / -	- / -

(*) First / second values correspond to modal and uniform distributions, respectively

Table 5-5 reveals that 53% of the cases exhibit a satisfactory performance (YES), 16% unsatisfactory (NO) and 31% highly unsatisfactory (-). In the MRF/CBF/EBF buildings, such percentages are 65/93/1%, 18/7/22% and 17/0/77%. In the 5/10/15-story buildings such percentages are 68/59/32%, 14/10/24% and 18/31/44%. For the IO/LS/CP limit states, the percentages are 54/56/57%, 32/11/0% and 14/33/43%. For the Modal/Uniform distributions, the percentages are 63/52%, 10/13% and 27/35%. No relevant differences have been observed for *x/y* directions.

Table 5-6**.** Response reduction factor *R* in the *x* / *y* directions. "Piedemonte A" zone (new microzonation)

Building	Over-strength factor (Ω)(*)		Ductility factor R_d(*)		*R* factor ($R = \Omega R_d$) (*)	
	Direction *x*	Direction *y*	Direction *x*	Direction *y*	Direction *x*	Direction *y*
5 – 6 × 6 – MRF	1.43 / 1.42	1.47 / 1.42	4.67 / 4.37	2.92 / 4.85	6.69 / 6.20	4.29 / 6.89
5 – 8 × 8 – MRF	1.37 / 1.31	1.25 / 1.24	3.16 / 3.20	2.71 / 2.98	4.33 / 4.19	3.39 / 3.70
5 – 6 × 6 – CBF	1.55 / 1.60	1.46 / 1.60	4.77 / 4.46	4.11 / 4.13	7.40 / 7.13	6.00 / 6.61
5 – 8 × 8 – CBF	1.46 / 1.52	1.43 / 1.51	4.63 / 4.36	4.41 / 4.34	6.76 / 6.64	6.30 / 6.56
5 – 6 × 6 – EBF	1.47 / 1.49	1.27 / 1.30	2.22 / 2.32	2.14 / 2.12	3.26 / 3.46	2.72 / 2.75
5 – 8 × 8 – EBF	1.38 / 1.38	1.21 / 1.22	3.80 / 2.41	2.18 / 2.25	5.25 / 3.32	2.64 / 2.74
10 – 6 × 6 – MRF	1.33 / 1.30	1.22 / 1.20	3.80 / 2.75	1.73 / 1.53	5.05 / 3.58	2.11 / 1.84
10 – 8 × 8 – MRF	1.29 / 1.24	1.24 / 1.27	1.53 / 2.06	1.66 / 1.99	1.98 / 2.56	2.06 / 2.53
10 – 6 × 6 – CBF	1.47 / 1.56	1.44 / 1.44	3.26 / 2.99	3.23 / 2.58	4.79 / 4.66	4.65 / 3.72
10 – 8 × 8 – CBF	1.71 / 1.67	1.86 / 1.84	2.06 / 1.80	2.77 / 2.40	3.53 / 3.01	5.15 / 4.41
10 – 6 × 6 – EBF	1.38 / 1.49	1.34 / 1.36	1.72 / 1.86	1.59 / 1.69	2.37 / 2.77	2.13 / 2.30
10 – 8 × 8 – EBF	1.29 / 1.40	1.19 / 1.19	1.71 / 2.56	1.99 / 1.64	2.21 / 3.59	2.37 / 1.95
15 – 6 × 6 – MRF	1.47 / 1.29	1.29 / 1.22	3.18 / 1.25	1.03 / 1.27	4.67 / 1.61	1.33 / 1.55
15 – 8 × 8 – MRF	1.29 / 1.27	1.28 / 1.25	1.22 / 1.34	1.77 / 1.66	1.57 / 1.70	2.27 / 2.07
15 – 6 × 6 – CBF	3.27 / 3.36	2.26 / 2.34	3.69 / 2.74	2.94 / 2.65	12.08 / 9.23	6.64 / 6.19
15 – 8 × 8 – CBF	1.72 / 1.90	2.30 / 2.32	4.20 / 2.79	3.09 / 2.20	7.22 / 5.31	7.11 / 5.11
15 – 6 × 6 – EBF	1.29 / 1.50	1.25 / 1.39	1.77 / 1.79	1.57 / 1.44	2.28 / 2.68	1.96 / 2.00
15 – 8 × 8 – EBF	1.24 / 1.34	1.38 / 1.30	2.45 / 1.53	1.75 / 2.01	3.04 / 2.05	2.42 / 2.61

(*) First / second values correspond to modal and uniform distributions, respectively

Comparison among the values of *R* in Table 5-6 with the assumed factors in Table 4-23 shows that, in 65% of the cases, the analyzed buildings do not possess the required ductility. In the MRF/CBF/EBF buildings, such percentage is 79/17/100%. In the 5/10/15-story buildings such percentage is 54/79/63%. For the Modal/Uniform distributions, the percentages are 61/69%. No relevant differences have been observed for *x/y* directions.

5.3.5 "Piedemonte-B" Zone (new microzonation)

Figure 5-30, Figure 5-33 and Figure 5-36 display the capacity curves of the prototype buildings (Table 4-1) designed for the "Piedemonte-B" Zone (new microzonation, Figure 3-7); Figure 5-30, Figure 5-33 and Figure 5-36 refer to the MRF, CBF and EBF buildings, respectively.

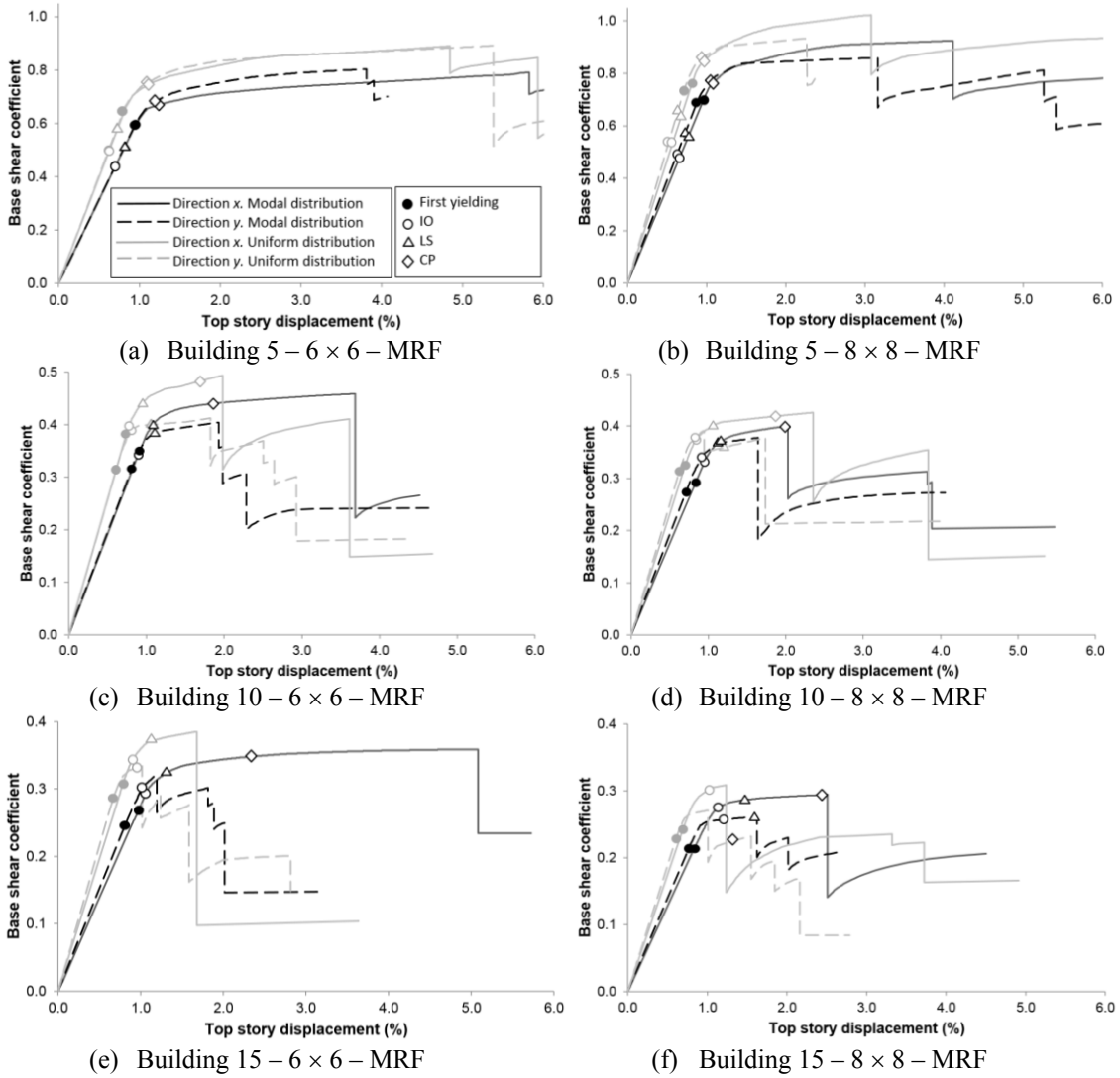

(a) Building 5 – 6 × 6 – MRF (b) Building 5 – 8 × 8 – MRF

(c) Building 10 – 6 × 6 – MRF (d) Building 10 – 8 × 8 – MRF

(e) Building 15 – 6 × 6 – MRF (f) Building 15 – 8 × 8 – MRF

Figure 5-30. Capacity curves and Target Drifts of buildings with Moment-Resisting Frames. Zone "Piedemonte-B" (new microzonation, Figure 3-7)

Most of the results in Figure 5-30 are regular and expected; subsection 5.3.12 holds deeper conclusions issued globally for all the cases. However, Figure 5-30.f shows that, for the 15 – 8 × 8 – MRF prototype building (Table 4-1) in *y* direction, the push-over analysis under modal force distribution predicts less initial stiffness, less force strength, and higher displacement ductility than the analysis under constant force distribution. To further investigate this issue, Figure 5-31 and Figure 5-32 display the damage progression of the 15 – 8 × 8 – MRF prototype building in *y*

direction designed for the "Piedemonte-B" Zone (new microzonation, Figure 3-7). Figure 5-31 and Figure 5-32 correspond to push-over analyses under modal and uniform force distribution, respectively (Figure 5-1).

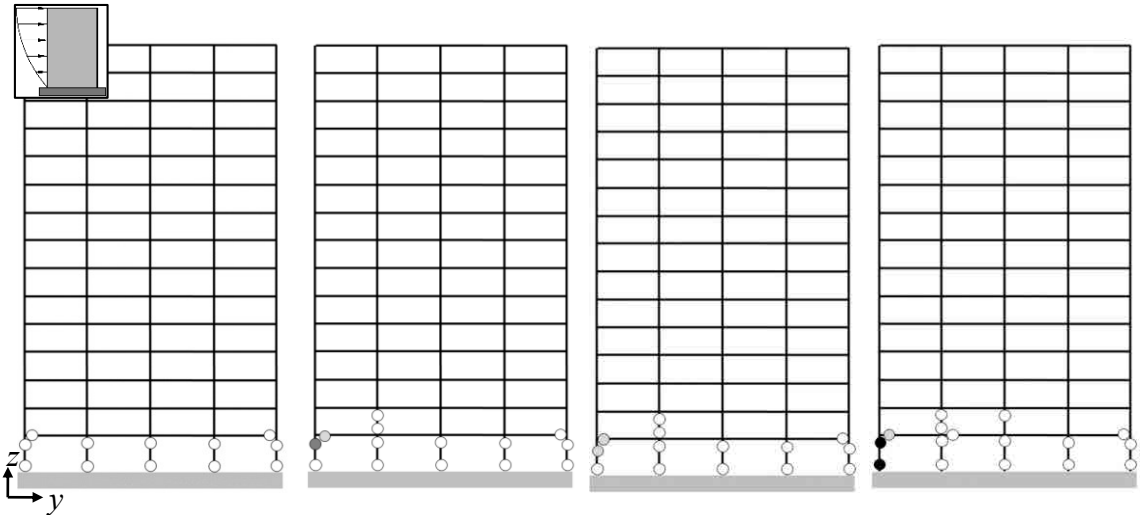

(a) Drift angle 1.01% (b) Drift angle 1.49% (c) Drift angle 1.62% (d) Drift angle 1.66%

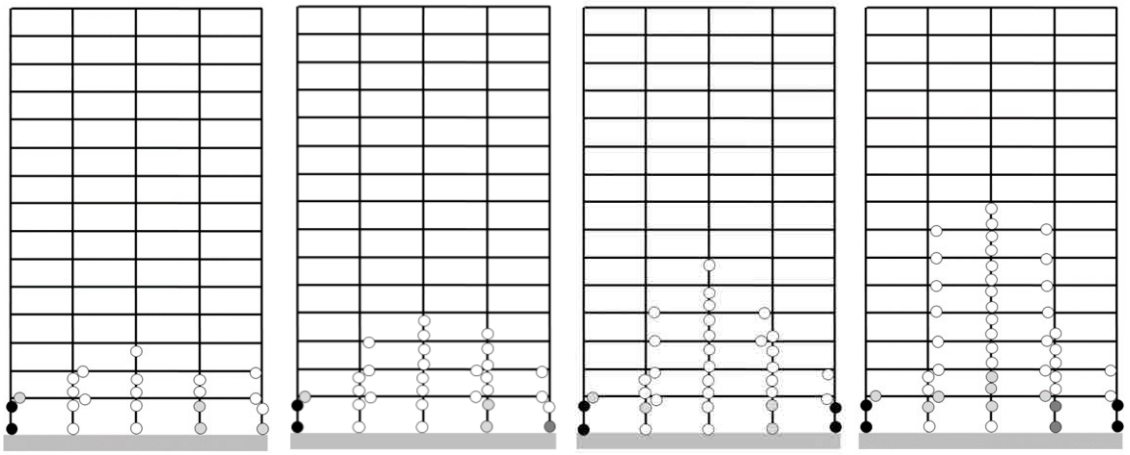

(e) Drift angle 1.93% (f) Drift angle 2.11% (g) Drift angle 2.25% (h) Drift angle 2.63%

Figure 5-31. Hinge progression sequence for the 15 – 8 × 8 – MRF building, modal distribution and *y* direction (right displacement). Zone "Piedemonte-B" (new microzonation, Figure 3-7). ○: yielding, ◎: IO, ◉: LS, ●: CP [FEMA 356 2000]

In Figure 5-31, each frame has four seismic bays (see Figure 4-3). Figure 5-31 represents the damage, in terms of the progression of plastic hinges at the ends of the members (beams and columns), for eight selected states corresponding to growing values of the drift angle. These values of the drift displacement have been chosen to highlight a number of characteristic points of the corresponding capacity curve (Figure 5-30.f), namely: onset of yielding (Figure 5-31.a), first sudden drop failure of the right bottom column (Figure 5-31.d), second sudden drop (Figure 5-31.e) and near collapse (Figure 5-31.h). Figure 5-31.h shows that the collapse mechanism is mainly concentrated in the bottom floor but it involves an important number of floors (both beams and columns).

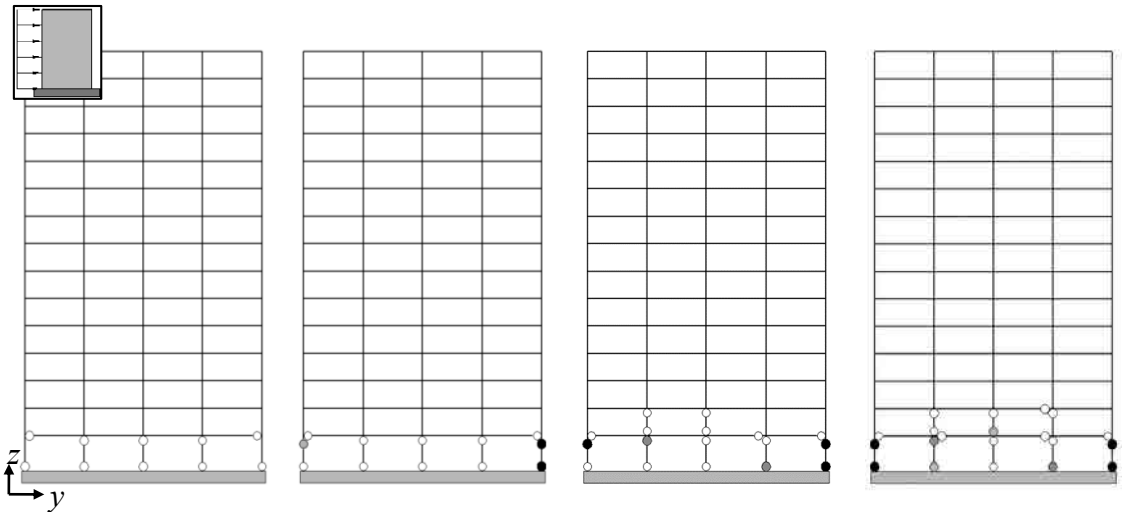

(a) Drift angle 0.72% (b) Drift angle 1.06% (c) Drift angle 1.46% (d) Drift angle 1.70%

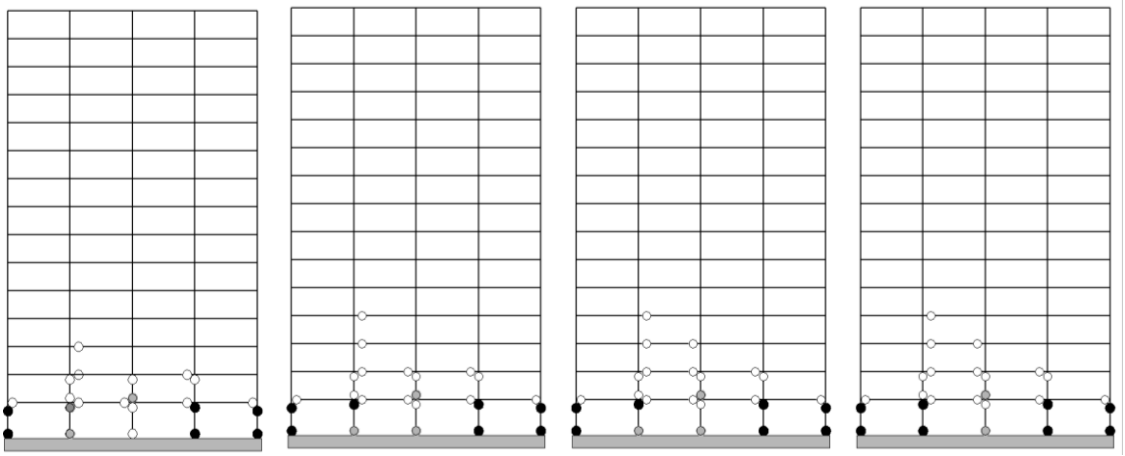

(e) Drift angle 2.02% (f) Drift angle 2.11% (g) Drift angle 2.16% (h) Drift angle 2.79%

Figure 5-32. Hinge progression sequence for the 15 – 8 × 8 – MRF building, uniform distribution and *y* direction (right displacement). Zone "Piedemonte-B" (new microzonation, Figure 3-7). ○: yielding, ◎: IO, ◉: LS, ●: CP [FEMA 356 2000]

Comparison between Figure 5-31 and Figure 5-32 shows that under modal force distribution, the collapse mechanism involves hinges in many levels of the building (up to the eighth level), while for uniform distribution, the hinges concentrate more in the lower levels, mainly in the bottom one (although in the collapse, there is a plastic hinge in a beam in the 4th story). This difference between modal and uniform pushing forces is consistent with the shear forces and bending moments distribution along the height of the building (Figure 5-1). Noticeably, Figure 5-31 and Figure 5-32 show that in most of the joints, hinges occur earlier in columns than in beams. This undesired brittle behavior arises from the lack of enforced requirements of the Colombian design codes [NSR-98 1998, NSR-10 2010] for guaranteeing the "strong column-weak beam" behavior for the intermediate seismicity zones, such as Bogotá (Figure 3-3). The observed collapse mechanisms show that this circumstance seriously reduces the structural ductility.

As previously announced, Figure 5-33 displays the capacity curves of the prototype CBF buildings (Table 4-1) designed for the "Piedemonte B" Zone (new microzonation, Figure 3-7).

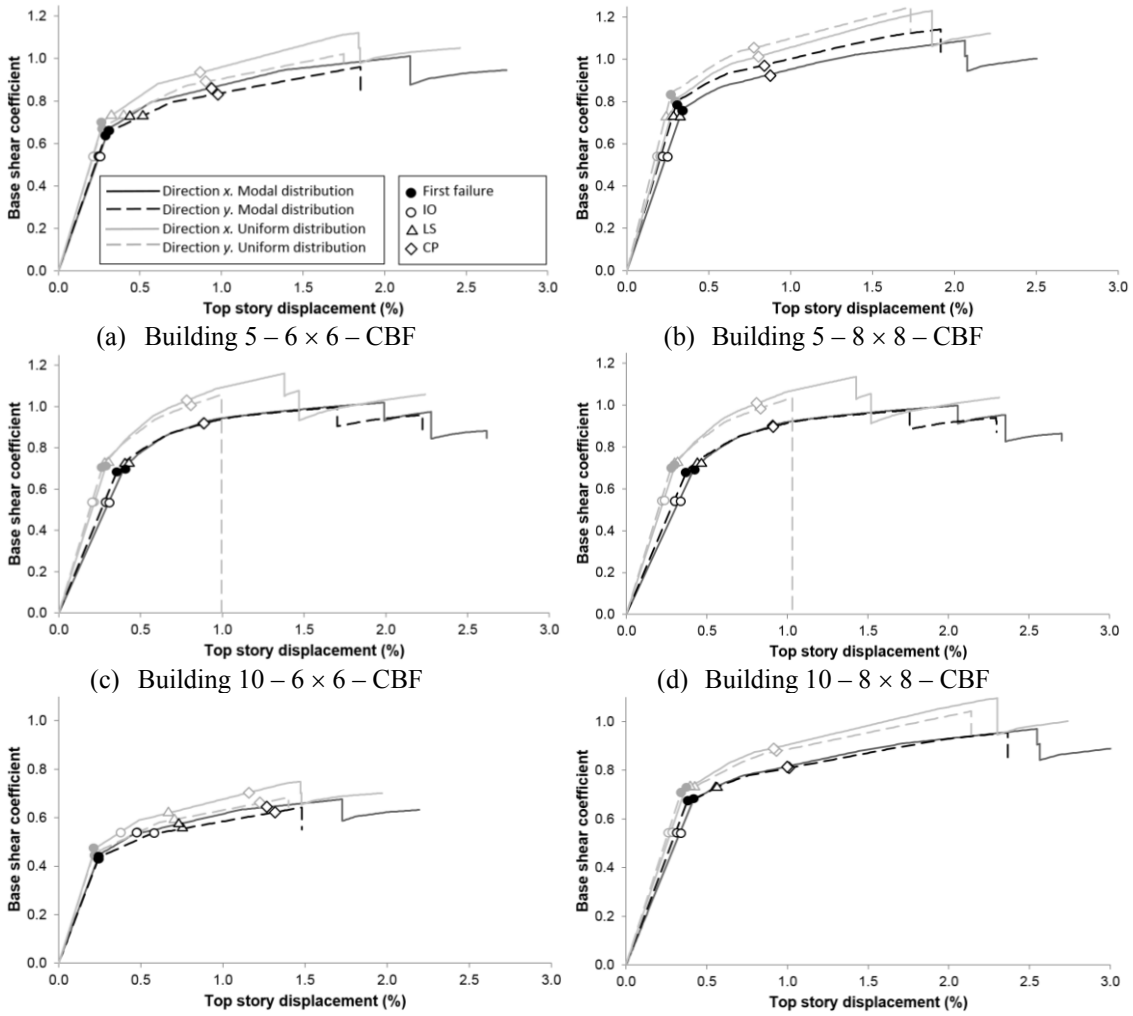

(a) Building 5 – 6 × 6 – CBF (b) Building 5 – 8 × 8 – CBF

(c) Building 10 – 6 × 6 – CBF (d) Building 10 – 8 × 8 – CBF

(e) Building 15 – 6 × 6 – CBF (f) Building 15 – 8 × 8 – CBF

Figure 5-33. Capacity curves and Target Drifts of buildings with Concentric-Braced Frames. Zone "Piedemonte-B" (new microzonation, Figure 3-7)

Most of the results in Figure 5-33 are regular and expected, thus illustrating the reliability and accuracy of the carried out analysis; subsection 5.3.12 holds deeper conclusions that are issued globally for all the cases. However, Figure 5-33.b shows that, for the 5 – 8 × 8 – CBF prototype building (Table 4-1) in *y* direction, the push-over analysis under modal force distribution predicts less initial stiffness and force strength, whereas that analysis predicts higher displacement ductility than the analysis under constant force distribution. To further investigate this issue, Figure 5-34 and Figure 5-35 display the damage progression of the 5 – 8 × 8 – CBF prototype building in *y* direction designed for the "Piedemonte B" Zone (new microzonation, Figure 3-7). Figure 5-34 and Figure 5-35 correspond to push-over analyses under modal and uniform force distribution, respectively (Figure 5-1).

Figure 5-34 and Figure 5-35 show that the damage progression follows regular and expected patterns: (i) the damage affects only the brace members (this fact points out that the protection of the main structural members is highly effective), (ii) inside each step, the damage in every level is almost uniform, (iii) the damage is progressing upwards, i.e. the damage in any floor is lower or equal than in the lowest ones, and (iv) for each pair of braces (e.g. those that belong to the same floor and the same bay), the compressed brace exhibits more damage than the tensioned one. This last fact is obviously related to the important deleterious influence of the buckling instability (see Figure 4-8.b).

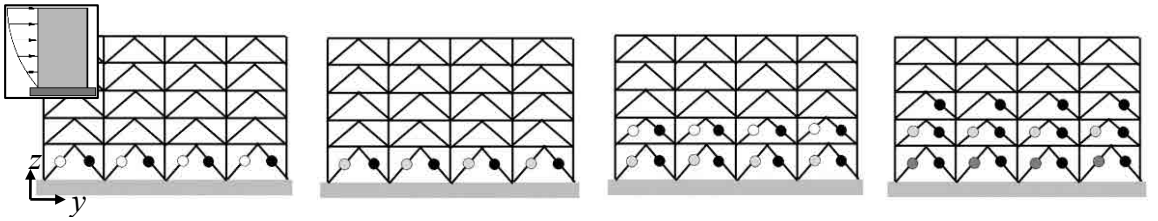

(a) Drift angle 0.40% (b) Drift angle 0.47% (c) Drift angle 0.72% (d) Drift angle 1.66%

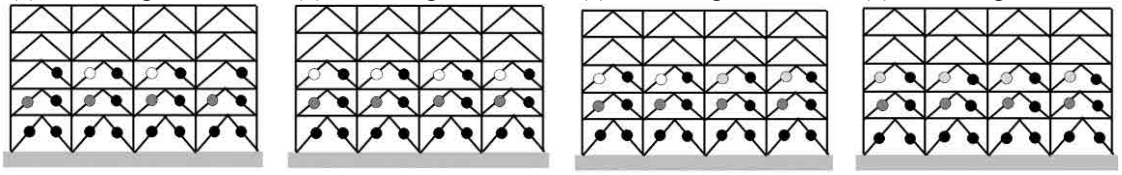

(e) Drift angle 1.89% (f) Drift angle 1.95% (g) Drift angle 2.02% (h) Drift angle 2.22%

Figure 5-34. Failure progression sequence for the 5 – 8 × 8 – CBF building, modal distribution and *y* direction (right displacement). Zone "Piedemonte-B" (new microzonation, Figure 3-7). ○: yielding, ◎: IO, ◉: LS, ●: CP [FEMA 356 2000]

In Figure 5-34 and Figure 5-35, each frame has four seismic bays (Figure 4-3). Figure 5-34 and Figure 5-35 represents the damage, in terms of the progression of plastic hinges at the ends of the members (braces), for eight selected states corresponding to growing values of the drift angle. These values of the drift displacement have been chosen to highlight a number of characteristic points of the corresponding capacity curve (Figure 5-33.b), namely: onset of yielding (Figure 5-34.a and Figure 5-35.a), and near collapse (Figure 5-34.h and Figure 5-35.h). The intermediate values correspond to relevant stages of the damage progression.

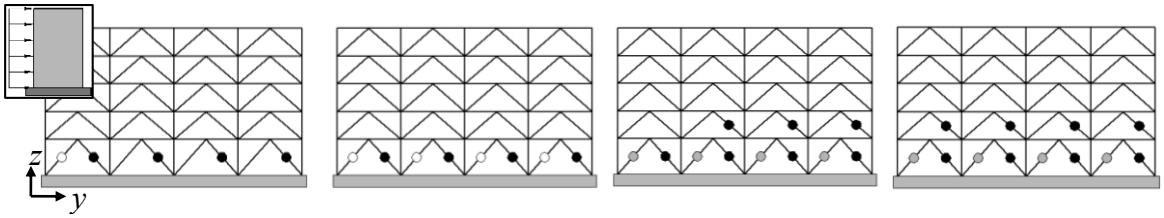

(a) Drift angle 0.32% (b) Drift angle 0.33% (c) Drift angle 0.66% (d) Drift angle 0.71%

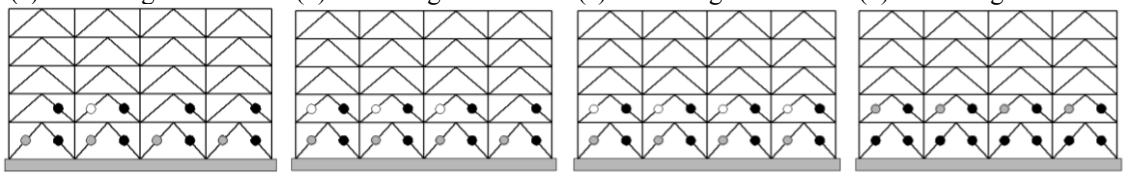

(e) Drift angle 0.80% (f) Drift angle 0.80% (g) Drift angle 0.96% (h) Drift angle 2.01%

Figure 5-35. Failure progression sequence for the 5 – 8 × 8 – CBF building, uniform distribution and *y* direction (right displacement). Zone "Piedemonte-B" (new microzonation, Figure 3-7). ○: yielding, ◎: IO, ◉: LS, ●: CP [FEMA 356 2000]

Comparison between Figure 5-34 and Figure 5-35 shows that, under modal force distribution (Figure 5-34), the collapse mechanism involves hinges in the bottom three levels of the building (even in the top one), while for uniform distribution (Figure 5-35) the hinges concentrate in the two lowest levels. This difference between modal and uniform pushing forces is consistent with the corresponding distribution laws of shear forces and bending moments along the height of the building (Figure 5-1).

As previously announced, Figure 5-36 displays the capacity curves of the prototype EBF

buildings (Table 4-1) designed for the "Piedemonte B" Zone (new microzonation, Figure 3-7).

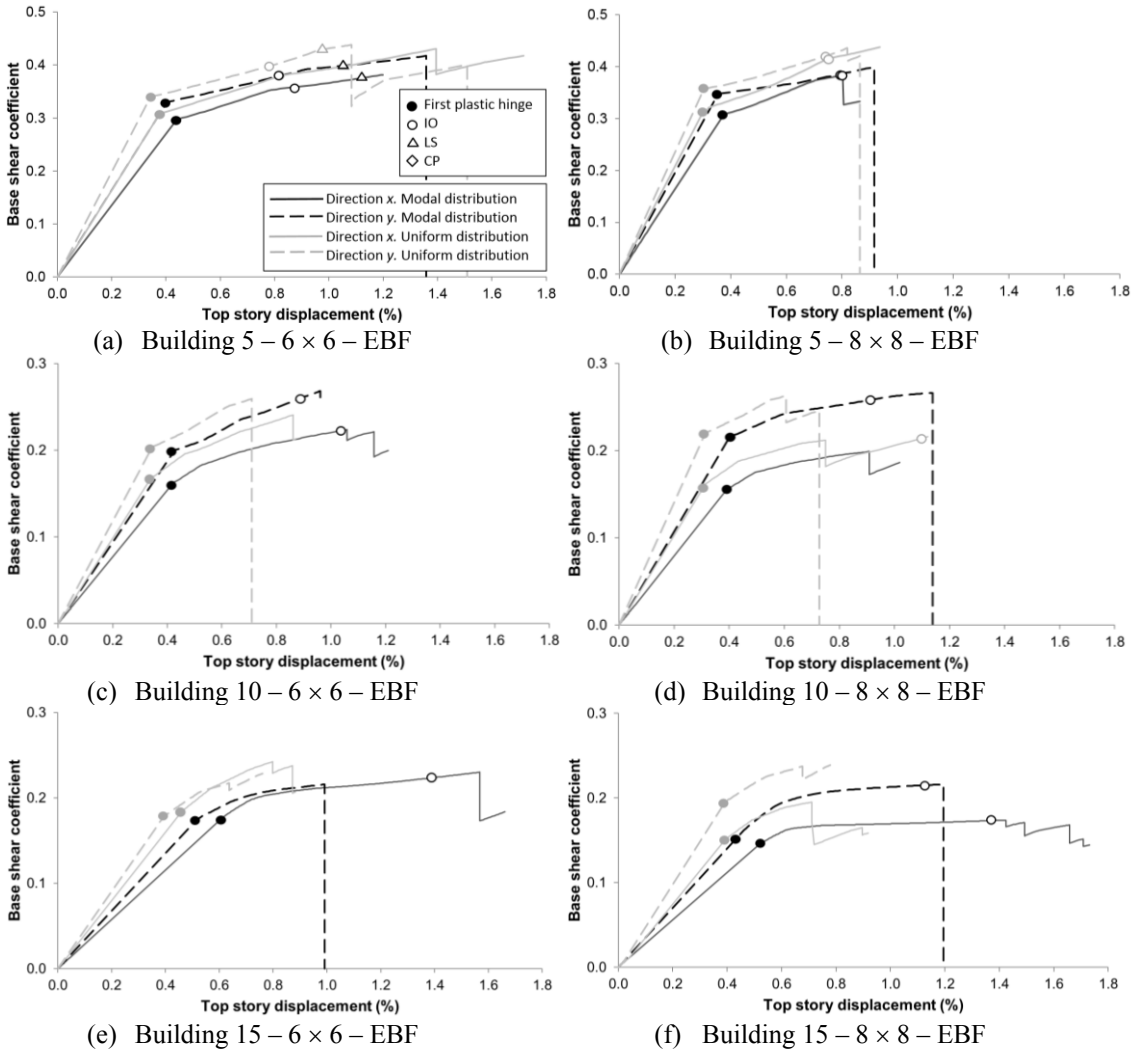

(a) Building 5 – 6 × 6 – EBF (b) Building 5 – 8 × 8 – EBF

(c) Building 10 – 6 × 6 – EBF (d) Building 10 – 8 × 8 – EBF

(e) Building 15 – 6 × 6 – EBF (f) Building 15 – 8 × 8 – EBF

Figure 5-36. Capacity curves and Target Drifts of buildings with Eccentric-Braced Frames. Zone "Piedemonte-B" (new microzonation, Figure 3-7)

Most of the results in Figure 5-36 are regular and expected; subsection 5.3.12 holds deeper conclusions issued globally for all the cases. However, Figure 5-36.b shows that, for the 5 – 8 × 8 – EBF prototype building (Table 4-1) in *y* direction, the push-over analysis under modal force distribution predicts less initial stiffness and force strength, whereas that analysis predicts a slightly higher displacement ductility than the analysis under constant force distribution. To further investigate this issue, Figure 5-37 and Figure 5-38 display the damage progression of the 5 – 8 × 8 – EBF prototype building in *y* direction designed for the "Piedemonte B" Zone (new microzonation, Figure 3-7). Figure 5-37 and Figure 5-38 correspond to push-over analyses under modal and uniform force distribution, respectively (Figure 5-1).

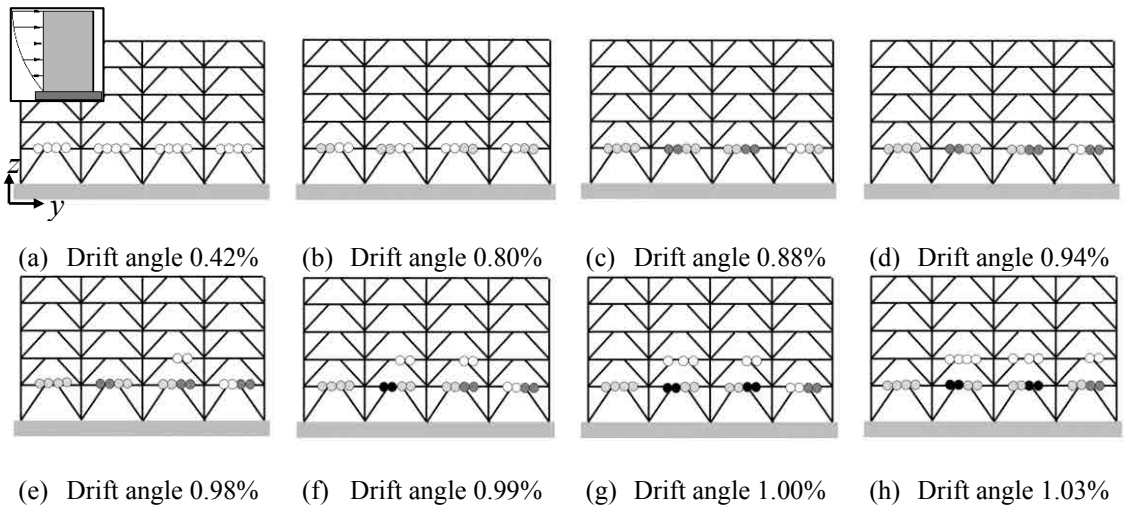

(a) Drift angle 0.42% (b) Drift angle 0.80% (c) Drift angle 0.88% (d) Drift angle 0.94%

(e) Drift angle 0.98% (f) Drift angle 0.99% (g) Drift angle 1.00% (h) Drift angle 1.03%

Figure 5-37. Hinge progression sequence for the 5 – 8 × 8 – EBF building, modal distribution and *y* direction (right displacement). Zone "Piedemonte-B" (new microzonation, Figure 3-7). ○: yielding, ◍: IO, ●: LS, ●: CP [FEMA 356 2000]

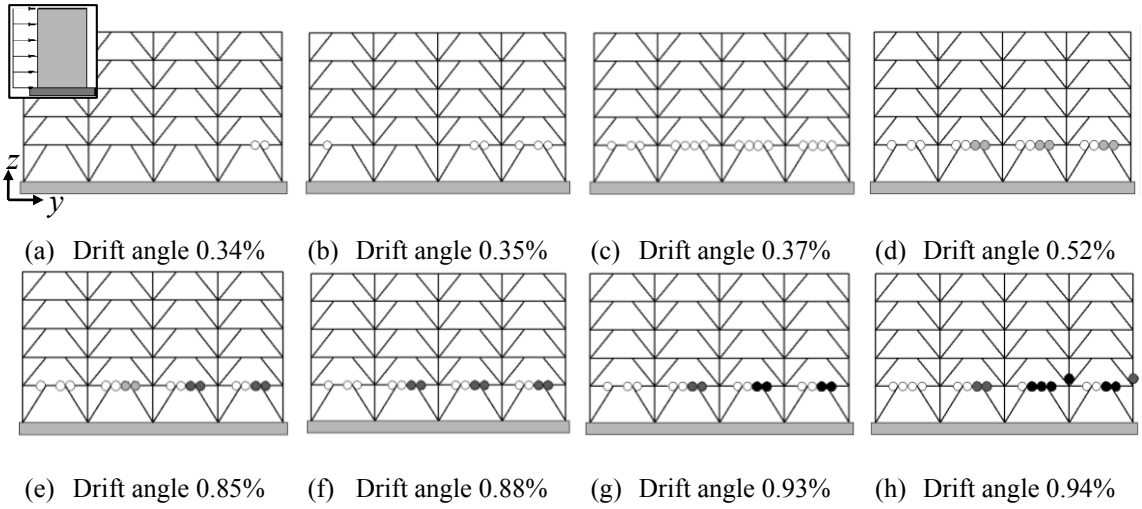

(a) Drift angle 0.34% (b) Drift angle 0.35% (c) Drift angle 0.37% (d) Drift angle 0.52%

(e) Drift angle 0.85% (f) Drift angle 0.88% (g) Drift angle 0.93% (h) Drift angle 0.94%

Figure 5-38. Hinge progression sequence for the 5 – 8 × 8 – EBF building, uniform distribution and *y* direction (right displacement). Zone "Piedemonte-B" (new microzonation, Figure 3-7). ○: yielding, ◍: IO, ●: LS, ●: CP [FEMA 356 2000]

Comparison between Figure 5-37 and Figure 5-38 shows that under modal force distribution (Figure 5-37), the collapse mechanism involves hinges in the bottom two levels of the building, although for uniform distribution (Figure 5-38), the hinges concentrate only in the link segments of the bottom (except for the hinges in the right second floor columns). This difference between modal and uniform pushing forces is consistent with the corresponding shear forces and bending moments distribution along the height of the building (Figure 5-1). Figure 5-37.h and Figure 5-38.h show that the collapse mechanism is similar to the one described by Figure 4-8.c; noticeably, the full collapse mechanism would involve (apart from the progression of the hinges in the link segments of the first floor beams) also the development of plastic hinges in columns and braces.

Table 5-7 and Table 5-8 show, respectively, the seismic performance and the response reduction factor (R, Ω and R_d) of the prototype buildings (Table 4-1) designed for the "Piedemonte B" Zone (new microzonation, Figure 3-7). Table 5-7 reveals that 48% of the cases exhibit a satisfactory performance (YES), 31% unsatisfactory (NO) and 21% highly unsatisfactory (-). In the MRF/CBF/EBF buildings, such percentages are 52/87/6%, 31/13/48% and 17/0/46%. In the

5/10/15-story buildings such percentages are 72/47/26%, 17/42/33% and 11/11/41%. For the IO/LS/CP limit states, the percentages are 42/48/58%, 45/21/0% and 13/31/42%. For the Modal/Uniform distributions, the percentages are 53/51%, 24/18% and 23/31%. No relevant differences have been observed for *x/y* directions.

Table 5-7. Seismic performance. "Piedemonte B" zone (new microzonation)

Building	Target Drift IO(*)		Target Drift LS(*)		Target Drift CP(*)	
	Direction *x*	Direction *y*	Direction *x*	Direction *y*	Direction *x*	Direction *y*
5 – 6 × 6 – MRF	YES / YES	YES / YES	YES / YES	YES / YES	YES / YES	YES / YES
5 – 8 × 8 – MRF	YES / YES	YES / YES	YES / YES	YES / YES	YES / YES	YES /YES
5 – 6 × 6 – CBF	YES / YES	YES / YES	YES / YES	YES / YES	YES / YES	YES / YES
5 – 8 × 8 – CBF	YES / YES	YES / YES	YES / YES	YES/YES	YES / YES	YES / YES
5 – 6 × 6 – EBF	**NO** / **NO**	**NO** / **NO**	**NO** / **NO**	**NO** / **NO**	YES / YES	YES / YES
5 – 8 × 8 – EBF	**NO** / **NO**	**NO** / **NO**	- / -	- / -	- / -	- / -
10 – 6 × 6 – MRF	YES / **NO**	**NO** / **NO**	YES / YES	YES / **NO**	YES / YES	- / -
10 – 8 × 8 – MRF	**NO** / **NO**	**NO** / **NO**	YES / YES	**NO** / **NO**	YES / YES	- / -
10 – 6 × 6 – CBF	YES / YES	YES / YES	YES / YES	YES / YES	YES / YES	YES / YES
10 – 8 × 8 – CBF	YES / YES	YES / YES	YES / YES	YES / YES	YES / YES	YES / YES
10 – 6 × 6 – EBF	**NO** / -	**NO** / -	- / -	- / -	- / -	- / -
10 – 8 × 8 – EBF	- / **NO**	**NO** / -	- / -	- / -	- / -	- / -
15 – 6 × 6 – MRF	**NO** / **NO**	**NO** / **NO**	YES / YES	**NO** / **NO**	YES / -	- / -
15 – 8 × 8 – MRF	**NO** / **NO**	**NO** / **NO**	**NO** / -	**NO** / -	YES / -	- / -
15 – 6 × 6 – CBF	**NO** / **NO**	**NO** / **NO**	**NO** / **NO**	**NO** / **NO**	YES / YES	YES / YES
15 – 8 × 8 – CBF	YES / YES	YES / YES	YES / YES	YES / YES	YES / YES	YES / YES
15 – 6 × 6 – EBF	**NO** / -	- / -	- / -	- / -	- / -	- / -
15 – 8 × 8 – EBF	**NO** / -	**NO** / -	- / -	- / -	- / -	- / -

(*) First / second values correspond to modal and uniform distributions, respectively

Table 5-8**.** Response reduction factor *R* in the *x* / *y* directions. "Piedemonte B" zone (new microzonation)

Building	Over-strength factor (Ω)(*)		Ductility factor R_d(*)		*R* factor ($R = \Omega R_d$) (*)	
	Direction *x*	Direction *y*	Direction *x*	Direction *y*	Direction *x*	Direction *y*
5 – 6 × 6 – MRF	1.45 / 1.41	1.47 / 1.39	4.77 / 4.34	2.81 / 4.87	6.91 / 6.11	4.14 / 6.77
5 – 8 × 8 – MRF	1.33 / 1.45	1.30 / 1.27	3.53 / 2.68	3.11 / 2.41	4.70 / 3.88	4.05 / 3.05
5 – 6 × 6 – CBF	1.49 / 1.59	1.52 / 1.49	4.69 / 4.38	3.99 / 4.02	7.00 / 6.95	6.05 / 6.00
5 – 8 × 8 – CBF	1.45 / 1.49	1.37 / 1.47	4.14 / 4.38	4.59 / 3.69	6.00 / 6.53	6.29 / 5.42
5 – 6 × 6 – EBF	1.27 / 1.41	1.26 / 1.32	2.44 / 2.61	2.69 / 2.34	3.09 / 3.68	3.40 / 3.08
5 – 8 × 8 – EBF	1.25 / 1.28	1.14 / 1.78	2.30 / 2.21	2.06 / 2.21	2.88 / 2.83	2.37 / 2.54
10 – 6 × 6 – MRF	1.30 / 1.23	1.28 / 1.05	3.06 / 2.07	1.84 / 2.85	3.98 / 2.55	2.36 / 3.00
10 – 8 × 8 – MRF	1.22 / 1.35	1.47 / 1.37	1.75 / 1.92	1.84 / 2.20	2.14 / 2.59	2.71 / 3.02
10 – 6 × 6 – CBF	1.54 / 1.64	1.45 / 1.43	3.32 / 3.07	3.15 / 2.37	5.11 / 5.04	4.57 / 3.38
10 – 8 × 8 – CBF	1.45 / 1.59	1.43 / 1.41	3.24 / 2.97	3.54 / 2.18	4.70 / 4.71	5.05 / 3.07
10 – 6 × 6 – EBF	1.39 / 1.43	1.35 / 1.30	1.80 / 1.78	1.70 / 1.60	2.50 / 2.54	2.31 / 2.08
10 – 8 × 8 – EBF	1.28 / 1.32	1.27 / 1.12	1.82 / 1.94	2.29 / 2.02	2.33 / 2.55	2.90 / 2.27
15 – 6 × 6 – MRF	1.22 / 1.33	1.33 / 1.06	3.96 / 3.76	2.27 / 2.48	4.83 / 2.16	3.03 / 2.64
15 – 8 × 8 – MRF	1.39 / 1.30	1.25 / 1.33	2.16 / 1.44	2.06 / 1.37	3.00 / 1.87	2.57 / 1.83
15 – 6 × 6 – CBF	1.54 / 1.59	1.49 / 1.43	4.34 / 3.95	3.56 / 4.07	6.67 / 6.27	5.31 / 5.81
15 – 8 × 8 – CBF	1.39 / 1.52	1.43 / 1.49	4.56 / 4.03	4.55 / 4.55	6.33 / 6.11	6.50 / 6.79
15 – 6 × 6 – EBF	1.30 / 1.30	1.28 / 1.39	1.96 / 2.11	1.56 / 1.56	2.55 / 2.75	2.00 / 2.17
15 – 8 × 8 – EBF	1.19 / 1.27	1.39 / 1.25	2.26 / 1.36	1.96 / 1.58	2.70 / 1.72	2.73 / 1.97

(*) First / second values correspond to modal and uniform distributions, respectively

Comparison among the values of *R* in Table 5-8 with the assumed factors in Table 4-24 shows that, in 63% of the cases, the analyzed buildings do not possess the required ductility. In the MRF/CBF/EBF buildings, such percentage is 79/8/100%. In the 5/10/15-story buildings such

percentage is 50/75/63%. For the Modal/Uniform distributions, the percentages are 58/67%. No relevant differences have been observed for *x/y* directions.

5.3.6 "Piedemonte-C" Zone (new microzonation)

Figure 5-39, Figure 5-42 and Figure 5-45 display the capacity curves of the prototype buildings (Table 4-1) designed for the "Piedemonte-C" Zone (new microzonation, Figure 3-7); Figure 5-39, Figure 5-42 and Figure 5-45 refer to the MRF, CBF and EBF buildings, respectively.

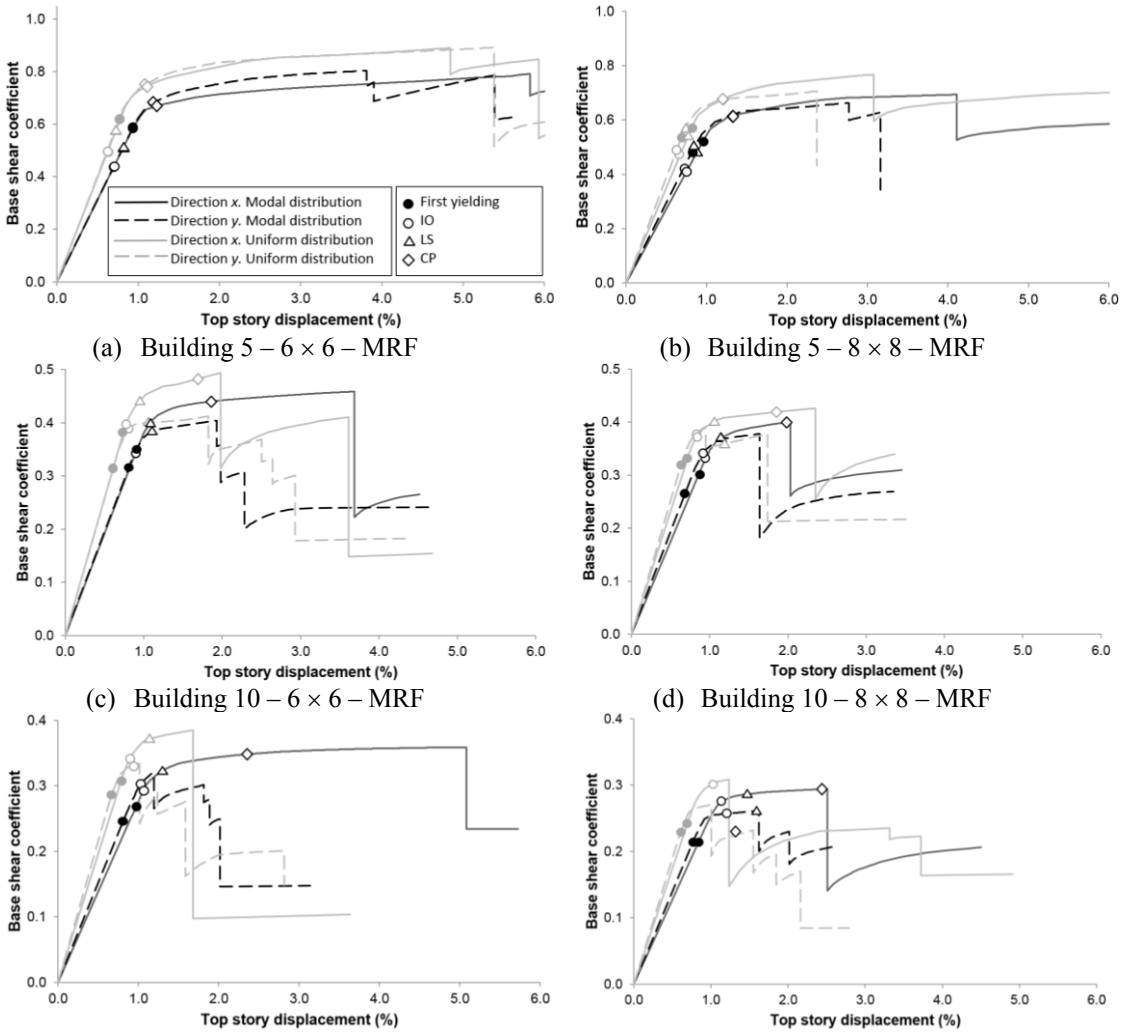

(a) Building 5 – 6 × 6 – MRF (b) Building 5 – 8 × 8 – MRF

(c) Building 10 – 6 × 6 – MRF (d) Building 10 – 8 × 8 – MRF

(e) Building 15 – 6 × 6 – MRF (f) Building 15 – 8 × 8 – MRF

Figure 5-39. Capacity curves and Target Drifts of buildings with Moment-Resisting Frames. Zone "Piedemonte-C" (new microzonation, Figure 3-7)

Most of the results in Figure 5-39 are regular and expected; subsection 5.3.12 holds deeper conclusions issued globally for all the cases. However, Figure 5-39.c shows that, for the 10 – 6 × 6 – MRF prototype building (Table 4-1) in *x* direction, the push-over analysis under modal force distribution predicts less initial stiffness, less force strength, and significantly higher displacement ductility than the analysis under constant force distribution. To further investigate this issue, Figure 5-40 and Figure 5-41 display the damage progression of the 10 – 6 × 6 – MRF prototype building in *x* direction designed for the "Piedemonte-C" Zone (new microzonation, Figure 3-7). Figure 5-40 and Figure 5-41 correspond to push-over analyses under modal and uniform force distribution, respectively (Figure 5-1).

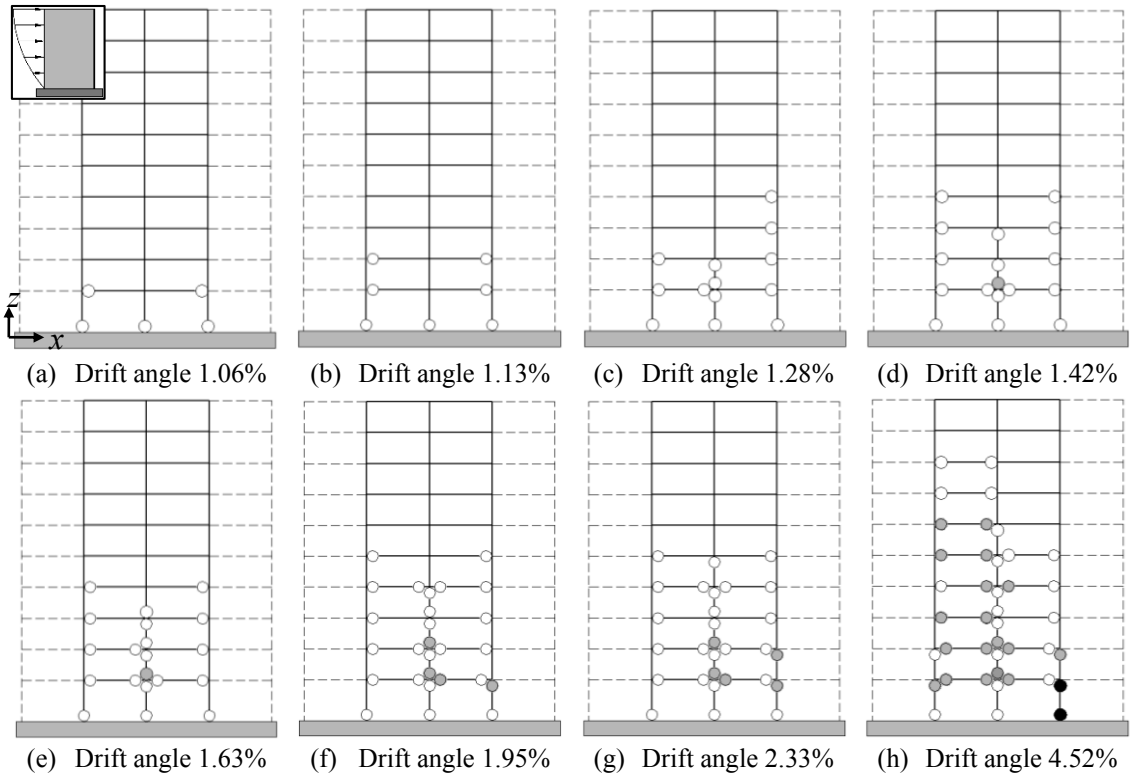

(a) Drift angle 1.06% (b) Drift angle 1.13% (c) Drift angle 1.28% (d) Drift angle 1.42%

(e) Drift angle 1.63% (f) Drift angle 1.95% (g) Drift angle 2.33% (h) Drift angle 4.52%

Figure 5-40. Hinge progression sequence for the 10 – 6 × 6 – MRF building, modal distribution and *x* direction (right displacement). Zone "Piedemonte-C" (new microzonation, Figure 3-7). ○: yielding, ◍: IO, ●: LS, ●: CP [FEMA 356 2000]

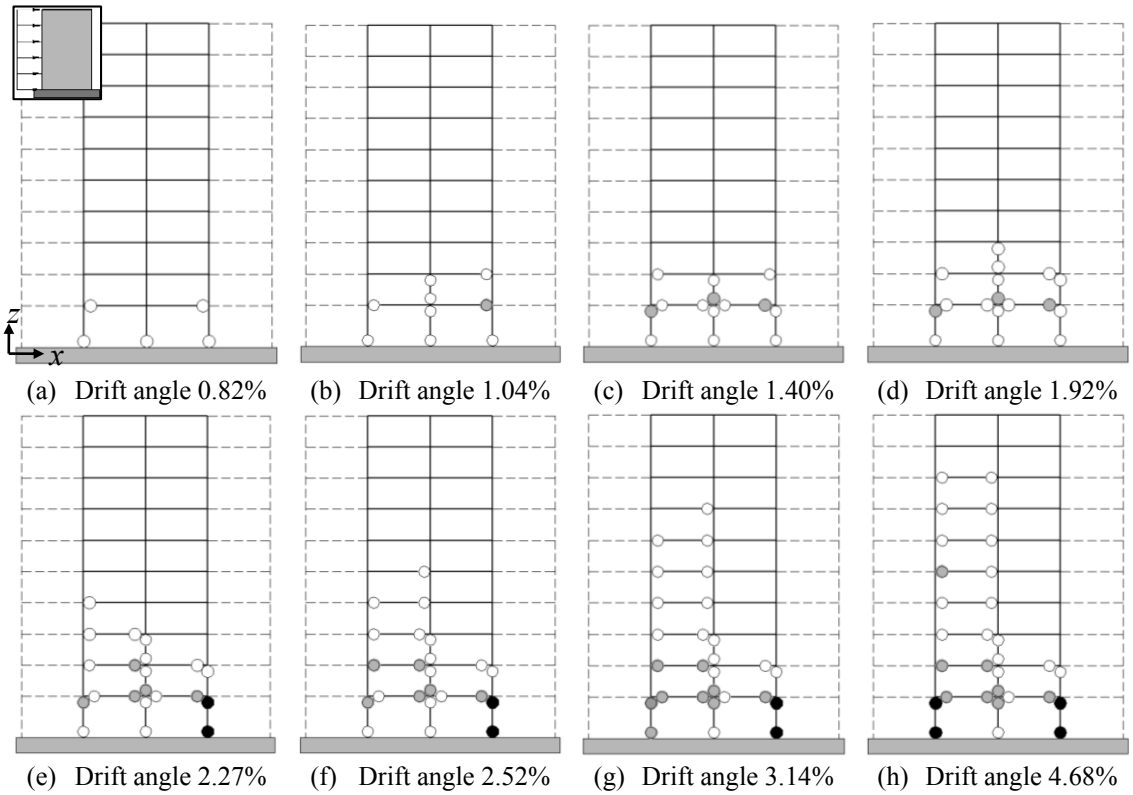

(a) Drift angle 0.82% (b) Drift angle 1.04% (c) Drift angle 1.40% (d) Drift angle 1.92%

(e) Drift angle 2.27% (f) Drift angle 2.52% (g) Drift angle 3.14% (h) Drift angle 4.68%

Figure 5-41. Hinge progression sequence for the 10 – 6 × 6 – MRF building, uniform distribution and *x* direction (right displacement). Zone "Piedemonte-C" (new microzonation, Figure 3-7). ○: yielding, ◍: IO, ●: LS, ●: CP [FEMA 356 2000]

Comparison between Figure 5-40 and Figure 5-41 shows that both under modal and uniform force distribution, the collapse mechanism involves hinges in many levels of the building (up to the eigth level). Nevertheless, for uniform distribution, the hinges concentrate more in the lower levels, mainly in the bottom one. This difference between modal and uniform pushing forces is consistent with the shear forces and bending moments distribution (Figure 5-1).

As previously announced, Figure 5-42 displays the capacity curves of the prototype CBF buildings (Table 4-1) designed for the "Piedemonte C" Zone (new microzonation, Figure 3-7).

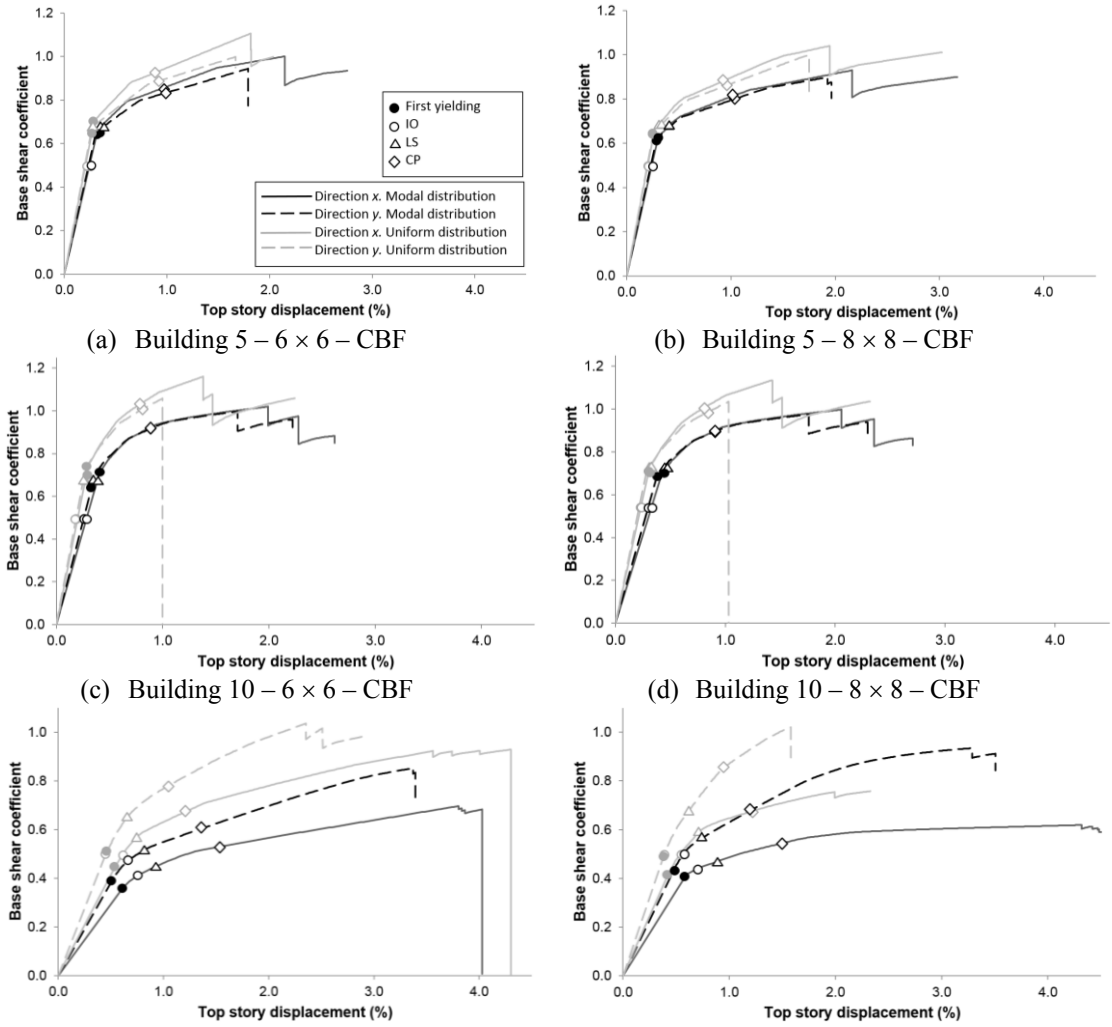

(a) Building 5 – 6 × 6 – CBF (b) Building 5 – 8 × 8 – CBF

(c) Building 10 – 6 × 6 – CBF (d) Building 10 – 8 × 8 – CBF

(e) Building 15 – 6 × 6 – CBF (f) Building 15 – 8 × 8 – CBF

Figure 5-42. Capacity curves and Target Drifts of buildings with Concentric-Braced Frames. Zone "Piedemonte-C" (new microzonation, Figure 3-7)

Most of the results in Figure 5-42 are regular and expected, thus illustrating the reliability and accuracy of the carried out analysis; subsection 5.3.12 holds deeper conclusions that are issued globally for all the cases. However, Figure 5-42.c shows that, for the 10 – 6 × 6 – CBF prototype building (Table 4-1) in *y* direction, the push-over analysis under modal force distribution predicts less initial stiffness and force strength, whereas that analysis predicts higher displacement ductility than the analysis under constant force distribution. To further investigate this issue, Figure 5-43 and Figure 5-44 display the damage progression of the 10 – 6 × 6 – CBF prototype building in *y* direction designed for the "Piedemonte C" Zone (new microzonation, Figure 3-7). Figure 5-43 and Figure 5-44 correspond to push-over analyses under modal and uniform force distribution, respectively (Figure 5-1).

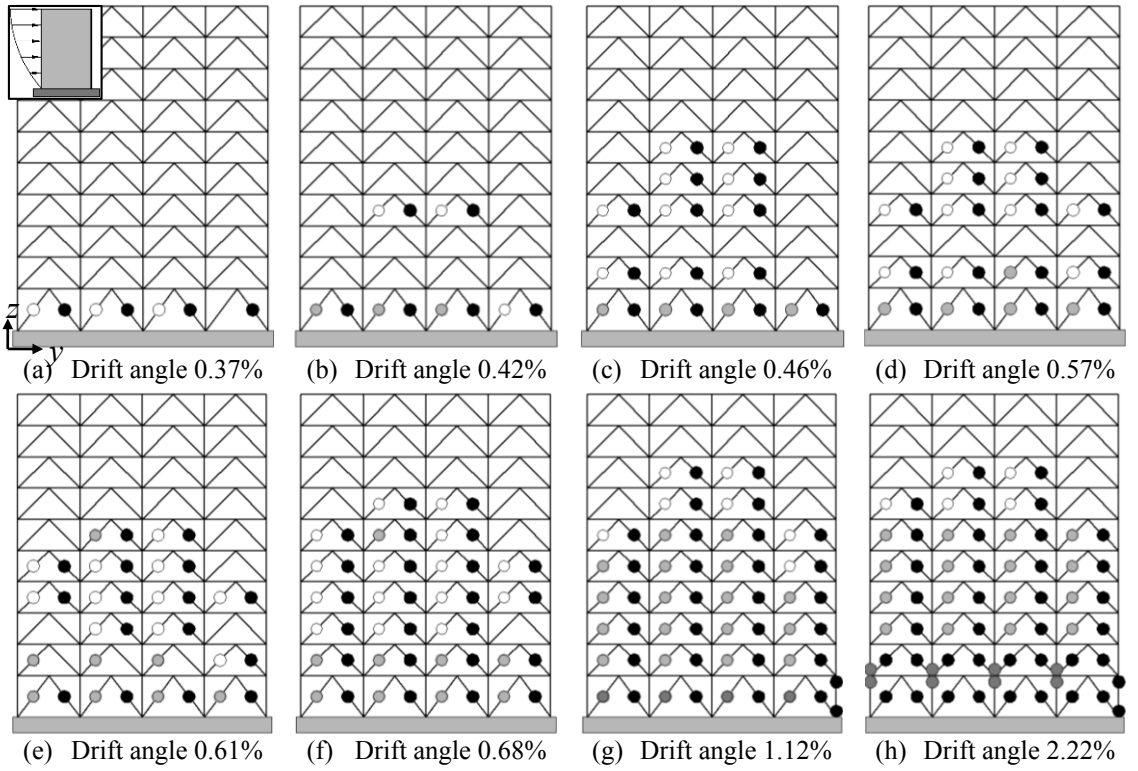

(a) Drift angle 0.37% (b) Drift angle 0.42% (c) Drift angle 0.46% (d) Drift angle 0.57%

(e) Drift angle 0.61% (f) Drift angle 0.68% (g) Drift angle 1.12% (h) Drift angle 2.22%

Figure 5-43. Hinge progression sequence for the 10 – 6 × 6 – CBF building, modal distribution and *y* direction (right displacement). Zone "Piedemonte-C" (new microzonation, Figure 3-7). ○: yielding, ◍: IO, ◉: LS, ●: CP [FEMA 356 2000]

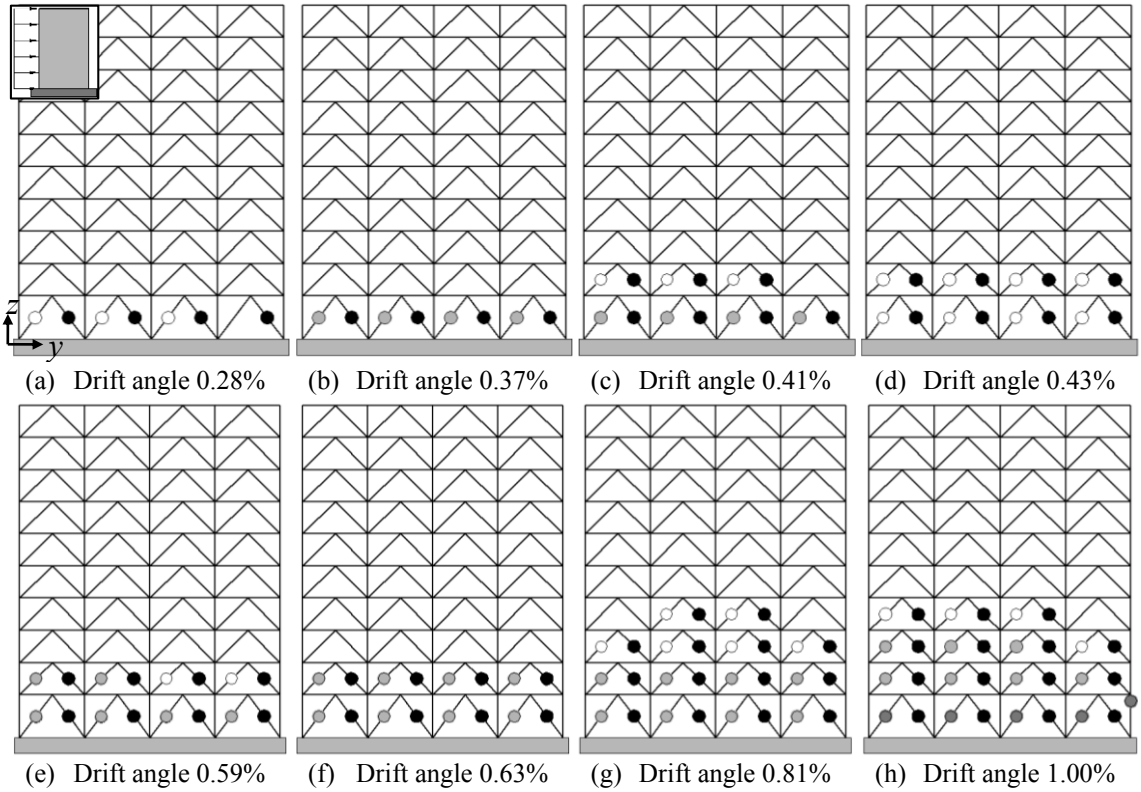

(a) Drift angle 0.28% (b) Drift angle 0.37% (c) Drift angle 0.41% (d) Drift angle 0.43%

(e) Drift angle 0.59% (f) Drift angle 0.63% (g) Drift angle 0.81% (h) Drift angle 1.00%

Figure 5-44. Hinge progression sequence for the 10 – 6 × 6 – CBF building, uniform distribution and *y* direction (right displacement). Zone "Piedemonte-C" (new microzonation, Figure 3-7). ○: yielding, ◍: IO, ◉: LS, ●: CP [FEMA 356 2000]

Comparison between Figure 5-43 and Figure 5-44 shows that, under modal force distribution (Figure 5-43), the collapse mechanism involves hinges in virtually all levels of the building (even in the top one), while for uniform distribution (Figure 5-44) the hinges concentrate in the four lowest levels. This difference between modal and uniform pushing forces is consistent with the corresponding distribution laws of shear forces and bending moments along the height of the building (Figure 5-1).

As previously announced, Figure 5-45 displays the capacity curves of the prototype EBF buildings (Table 4-1) designed for the "Piedemonte C" Zone (new microzonation, Figure 3-7).

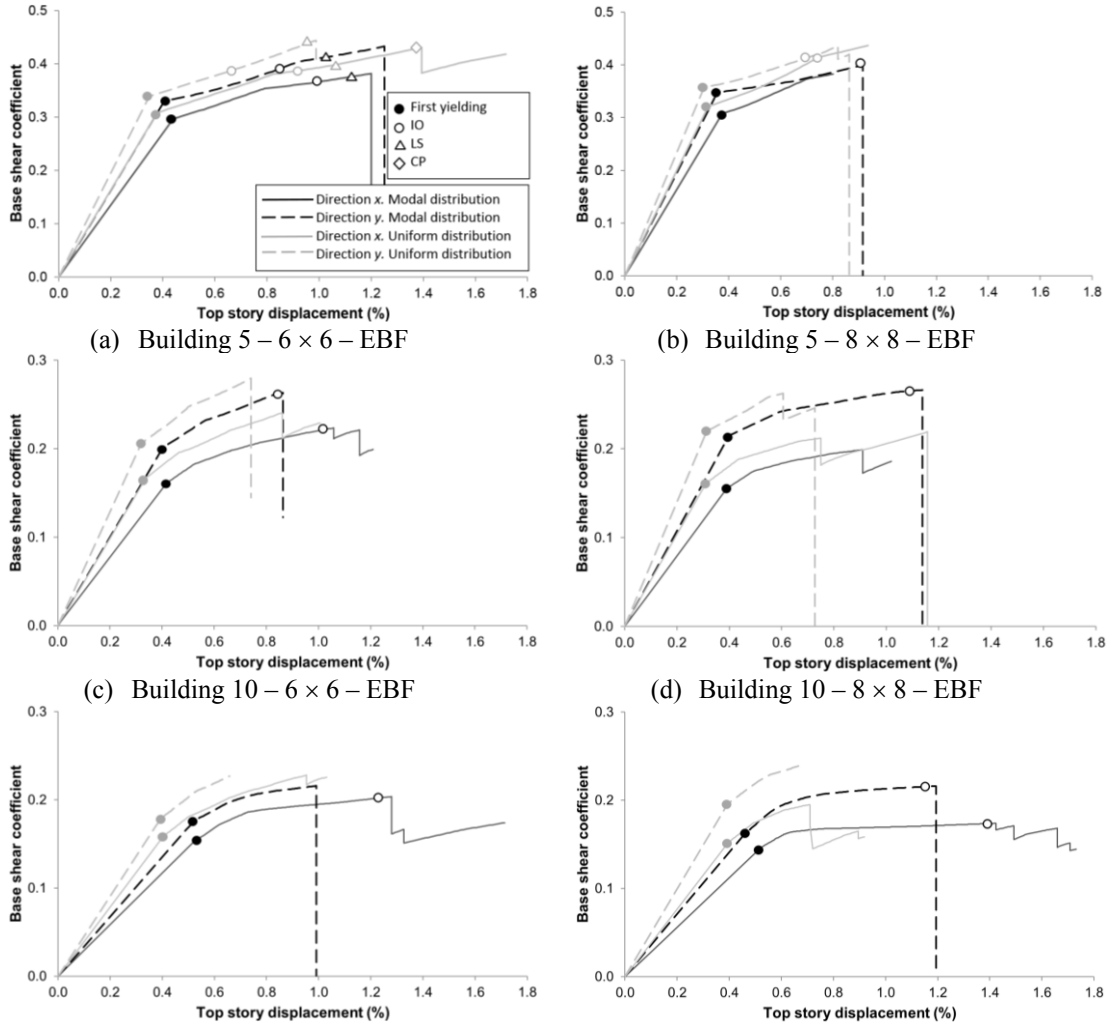

(a) Building 5 – 6 × 6 – EBF (b) Building 5 – 8 × 8 – EBF

(c) Building 10 – 6 × 6 – EBF (d) Building 10 – 8 × 8 – EBF

(e) Building 15 – 6 × 6 – EBF (f) Building 15 – 8 × 8 – EBF

Figure 5-45. Capacity curves and Target Drifts of buildings with Eccentric-Braced Frames. Zone "Piedemonte-C" (new microzonation, Figure 3-7)

Most of the results in Figure 5-45 are regular and expected; subsection 5.3.12 holds deeper conclusions issued globally for all the cases. However, Figure 5-45.b shows that, for the 5 – 8 × 8 – EBF prototype building (Table 4-1) in *y* direction, the push-over analysis under modal force distribution predicts less initial stiffness and force strength, whereas that analysis predicts a slightly higher displacement ductility than the analysis under constant force distribution. To further investigate this issue, Figure 5-46 and Figure 5-47 display the damage progression of the 5 – 8 × 8 – EBF prototype building in *y* direction designed for the "Piedemonte B" Zone (new microzonation, Figure 3-7). Figure 5-46 and Figure 5-47 correspond to push-over analyses under modal and uniform force distribution, respectively (Figure 5-1).

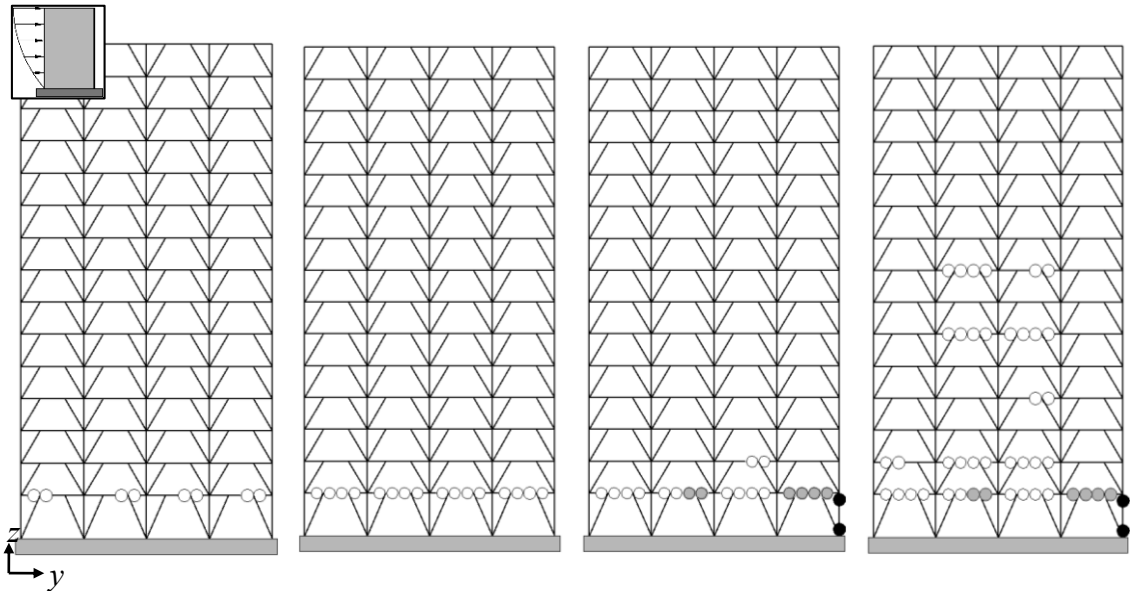

(a) Drift angle 0.52% (b) Drift angle 0.54% (c) Drift angle 0.63% (d) Drift angle 0.65%

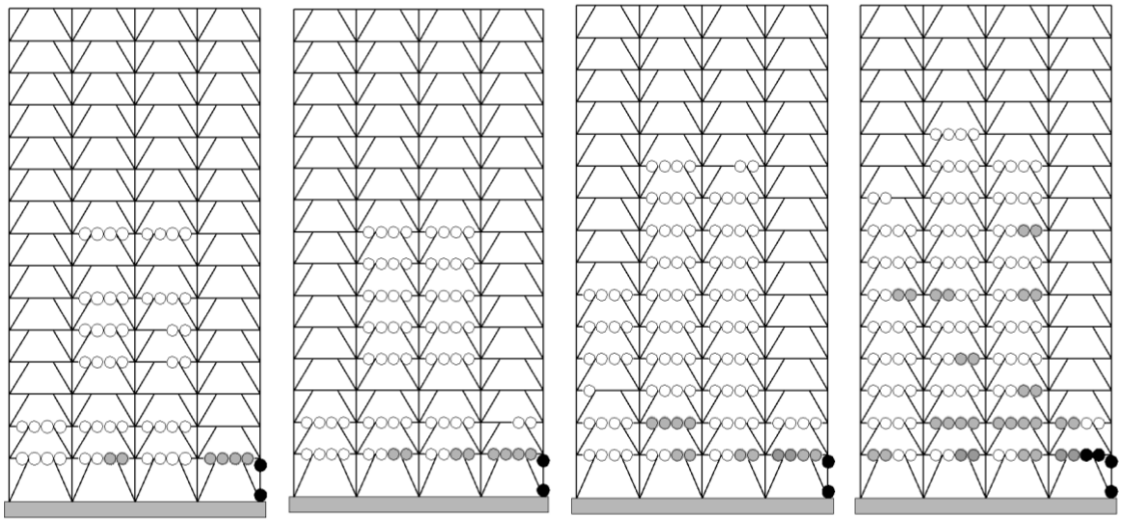

(e) Drift angle 0.67% (f) Drift angle 0.72% (g) Drift angle 0.81% (h) Drift angle 0.99%

Figure 5-46. Hinge progression sequence for the 15 – 6 × 6 – EBF building, modal distribution and *y* direction (right displacement). Zone "Piedemonte-C" (new microzonation, Figure 3-7). ○: yielding, ◎: IO, ◉: LS, ●: CP [FEMA 356 2000]

Figure 5-46 shows that the plastic hinges appear mainly in the link segments of the beams of the lowest levels, as expected. Nevertheless, the right column of the first story experiences early severe damage, since Figure 5-46.c shows that two full plastic hinges develop, thus reducing all the lateral stiffness of this member. This fact can be read again as a lack of fulfillment of the overall principle "strong column-weak beam". As discussed previously, the Colombian seismic design guidelines [NSR-98 1998; NSR-10 2010] do not enforce this verification for medium-seismicity regions, like Bogotá. Noticeably, this type of behavior cannot be observed for uniform distribution of the pushing forces (Figure 5-47).

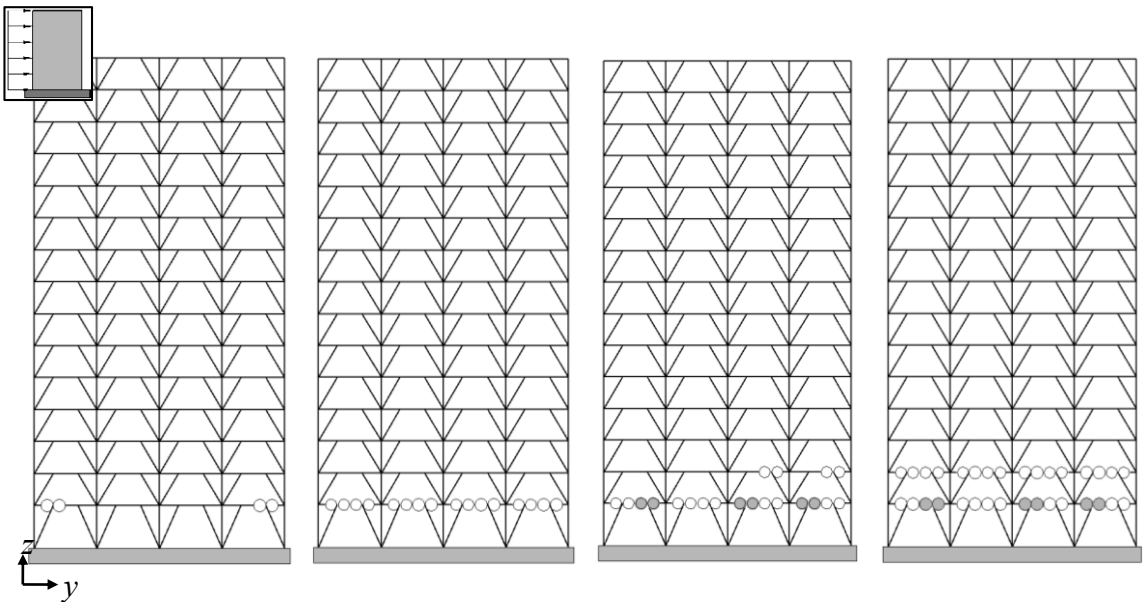

(a) Drift angle 0.38% (b) Drift angle 0.40% (c) Drift angle 0.52% (d) Drift angle 0.54%

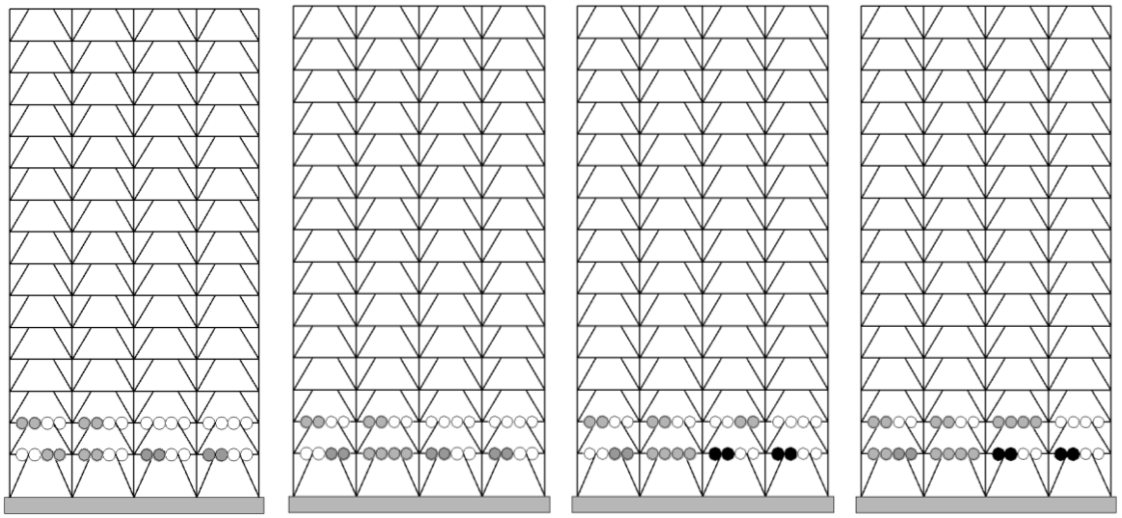

(e) Drift angle 0.58% (f) Drift angle 0.62% (g) Drift angle 0.64% (h) Drift angle 0.66%

Figure 5-47. Hinge progression sequence for the 15 – 6 × 6 – EBF building, uniform distribution and *y* direction (right displacement). Zone "Piedemonte-C" (new microzonation, Figure 3-7). ○: yielding, ◍: IO, ◉: LS, ●: CP [FEMA 356 2000]

Comparison between Figure 5-46 and Figure 5-47 shows that under modal force distribution (Figure 5-46), the collapse mechanism involves hinges up to the eleventh level of the building, although for uniform distribution (Figure 5-47), the hinges concentrate only in the link segments of the two bottom floors. This difference between modal and uniform pushing forces is consistent with the corresponding shear forces and bending moments distribution along the height of the building (Figure 5-1). Figure 5-46.h and Figure 5-47.h show that the collapse mechanism is similar to the one described by Figure 4-8.c; noticeably, the full collapse mechanism would involve (apart from the progression of the hinges in the link segments of the first floor beams) also the development of plastic hinges in columns and braces.

Table 5-9 and Table 5-10 show, respectively, the seismic performance and the response reduction factor (R, Ω and R_d) of the prototype buildings (Table 4-1) designed for the "Piedemonte C" Zone (new microzonation, Figure 3-7). Table 5-9 reveals that 49% of the cases exhibit a satisfactory performance (YES), 21% unsatisfactory (NO) and 30% highly unsatisfactory (-). In the

MRF/CBF/EBF buildings, such percentages are 54/29/17%, 92/8/25% and 17/0/74%. In the 5/10/15-story buildings such percentages are 68/48/31%, 17/17/29% and 15/35/40%. For the IO/LS/CP limit states, the percentages are 39/53/57%, 48/14/0% and 13/33/43%. For the Modal/Uniform distributions, the percentages are 51/49%, 24/17% and 25/34%. No relevant differences have been observed for *x/y* directions.

Table 5-9. Seismic performance. "Piedemonte C" zone (new microzonation)

Building	Target Drift IO(*)		Target Drift LS(*)		Target Drift CP(*)	
	Direction *x*	Direction *y*	Direction *x*	Direction *y*	Direction *x*	Direction *y*
5 – 6 × 6 – MRF	YES / YES	YES / YES	YES / YES	YES / YES	YES / YES	YES / YES
5 – 8 × 8 – MRF	YES / YES	YES / YES	YES / YES	YES / YES	YES / YES	YES / YES
5 – 6 × 6 – CBF	YES / YES	YES / YES	YES / YES	YES / YES	YES / YES	YES / YES
5 – 8 × 8 – CBF	YES / YES	YES / YES	YES / YES	YES / YES	YES / YES	YES / YES
5 – 6 × 6 – EBF	**NO** / **NO**	**NO** / **NO**	**NO** / **NO**	**NO** / **NO**	- / YES	- / -
5 – 8 × 8 – EBF	**NO** / **NO**	**NO** / **NO**	- / -	- / -	- / -	- / -
10 – 6 × 6 – MRF	YES / **NO**	**NO** / **NO**	YES / YES	YES / **NO**	YES / YES	- / -
10 – 8 × 8 – MRF	**NO** / **NO**	**NO** / **NO**	YES / YES	**NO** / -	YES / YES	YES / -
10 – 6 × 6 – CBF	YES / YES	YES / YES	YES / YES	YES / YES	YES / YES	YES / YES
10 – 8 × 8 – CBF	YES / YES	YES / YES	YES / YES	YES / YES	YES / YES	YES / YES
10 – 6 × 6 – EBF	**NO** / **-**	**NO** / **-**	- / -	- / -	- / -	- / -
10 – 8 × 8 – EBF	**-** / **-**	**NO** / -	- / -	- / -	- / -	- / -
15 – 6 × 6 – MRF	**NO** / **NO**	**NO** / **NO**	YES / **NO**	**NO** / -	YES / YES	- / -
15 – 8 × 8 – MRF	**NO** / **NO**	**NO** / **NO**	**NO** / -	**NO** / -	YES / -	- / -
15 – 6 × 6 – CBF	**NO** / **NO**	**NO** / YES	YES / YES	YES / YES	YES / YES	YES / YES
15 – 8 × 8 – CBF	**NO** / **NO**	**NO** / YES	YES / YES	YES / YES	YES / YES	YES / YES
15 – 6 × 6 – EBF	**NO** / **-**	**-** / -	- / -	- / -	- / -	- / -
15 – 8 × 8 – EBF	**NO** / **-**	**NO** / **-**	- / -	- / -	- / -	- / -

(*) First / second values correspond to modal and uniform distributions, respectively

Table 5-10**.** Response reduction factor *R* in the *x* / *y* directions. "Piedemonte C" zone (new microzonation)

Building	Over-strength factor (Ω)(*)		Ductility factor R_d(*)		R factor ($R = \Omega R_d$) (*)	
	Direction x	Direction y	Direction x	Direction y	Direction x	Direction y
5 – 6 × 6 – MRF	1.48 / 1.42	1.48 / 1.41	4.55 / 4.34	2.95 / 4.84	6.74 / 6.16	4.37 / 6.82
5 – 8 × 8 – MRF	1.34 / 1.35	1.39 / 1.33	3.22 / 2.75	2.42 / 2.56	4.31 / 3.71	3.37 / 3.41
5 – 6 × 6 – CBF	1.53 / 1.57	1.46 / 1.56	4.18 / 4.10	3.99 / 3.95	6.39 / 6.44	5.82 / 6.16
5 – 8 × 8 – CBF	1.50 / 1.60	1.47 / 1.56	4.85 / 4.97	4.54 / 4.38	7.27 / 7.95	6.67 / 6.84
5 – 6 × 6 – EBF	1.30 / 1.41	1.32 / 1.31	2.12 / 2.65	2.33 / 2.20	2.76 / 3.74	3.08 / 2.88
5 – 8 × 8 – EBF	1.24 / 1.37	1.16 / 1.24	1.74 / 2.18	2.23 / 2.19	2.17 / 2.98	2.59 / 2.72
10 – 6 × 6 – MRF	1.30 / 1.25	1.31 / 1.36	3.08 / 2.08	1.87 / 2.26	4.01 / 2.60	2.45 / 3.08
10 – 8 × 8 – MRF	1.22 / 1.37	1.45 / 1.38	1.75 / 2.53	1.67 / 1.21	2.12 / 3.46	2.42 / 1.67
10 – 6 × 6 – CBF	1.44 / 1.66	1.56 / 1.43	3.38 / 2.77	3.35 / 2.48	4.86 / 4.60	5.22 / 3.54
10 – 8 × 8 – CBF	1.44 / 1.59	1.46 / 1.47	3.28 / 2.79	3.32 / 2.39	4.73 / 4.43	4.85 / 3.52
10 – 6 × 6 – EBF	1.42 / 1.48	1.32 / 1.38	1.79 / 1.78	1.64 / 1.69	2.54 / 2.63	2.17 / 2.33
10 – 8 × 8 – EBF	1.28 / 1.33	1.24 / 1.19	1.83 / 1.82	3.34 / 1.64	2.34 / 2.42	2.90 / 1.95
15 – 6 × 6 – MRF	1.22 / 1.33	1.46 / 1.32	3.88 / 1.71	1.11 / 1.31	4.73 / 2.28	1.63 / 1.73
15 – 8 × 8 – MRF	1.38 / 1.27	1.22 / 1.35	2.14 / 1.39	1.75 / 1.37	2.96 / 1.76	2.14 / 1.85
15 – 6 × 6 – CBF	1.93 / 2.10	2.21 / 2.03	3.23 / 3.85	3.03 / 2.52	6.24 / 8.08	6.70 / 5.12
15 – 8 × 8 – CBF	1.53 / 1.84	2.17 / 2.05	4.90 / 3.01	3.09 / 2.00	7.50 / 5.54	6.71 / 4.10
15 – 6 × 6 – EBF	1.33 / 1.45	1.23 / 1.28	1.81 / 1.64	1.56 / 1.30	2.41 / 2.38	1.92 / 1.67
15 – 8 × 8 – EBF	1.21 / 1.29	1.33 / 1.22	2.55 / 1.40	1.94 / 1.39	3.09 / 1.81	2.58 / 1.70

(*) First / second values correspond to modal and uniform distributions, respectively

Comparison among the values of *R* in Table 5-10 with the assumed factors in Table 4-25 shows that, in 67% of the cases, the analyzed buildings do not possess the required ductility. In the

MRF/CBF/EBF buildings such percentage is 83/17/100%. In the 5/10/15-story buildings such percentage is 54/79/67%. For the Modal/Uniform distributions, the percentages are 61/72%. No relevant differences have been observed for *x/y* directions.

5.3.7 "Lacustre-50" Zone (new microzonation)

Figure 5-48, Figure 5-51 and Figure 5-54 display the capacity curves of the prototype buildings (Table 4-1) designed for the "Lacustre-50" Zone (new microzonation, Figure 3-7); Figure 5-48, Figure 5-51 and Figure 5-54 refer to the MRF, CBF and EBF buildings, respectively.

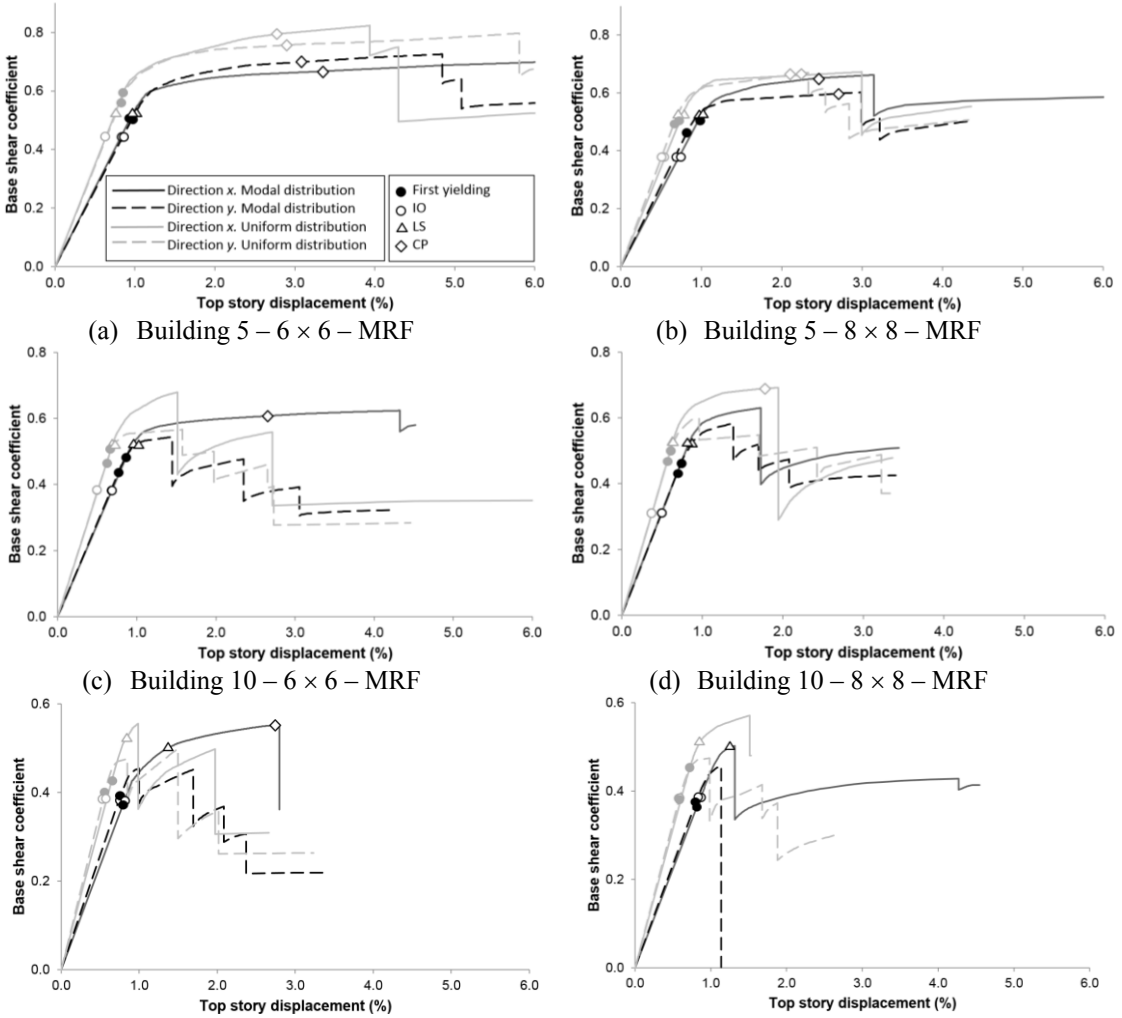

(a) Building 5 – 6 × 6 – MRF (b) Building 5 – 8 × 8 – MRF

(c) Building 10 – 6 × 6 – MRF (d) Building 10 – 8 × 8 – MRF

(e) Building 15 – 6 × 6 – MRF (f) Building 15 – 8 × 8 – MRF

Figure 5-48. Capacity curves and Target Drifts of buildings with Moment-Resisting Frames. Zone "Lacustre-50" (new microzonation, Figure 3-7)

Most of the results in Figure 5-48 are regular and expected; subsection 5.3.12 holds deeper conclusions issued globally for all the cases. However, Figure 5-48.f shows that, for the 15 – 8 × 8 – MRF prototype building (Table 4-1) in *x* direction, the push-over analysis under modal force distribution predicts less initial stiffness, less force strength, and significantly higher displacement ductility than the analysis under constant force distribution. To further investigate this issue, Figure 5-49 and Figure 5-50 display the damage progression of the 15 – 8 × 8 – MRF prototype building in *x* direction designed for the "Lacustre-50" Zone (new microzonation, Figure 3-7). Figure 5-49 and Figure 5-50 correspond to push-over analyses under modal and uniform force distribution, respectively (Figure 5-1).

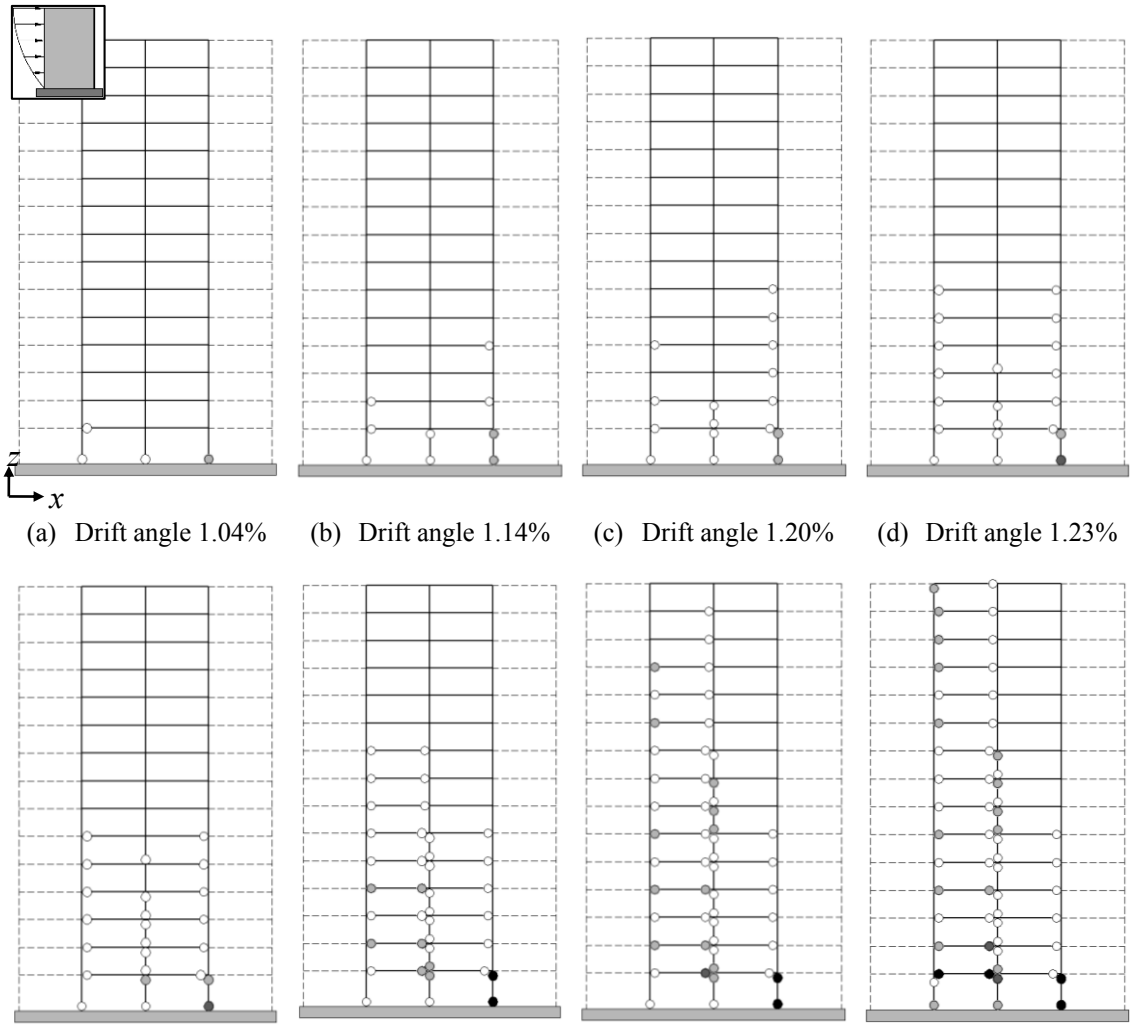

(a) Drift angle 1.04% (b) Drift angle 1.14% (c) Drift angle 1.20% (d) Drift angle 1.23%

(e) Drift angle 1.30% (f) Drift angle 1.94% (g) Drift angle 3.06% (h) Drift angle 4.55%

Figure 5-49. Hinge progression sequence for the 15 – 8 × 8 – MRF building, modal distribution and *x* direction (right displacement). Zone "Lacustre-50" (new microzonation, Figure 3-7). ○: yielding, ○: IO, ●: LS, ●: CP [FEMA 356 2000]

In Figure 5-49, each frame has two seismic bays (see Figure 4-3). Figure 5-49 represents the damage, in terms of the progression of plastic hinges at the ends of beams and columns, for eight selected states corresponding to growing values of the drift angle. These values of the drift displacement have been chosen to highlight a number of characteristic points of the corresponding capacity curve (Figure 5-48.f), namely: onset of yielding (Figure 5-49.a), sudden drop (Figure 5-49.e) and near collapse (Figure 5-49.h). Figure 5-49.h shows that the collapse mechanism involves all the floors although it is mainly concentrated in the first floor columns. A more detailed observation of Figure 5-49 shows that, after the development of two full plastic hinges in the right column of the first floor (Figure 5-49.f), the demands concentrate almost exclusively in the left seismic bay.

As in Figure 5-50 each frame has two seismic bays. The growing values of the drift displacement have been chosen to highlight a number of characteristic points of the corresponding capacity curve (Figure 5-48.f), namely: onset of yielding (Figure 5-50.a) and near collapse (Figure 5-50.h).

Figure 5-50.h shows that the collapse mechanism involves the four bottom floors being mainly concentrated in the first floor columns.

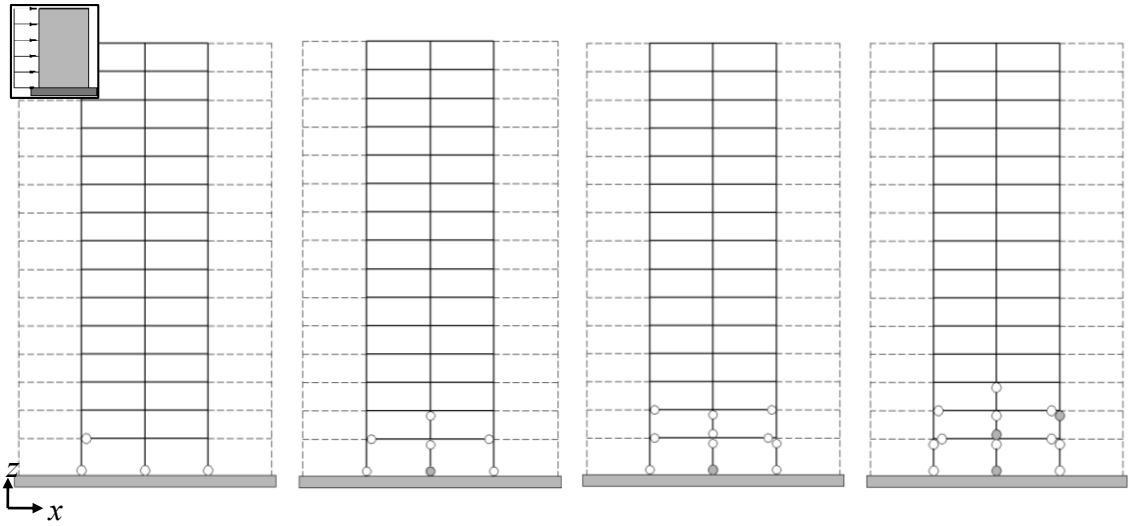

(a) Drift angle 0.79% (b) Drift angle 0.88% (c) Drift angle 0.95% (d) Drift angle 1.18%

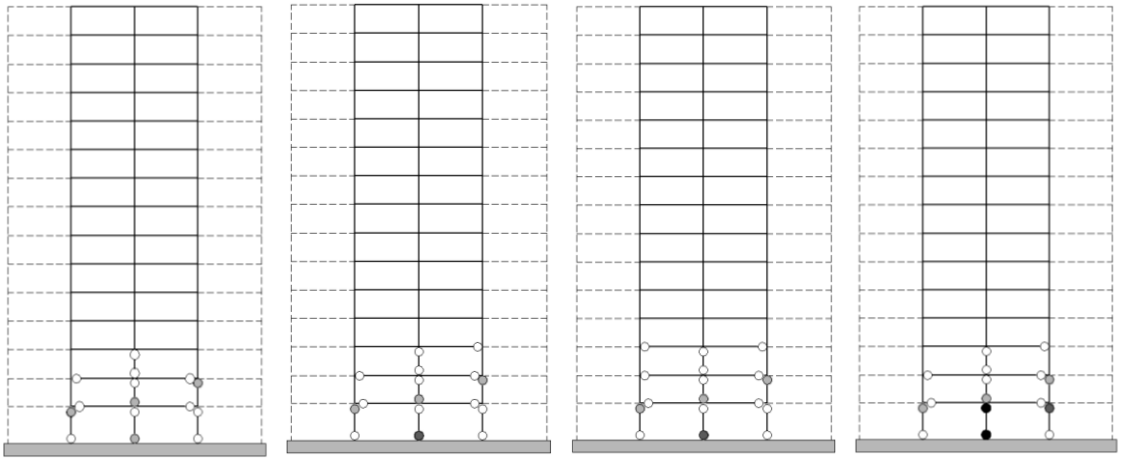

(e) Drift angle 1.24% (f) Drift angle 1.32% (g) Drift angle 1.37% (h) Drift angle 1.53%

Figure 5-50. Hinge progression sequence for the 15 – 8 × 8 – MRF building, uniform distribution and *x* direction (right displacement). Zone "Lacustre-50" (new microzonation, Figure 3-7). ○: yielding, ◎: IO, ◉: LS, ●: CP [FEMA 356 2000]

Comparison between Figure 5-49 and Figure 5-50 shows that the collapse mechanisms for modal and uniform force distribution (Figure 5-49 and Figure 5-50, respectively) are completely different: the mechanism for modal distribution is highly ductile, involving all the levels of the building, while the mechanism for uniform distribution is highly brittle, affecting only the three lowest floors and being concentrated in the first story columns (soft-story mechanism). This difference between modal and uniform pushing forces is consistent with the shear forces and bending moments distribution (Figure 5-1).

As previously announced, Figure 5-51 displays the capacity curves of the prototype CBF buildings (Table 4-1) designed for the "Lacustre-50" Zone (new microzonation, Figure 3-7).

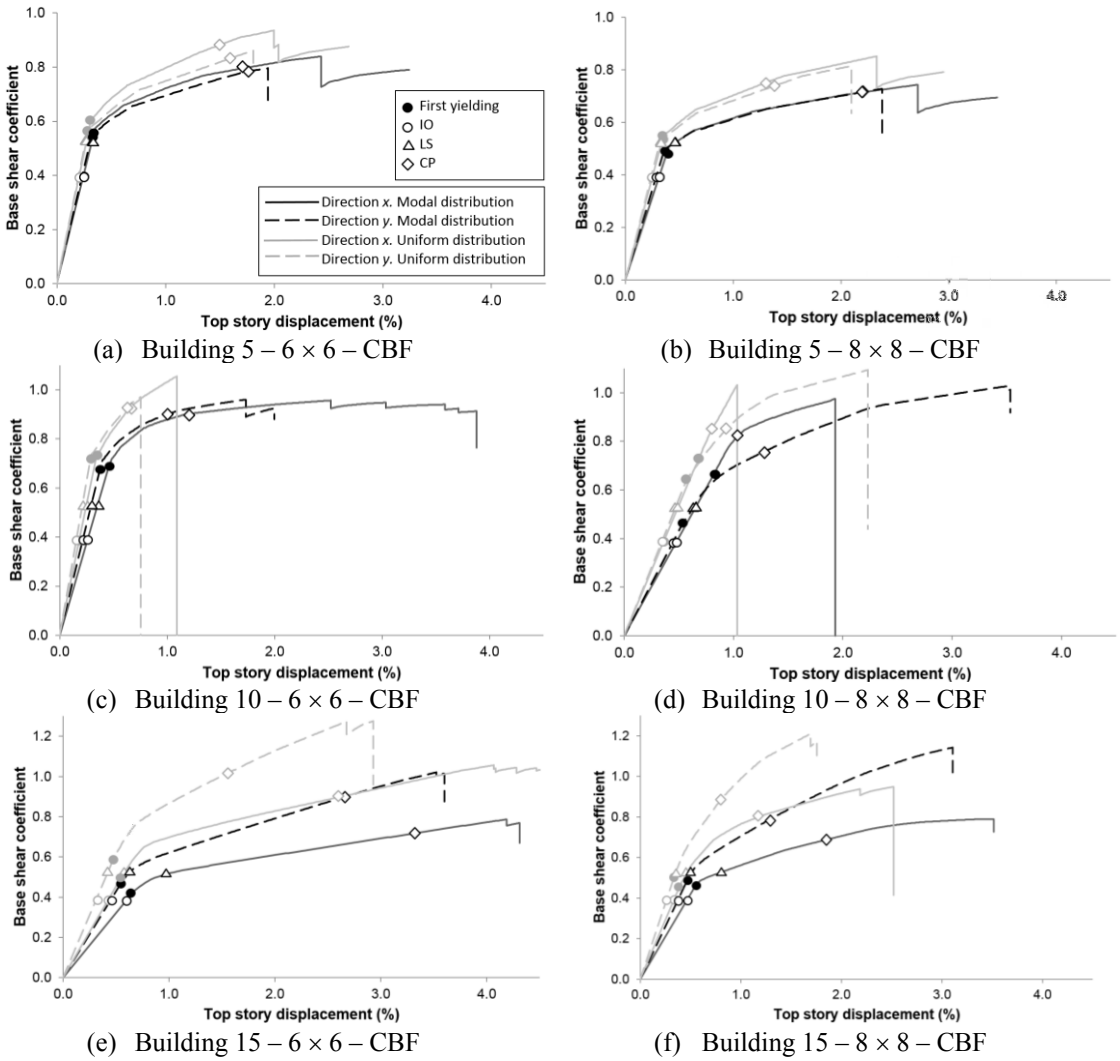

(a) Building 5 – 6 × 6 – CBF

(b) Building 5 – 8 × 8 – CBF

(c) Building 10 – 6 × 6 – CBF

(d) Building 10 – 8 × 8 – CBF

(e) Building 15 – 6 × 6 – CBF

(f) Building 15 – 8 × 8 – CBF

Figure 5-51. Capacity curves and Target Drifts of buildings with Concentric-Braced Frames. Zone "Lacustre-50" (new microzonation, Figure 3-7)

Most of the results in Figure 5-51 are regular and expected, thus illustrating the reliability and accuracy of the carried out analysis; subsection 5.3.12 holds deeper conclusions that are issued globally for all the cases. However, Figure 5-51.d shows that, for the 10 – 8 × 8 – CBF prototype building (Table 4-1) in *y* direction, the push-over analysis under modal force distribution predicts less initial stiffness and slightly less force strength, whereas that analysis also predicts higher displacement ductility than the analysis under constant force distribution. To further investigate this issue, Figure 5-52 and Figure 5-53 display the damage progression of the 10 – 8 × 8 – CBF prototype building in *y* direction designed for the "Lacustre-50" Zone (new microzonation, Figure 3-7). Figure 5-52 and Figure 5-53 correspond to push-over analyses under modal and uniform force distribution, respectively (Figure 5-1).

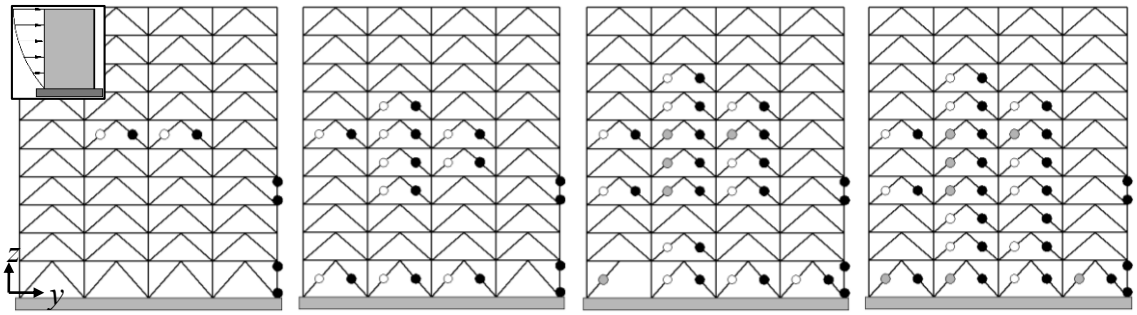

(a) Drift angle 0.42% (b) Drift angle 0.49% (c) Drift angle 0.56% (d) Drift angle 0.58%

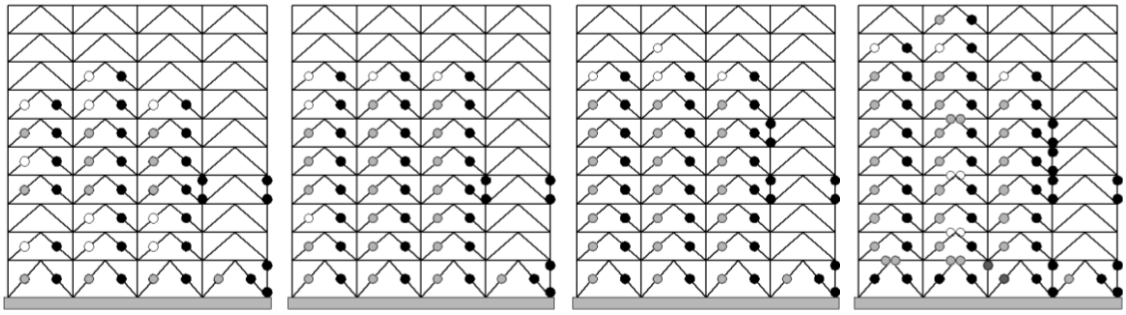

(e) Drift angle 0.64% (f) Drift angle 0.76% (g) Drift angle 1.14% (h) Drift angle 2.14%

Figure 5-52. Hinge progression sequence for the 10 – 8 × 8 – CBF building, modal distribution and *y* direction (right displacement). Zone "Lacustre-50" (new microzonation, Figure 3-7). ○: yielding, ◎: IO, ◉: LS, ●: CP [FEMA 356 2000]

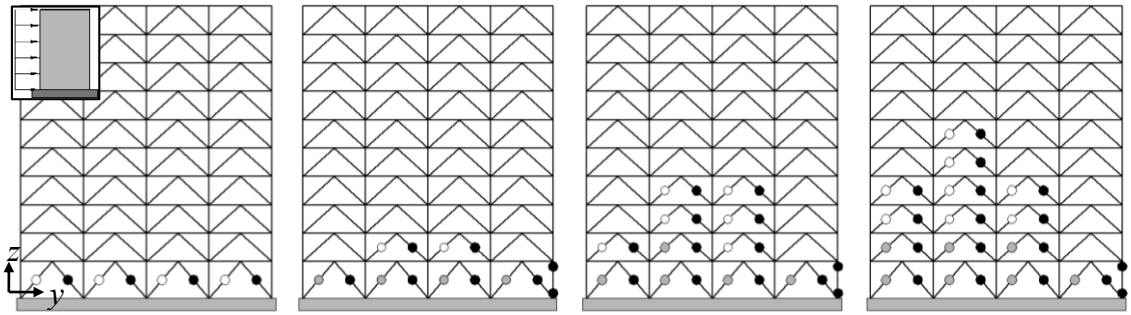

(a) Drift angle 0.32% (b) Drift angle 0.45% (c) Drift angle 0.54% (d) Drift angle 0.59%

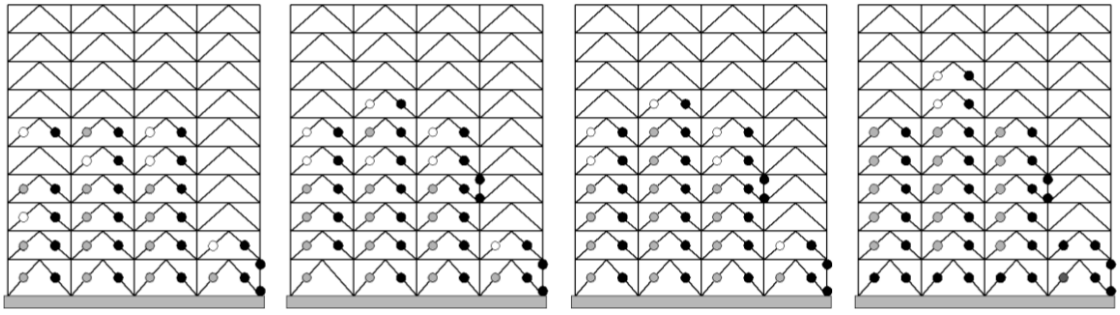

(e) Drift angle 0.69% (f) Drift angle 0.76% (g) Drift angle 0.99% (h) Drift angle 1.24%

Figure 5-53. Hinge progression sequence for the 10 – 8 × 8 – CBF building, uniform distribution and *y* direction (right displacement). Zone "Lacustre-50" (new microzonation, Figure 3-7). ○: yielding, ◎: IO, ◉: LS, ●: CP [FEMA 356 2000]

Comparison between Figure 5-52 and Figure 5-53 shows that, under modal force distribution (Figure 5-52), the collapse mechanism involves hinges in all levels of the building (noticeably, even in the top one), while for uniform distribution (Figure 5-53) the hinges concentrate more in

the lowest levels, although they affect even the eighth story. This difference between modal and uniform pushing forces is consistent with the corresponding distribution laws of shear forces and bending moments along the height of the building (Figure 5-1).

As previously announced, Figure 5-54 displays the capacity curves of the prototype EBF buildings (Table 4-1) designed for the "Lacustre-50" Zone (new microzonation, Figure 3-7).

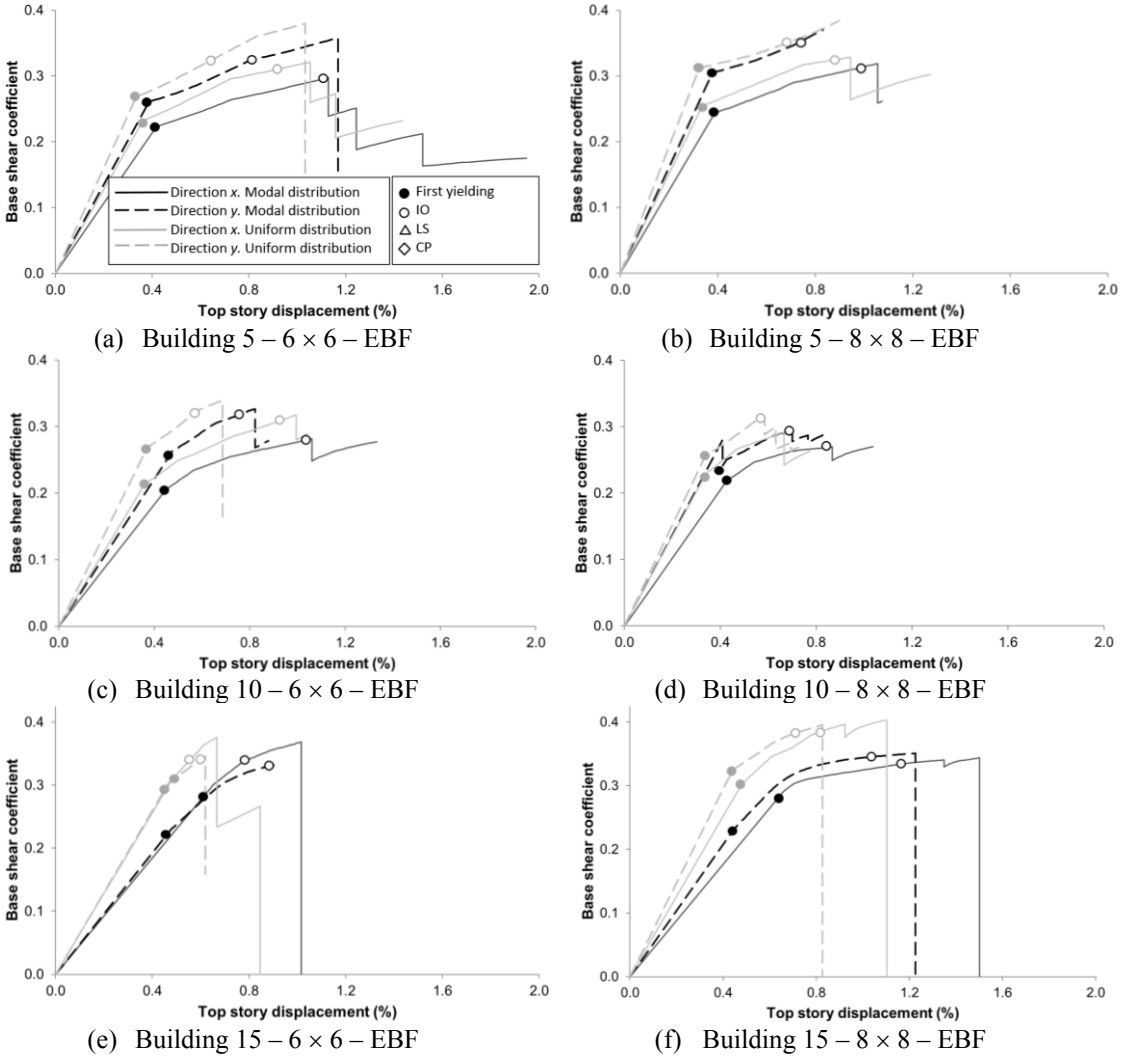

(a) Building 5 – 6 × 6 – EBF (b) Building 5 – 8 × 8 – EBF

(c) Building 10 – 6 × 6 – EBF (d) Building 10 – 8 × 8 – EBF

(e) Building 15 – 6 × 6 – EBF (f) Building 15 – 8 × 8 – EBF

Figure 5-54. Capacity curves and Target Drifts of buildings with Eccentric-Braced Frames. Zone "Lacustre-50" (new microzonation, Figure 3-7)

Most of the results in Figure 5-54 are regular and expected; subsection 5.3.12 holds deeper conclusions issued globally for all the cases. However, Figure 5-54.e shows that, for the 15 – 6 × 6 – EBF prototype building (Table 4-1) in *y* direction, the push-over analysis under modal force distribution predicts less initial stiffness and force strength, whereas that analysis predicts a slightly higher displacement ductility than the analysis under constant force distribution (in fact, both collapse mechanisms are rather brittle). To further investigate this issue, Figure 5-55 and Figure 5-56 display the damage progression of the 15 – 6 × 6 – EBF prototype building in *y* direction designed for the "Lacustre-50" Zone (new microzonation, Figure 3-7). Figure 5-55 and Figure 5-56 correspond to push-over analyses under modal and uniform force distribution, respectively (Figure 5-1).

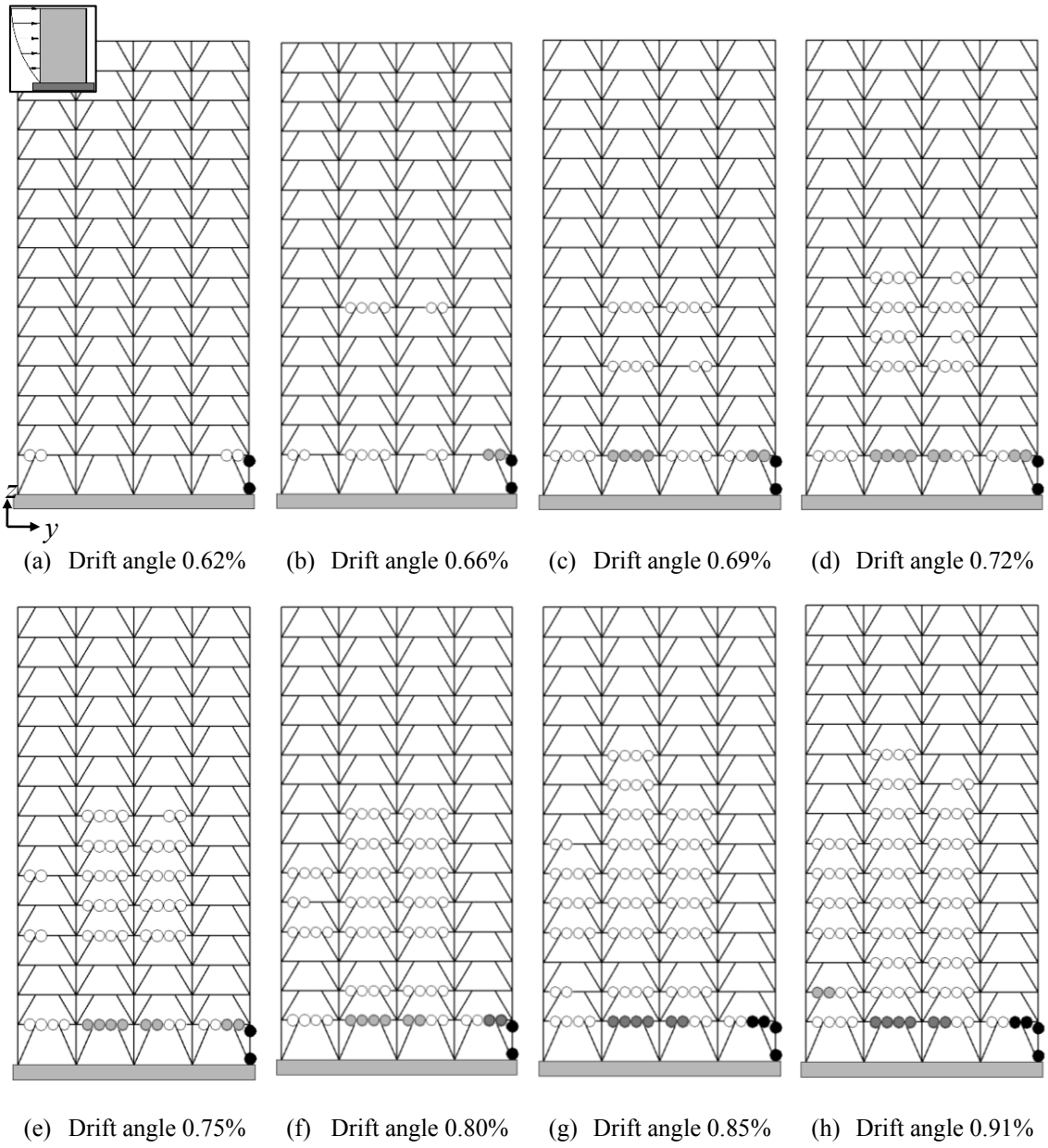

(a) Drift angle 0.62% (b) Drift angle 0.66% (c) Drift angle 0.69% (d) Drift angle 0.72%

(e) Drift angle 0.75% (f) Drift angle 0.80% (g) Drift angle 0.85% (h) Drift angle 0.91%

Figure 5-55. Hinge progression sequence for the 15 – 6 × 6 – EBF building, modal distribution and *y* direction (right displacement). Zone "Lacustre-50" (new microzonation, Figure 3-7). ○: yielding, ○: IO, ●: LS, ●: CP [FEMA 356 2000]

Figure 5-55 shows that the plastic hinges appear mainly in the link segments of the beams of the lowest levels, as expected. Nevertheless, the right column of the first story experiences extremely early severe damage, since Figure 5-55.a shows that two full plastic hinges develop, thus reducing the lateral stiffness of this member. This fact can be read again as a lack of fulfillment of the overall principle "strong column-weak beam". As discussed previously, the Colombian seismic design guidelines [NSR-98 1998; NSR-10 2010] do not enforce this verification for medium-seismicity regions, like Bogotá. Noticeably, this type of behavior cannot be observed for uniform distribution of the pushing forces (Figure 5-56).

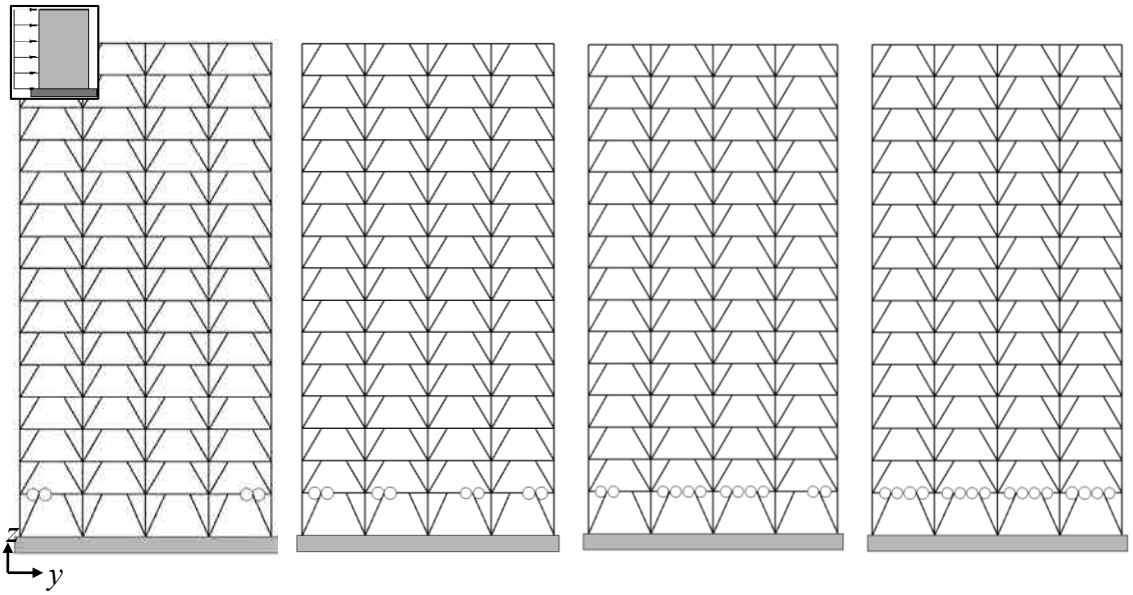

(a) Drift angle 0.45% (b) Drift angle 0.47% (c) Drift angle 0.47% (d) Drift angle 0.48%

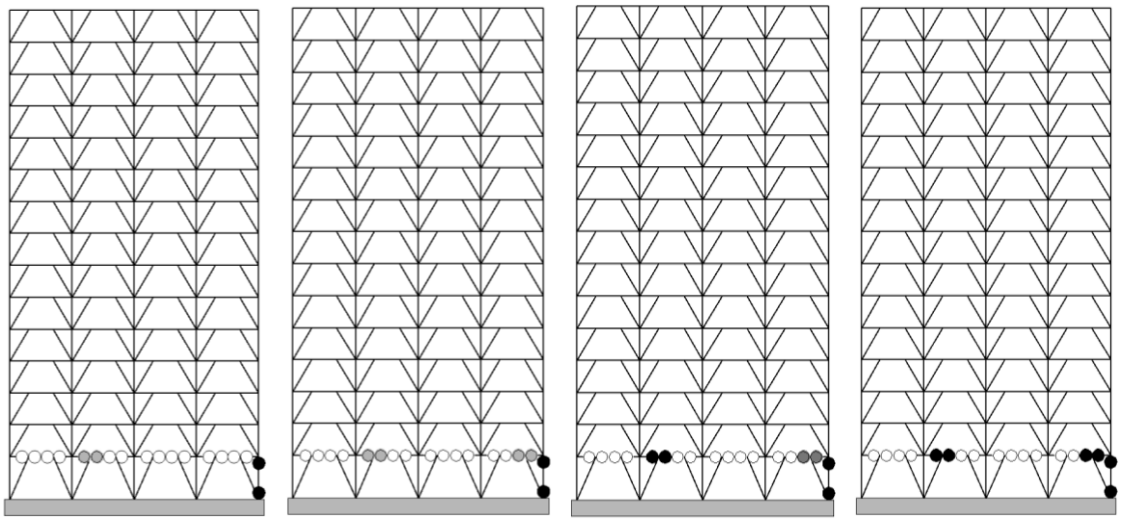

(e) Drift angle 0.50% (f) Drift angle 0.52% (g) Drift angle 0.60% (h) Drift angle 0.62%

Figure 5-56. Hinge progression sequence for the 15 – 6 × 6 – EBF building, uniform distribution and *y* direction (right displacement). Zone "Lacustre-50" (new microzonation, Figure 3-7). ○: yielding, ◎: IO, ●: LS, ●: CP [FEMA 356 2000]

Comparison between Figure 5-55 and Figure 5-56 shows that under modal force distribution (Figure 5-55), the collapse mechanism involves hinges up to the tenth level of the building, although for uniform distribution (Figure 5-56), the hinges concentrate only in the link segments and the right column of the bottom floor. This difference between modal and uniform pushing forces is consistent with the corresponding shear forces and bending moments distribution along the height of the building (Figure 5-1). Figure 5-55.h and Figure 5-56.h show that the collapse mechanism is similar to the one described by Figure 4-8.c; noticeably, the full collapse mechanism would involve (apart from the progression of the hinges in the link segments of the first floor beams) also the development of plastic hinges in columns and braces.

Table 5-11 and Table 5-12 show, respectively, the seismic performance and the response reduction factor (R, Ω and R_d) of the prototype buildings (Table 4-1) designed for the "Lacustre-50" Zone (new microzonation, Figure 3-7).

Table 5-11. Seismic performance. "Lacustre-50" zone (new microzonation)

Building	Target Drift IO(*)		Target Drift LS(*)		Target Drift CP(*)	
	Direction *x*	Direction *y*	Direction *x*	Direction *y*	Direction *x*	Direction *y*
5 – 6 × 6 – MRF	YES / YES	YES / YES	YES / YES	YES / YES	YES / YES	YES / YES
5 – 8 × 8 – MRF	YES / YES	YES / YES	YES / YES	YES / YES	YES / YES	YES / YES
5 – 6 × 6 – CBF	YES / YES	YES / YES	YES / YES	YES / YES	YES / YES	YES / YES
5 – 8 × 8 – CBF	YES / YES	YES / YES	YES / YES	YES / YES	YES / YES	YES / YES
5 – 6 × 6 – EBF	**NO** / **NO**	**NO** / **NO**	- / -	- / -	- / -	- / -
5 – 8 × 8 – EBF	**NO** / **NO**	**NO** / **NO**	- / -	- / -	- / -	- / -
10 – 6 × 6 – MRF	YES / YES	YES / YES	YES / YES	YES / YES	YES / -	- / -
10 – 8 × 8 – MRF	YES / YES	YES / YES	YES / YES	YES / YES	- / YES	- / -
10 – 6 × 6 – CBF	YES / YES	YES / YES	YES / YES	YES / YES	YES / YES	YES / YES
10 – 8 × 8 – CBF	YES / YES	YES / YES	YES / YES	YES / YES	YES / YES	YES / YES
10 – 6 × 6 – EBF	**NO** / **NO**	**NO** / **NO**	- / -	- / -	- / -	- / -
10 – 8 × 8 – EBF	**NO** / **NO**	**NO** / **NO**	- / -	- / -	- / -	- / -
15 – 6 × 6 – MRF	**NO** / YES	YES / YES	**NO** / YES	- / -	YES / -	- / -
15 – 8 × 8 – MRF	**NO** / **NO**	**NO** / **NO**	**NO** / YES	- / -	- / -	- / -
15 – 6 × 6 – CBF	YES / YES	YES / YES	YES / YES	YES / YES	YES / YES	YES / YES
15 – 8 × 8 – CBF	YES / YES	YES / YES	YES / YES	YES / YES	YES / YES	YES / YES
15 – 6 × 6 – EBF	**NO** / **NO**	**NO** / **NO**	- / -	- / -	- / -	- / -
15 – 8 × 8 – EBF	**NO** / **NO**	**NO** / **NO**	- / -	- / -	- / -	- / -

(*) First / second values correspond to modal and uniform distributions, respectively

Table 5-11 reveals that 56% of the cases exhibit a satisfactory performance (YES), 14% unsatisfactory (NO) and 30% highly unsatisfactory (-). In the MRF/CBF/EBF buildings, such percentages are 66/100/0%, 10/0/33% and 24/0/67%. In the 5/10/15-story buildings such percentages are 67/58/42%, 11/11/21% and 22/31/37%. For the IO/LS/CP limit states, the percentages are 60/58/49%, 40/3/0% and 0/39/51%. For the Modal/Uniform distributions, the percentages are 55/56%, 16/13% and 29/31%. No relevant differences have been observed for *x/y* directions.

Table 5-12**.** Response reduction factor R in the x / y directions. "Lacustre-50" zone (new microzonation)

Building	Over-strength factor (Ω)(*)		Ductility factor R_d(*)		*R* factor ($R = \Omega R_d$) (*)	
	Direction *x*	Direction *y*	Direction *x*	Direction *y*	Direction *x*	Direction *y*
5 – 6 × 6 – MRF	1.37 / 1.39	1.45 / 1.43	4.77 / 3.32	3.48 / 4.90	6.53 / 4.62	5.04 / 7.01
5 – 8 × 8 – MRF	1.32 / 1.33	1.30 / 1.35	2.40 / 3.11	2.81 / 2.58	3.17 / 4.13	3.65 / 3.48
5 – 6 × 6 – CBF	1.51 / 1.55	1.46 / 1.53	4.89 / 4.24	4.14 / 4.22	7.39 / 6.57	6.04 / 6.47
5 – 8 × 8 – CBF	1.55 / 1.54	1.48 / 1.51	4.63 / 4.29	4.50 / 4.23	7.17 / 6.60	6.66 / 6.39
5 – 6 × 6 – EBF	1.34 / 1.41	1.38 / 1.42	2.04 / 2.06	2.25 / 2.23	2.73 / 2.90	3.10 / 3.14
5 – 8 × 8 – EBF	1.31 / 1.30	1.21 / 1.24	2.53 / 2.15	1.83 / 2.25	2.31 / 2.79	2.21 / 2.79
10 – 6 × 6 – MRF	1.30 / 1.34	1.26 / 1.23	3.85 / 1.64	1.48 / 2.05	5.00 / 2.20	1.87 / 2.52
10 – 8 × 8 – MRF	1.37 / 1.38	1.26 / 1.19	1.69 / 2.34	1.49 / 1.34	2.31 / 3.23	1.88 / 1.60
10 – 6 × 6 – CBF	1.40 / 1.46	1.42 / 1.35	5.56 / 2.13	3.30 / 1.93	7.79 / 3.11	4.72 / 2.61
10 – 8 × 8 – CBF	1.49 / 1.42	2.21 / 1.71	1.55 / 1.08	2.99 / 2.30	2.31 / 1.53	6.61 / 3.94
10 – 6 × 6 – EBF	1.37 / 1.49	1.27 / 1.27	1.74 / 1.89	1.41 / 1.48	2.39 / 2.78	1.79 / 1.88
10 – 8 × 8 – EBF	1.24 / 1.29	1.18 / 1.22	1.94 / 1.53	1.42 / 1.41	2.43 / 1.98	1.68 / 1.74
15 – 6 × 6 – MRF	1.49 / 1.30	1.17 / 1.18	2.39 / 1.15	1.13 / 1.30	3.56 / 1.50	1.32 / 1.53
15 – 8 × 8 – MRF	1.38 / 1.26	1.21 / 1.22	1.14 / 1.65	1.18 / 1.36	1.58 / 2.08	1.44 / 1.67
15 – 6 × 6 – CBF	1.89 / 2.11	2.15 / 2.17	3.44 / 3.53	3.08 / 2.86	6.51 / 7.45	6.63 / 6.20
15 – 8 × 8 – CBF	1.73 / 2.11	2.39 / 2.36	3.69 / 3.14	2.82 / 2.09	6.39 / 6.63	6.74 / 4.93
15 – 6 × 6 – EBF	1.30 / 1.22	1.49 / 1.17	1.27 / 1.11	1.34 / 1.18	1.65 / 1.35	1.99 / 1.38
15 – 8 × 8 – EBF	1.22 / 1.35	1.54 / 1.22	1.93 / 1.71	1.80 / 1.54	2.36 / 2.31	2.77 / 1.90

(*) First / second values correspond to modal and uniform distributions, respectively

Comparison among the values of *R* in Table 5-12 with the assumed factors in Table 4-26 shows

that, in 67% of the cases, the analyzed buildings do not possess the required ductility. In the MRF/CBF/EBF buildings, such percentage is 79/21/100%. In the 5/10/15-story buildings such percentage is 50/83/67%. For the Modal/Uniform distributions, the percentages are 61/72%. No relevant differences have been observed for *x/y* directions.

5.3.8 "Lacustre-100" Zone (new microzonation)

Figure 5-57, Figure 5-60 and Figure 5-63 display the capacity curves of the prototype buildings (Table 4-1) designed for the "Lacustre-100" Zone (new microzonation, Figure 3-7); Figure 5-57, Figure 5-60 and Figure 5-63 refer to the MRF, CBF and EBF buildings, respectively.

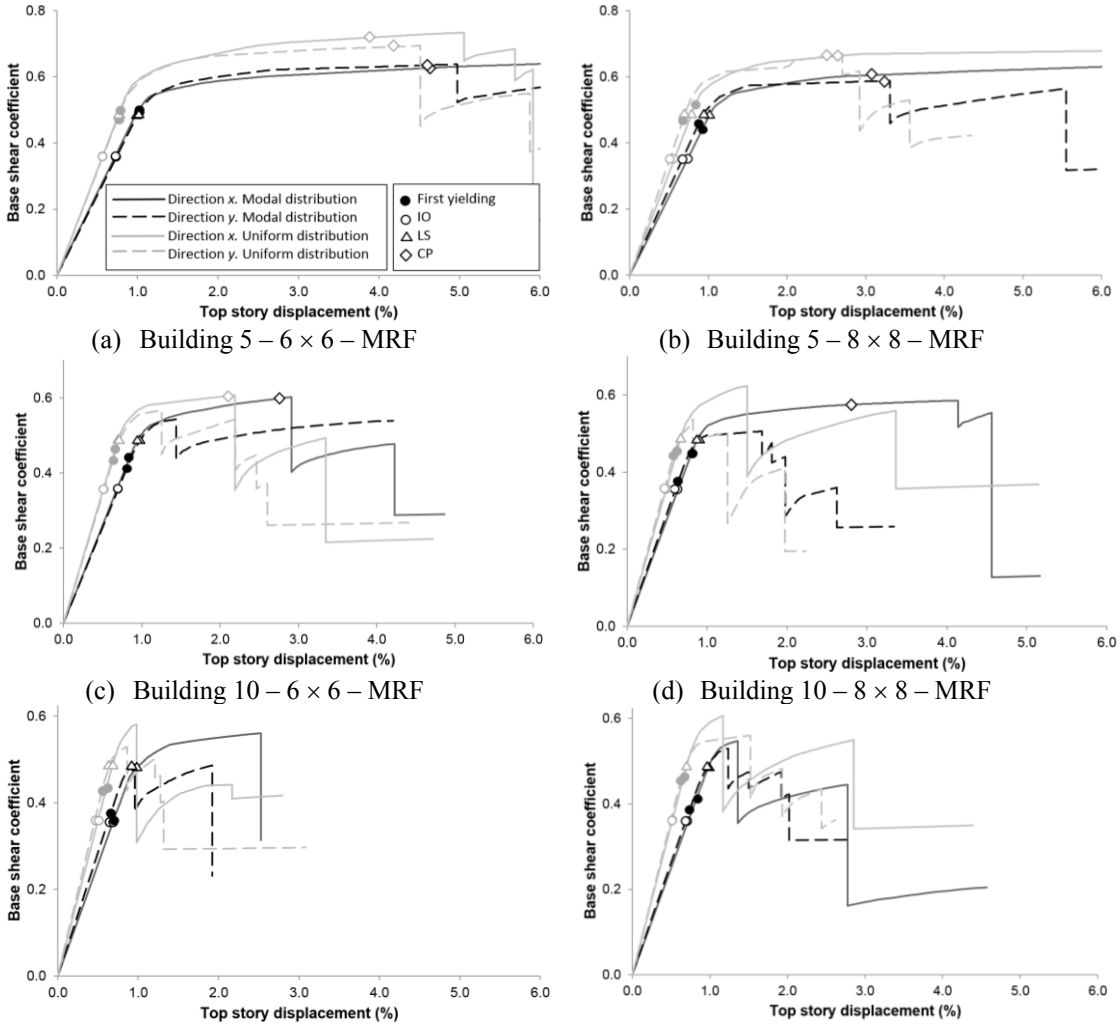

(a) Building 5 – 6 × 6 – MRF (b) Building 5 – 8 × 8 – MRF

(c) Building 10 – 6 × 6 – MRF (d) Building 10 – 8 × 8 – MRF

(e) Building 15 – 6 × 6 – MRF (f) Building 15 – 8 × 8 – MRF

Figure 5-57. Capacity curves and Target Drifts of buildings with Moment-Resisting Frames. Zone "Lacustre-100" (new microzonation, Figure 3-7)

Most of the results in Figure 5-57 are regular and expected; subsection 5.3.12 holds deeper conclusions issued globally for all the cases. Figure 5-57.f shows that, for the 15 – 8 × 8 – MRF prototype building (Table 4-1) in *y* direction, the push-over analysis under modal force distribution predicts less initial stiffness, similar force strength, and similar displacement ductility than the analysis under constant force distribution. To further investigate this issue, Figure 5-58 and Figure 5-59 display the damage progression of the 15 – 8 × 8 – MRF prototype building in *y* direction designed for the "Lacustre-100" Zone (new microzonation, Figure 3-7). Figure 5-58 and Figure 5-59 correspond to push-over analyses under modal and uniform force distribution, respectively (Figure 5-1).

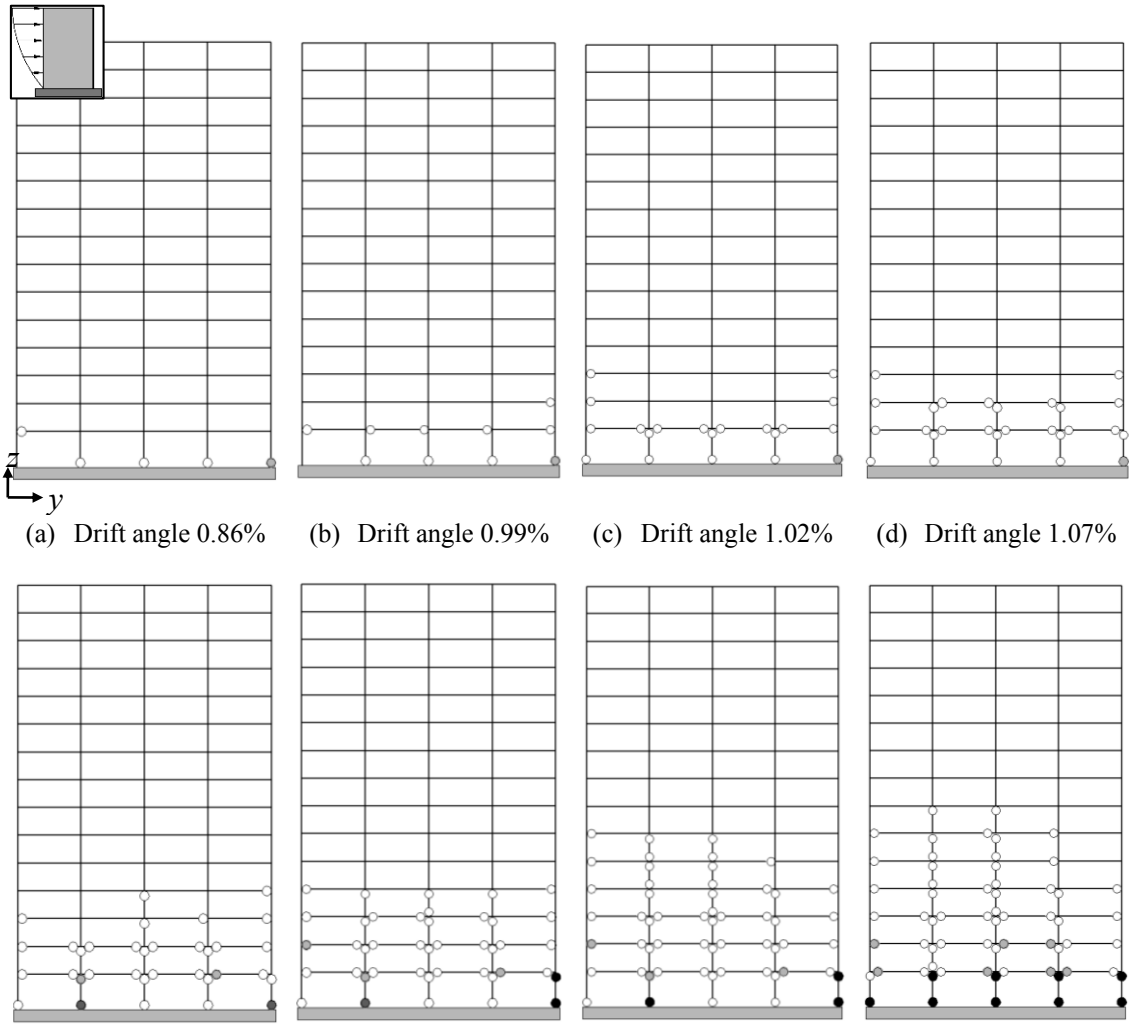

(a) Drift angle 0.86% (b) Drift angle 0.99% (c) Drift angle 1.02% (d) Drift angle 1.07%

(e) Drift angle 1.18% (f) Drift angle 1.24% (g) Drift angle 1.41% (h) Drift angle 2.84%

Figure 5-58. Hinge progression sequence for the 15 – 8 × 8 – MRF building, modal distribution and *y* direction (right displacement). Zone "Lacustre-100" (new microzonation, Figure 3-7). ○: yielding, ◎: IO, ◉: LS, ●: CP [FEMA 356 2000]

In Figure 5-58, each frame has four seismic bays (see Figure 4-3). Figure 5-58 represents the damage, in terms of the progression of plastic hinges at the ends of beams and columns, for eight selected states corresponding to growing values of the drift angle. These values of the drift displacement have been chosen to highlight a number of characteristic points of the corresponding capacity curve (Figure 5-57.f), namely: onset of yielding (Figure 5-58.a), first sudden drop (Figure 5-58.e) and near collapse (Figure 5-58.h). Figure 5-58.h shows that the collapse mechanism involves the seven lowest floors although it is mainly concentrated in the first floor columns.

As in Figure 5-58, in Figure 5-59 each frame has four seismic bays. The growing values of the drift displacement have been chosen to highlight a number of characteristic points of the corresponding capacity curve (Figure 5-57.f), namely: onset of yielding (Figure 5-59.a), first sudden drop (Figure 5-59.d) and near collapse (Figure 5-59.h). Figure 5-59.h shows that the collapse mechanism involves the seven bottom floors being mainly concentrated in the first floor columns.

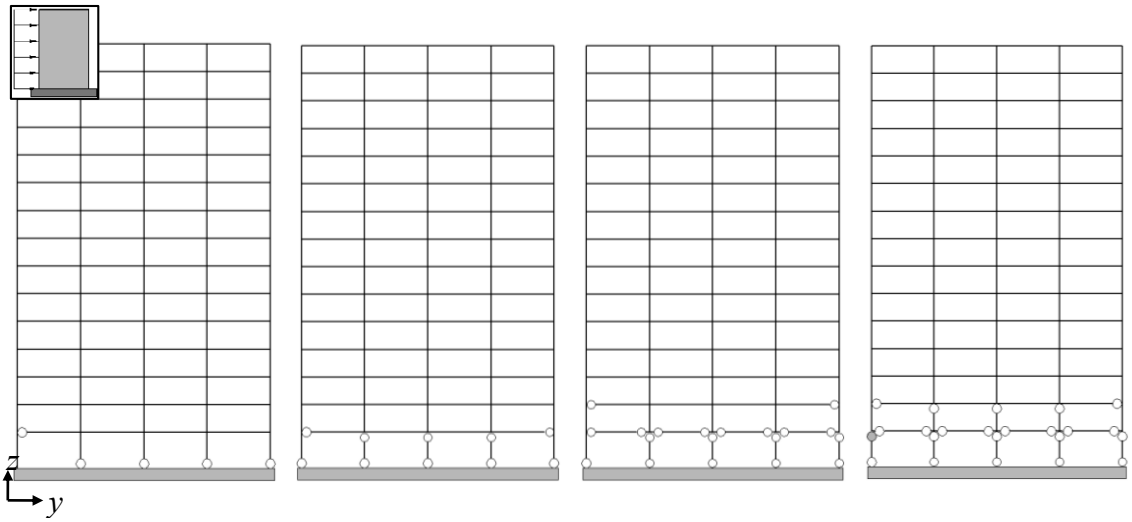

(a) Drift angle 0.65% (b) Drift angle 0.79% (c) Drift angle 0.83% (d) Drift angle 1.20%

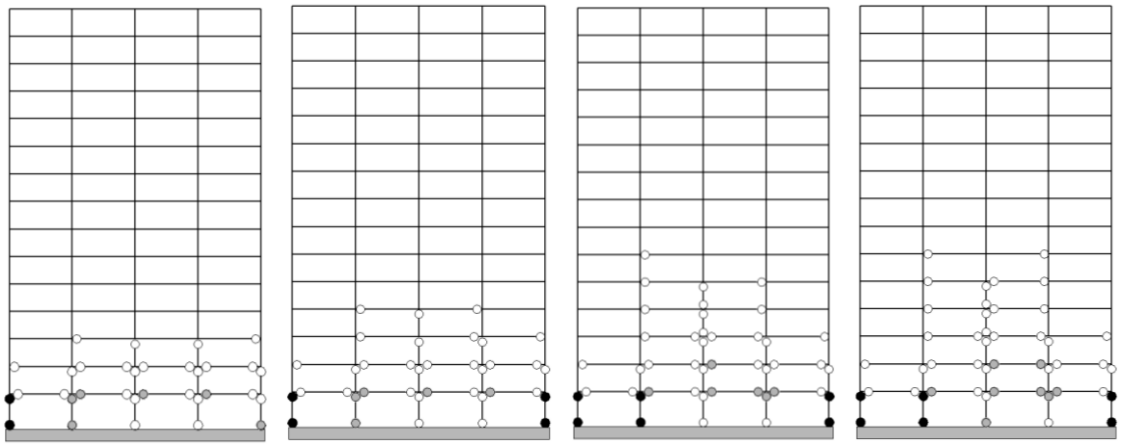

(e) Drift angle 1.84% (f) Drift angle 2.14% (g) Drift angle 2.46% (h) Drift angle 2.62%

Figure 5-59. Hinge progression sequence for the 15 – 8 × 8 – MRF building, uniform distribution and *y* direction (right displacement). Zone "Lacustre-100" (new microzonation, Figure 3-7). ○: yielding, ◎: IO, ◉: LS, ●: CP [FEMA 356 2000]

Comparison between Figure 5-58 and Figure 5-59 shows that the collapse mechanisms for modal and uniform force distribution (Figure 5-58 and Figure 5-59, respectively) are similar, although the mechanism for modal distribution is slightly more ductile. This difference between modal and uniform pushing forces is consistent with the shear forces and bending moments distribution (Figure 5-1).

As previously announced, Figure 5-60 displays the capacity curves of the prototype CBF buildings (Table 4-1) designed for the "Lacustre-100" Zone (new microzonation, Figure 3-7).

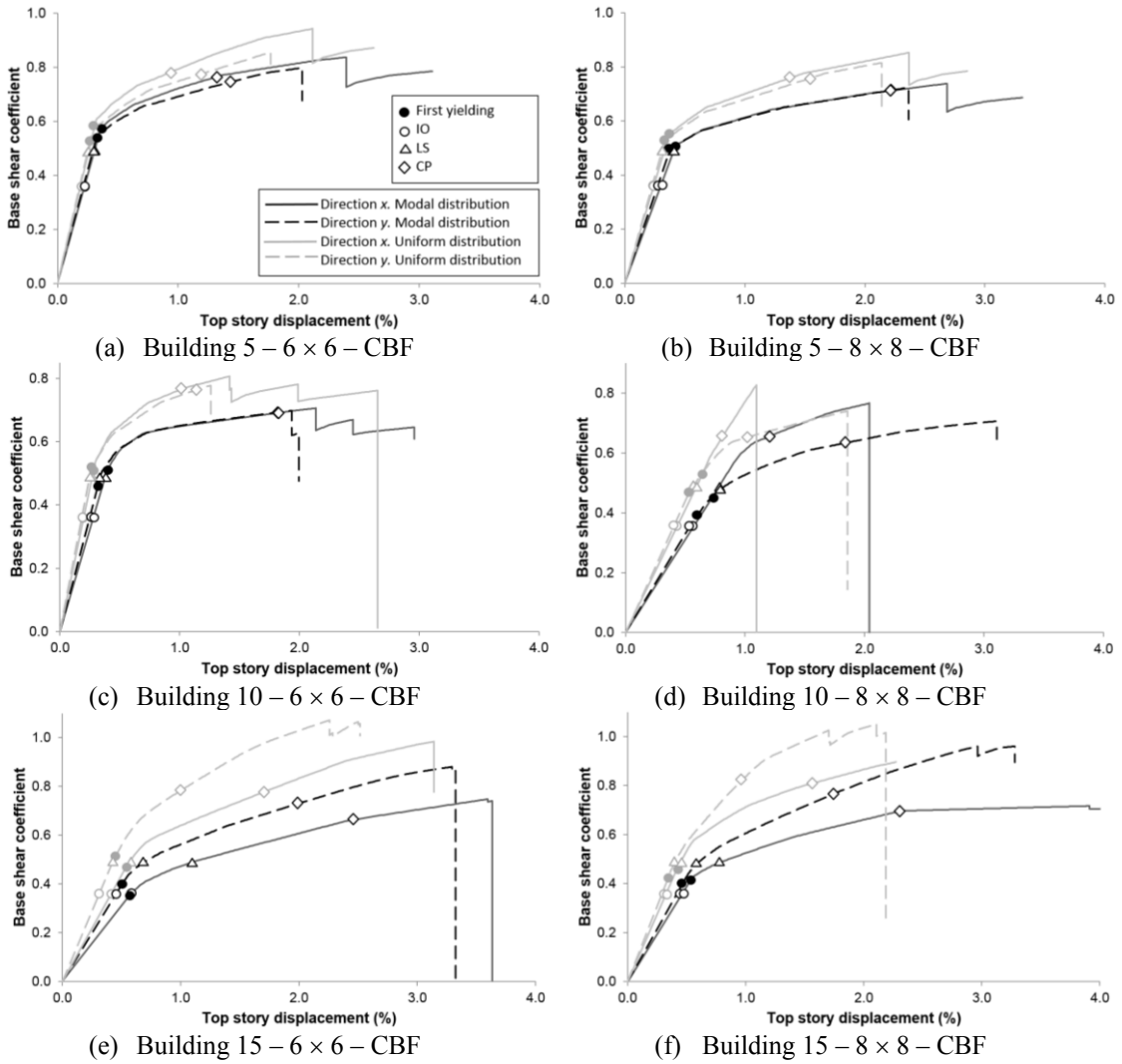

(a) Building 5 – 6 × 6 – CBF (b) Building 5 – 8 × 8 – CBF

(c) Building 10 – 6 × 6 – CBF (d) Building 10 – 8 × 8 – CBF

(e) Building 15 – 6 × 6 – CBF (f) Building 15 – 8 × 8 – CBF

Figure 5-60. Capacity curves and Target Drifts of buildings with Concentric-Braced Frames. Zone "Lacustre-100" (new microzonation, Figure 3-7)

Most of the results in Figure 5-60 are regular and expected, thus illustrating the reliability and accuracy of the carried out analysis; subsection 5.3.12 holds deeper conclusions that are issued globally for all the cases. However, Figure 5-60.d shows that, for the 10 – 8 × 8 – CBF prototype building (Table 4-1) in *y* direction, the push-over analysis under modal force distribution predicts less initial stiffness and slightly less force strength, whereas that analysis also predicts higher displacement ductility than the analysis under constant force distribution. To further investigate this issue, Figure 5-61 and Figure 5-62 display the damage progression of the 10 – 8 × 8 – CBF prototype building in *y* direction designed for the "Lacustre-100" Zone (new microzonation, Figure 3-7). Figure 5-61 and Figure 5-62 correspond to push-over analyses under modal and uniform force distribution, respectively (Figure 5-1).

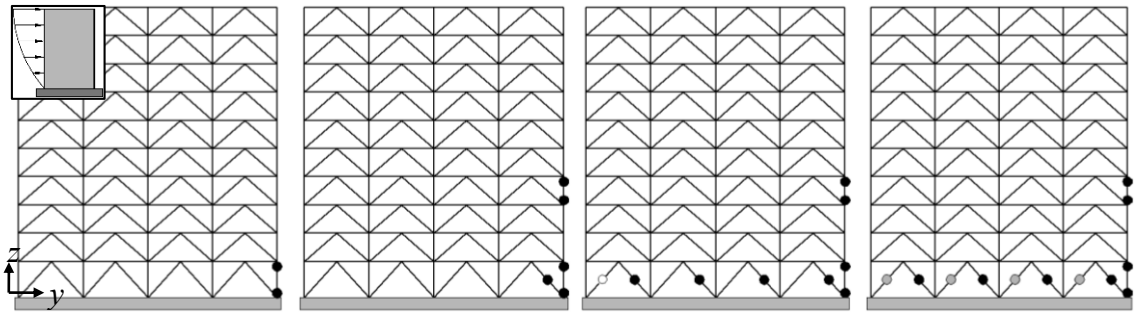

(a) Drift angle 0.42% (b) Drift angle 0.45% (c) Drift angle 0.47% (d) Drift angle 0.54%

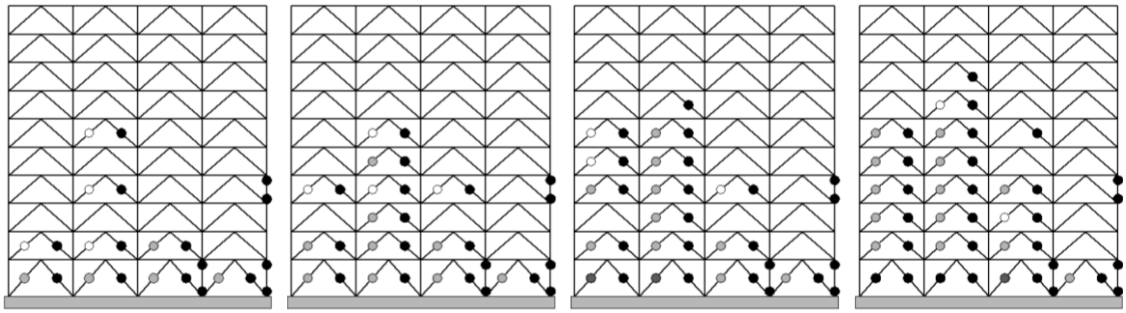

(e) Drift angle 0.67% (f) Drift angle 0.85% (g) Drift angle 1.51% (h) Drift angle 1.88%

Figure 5-61. Hinge progression sequence for the 10 – 8 × 8 – CBF building, modal distribution and *y* direction (right displacement). Zone "Lacustre-100" (new microzonation, Figure 3-7). ○: yielding, ◎: IO, ◉: LS, ●: CP [FEMA 356 2000]

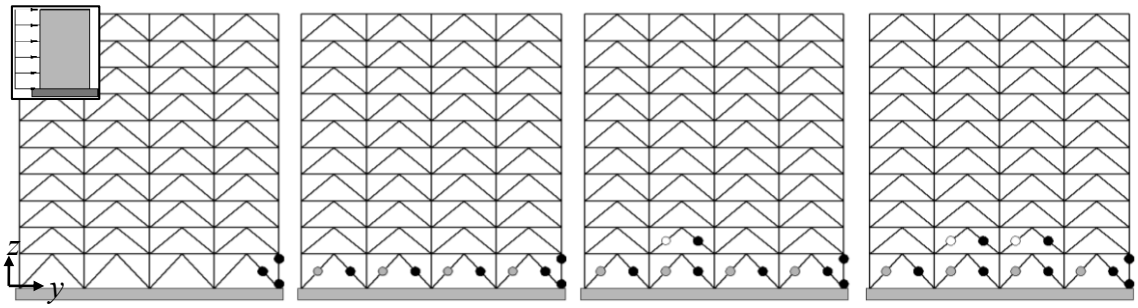

(a) Drift angle 0.33% (b) Drift angle 0.40% (c) Drift angle 0.45% (d) Drift angle 0.49%

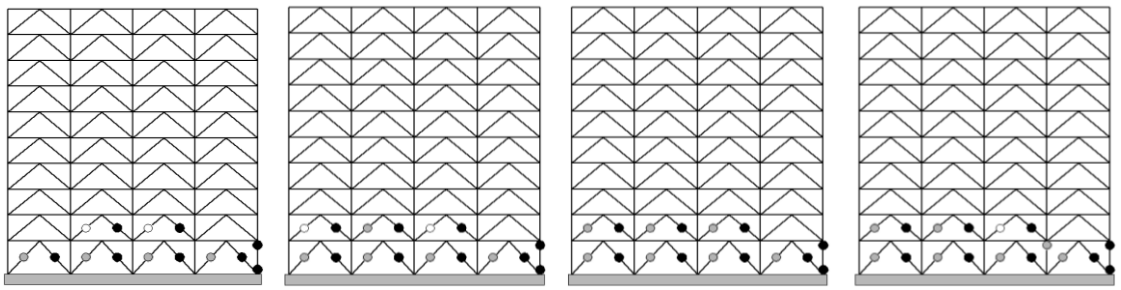

(e) Drift angle 0.55% (f) Drift angle 0.64% (g) Drift angle 0.84% (h) Drift angle 1.06%

Figure 5-62. Hinge progression sequence for the 10 – 8 × 8 – CBF building, uniform distribution and *y* direction (right displacement). Zone "Lacustre-100" (new microzonation, Figure 3-7). ○: yielding, ◎: IO, ◉: LS, ●: CP [FEMA 356 2000]

Comparison between Figure 5-61 and Figure 5-62 shows that, under modal force distribution (Figure 5-61), the collapse mechanism involves hinges in all levels of the building (noticeably, even in the top one), while for uniform distribution (Figure 5-62) the hinges concentrate more in

the lowest levels, although they affect even the seventh story. This difference between modal and uniform pushing forces is consistent with the corresponding distribution laws of shear forces and bending moments along the height of the building (Figure 5-1).

As previously announced, Figure 5-63 displays the capacity curves of the prototype EBF buildings (Table 4-1) designed for the "Lacustre-100" Zone (new microzonation, Figure 3-7).

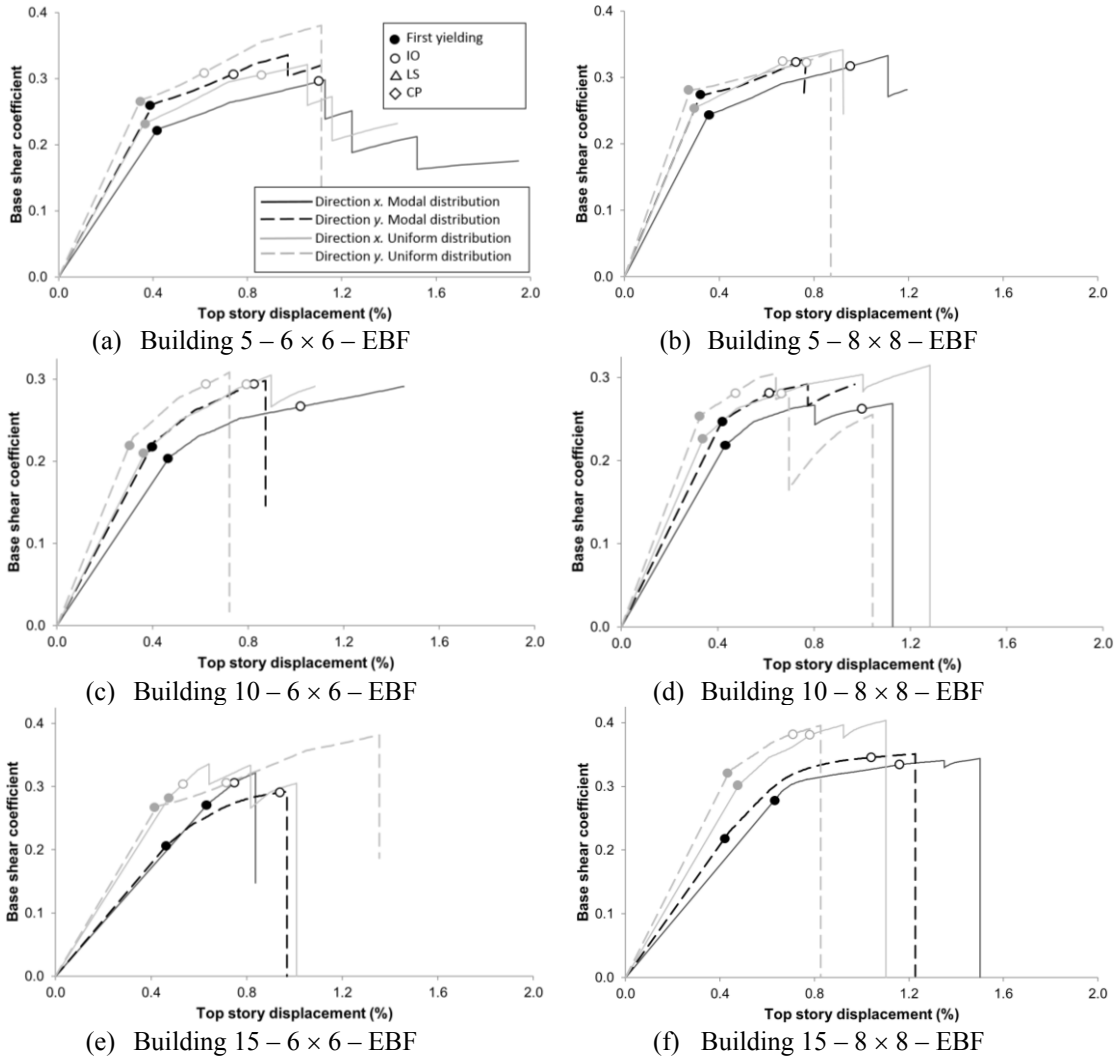

(a) Building 5 – 6 × 6 – EBF (b) Building 5 – 8 × 8 – EBF

(c) Building 10 – 6 × 6 – EBF (d) Building 10 – 8 × 8 – EBF

(e) Building 15 – 6 × 6 – EBF (f) Building 15 – 8 × 8 – EBF

Figure 5-63. Capacity curves and Target Drifts of buildings with Eccentric-Braced Frames. Zone "Lacustre-100" (new microzonation, Figure 3-7)

Most of the results in Figure 5-63 are regular and expected; subsection 5.3.12 holds deeper conclusions issued globally for all the cases. However, Figure 5-63.c shows that, for the 10 – 6 × 6 – EBF prototype building (Table 4-1) in *x* direction, the push-over analysis under modal force distribution predicts less initial stiffness and force strength, whereas that analysis predicts higher displacement ductility than the analysis under constant force distribution. To further investigate this issue, Figure 5-64 and Figure 5-65 display the damage progression of the 10 – 6 × 6 – EBF prototype building in *x* direction designed for the "Lacustre-100" Zone (new microzonation, Figure 3-7). Figure 5-64 and Figure 5-65 correspond to push-over analyses under modal and uniform force distribution, respectively (Figure 5-1).

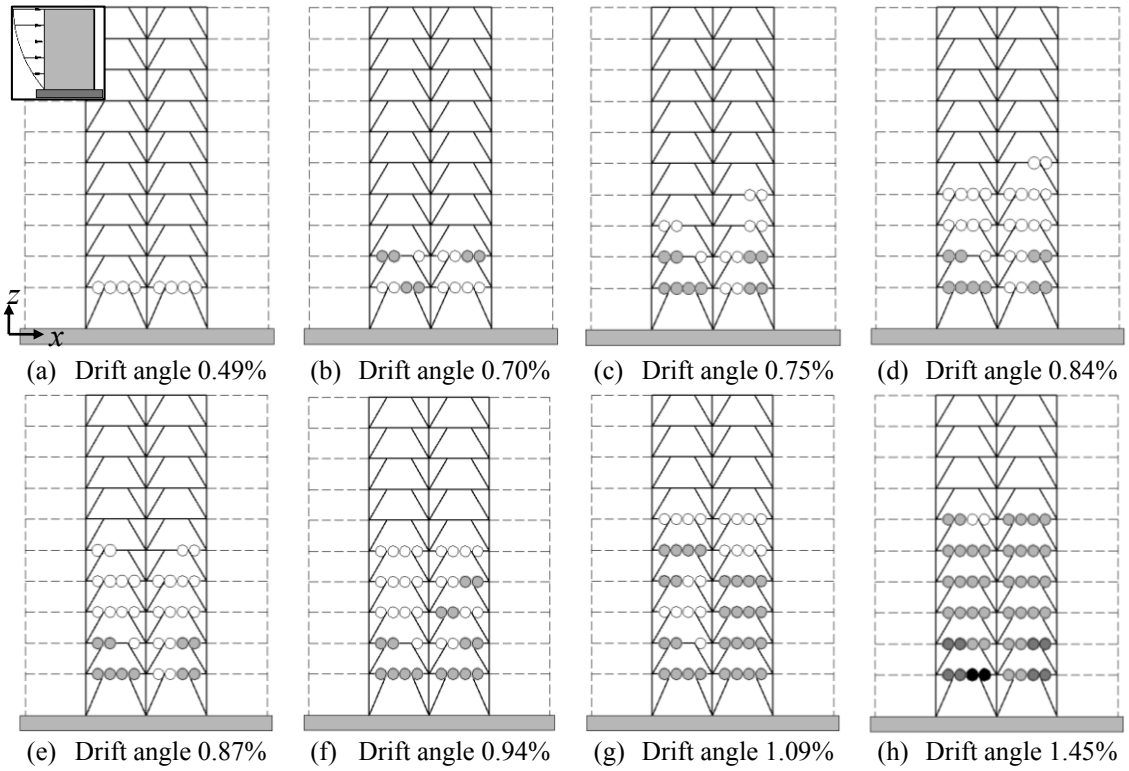

(a) Drift angle 0.49% (b) Drift angle 0.70% (c) Drift angle 0.75% (d) Drift angle 0.84%

(e) Drift angle 0.87% (f) Drift angle 0.94% (g) Drift angle 1.09% (h) Drift angle 1.45%

Figure 5-64. Hinge progression sequence for the 10 – 6 × 6 – EBF building, modal distribution and *x* direction (right displacement). Zone "Lacustre-100" (new microzonation, Figure 3-7). ○: yielding, ◎: IO, ◍: LS, ●: CP [FEMA 356 2000]

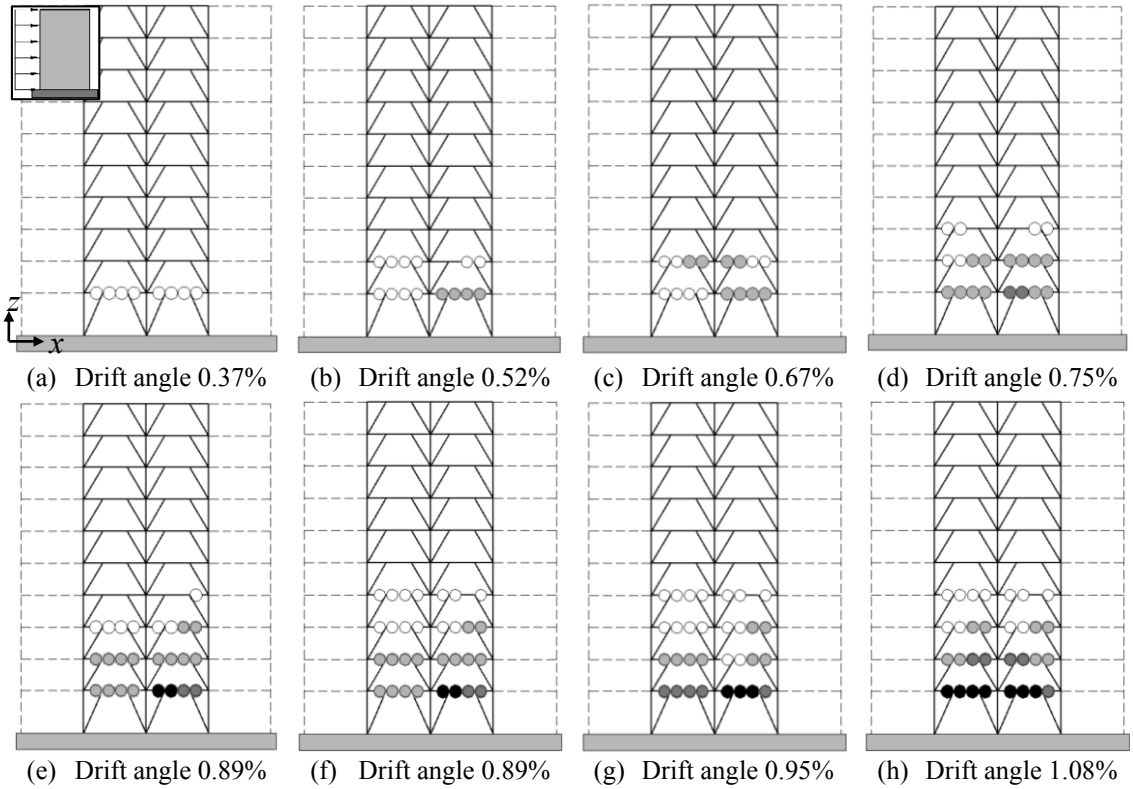

(a) Drift angle 0.37% (b) Drift angle 0.52% (c) Drift angle 0.67% (d) Drift angle 0.75%

(e) Drift angle 0.89% (f) Drift angle 0.89% (g) Drift angle 0.95% (h) Drift angle 1.08%

Figure 5-65. Hinge progression sequence for the 10 – 6 × 6 – EBF building, uniform distribution and *x* direction (right displacement). Zone "Lacustre-100" (new microzonation, Figure 3-7). ○: yielding, ◎: IO, ◍: LS, ●: CP [FEMA 356 2000]

Figure 5-64 and Figure 5-65 shows that under modal force distribution (Figure 5-64), the collapse mechanism involves hinges up to the sixth level of the building, and for uniform distribution (Figure 5-65), the hinges concentrate only in the link segments of the four lowest levels. This difference between modal and uniform pushing forces is consistent with the corresponding shear forces and bending moments distribution along the height of the building (Figure 5-1).

Table 5-13 and Table 5-14 display, respectively, the seismic performance and the response reduction factor (R, Ω and R_d) of the prototype buildings (Table 4-1) designed for the "Lacustre-100" Zone (new microzonation, Figure 3-7).

Table 5-13. Seismic performance. "Lacustre-100" zone (new microzonation)

Building	Target Drift IO(*)		Target Drift LS(*)		Target Drift CP(*)	
	Direction *x*	Direction *y*	Direction *x*	Direction *y*	Direction *x*	Direction *y*
5 – 6 × 6 – MRF	YES / YES	YES / YES	YES / YES	YES / YES	YES / YES	YES / YES
5 – 8 × 8 – MRF	YES / YES	YES / YES	YES / YES	YES / YES	YES / YES	YES / YES
5 – 6 × 6 – CBF	YES / YES	YES / YES	YES / YES	YES / YES	YES / YES	YES / YES
5 – 8 × 8 – CBF	YES / YES	YES / YES	YES / YES	YES / YES	YES / YES	YES / YES
5 – 6 × 6 – EBF	**NO** / **NO**	**NO** / **NO**	- / -	- / -	- / -	- / -
5 – 8 × 8 – EBF	**NO** / **NO**	**NO** / **NO**	- / -	- / -	- / -	- / -
10 – 6 × 6 – MRF	YES / YES	YES / YES	YES / YES	YES / YES	YES / YES	- / -
10 – 8 × 8 – MRF	YES / YES	YES / YES	YES / YES	YES / **NO**	YES / -	- / -
10 – 6 × 6 – CBF	YES / YES	YES / YES	YES / YES	YES / YES	YES / YES	YES / YES
10 – 8 × 8 – CBF	YES / YES	YES / YES	YES / YES	YES / YES	YES / YES	YES / YES
10 – 6 × 6 – EBF	**NO** / **NO**	**NO** / **NO**	- / -	- / -	- / -	- / -
10 – 8 × 8 – EBF	**NO** / **NO**	**NO** / **NO**	- / -	- / -	- / -	- / -
15 – 6 × 6 – MRF	YES / YES	YES / YES	YES / YES	YES / YES	- / -	- / -
15 – 8 × 8 – MRF	YES / YES	YES / YES	YES / YES	**NO** / YES	- / -	- / -
15 – 6 × 6 – CBF	YES / YES	YES / YES	YES / YES	YES / YES	YES / YES	YES / YES
15 – 8 × 8 – CBF	YES / YES	YES / YES	YES / YES	YES / YES	YES / YES	YES / YES
15 – 6 × 6 – EBF	**NO** / **NO**	NO / -	- / -	- / -	- / -	- / -
15 – 8 × 8 – EBF	**NO** / **NO**	NO / NO	- / -	- / -	- / -	- / -

(*) First / second values correspond to modal and uniform distributions, respectively

Table 5-13 reveals that 61% of the cases exhibit a satisfactory performance (YES), 12% unsatisfactory (NO) and 27% highly unsatisfactory (-). In the MRF/CBF/EBF buildings, such percentages are 84/100/0%, 3/0/32% and 13/0/68%. In the 5/10/15-story buildings such percentages are 67/58/60%, 11/13/11% and 22/29/29%. For the IO/LS/CP limit states, the percentages are 67/64/49%, 32/3/0% and 1/33/51%. For the Modal/Uniform distributions, the percentages are 60/60%, 12/10% and 28/30%. No relevant differences have been observed for *x*/*y* directions.

Table 5-14. Response reduction factor R in the x / y directions. "Lacustre-100" zone (new microzonation)

Building	Over-strength factor (Ω)(*)		Ductility factor R_d(*)		R factor ($R = \Omega R_d$) (*)	
	Direction x	Direction y	Direction x	Direction y	Direction x	Direction y
5 – 6 × 6 – MRF	1.26 / 1.48	1.28 / 1.46	4.67 / 4.35	3.77 / 4.10	5.88 / 6.44	4.82 / 5.99
5 – 8 × 8 – MRF	1.42 / 1.31	1.29 / 1.44	4.52 / 5.47	2.90 / 2.76	6.46 / 7.16	3.74 / 3.97
5 – 6 × 6 – CBF	1.47 / 1.61	1.49 / 1.62	4.45 / 4.48	4.13 / 4.04	6.58 / 7.22	6.15 / 6.55
5 – 8 × 8 – CBF	1.46 / 1.55	1.45 / 1.54	4.34 / 4.19	4.44 / 4.14	6.33 / 6.50	6.44 / 6.42
5 – 6 × 6 – EBF	1.34 / 1.38	1.30 / 1.43	2.04 / 2.10	1.94 / 2.26	2.73 / 2.90	2.52 / 3.23
5 – 8 × 8 – EBF	1.37 / 1.36	1.18 / 1.20	2.27 / 2.31	2.00 / 2.67	3.11 / 3.14	2.38 / 3.21
10 – 6 × 6 – MRF	1.36 / 1.32	1.30 / 1.30	2.58 / 2.49	1.38 / 1.54	3.51 / 3.29	1.79 / 2.00
10 – 8 × 8 – MRF	1.30 / 1.37	1.35 / 1.21	3.89 / 1.73	1.97 / 1.17	5.06 / 2.37	2.66 / 1.42
10 – 6 × 6 – CBF	1.39 / 1.59	1.51 / 1.50	3.79 / 3.11	3.97 / 3.25	5.27 / 4.95	5.99 / 4.87
10 – 8 × 8 – CBF	1.72 / 1.56	1.78 / 1.58	1.60 / 1.08	2.93 / 2.16	2.75 / 1.69	5.22 / 3.42
10 – 6 × 6 – EBF	1.41 / 1.45	1.37 / 1.40	2.21 / 1.71	1.61 / 1.68	3.13 / 2.48	2.20 / 2.35
10 – 8 × 8 – EBF	1.22 / 1.34	1.19 / 1.21	2.11 / 2.22	1.57 / 1.64	2.59 / 2.97	1.85 / 1.97
15 – 6 × 6 – MRF	1.56 / 1.33	1.30 / 1.23	2.30 / 1.20	1.11 / 1.27	3.59 / 1.59	1.44 / 1.56
15 – 8 × 8 – MRF	1.33 / 1.31	1.37 / 1.24	1.20 / 1.34	1.24 / 1.98	1.60 / 1.76	1.70 / 2.45
15 – 6 × 6 – CBF	2.12 / 2.09	2.21 / 2.09	2.95 / 2.79	2.92 / 2.40	6.25 / 5.83	6.46 / 5.02
15 – 8 × 8 – CBF	1.74 / 1.94	2.39 / 2.49	4.19 / 2.74	2.70 / 2.49	7.29 / 5.31	6.46 / 6.20
15 – 6 × 6 – EBF	1.19 / 1.18	1.42 / 1.43	1.11 / 1.14	1.46 / 2.38	1.32 / 1.35	2.09 / 3.41
15 – 8 × 8 – EBF	1.24 / 1.33	1.62 / 1.23	1.92 / 1.74	1.79 / 1.54	2.38 / 2.31	2.90 / 1.90

(*) First / second values correspond to modal and uniform distributions, respectively

Comparison among the values of R in Table 5-14 with the assumed factors in Table 4-27 shows that, in 61% of the cases, the analyzed buildings do not possess the required ductility. In the MRF/CBF/EBF buildings, such percentage is 71/13/100%. In the 5/10/15-story buildings such percentage is 42/75/67%. For the Modal/Uniform distributions, the percentages are 58/64%. No relevant differences have been observed for *x/y* directions.

5.3.9 "Lacustre-200" Zone (new microzonation)

Figure 5-66, Figure 5-69 and Figure 5-72 display the capacity curves of the prototype buildings (Table 4-1) designed for the "Lacustre-200" Zone (new microzonation, Figure 3-7); Figure 5-66, Figure 5-69 and Figure 5-72 refer to the MRF, CBF and EBF buildings, respectively.

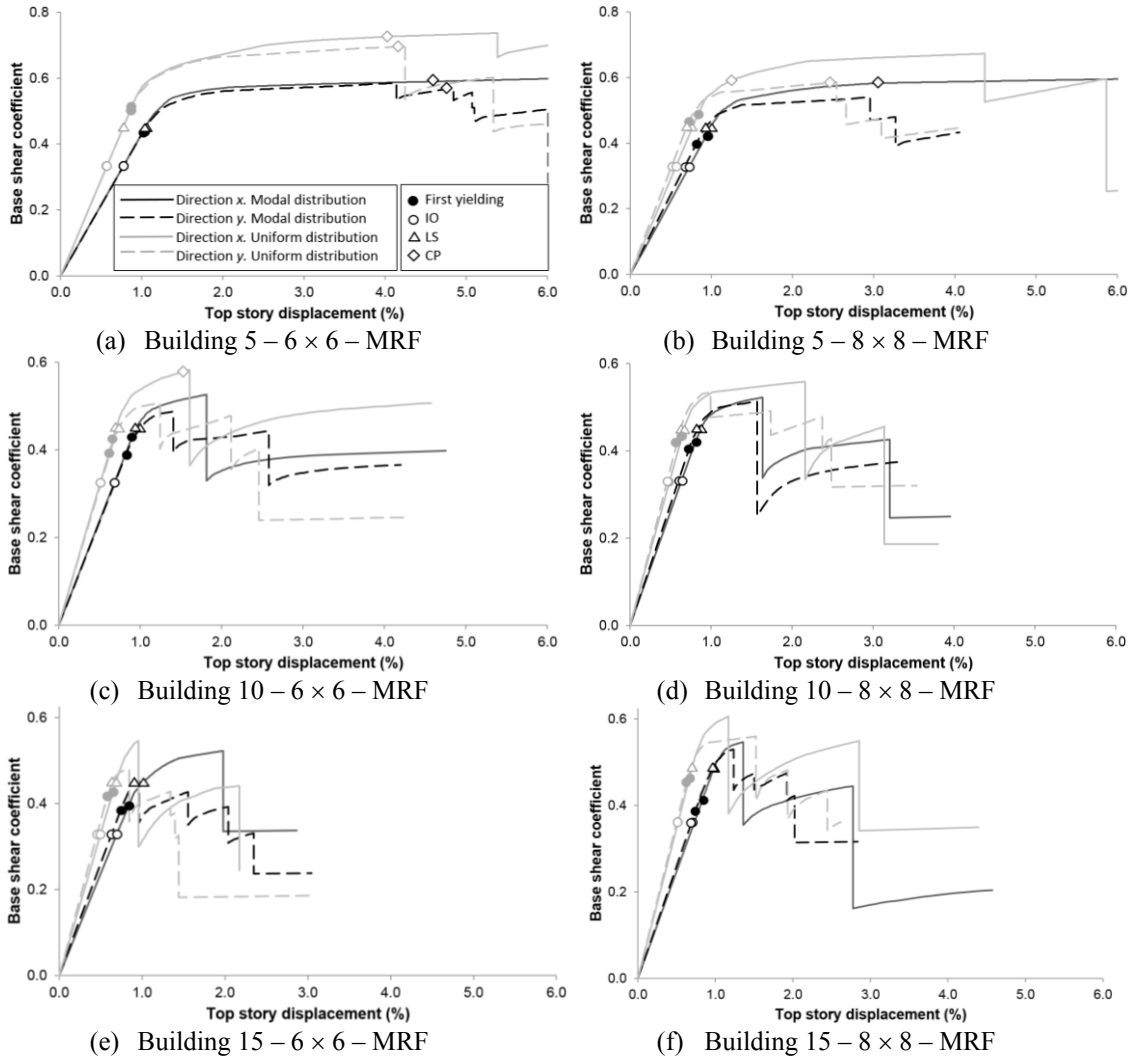

(a) Building 5 – 6 × 6 – MRF (b) Building 5 – 8 × 8 – MRF

(c) Building 10 – 6 × 6 – MRF (d) Building 10 – 8 × 8 – MRF

(e) Building 15 – 6 × 6 – MRF (f) Building 15 – 8 × 8 – MRF

Figure 5-66. Capacity curves and Target Drifts of buildings with Moment-Resisting Frames. Zone "Lacustre-200" (new microzonation, Figure 3-7)

Most of the results in Figure 5-66 are regular and expected; subsection 5.3.12 holds deeper conclusions issued globally for all the cases. Figure 5-66.d shows that, for the 10 – 8 × 8 – MRF prototype building (Table 4-1) in *x* direction, the push-over analysis under modal force distribution predicts less initial stiffness, similar force strength, and similar displacement ductility than the analysis under constant force distribution, although the first sudden (abrupt) drop (descent) is earlier for the modal distribution than for the uniform one. To further investigate this issue, Figure 5-67 and Figure 5-68 display the damage progression of the 10 – 8 × 8 – MRF prototype building in *x* direction designed for the "Lacustre-200" Zone (new microzonation, Figure 3-7). Figure 5-67 and Figure 5-68 correspond to push-over analyses under modal and uniform force distribution, respectively (Figure 5-1).

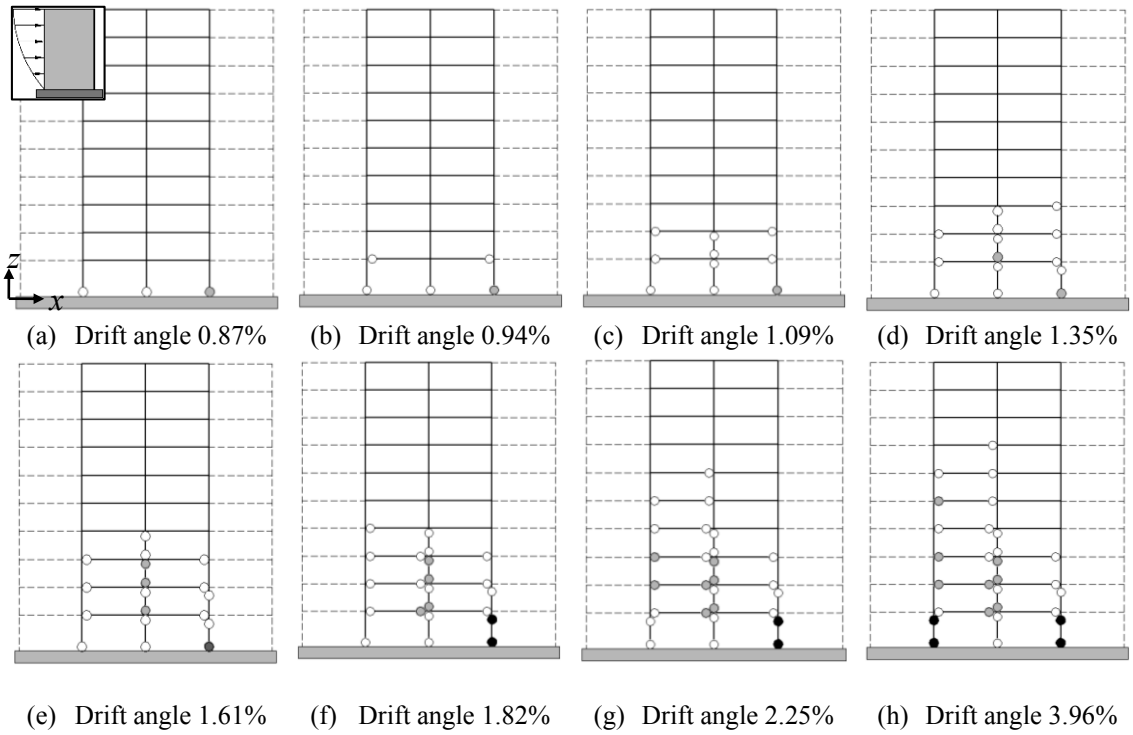

(a) Drift angle 0.87% (b) Drift angle 0.94% (c) Drift angle 1.09% (d) Drift angle 1.35%

(e) Drift angle 1.61% (f) Drift angle 1.82% (g) Drift angle 2.25% (h) Drift angle 3.96%

Figure 5-67. Hinge progression sequence for the 10 – 8 × 8 – MRF building, modal distribution and *x* direction (right displacement). Zone "Lacustre-200" (new microzonation, Figure 3-7). ○: yielding, ◎: IO, ◉: LS, ●: CP [FEMA 356 2000]

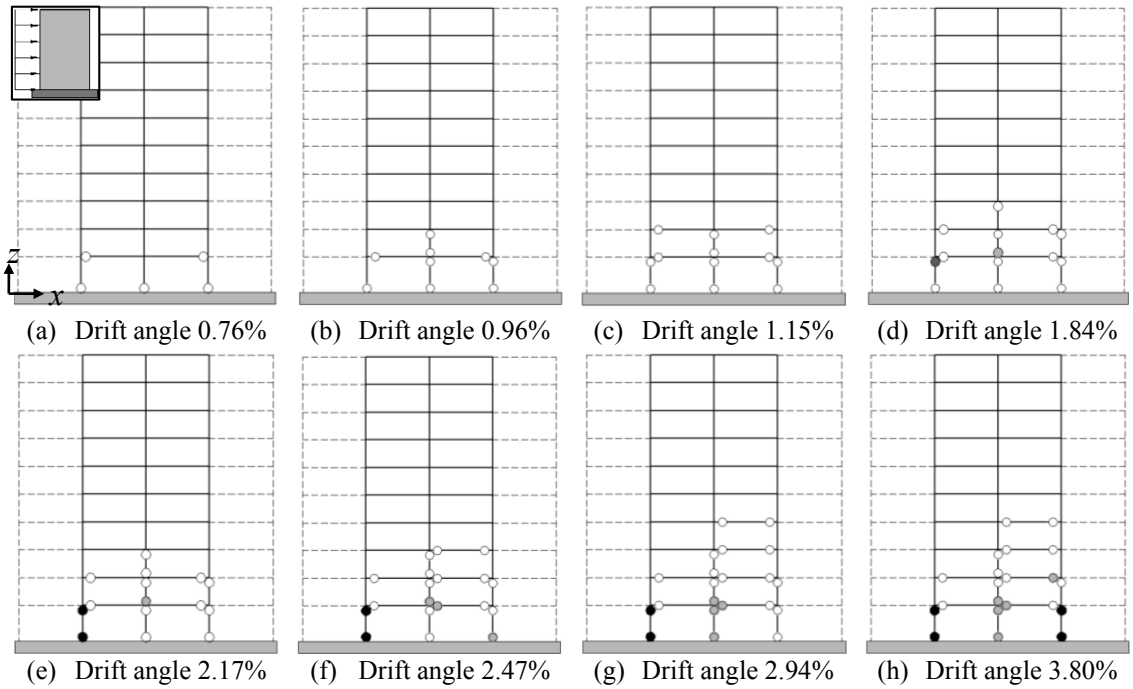

(a) Drift angle 0.76% (b) Drift angle 0.96% (c) Drift angle 1.15% (d) Drift angle 1.84%

(e) Drift angle 2.17% (f) Drift angle 2.47% (g) Drift angle 2.94% (h) Drift angle 3.80%

Figure 5-68. Hinge progression sequence for the 10 – 8 × 8 – MRF building, uniform distribution and *x* direction (right displacement). Zone "Lacustre-200" (new microzonation, Figure 3-7). ○: yielding, ◎: IO, ◉: LS, ●: CP [FEMA 356 2000]

Comparison between Figure 5-67 and Figure 5-68 shows that the collapse mechanisms for modal and uniform force distribution (Figure 5-67 and Figure 5-68, respectively) are rather similar since in both the plastic hinges are concentrated in the first floor columns; however, the mechanism for

modal distribution is slightly more ductile since involves up to the seventh floor while the mechanism for uniform distribution involves only the four bottom floors. This difference between modal and uniform pushing forces is consistent with the shear forces and bending moments distribution (Figure 5-1). The first brusque drop for the modal distribution corresponds basically to the difference between Figure 5-67.e and Figure 5-67.f; abrupt descent for the uniform distribution corresponds to Figure 5-68.e.

As previously announced, Figure 5-69 displays the capacity curves of the prototype CBF buildings (Table 4-1) designed for the "Lacustre-200" Zone (new microzonation, Figure 3-7).

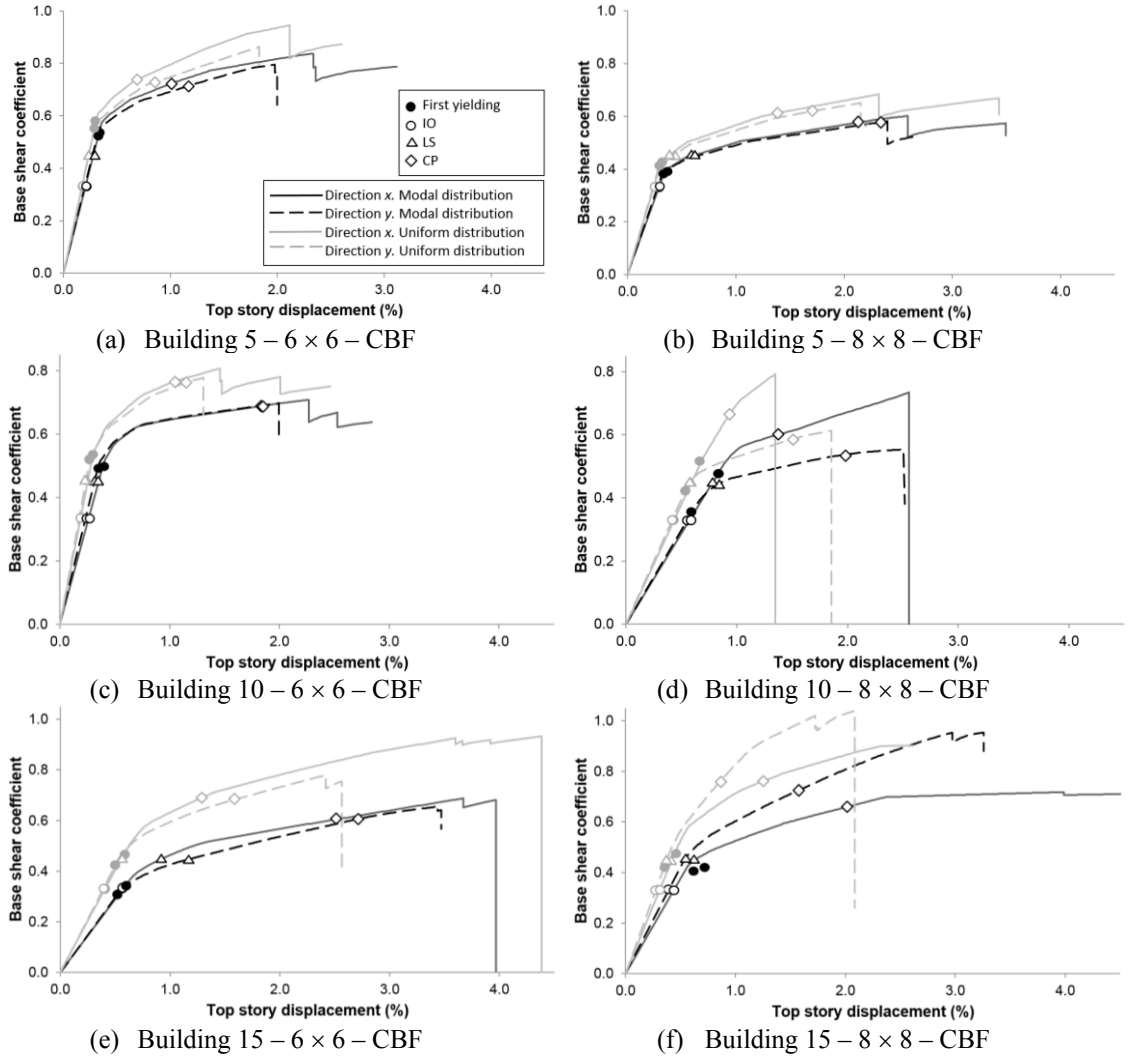

(a) Building 5 – 6 × 6 – CBF (b) Building 5 – 8 × 8 – CBF

(c) Building 10 – 6 × 6 – CBF (d) Building 10 – 8 × 8 – CBF

(e) Building 15 – 6 × 6 – CBF (f) Building 15 – 8 × 8 – CBF

Figure 5-69. Capacity curves and Target Drifts of buildings with Concentric-Braced Frames. Zone "Lacustre-200" (new microzonation, Figure 3-7)

Most of the results in Figure 5-69 are regular and expected, thus illustrating the reliability and accuracy of the carried out analysis; subsection 5.3.12 holds deeper conclusions that are issued globally for all the cases. However, Figure 5-69.f shows that, for the 15 – 8 × 8 – CBF prototype building (Table 4-1) in *x* direction, the push-over analysis under modal force distribution predicts less initial stiffness and less force strength, whereas that analysis also predicts higher displacement ductility than the analysis under constant force distribution. To further investigate this issue, Figure 5-70 and Figure 5-71 display the damage progression of the 15 – 8 × 8 – CBF prototype building in *x* direction designed for the "Lacustre-200" Zone (new microzonation, Figure 3-7). Figure 5-70 and Figure 5-71 correspond to push-over analyses under modal and uniform force distribution, respectively (Figure 5-1).

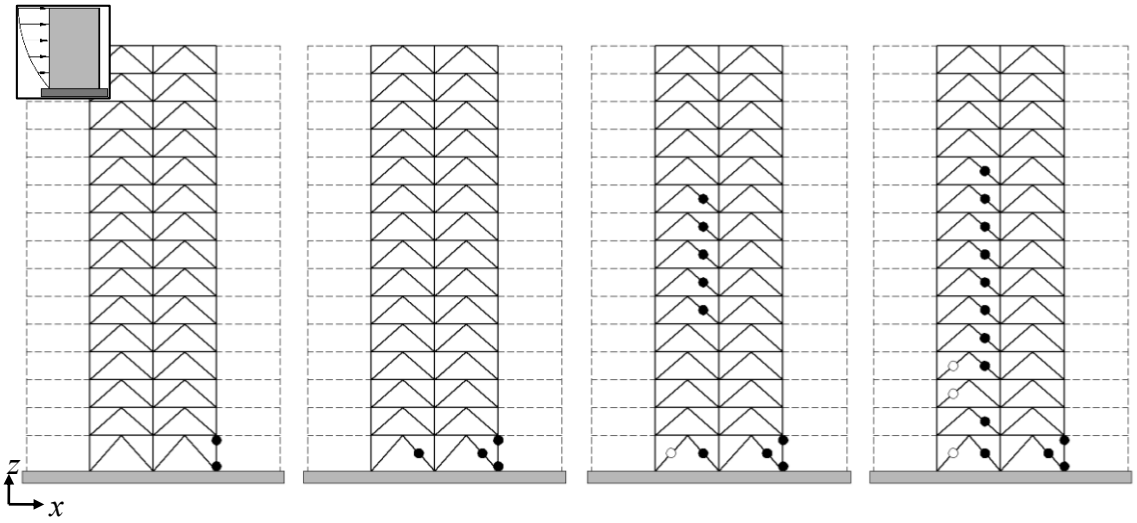

(a) Drift angle 0.63% (b) Drift angle 0.70% (c) Drift angle 0.82% (d) Drift angle 1.02%

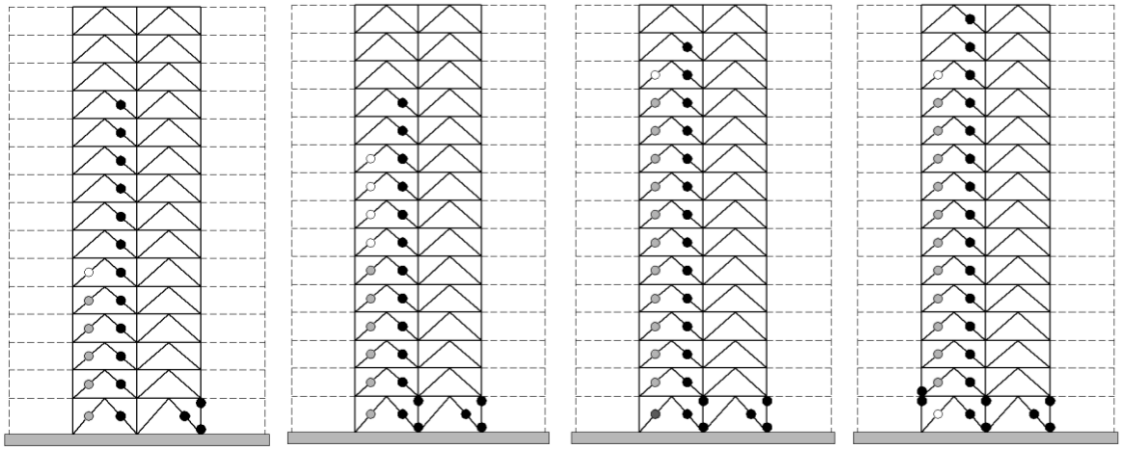

(e) Drift angle 1.44% (f) Drift angle 2.01% (g) Drift angle 2.75% (h) Drift angle 3.12%

Figure 5-70. Hinge progression sequence for the 15 – 8 × 8 – CBF building, modal distribution and *x* direction (right displacement). Zone "Lacustre-200" (new microzonation, Figure 3-7). ○: yielding, ◎: IO, ◉: LS, ●: CP [FEMA 356 2000]

Figure 5-70 shows that the plastic hinges appear mainly in the braces, as expected (those elements are designed to protect the main structural members, e.g. beams and columns). Figure 5-70.a shows that the right column of the first floor undergoes extremely early damage, vanishing almost completely its lateral stiffness; this fact is due to the severe interaction with the high compressive axial force generated by the horizontal pushing forces. Noticeably, the early failure of the right bottom column causes that most of the damage concentrates in the left bay since it does not transmit neither any horizontal force nor any flexure to the above stories.

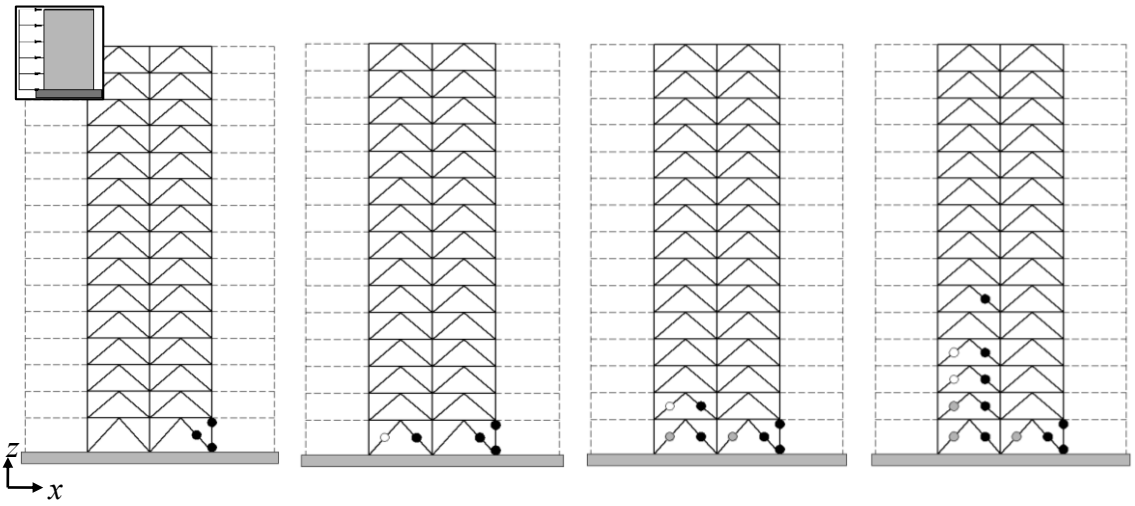

(a) Drift angle 0.54% (b) Drift angle 0.63 (c) Drift angle 0.87% (d) Drift angle 0.98%

(e) Drift angle 1.10% (f) Drift angle 1.24% (g) Drift angle 1.98% (h) Drift angle 2.63%

Figure 5-71. Hinge progression sequence for the 15 – 8 × 8 – CBF building, uniform distribution and *x* direction (right displacement). Zone "Lacustre-200" (new microzonation, Figure 3-7). ○: yielding, ○: IO, ●: LS, ●: CP [FEMA 356 2000]

Comparison between Figure 5-70 and Figure 5-71 shows that, both under modal and uniform force distributions, the collapse mechanisms involve hinges in all levels of the building (noticeably, even in the top one); nevertheless, for uniform distribution (Figure 5-71) the hinges concentrate more in the lowest levels. This difference between modal and uniform pushing forces is consistent with the corresponding distribution laws of shear forces and bending moments along the height of the building (Figure 5-1).

As previously announced, Figure 5-72 displays the capacity curves of the prototype EBF buildings (Table 4-1) designed for the "Lacustre-200" Zone (new microzonation, Figure 3-7).

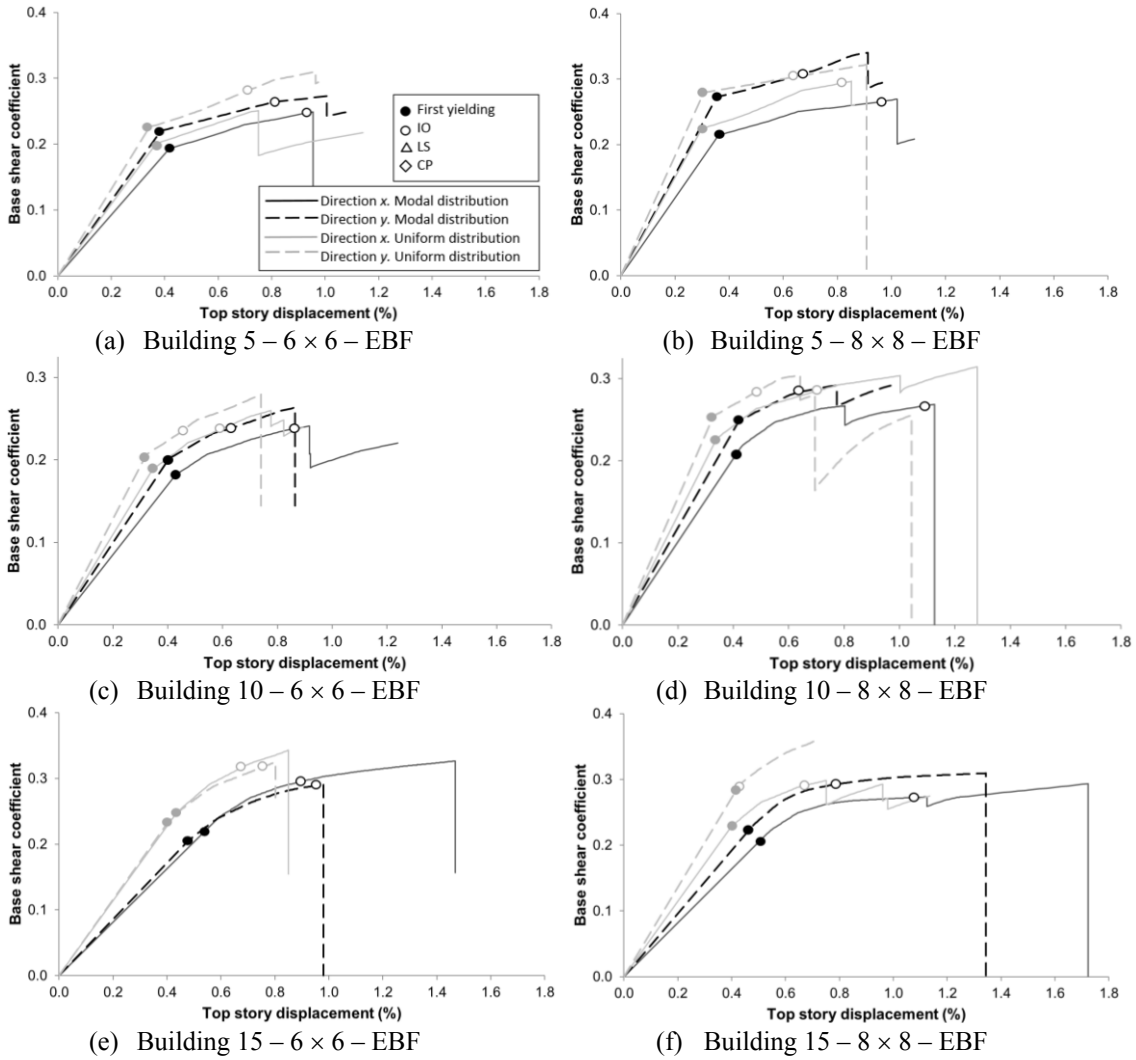

(a) Building 5 – 6 × 6 – EBF (b) Building 5 – 8 × 8 – EBF

(c) Building 10 – 6 × 6 – EBF (d) Building 10 – 8 × 8 – EBF

(e) Building 15 – 6 × 6 – EBF (f) Building 15 – 8 × 8 – EBF

Figure 5-72. Capacity curves and Target Drifts of buildings with Eccentric-Braced Frames. Zone "Lacustre-200" (new microzonation, Figure 3-7)

Most of the results in Figure 5-72 are regular and expected; subsection 5.3.12 holds deeper conclusions issued globally for all the cases. However, Figure 5-72.e shows that, for the 15 – 6 × 6 – EBF prototype building (Table 4-1) in *x* direction, the push-over analysis under modal force distribution predicts less initial stiffness and similar force strength, whereas that analysis predicts higher displacement ductility than the analysis under constant force distribution. To further investigate this issue, Figure 5-73 and Figure 5-74 display the damage progression of the 15 – 6 × 6 – EBF prototype building in *x* direction designed for the "Lacustre-200" Zone (new microzonation, Figure 3-7). Figure 5-73 and Figure 5-74 correspond to push-over analyses under modal and uniform force distribution, respectively (Figure 5-1).

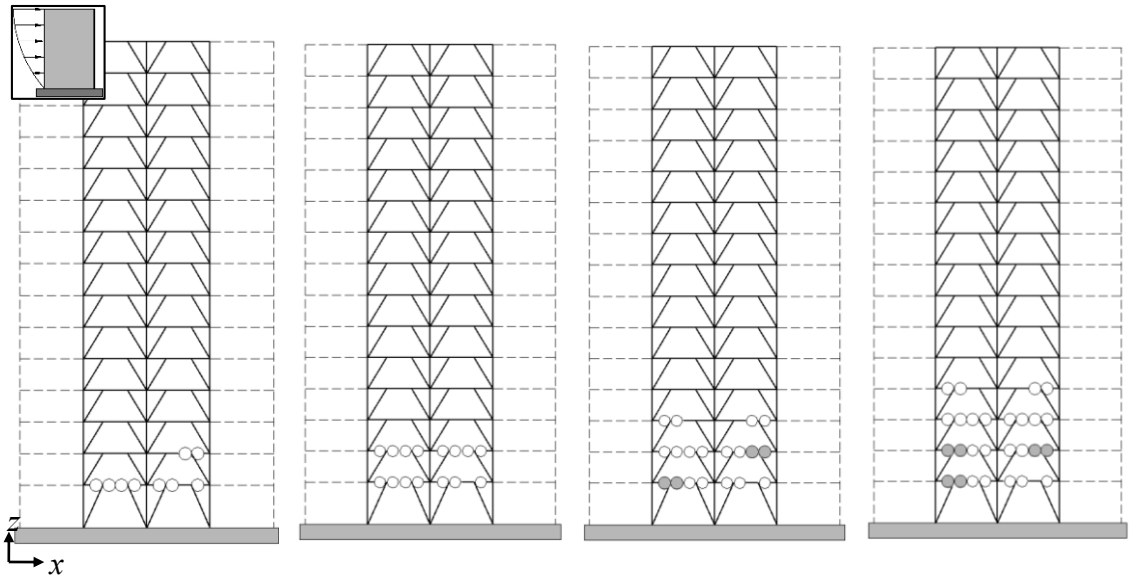

(a) Drift angle 0.68% (b) Drift angle 0.72% (c) Drift angle 0.80% (d) Drift angle 0.88%

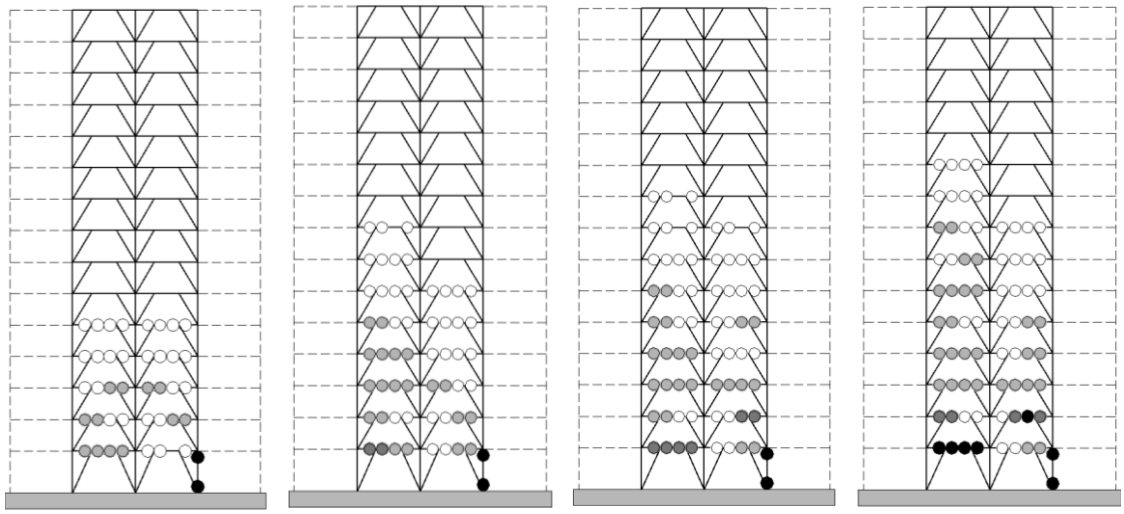

(e) Drift angle 0.97% (f) Drift angle 1.14% (g) Drift angle 1.30% (h) Drift angle 1.45%

Figure 5-73. Hinge progression sequence for the 15 – 6 × 6 – EBF building, modal distribution and *x* direction (right displacement). Zone "Lacustre-200" (new microzonation, Figure 3-7). ○: yielding, ◎: IO, ◍: LS, ●: CP [FEMA 356 2000]

Figure 5-73 shows that the plastic hinges appear mainly in the link segments of the beams of the lowest levels, as expected. Nevertheless, the right column of the first story experiences early severe damage, since Figure 5-73.e shows that two full plastic hinges develop, thus reducing all the lateral stiffness of this member. This fact can be read again as a lack of fulfillment of the overall principle "strong column-weak beam". As discussed previously, the Colombian seismic design guidelines [NSR-98 1998; NSR-10 2010] do not enforce this verification for medium-seismicity regions, like Bogotá. Noticeably, this type of behavior cannot be observed for uniform distribution of the pushing forces (Figure 5-74).

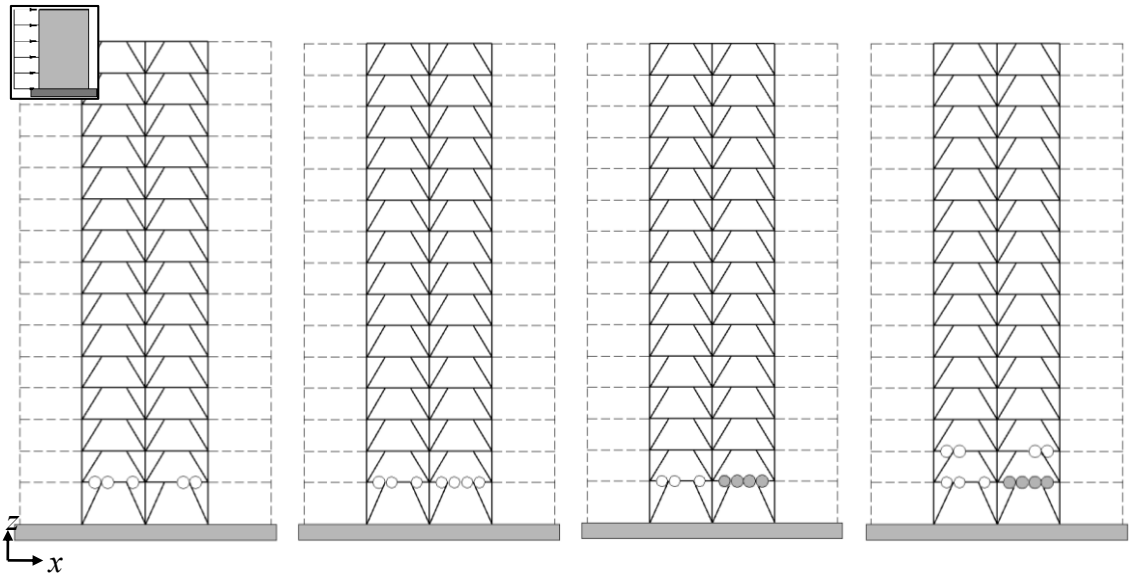

(a) Drift angle 0.43% (b) Drift angle 0.47% (c) Drift angle 0.53% (d) Drift angle 0.55%

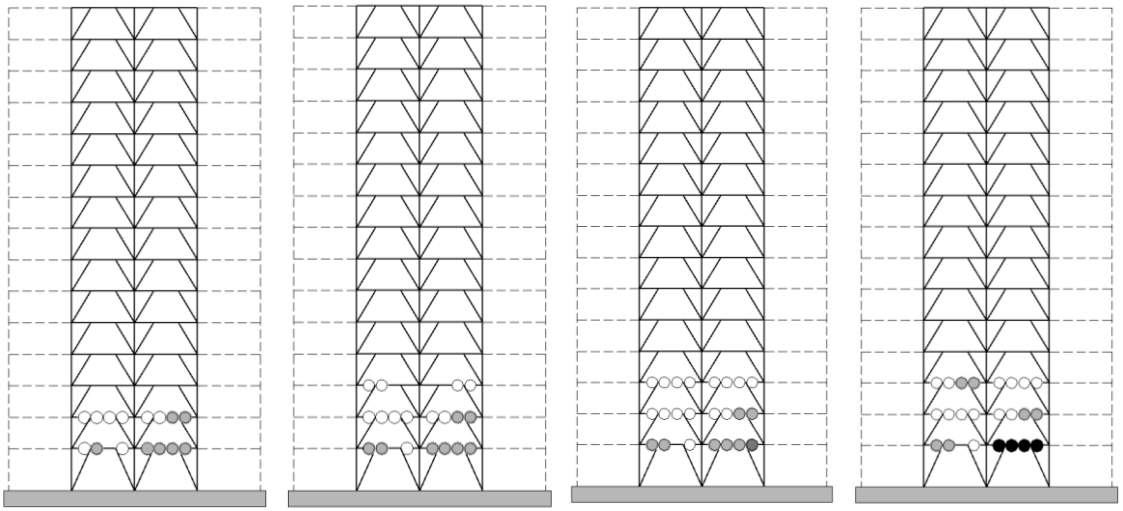

(e) Drift angle 0.62% (f) Drift angle 0.69% (g) Drift angle 0.71% (h) Drift angle 0.84%

Figure 5-74. Hinge progression sequence for the 15 – 6 × 6 – EBF building, uniform distribution and *x* direction (right displacement). Zone "Lacustre-200" (new microzonation, Figure 3-7). ○: yielding, ◎: IO, ◉: LS, ●: CP [FEMA 356 2000]

Comparison between Figure 5-73 and Figure 5-74 shows that under modal force distribution (Figure 5-73), the collapse mechanism involves hinges up to the tenth level of the building, although for uniform distribution (Figure 5-74), the hinges concentrate only in the link segments of the three bottom floors. This difference between modal and uniform pushing forces is consistent with the corresponding shear forces and bending moments distribution along the height of the building (Figure 5-1). Figure 5-73.h and Figure 5-74.h show that the collapse mechanism is similar to the one described by Figure 4-8.c; noticeably, the full collapse mechanism would involve (apart from the progression of the hinges in the link segments of the first floor beams) also the development of plastic hinges in columns and braces.

Table 5-15 and Table 5-16 display, respectively, the seismic performance and the response reduction factor (R, Ω and R_d) of the prototype buildings (Table 4-1) designed for the "Lacustre-200" Zone (new microzonation, Figure 3-7).

Table 5-15. Seismic performance. "Lacustre-200" zone (new microzonation)

Building	Target Drift IO(*)		Target Drift LS(*)		Target Drift CP(*)	
	Direction *x*	Direction *y*	Direction *x*	Direction *y*	Direction *x*	Direction *y*
5 – 6 × 6 – MRF	YES / YES	YES / YES	YES / YES	YES / YES	YES / YES	YES / YES
5 – 8 × 8 – MRF	YES / YES	YES / YES	YES / YES	YES / YES	YES / YES	- / YES
5 – 6 × 6 – CBF	YES / YES	YES / YES	YES / YES	YES / YES	YES / YES	YES / YES
5 – 8 × 8 – CBF	YES / YES	YES / YES	YES / YES	YES / YES	YES / YES	YES / YES
5 – 6 × 6 – EBF	**NO** / **NO**	**NO** / **NO**	- / -	- / -	- / -	- / -
5 – 8 × 8 – EBF	**NO** / **NO**	**NO** / **NO**	- / -	- / -	- / -	- / -
10 – 6 × 6 – MRF	YES / YES	YES / YES	YES / YES	YES / YES	- / YES	- / -
10 – 8 × 8 – MRF	YES / YES	YES / YES	YES / YES	YES / YES	- / -	- / -
10 – 6 × 6 – CBF	YES / YES	YES / YES	YES / YES	YES / YES	YES / YES	YES / YES
10 – 8 × 8 – CBF	YES / YES	YES / YES	YES / YES	YES / YES	YES / YES	YES / YES
10 – 6 × 6 – EBF	**NO** / **NO**	**NO** / **NO**	- / -	- / -	- / -	- / -
10 – 8 × 8 – EBF	**NO** / **NO**	**NO** / **NO**	- / -	- / -	- / -	- / -
15 – 6 × 6 – MRF	YES / YES	YES / YES	YES / YES	YES / YES	- / -	- / -
15 – 8 × 8 – MRF	YES / YES	YES / YES	YES / YES	YES / YES	- / -	- / -
15 – 6 × 6 – CBF	YES / YES	YES / YES	YES / YES	YES / YES	YES / YES	YES / YES
15 – 8 × 8 – CBF	YES / YES	YES / YES	YES / YES	YES / YES	YES / YES	YES / YES
15 – 6 × 6 – EBF	YES / YES	**NO** / YES	- / -	- / -	- / -	- / -
15 – 8 × 8 – EBF	**NO** / YES	YES / YES	- / -	- / -	- / -	- / -

(*) First / second values correspond to modal and uniform distributions, respectively

Table 5-15 reveals that 61% of the cases exhibit a satisfactory performance (YES), 9% unsatisfactory (NO) and 30% highly unsatisfactory (-). In the MRF/CBF/EBF buildings, such percentages are 77/100/8%, 1/0/25% and 22/0/67%. In the 5/10/15-story buildings such percentages are 63/57/64%, 13/11/3% and 24/32/33%. For the IO/LS/CP limit states, the percentages are 75/67/44%, 25/0/0% and 0/33/56%. For the Modal/Uniform distributions, the percentages are 62/64%, 9/7% and 29/29%. No relevant differences have been observed for *x/y* directions.

Table 5-16**.** Response reduction factor *R* in the *x* / *y* directions. "Lacustre-200" zone (new microzonation)

Building	Over-strength factor (Ω)(*)		Ductility factor R_d(*)		*R* factor ($R = \Omega R_d$) (*)	
	Direction *x*	Direction *y*	Direction *x*	Direction *y*	Direction *x*	Direction *y*
5 – 6 × 6 – MRF	1.37 / 1.36	1.35 / 1.37	4.24 / 3.57	2.99 / 3.55	5.82 / 4.85	4.03 / 4.86
5 – 8 × 8 – MRF	1.41 / 1.38	1.36 / 1.27	4.43 / 3.70	2.68 / 2.76	6.25 / 5.11	3.65 / 3.50
5 – 6 × 6 – CBF	1.58 / 1.61	1.50 / 1.56	4.51 / 4.29	3.99 / 4.01	7.12 / 6.95	5.99 / 6.26
5 – 8 × 8 – CBF	1.53 / 1.61	1.52 / 1.57	4.88 / 4.34	4.84 / 4.69	7.46 / 7.79	7.36 / 7.69
5 – 6 × 6 – EBF	1.29 / 1.26	1.24 / 1.15	1.76 / 1.61	2.13 / 2.09	2.29 / 2.03	2.67 / 2.87
5 – 8 × 8 – EBF	1.25 / 1.32	1.24 / 1.15	2.24 / 2.15	2.02 / 2.62	2.80 / 2.84	2.51 / 3.02
10 – 6 × 6 – MRF	1.23 / 1.36	1.25 / 1.30	1.63 / 1.79	1.35 / 1.55	2.01 / 2.43	2.70 / 2.10
10 – 8 × 8 – MRF	1.25 / 1.29	1.28 / 1.28	1.59 / 2.65	1.73 / 1.34	1.99 / 3.42	2.21 / 1.72
10 – 6 × 6 – CBF	1.43 / 1.50	1.41 / 1.50	4.01 / 3.21	4.02 / 3.30	5.74 / 4.81	5.71 / 4.95
10 – 8 × 8 – CBF	1.54 / 1.53	1.55 / 1.45	1.96 / 1.29	2.80 / 2.39	3.03 / 2.00	4.34 / 3.46
10 – 6 × 6 – EBF	1.33 / 1.38	1.32 / 1.38	1.60 / 1.59	1.62 / 1.70	2.13 / 2.19	2.14 / 2.34
10 – 8 × 8 – EBF	1.29 / 1.39	1.17 / 1.19	2.12 / 2.75	1.97 / 1.66	2.74 / 3.82	2.31 / 1.99
15 – 6 × 6 – MRF	1.33 / 1.27	1.17 / 1.15	1.77 / 1.50	1.10 / 1.27	2.36 / 1.46	1.29 / 1.46
15 – 8 × 8 – MRF	1.32 / 1.30	1.37 / 1.22	1.20 / 1.35	1.24 / 2.01	1.60 / 1.75	1.70 / 2.47
15 – 6 × 6 – CBF	2.00 / 2.02	2.14 / 1.82	3.06 / 3.71	3.08 / 2.62	6.11 / 7.50	6.08 / 4.76
15 – 8 × 8 – CBF	1.70 / 1.89	2.35 / 2.49	6.66 / 2.73	2.62 / 2.43	6.23 / 5.16	6.16 / 6.04
15 – 6 × 6 – EBF	1.49 / 1.38	1.41 / 1.39	1.81 / 1.41	1.45 / 1.45	2.70 / 1.95	2.06 / 2.01
15 – 8 × 8 – EBF	1.42 / 1.30	2.37 / 1.24	1.38 / 1.44	2.09 / 1.36	3.39 / 1.87	2.91 / 1.69

(*) First / second values correspond to modal and uniform distributions, respectively

Comparison among the values of *R* in Table 5-16 with the assumed factors in Table 4-28 shows that, in 65% of the cases, the analyzed buildings do not possess the required ductility. In the MRF/CBF/EBF buildings, such percentage is 79/17/100%. In the 5/10/15-story buildings such percentage is 46/83/67%. For the Modal/Uniform distributions, the percentages are 67/64%. No relevant differences have been observed for *x/y* directions.

5.3.10 "Lacustre-300" Zone (new microzonation)

Figure 5-75, Figure 5-78 and Figure 5-81 display the capacity curves of the prototype buildings (Table 4-1) designed for the "Lacustre-300" Zone (new microzonation, Figure 3-7); Figure 5-75, Figure 5-78 and Figure 5-81 refer to the MRF, CBF and EBF buildings, respectively.

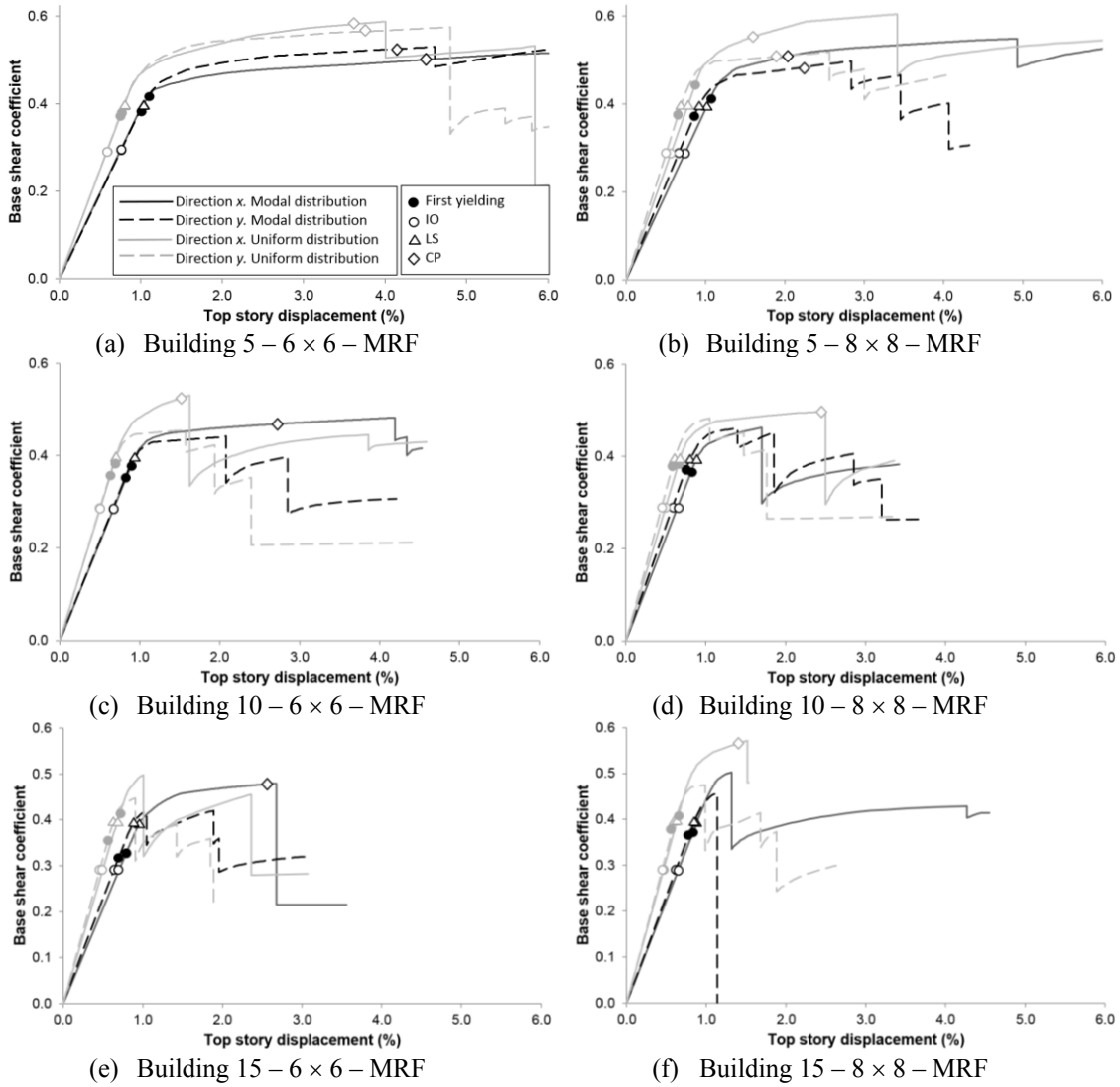

(a) Building 5 – 6 × 6 – MRF (b) Building 5 – 8 × 8 – MRF

(c) Building 10 – 6 × 6 – MRF (d) Building 10 – 8 × 8 – MRF

(e) Building 15 – 6 × 6 – MRF (f) Building 15 – 8 × 8 – MRF

Figure 5-75. Capacity curves and Target Drifts of buildings with Moment-Resisting Frames. Zone "Lacustre-300" (new microzonation, Figure 3-7)

Most of the results in Figure 5-75 are regular and expected; subsection 5.3.12 holds deeper conclusions issued globally for all the cases. Figure 5-75.f shows that, for the 15 – 8 × 8 – MRF prototype building (Table 4-1) in *x* direction, the push-over analysis under modal force distribution predicts less initial stiffness, similar force strength, and much higher displacement ductility than the analysis under constant force distribution. To further investigate this issue, Figure 5-76 and Figure 5-77 display the damage progression of the 15 – 8 × 8 – MRF prototype building in *x* direction designed for the "Lacustre-300" Zone (new microzonation, Figure 3-7).

Figure 5-76 and Figure 5-77 correspond to push-over analyses under modal and uniform force distribution, respectively (Figure 5-1).

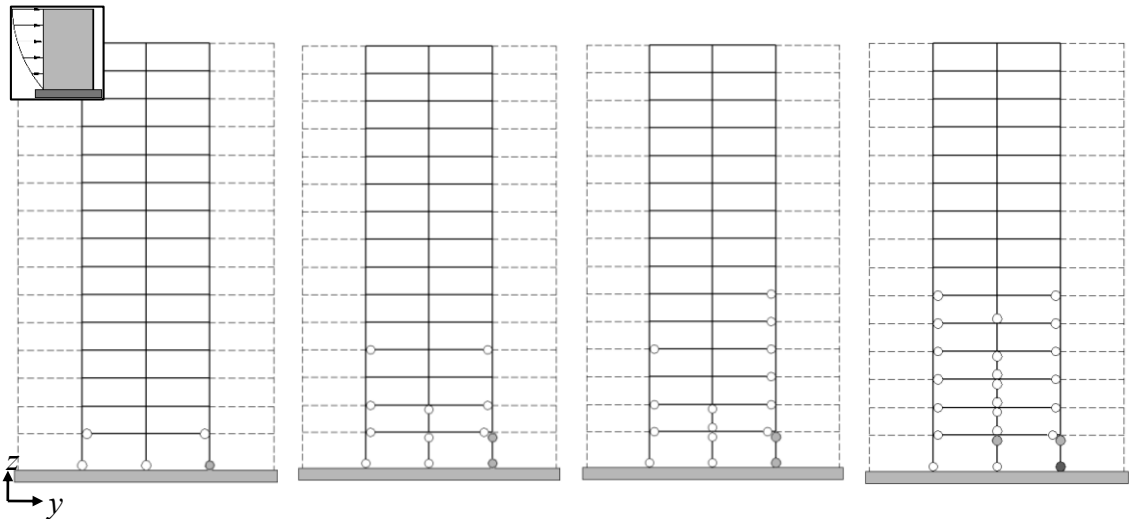

(a) Drift angle 1.06% (b) Drift angle 1.14% (c) Drift angle 1.21% (d) Drift angle 1.28%

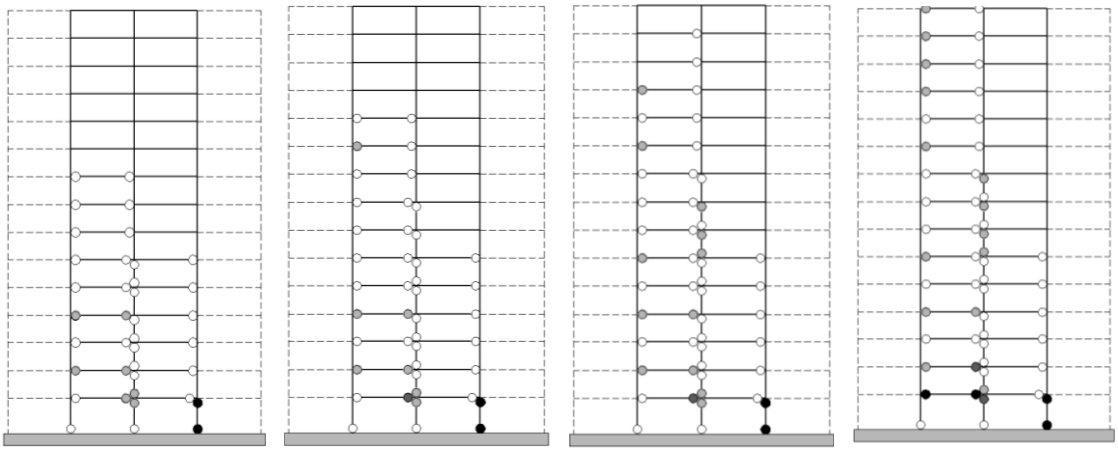

(e) Drift angle 1.94% (f) Drift angle 2.44% (g) Drift angle 3.06% (h) Drift angle 4.55%

Figure 5-76. Hinge progression sequence for the 15 – 8 × 8 – MRF building, modal distribution and *x* direction (right displacement). Zone "Lacustre-300" (new microzonation, Figure 3-7). ○: yielding, ○: IO, ●: LS, ●: CP [FEMA 356 2000]

In Figure 5-76, each frame has two seismic bays (see Figure 4-3). Figure 5-76 represents the damage, in terms of the progression of plastic hinges at the ends of beams and columns, for eight selected states corresponding to growing values of the drift angle. These values of the drift displacement have been chosen to highlight a number of characteristic points of the corresponding capacity curve (Figure 5-75.f), namely: onset of yielding (Figure 5-76.a), first sudden drop (Figure 5-76.d) and near collapse (Figure 5-76.h). Figure 5-76.h shows that the collapse mechanism involves all the floors although it is mainly concentrated in the bottom floor.

As in Figure 5-76, in Figure 5-77 each frame has two seismic bays. The growing values of the drift displacement have been chosen to highlight a number of characteristic points of the corresponding capacity curve (Figure 5-57.f), namely: onset of yielding (Figure 5-77.a), first sudden drop (Figure 5-75.f) and near collapse (Figure 5-77.h). Figure 5-77.h shows that the collapse mechanism involves the three bottom floors being mainly concentrated in the first floor columns.

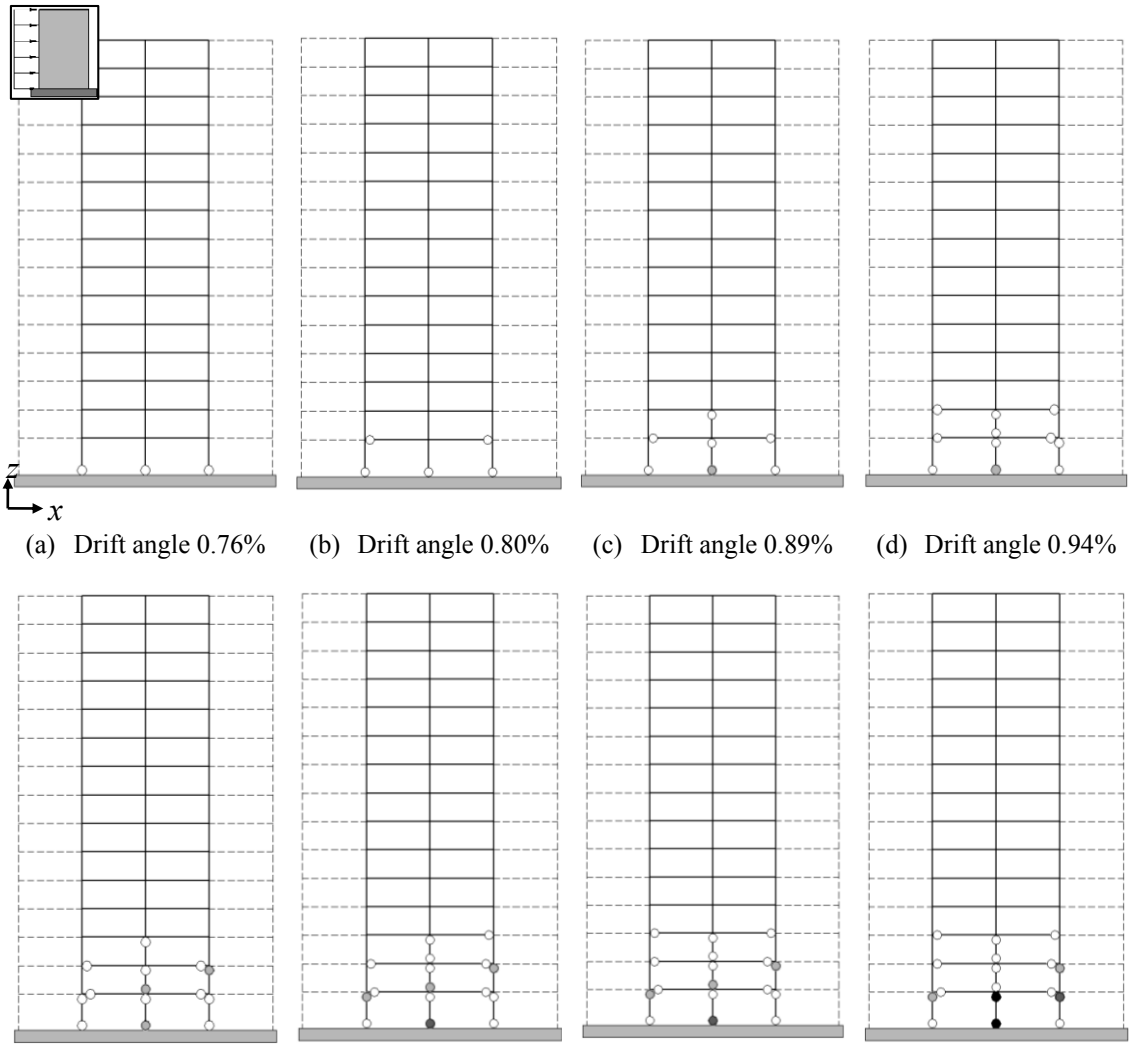

(a) Drift angle 0.76% (b) Drift angle 0.80% (c) Drift angle 0.89% (d) Drift angle 0.94%

(e) Drift angle 1.13% (f) Drift angle 1.31% (g) Drift angle 1.40% (h) Drift angle 1.53%

Figure 5-77. Hinge progression sequence for the 15 – 8 × 8 – MRF building, uniform distribution and *x* direction (right displacement). Zone "Lacustre-300" (new microzonation, Figure 3-7). ○: yielding, ◎: IO, ◉: LS, ●: CP [FEMA 356 2000]

Comparison between Figure 5-76 and Figure 5-77 shows that the collapse mechanisms for modal and uniform force distribution (Figure 5-76 and Figure 5-77, respectively) are very different: for modal distribution the plastic hinges are spread along the whole height of the building, while for uniform distribution the plastic hinges are mainly concentrated in the first floor columns; therefore, the mechanism for modal distribution is significantly more ductile. This difference between modal and uniform pushing forces is consistent with the shear forces and bending moments distribution (Figure 5-1).

As previously announced, Figure 5-78 displays the capacity curves of the prototype CBF buildings (Table 4-1) designed for the "Lacustre-300" Zone (new microzonation, Figure 3-7).

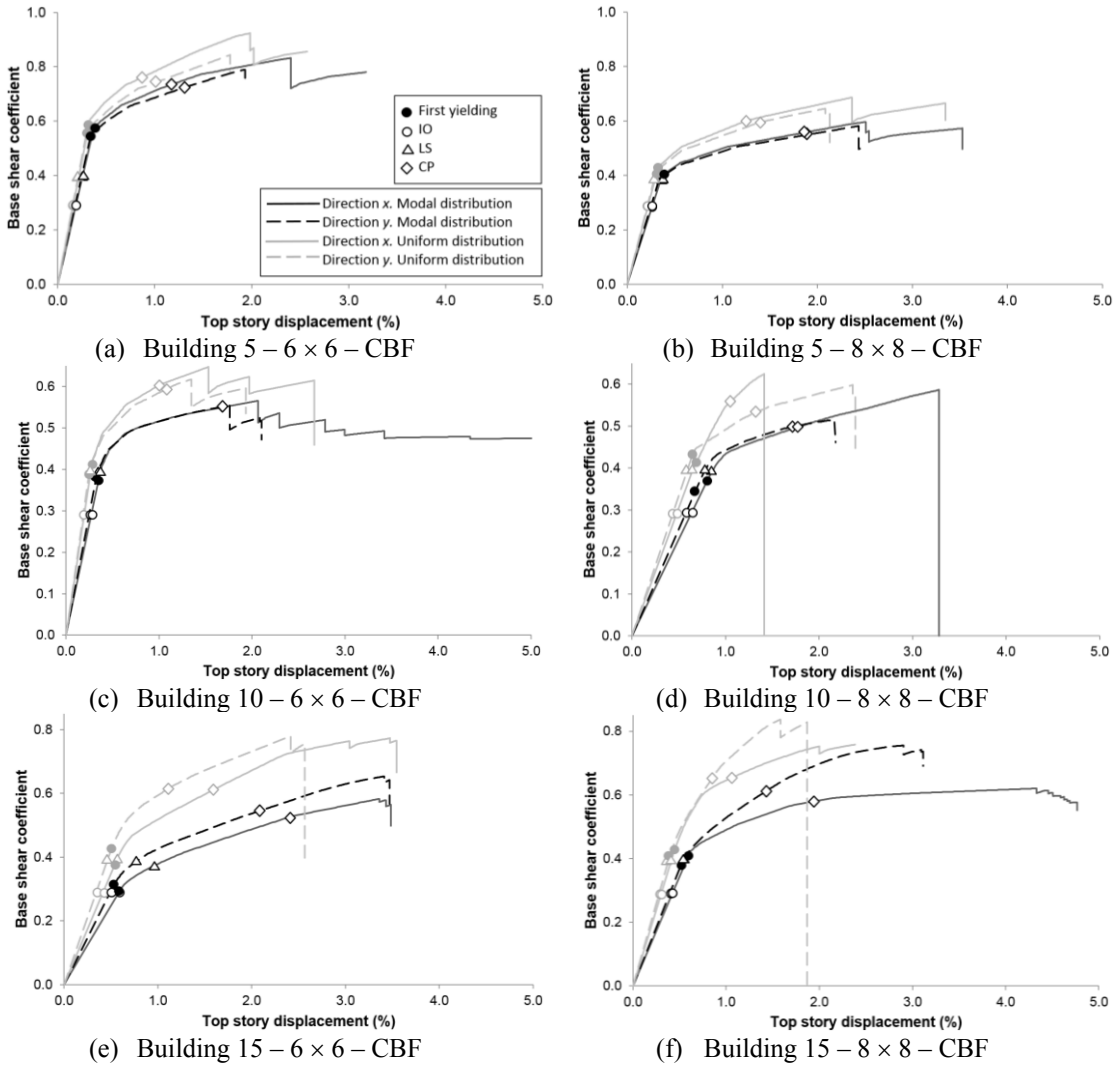

(a) Building 5 – 6 × 6 – CBF (b) Building 5 – 8 × 8 – CBF

(c) Building 10 – 6 × 6 – CBF (d) Building 10 – 8 × 8 – CBF

(e) Building 15 – 6 × 6 – CBF (f) Building 15 – 8 × 8 – CBF

Figure 5-78. Capacity curves and Target Drifts of buildings with Concentric-Braced Frames. Zone "Lacustre-300" (new microzonation, Figure 3-7)

Most of the results in Figure 5-78 are regular and expected, thus illustrating the reliability and accuracy of the carried out analysis; subsection 5.3.12 holds deeper conclusions that are issued globally for all the cases. However, Figure 5-78.c shows that, for the 10 – 6 × 6 – CBF prototype building (Table 4-1) in *x* direction, the push-over analysis under modal force distribution predicts less initial stiffness and less force strength, whereas that analysis also predicts higher displacement ductility than the analysis under constant force distribution. To further investigate this issue, Figure 5-79 and Figure 5-80 display the damage progression of the 10 – 6 × 6 – CBF prototype building in *x* direction designed for the "Lacustre-300" Zone (new microzonation, Figure 3-7). Figure 5-79 and Figure 5-80 correspond to push-over analyses under modal and uniform force distribution, respectively (Figure 5-1).

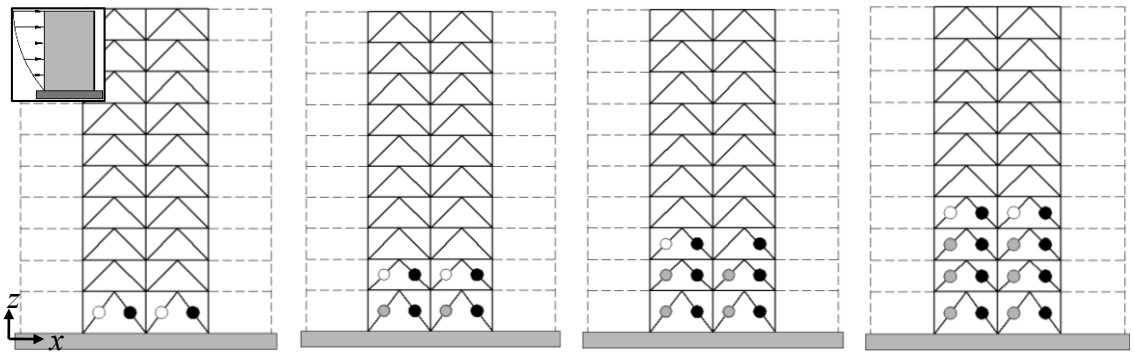

(a) Drift angle 0.39% (b) Drift angle 0.49% (c) Drift angle 0.63% (d) Drift angle 0.77%

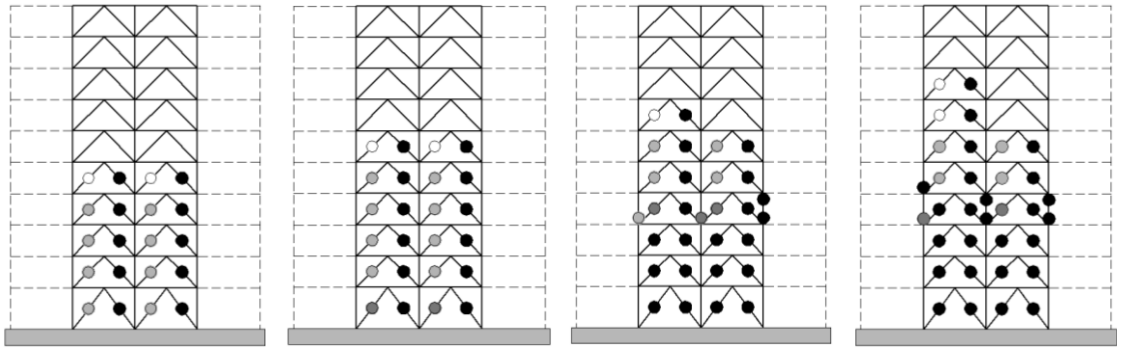

(e) Drift angle 1.13% (f) Drift angle 1.49% (g) Drift angle 3.29% (h) Drift angle 5.36%

Figure 5-79. Hinge progression sequence for the 10 – 6 × 6 – CBF building, modal distribution and *x* direction (right displacement). Zone "Lacustre-300" (new microzonation, Figure 3-7). ○: yielding, ◎: IO, ◉: LS, ●: CP [FEMA 356 2000]

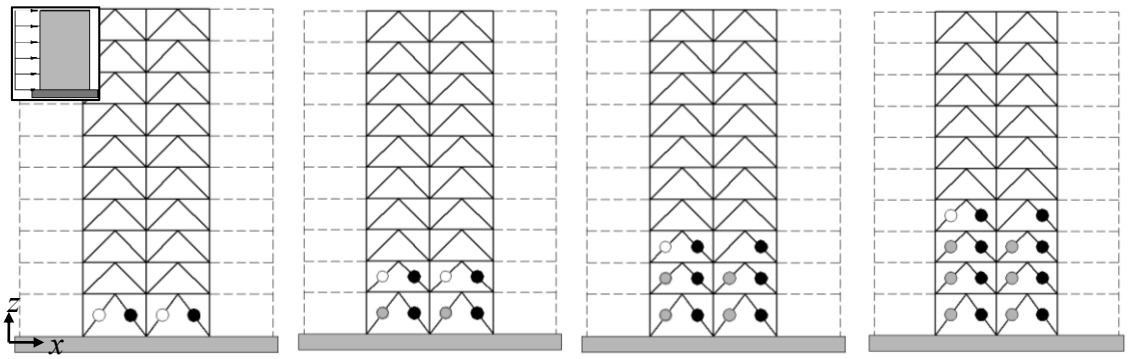

(a) Drift angle 0.29% (b) Drift angle 0.40% (c) Drift angle 0.64% (d) Drift angle 1.00%

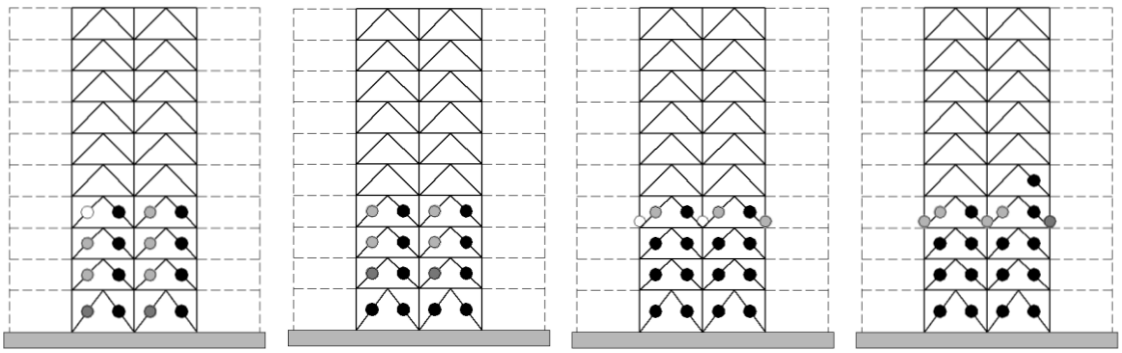

(e) Drift angle 1.13% (f) Drift angle 1.49% (g) Drift angle 2.52% (h) Drift angle 2.67%

Figure 5-80. Hinge progression sequence for the 10 – 6 × 6 – CBF building, uniform distribution and *x* direction (right displacement). Zone "Lacustre-300" (new microzonation, Figure 3-7). ○: yielding, ◎: IO, ◉: LS, ●: CP [FEMA 356 2000]

Comparison between Figure 5-79 and Figure 5-80 shows that, both under modal and uniform force distributions, the collapse mechanisms involve hinges in most of the levels of the building (noticeably, even in the top one); nevertheless, for uniform distribution (Figure 5-80) the hinges concentrate more in the lowest levels. This difference between modal and uniform pushing forces is consistent with the corresponding distribution laws of shear forces and bending moments along the height of the building (Figure 5-1).

As previously announced, Figure 5-81 displays the capacity curves of the prototype EBF buildings (Table 4-1) designed for the "Lacustre-300" Zone (new microzonation, Figure 3-7).

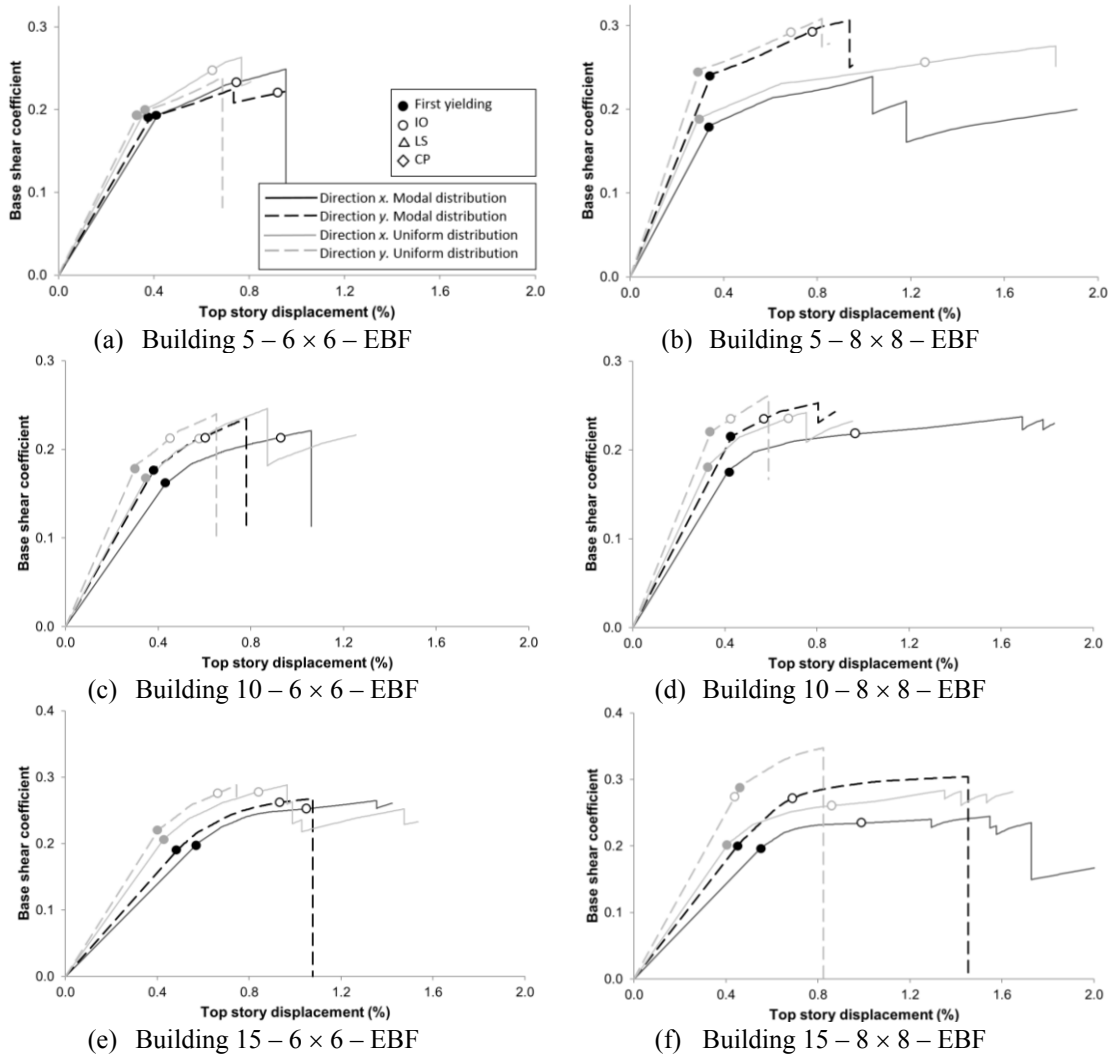

(a) Building 5 – 6 × 6 – EBF (b) Building 5 – 8 × 8 – EBF

(c) Building 10 – 6 × 6 – EBF (d) Building 10 – 8 × 8 – EBF

(e) Building 15 – 6 × 6 – EBF (f) Building 15 – 8 × 8 – EBF

Figure 5-81. Capacity curves and Target Drifts of buildings with Eccentric-Braced Frames. Zone "Lacustre-300" (new microzonation, Figure 3-7)

Most of the results in Figure 5-81 are regular and expected; subsection 5.3.12 holds deeper conclusions issued globally for all the cases. However, Figure 5-81.d shows that, for the 10 – 8 × 8 – EBF prototype building (Table 4-1) in *x* direction, the push-over analysis under modal force distribution predicts less initial stiffness and similar force strength, whereas that analysis predicts significantly higher displacement ductility than the analysis under constant force distribution. To further investigate this issue, Figure 5-82 and Figure 5-83 display the damage progression of the 10 – 8 × 8 – EBF prototype building in *x* direction designed for the "Lacustre-300" Zone (new microzonation, Figure 3-7). Figure 5-82 and Figure 5-83 correspond to push-over analyses under modal and uniform force distribution, respectively (Figure 5-1).

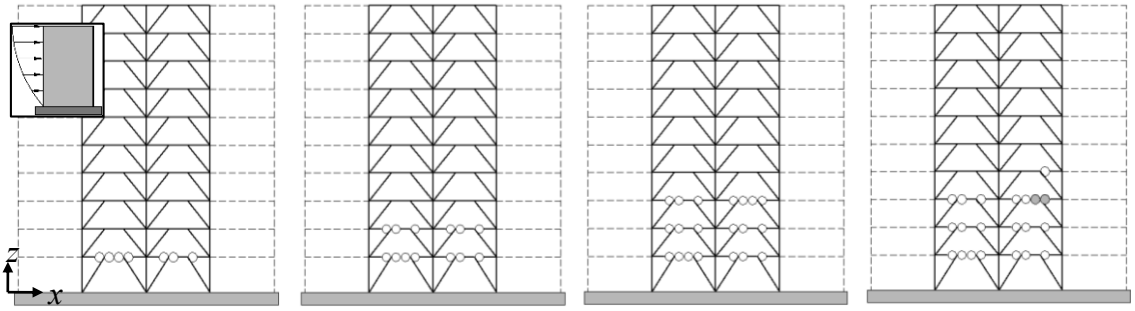

(a) Drift angle 0.51% (b) Drift angle 0.60% (c) Drift angle 0.71% (d) Drift angle 0.88%

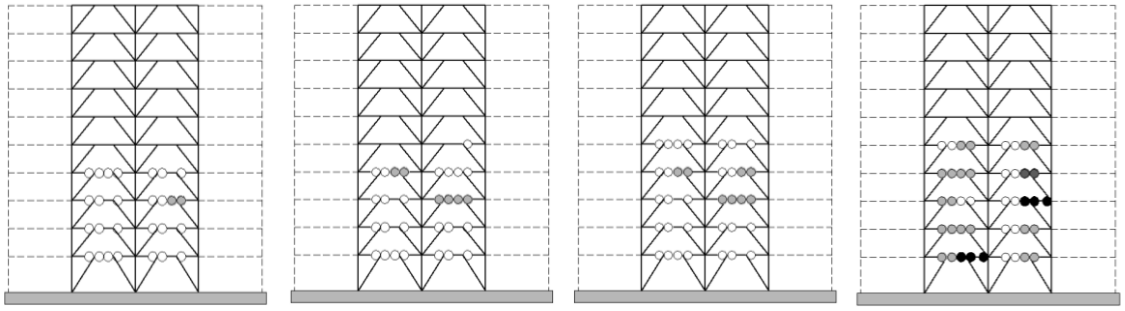

(e) Drift angle 0.90% (f) Drift angle 1.28% (g) Drift angle 1.32% (h) Drift angle 1.83%

Figure 5-82. Hinge progression sequence for the 10 – 8 × 8 – EBF building, modal distribution and *x* direction (right displacement). Zone "Lacustre-300" (new microzonation, Figure 3-7). ○: yielding, ◎: IO, ◉: LS, ●: CP [FEMA 356 2000]

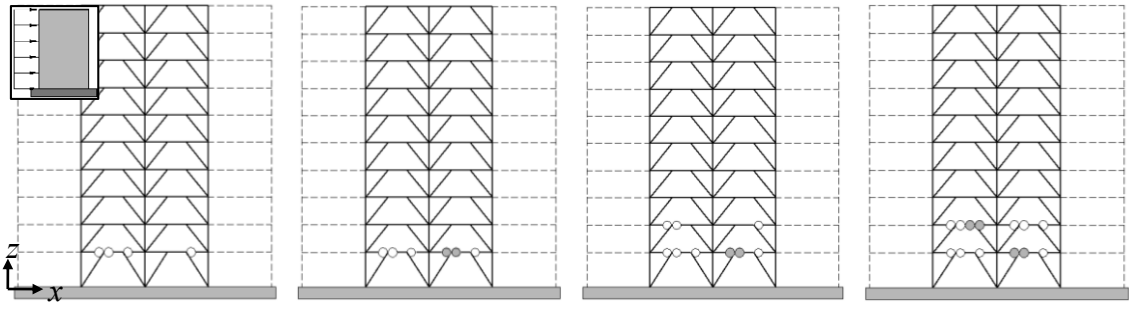

(a) Drift angle 0.33% (b) Drift angle 0.40% (c) Drift angle 0.46% (d) Drift angle 0.55%

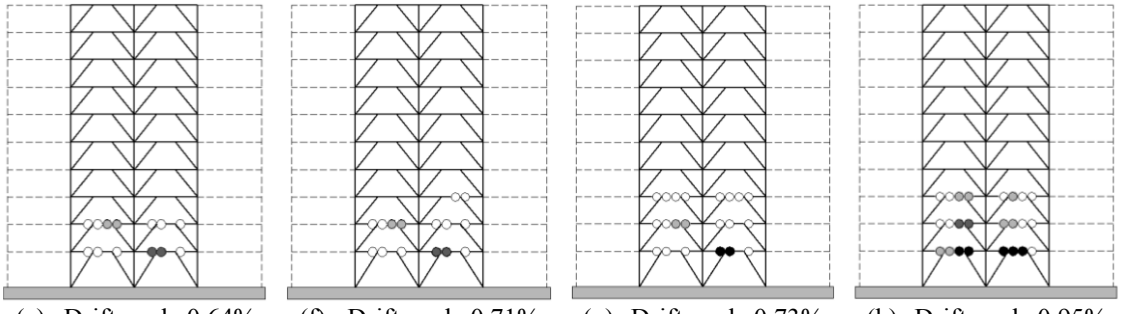

(e) Drift angle 0.64% (f) Drift angle 0.71% (g) Drift angle 0.73% (h) Drift angle 0.95%

Figure 5-83. Hinge progression sequence for the 10 – 8 × 8 – EBF building, uniform distribution and *x* direction (right displacement). Zone "Lacustre-300" (new microzonation, Figure 3-7). ○: yielding, ◎: IO, ◉: LS, ●: CP [FEMA 356 2000]

Comparison between Figure 5-82 and Figure 5-83 shows that under modal force distribution (Figure 5-82), the collapse mechanism involves hinges up to the fifth level of the building, although for uniform distribution (Figure 5-83), the hinges concentrate only in the link segments of the three bottom floors. This difference between modal and uniform pushing forces is consistent with the corresponding shear forces and bending moments distribution along the height

of the building (Figure 5-1).

Table 5-17 and Table 5-18 display, respectively, the seismic performance and the response reduction factor (R, Ω and R_d) of the prototype buildings (Table 4-1) designed for the "Lacustre-300" Zone (new microzonation, Figure 3-7).

Table 5-17. Seismic performance. "Lacustre-300" zone (new microzonation)

Building	Target Drift IO(*)		Target Drift LS(*)		Target Drift CP(*)	
	Direction x	Direction y	Direction x	Direction y	Direction x	Direction y
5 – 6 × 6 – MRF	YES / YES	YES / YES	YES / YES	YES / YES	YES / YES	YES / YES
5 – 8 × 8 – MRF	YES / YES	YES / YES	YES / YES	YES / YES	YES / YES	YES / YES
5 – 6 × 6 – CBF	YES / YES	YES / YES	YES / YES	YES / YES	YES / YES	YES / YES
5 – 8 × 8 – CBF	YES / YES	YES / YES	YES / YES	YES / YES	YES / YES	YES / YES
5 – 6 × 6 – EBF	**NO** / **NO**	**NO** / -	- / -	- / -	- / -	- / -
5 – 8 × 8 – EBF	**-** / **NO**	**NO** / **NO**	- / -	- / -	- / -	- / -
10 – 6 × 6 – MRF	YES / YES	YES / YES	YES / YES	YES / YES	YES / YES	- / -
10 – 8 × 8 – MRF	YES / YES	YES / YES	YES / YES	YES / YES	- / YES	- / -
10 – 6 × 6 – CBF	YES / YES	YES / YES	YES / YES	YES / YES	YES / YES	YES / YES
10 – 8 × 8 – CBF	YES / YES	YES / YES	**NO** / **NO**	YES / YES	YES / **NO**	YES / **NO**
10 – 6 × 6 – EBF	**NO** / **NO**	**NO** / YES	- / -	- / -	- / -	- / -
10 – 8 × 8 – EBF	**NO** / **NO**	**NO** / **NO**	- / -	- / -	- / -	- / -
15 – 6 × 6 – MRF	YES / YES	YES / YES	YES / YES	YES / **NO**	YES / -	- / -
15 – 8 × 8 – MRF	YES / YES	YES / YES	YES / YES	YES / YES	- / YES	- / -
15 – 6 × 6 – CBF	YES / YES	YES / YES	YES / YES	YES / YES	YES / YES	YES / YES
15 – 8 × 8 – CBF	YES / YES	YES / YES	YES / YES	YES / YES	YES / YES	YES / YES
15 – 6 × 6 – EBF	**NO** / **NO**	**NO** / **NO**	- / -	- / -	- / -	- / -
15 – 8 × 8 – EBF	**NO** / **NO**	**NO** / YES	- / -	- / -	- / -	- / -

(*) First / second values correspond to modal and uniform distributions, respectively

Table 5-17 reveals that 60% of the cases exhibit a satisfactory performance (YES), 12% unsatisfactory (NO) and 28% highly unsatisfactory (-). In the MRF/CBF/EBF buildings, such percentages are 84/94/2%, 1/6/29% and 15/0/69%. In the 5/10/15-story buildings such percentages are 67/54/58%, 8/17/11% and 25/29/31%. For the IO/LS/CP limit states, the percentages are 68/63/50%, 29/4/3% and 3/33/47%. For the Modal/Uniform distributions, the percentages are 60/59%, 11/13% and 29/28%. No relevant differences have been observed for *x/y* directions.

Table 5-18**.** Response reduction factor R in the x / y directions. "Lacustre-300" zone (new microzonation)

Building	Over-strength factor (Ω)(*)		Ductility factor R_d(*)		R factor ($R = \Omega R_d$) (*)	
	Direction x	Direction y	Direction x	Direction y	Direction x	Direction y
5 – 6 × 6 – MRF	1.35 / 1.58	1.27 / 1.50	4.47 / 3.34	3.31 / 4.19	6.04 / 5.27	4.20 / 6.28
5 – 8 × 8 – MRF	1.34 / 1.37	1.33 / 1.36	3.42 / 2.85	2.46 / 2.84	4.58 / 3.90	3.27 / 3.89
5 – 6 × 6 – CBF	1.45 / 1.57	1.46 / 1.51	4.30 / 4.10	3.85 / 3.88	6.24 / 6.44	5.62 / 5.86
5 – 8 × 8 – CBF	1.48 / 1.60	1.44 / 1.60	4.35 / 4.78	4.33 / 4.22	6.44 / 7.65	6.23 / 6.76
5 – 6 × 6 – EBF	2.06 / 1.32	1.30 / 1.22	2.01 / 1.61	1.96 / 1.73	4.14 / 2.12	2.55 / 2.10
5 – 8 × 8 – EBF	1.34 / 1.63	1.28 / 1.27	2.25 / 3.94	2.16 / 2.23	3.02 / 6.43	2.76 / 2.83
10 – 6 × 6 – MRF	1.29 / 1.39	1.26 / 1.28	3.62 / 1.67	2.01 / 1.95	4.67 / 2.33	2.53 / 2.50
10 – 8 × 8 – MRF	1.26 / 1.30	1.24 / 1.28	1.63 / 2.91	1.49 / 1.43	2.05 / 3.78	1.86 / 1.83
10 – 6 × 6 – CBF	1.51 / 1.57	1.45 / 1.59	3.72 / 3.54	3.70 / 3.40	5.62 / 5.55	5.36 / 5.40
10 – 8 × 8 – CBF	1.58 / 1.50	1.49 / 1.37	2.55 / 1.34	2.16 / 2.66	4.03 / 2.02	3.22 / 3.65
10 – 6 × 6 – EBF	1.36 / 1.48	1.32 / 1.34	1.81 / 1.70	1.55 / 1.63	2.46 / 2.52	2.04 / 2.19
10 – 8 × 8 – EBF	1.37 / 1.34	1.18 / 1.19	2.93 / 1.72	1.59 / 1.46	4.02 / 2.32	1.88 / 1.73
15 – 6 × 6 – MRF	1.48 / 1.21	1.31 / 1.26	2.26 / 1.16	1.15 / 1.29	3.35 / 1.40	1.50 / 1.62
15 – 8 × 8 – MRF	1.35 / 1.41	1.25 / 1.25	1.16 / 1.64	1.18 / 1.45	1.57 / 2.31	1.47 / 1.81
15 – 6 × 6 – CBF	1.98 / 2.06	2.08 / 1.82	2.83 / 3.10	3.08 / 2.64	5.64 / 6.39	6.41 / 4.81
15 – 8 × 8 – CBF	1.53 / 1.79	2.00 / 2.06	4.75 / 2.97	2.81 / 2.01	7.26 / 5.31	5.61 / 4.14
15 – 6 × 6 – EBF	1.34 / 1.42	1.41 / 1.31	1.78 / 1.58	1.57 / 1.42	2.38 / 2.24	2.22 / 1.86
15 – 8 × 8 – EBF	1.26 / 1.40	1.53 / 1.21	2.21 / 2.51	2.10 / 1.49	2.79 / 3.52	3.22 / 1.79

(*) First / second values correspond to modal and uniform distributions, respectively

Comparison among the values of R in Table 5-18 with the assumed factors in Table 4-29 shows that, in 67% of the cases, the analyzed buildings do not possess the required ductility. In the MRF/CBF/EBF buildings, such percentage is 79/21/100%. In the 5/10/15-story buildings such percentage is 50/79/71%. For the Modal/Uniform distributions, the percentages are 64/69%. No relevant differences have been observed for *x/y* directions.

5.3.11 "Lacustre-500" Zone (new microzonation)

Figure 5-84, Figure 5-87 and Figure 5-90 display the capacity curves of the prototype buildings (Table 4-1) designed for the "Lacustre-500" Zone (new microzonation, Figure 3-7); Figure 5-84, Figure 5-87 and Figure 5-90 refer to the MRF, CBF and EBF buildings, respectively.

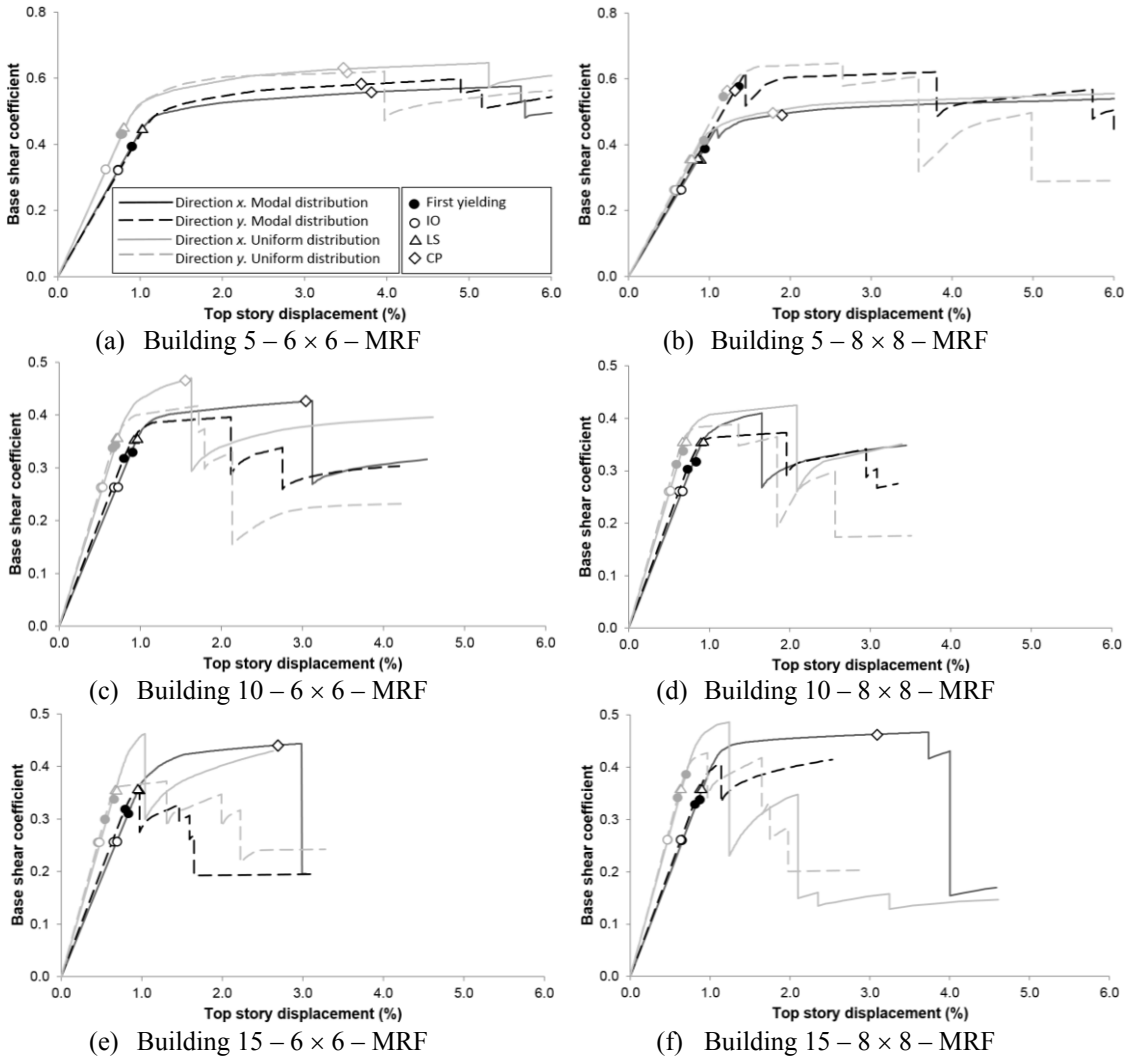

(a) Building 5 – 6 × 6 – MRF (b) Building 5 – 8 × 8 – MRF

(c) Building 10 – 6 × 6 – MRF (d) Building 10 – 8 × 8 – MRF

(e) Building 15 – 6 × 6 – MRF (f) Building 15 – 8 × 8 – MRF

Figure 5-84. Capacity curves and Target Drifts of buildings with Moment-Resisting Frames. Zone "Lacustre-500" (new microzonation, Figure 3-7)

Most of the results in Figure 5-84 are regular and expected; subsection 5.3.12 holds deeper conclusions issued globally for all the cases. Figure 5-84.c shows that, for the 15 – 8 × 8 – MRF prototype building (Table 4-1) in *x* direction, the push-over analysis under modal force distribution predicts less initial stiffness, similar force strength, and similar displacement ductility than the analysis under constant force distribution. To further investigate this issue, Figure 5-85 and Figure 5-86 display the damage progression of the 10 – 6 × 6 – MRF prototype building in *x* direction designed for the "Lacustre-500" Zone (new microzonation, Figure 3-7). Figure 5-85 and Figure 5-86 correspond to push-over analyses under modal and uniform force distribution, respectively (Figure 5-1).

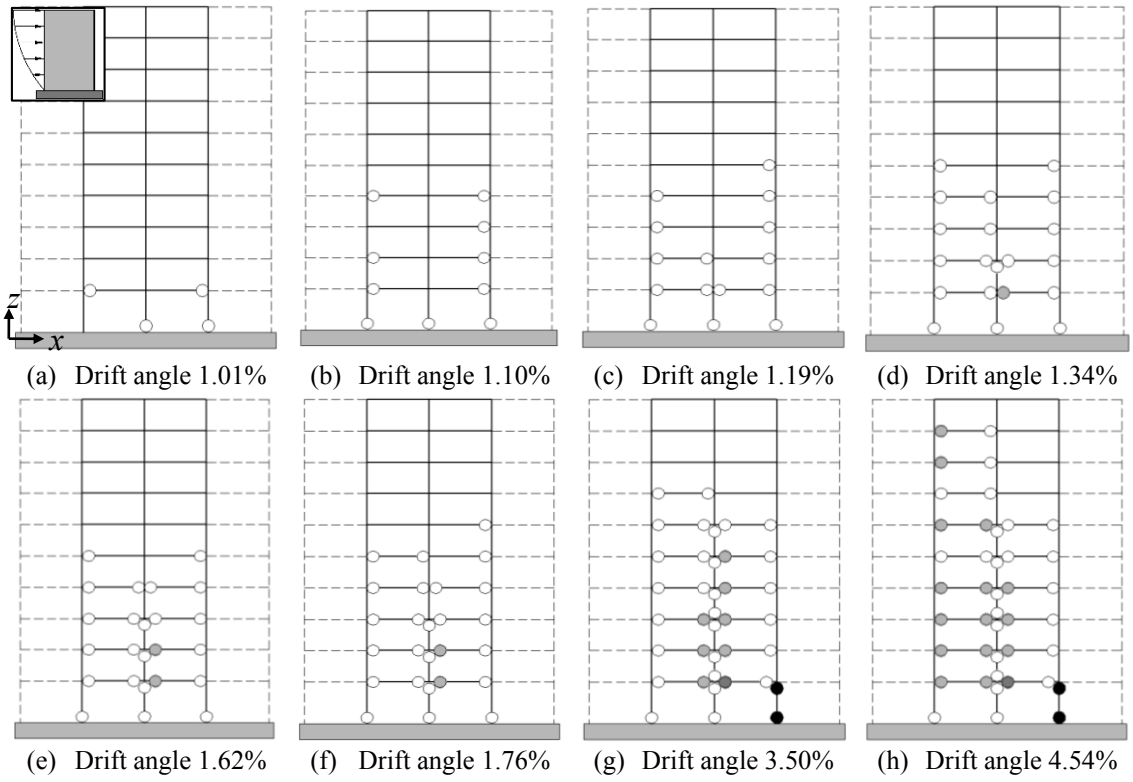

(a) Drift angle 1.01% (b) Drift angle 1.10% (c) Drift angle 1.19% (d) Drift angle 1.34%

(e) Drift angle 1.62% (f) Drift angle 1.76% (g) Drift angle 3.50% (h) Drift angle 4.54%

Figure 5-85. Hinge progression sequence for the 10 – 6 × 6 – MRF building, modal distribution and *x* direction (right displacement). Zone "Lacustre-500" (new microzonation, Figure 3-7). ○: yielding, ◎: IO, ◉: LS, ●: CP [FEMA 356 2000]

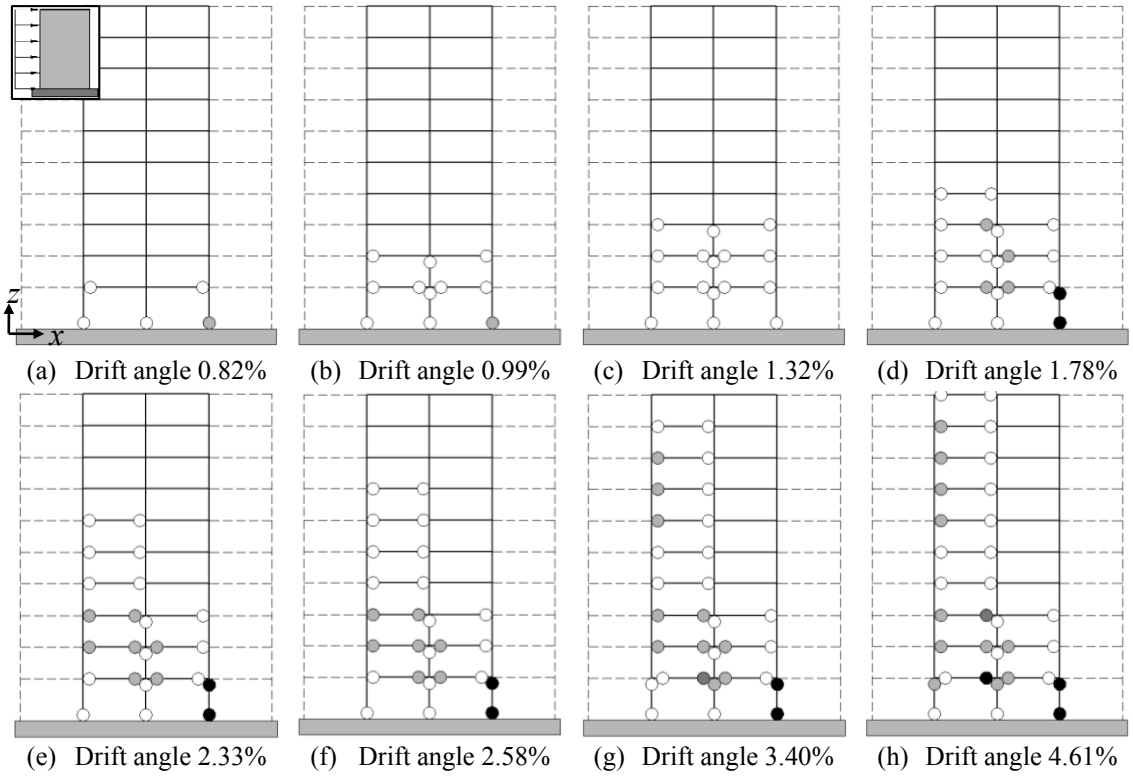

(a) Drift angle 0.82% (b) Drift angle 0.99% (c) Drift angle 1.32% (d) Drift angle 1.78%

(e) Drift angle 2.33% (f) Drift angle 2.58% (g) Drift angle 3.40% (h) Drift angle 4.61%

Figure 5-86. Hinge progression sequence for the 10 – 6 × 6 – MRF building, uniform distribution and *x* direction (right displacement). Zone "Lacustre-500" (new microzonation, Figure 3-7). ○: yielding, ◎: IO, ◉: LS, ●: CP [FEMA 356 2000]

Comparison between Figure 5-85 and Figure 5-86 shows that the collapse mechanisms for modal and uniform force distribution (Figure 5-85 and Figure 5-86, respectively) are different: for both distributions they extend along the whole height of the building but for uniform distribution the plastic hinges are mainly concentrated in the lowest columns; therefore, the mechanism for modal distribution is more ductile. This difference between modal and uniform pushing forces is consistent with the shear forces and bending moments distribution (Figure 5-1).

As previously announced, Figure 5-87 displays the capacity curves of the prototype CBF buildings (Table 4-1) designed for the "Lacustre-500" Zone (new microzonation, Figure 3-7).

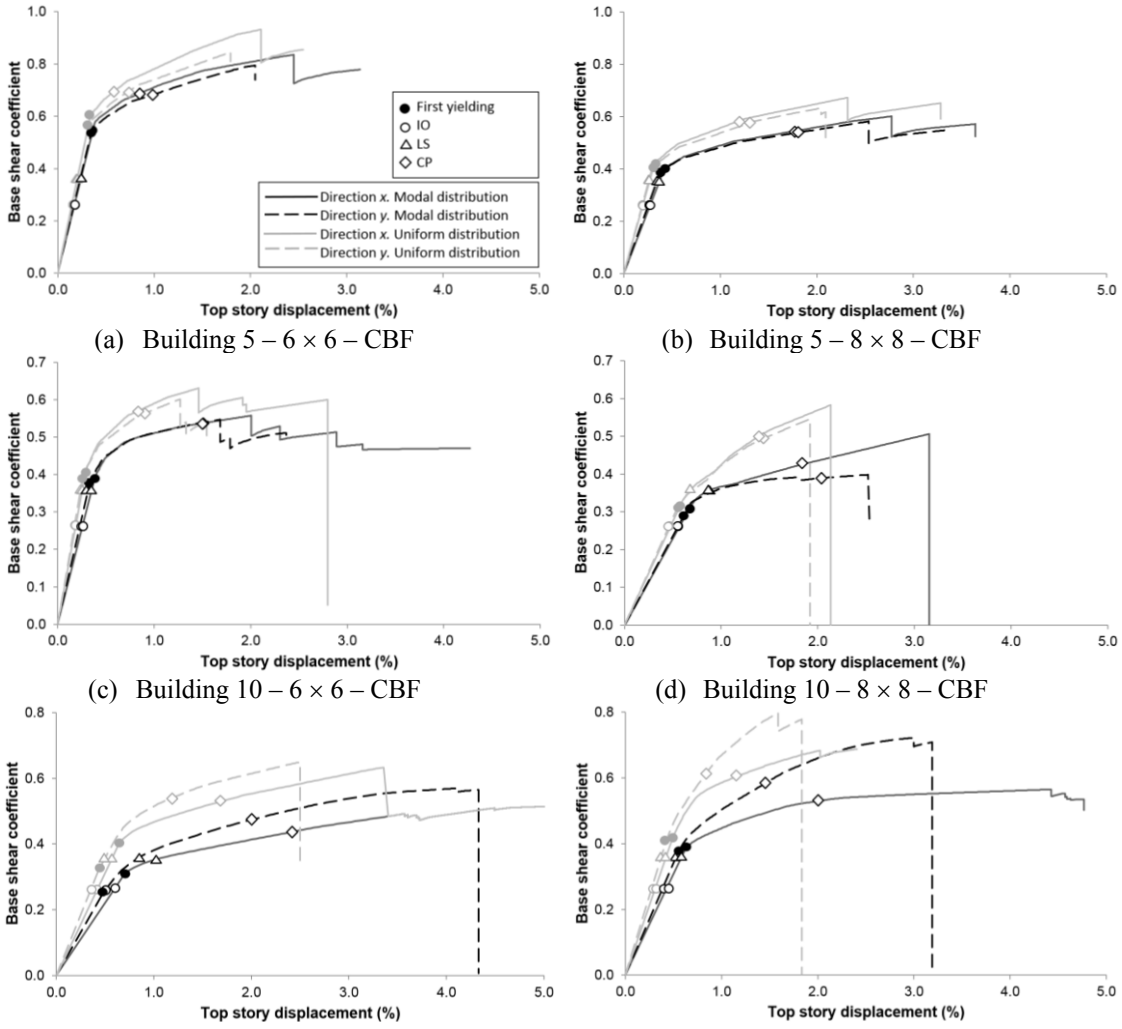

(a) Building 5 – 6 × 6 – CBF (b) Building 5 – 8 × 8 – CBF

(c) Building 10 – 6 × 6 – CBF (d) Building 10 – 8 × 8 – CBF

(e) Building 15 – 6 × 6 – CBF (f) Building 15 – 8 × 8 – CBF

Figure 5-87. Capacity curves and Target Drifts of buildings with Concentric-Braced Frames. Zone "Lacustre-500" (new microzonation, Figure 3-7)

Most of the results in Figure 5-87 are regular and expected, thus illustrating the reliability and accuracy of the carried out analysis; subsection 5.3.12 holds deeper conclusions that are issued globally for all the cases. However, Figure 5-87.c shows that, for the 10 – 6 × 6 – CBF prototype building (Table 4-1) in *y* direction, the push-over analysis under modal force distribution predicts less initial stiffness and force strength, but higher displacement ductility than the analysis under constant force distribution. To further investigate this issue, Figure 5-88 and Figure 5-89 display the damage progression of the 10 – 6 × 6 – CBF prototype building in *y* direction designed for the "Lacustre-500" Zone (new microzonation, Figure 3-7). Figure 5-88 and Figure 5-89 correspond to push-over analyses under modal and uniform force distribution, respectively (Figure 5-1).

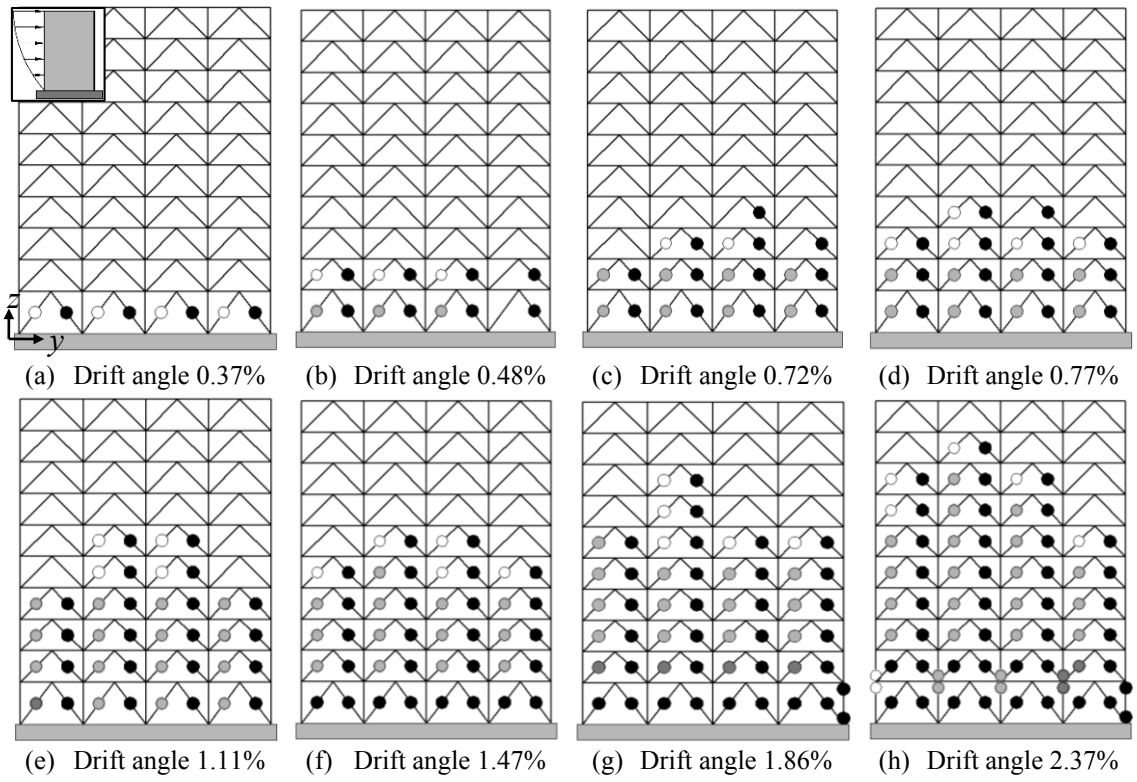

(a) Drift angle 0.37% (b) Drift angle 0.48% (c) Drift angle 0.72% (d) Drift angle 0.77%

(e) Drift angle 1.11% (f) Drift angle 1.47% (g) Drift angle 1.86% (h) Drift angle 2.37%

Figure 5-88. Hinge progression sequence for the 10 – 6 × 6 – CBF building, modal distribution and *y* direction (right displacement). Zone "Lacustre-500" (new microzonation, Figure 3-7). ○: yielding, ◍: IO, ●: LS, ●: CP [FEMA 356 2000]

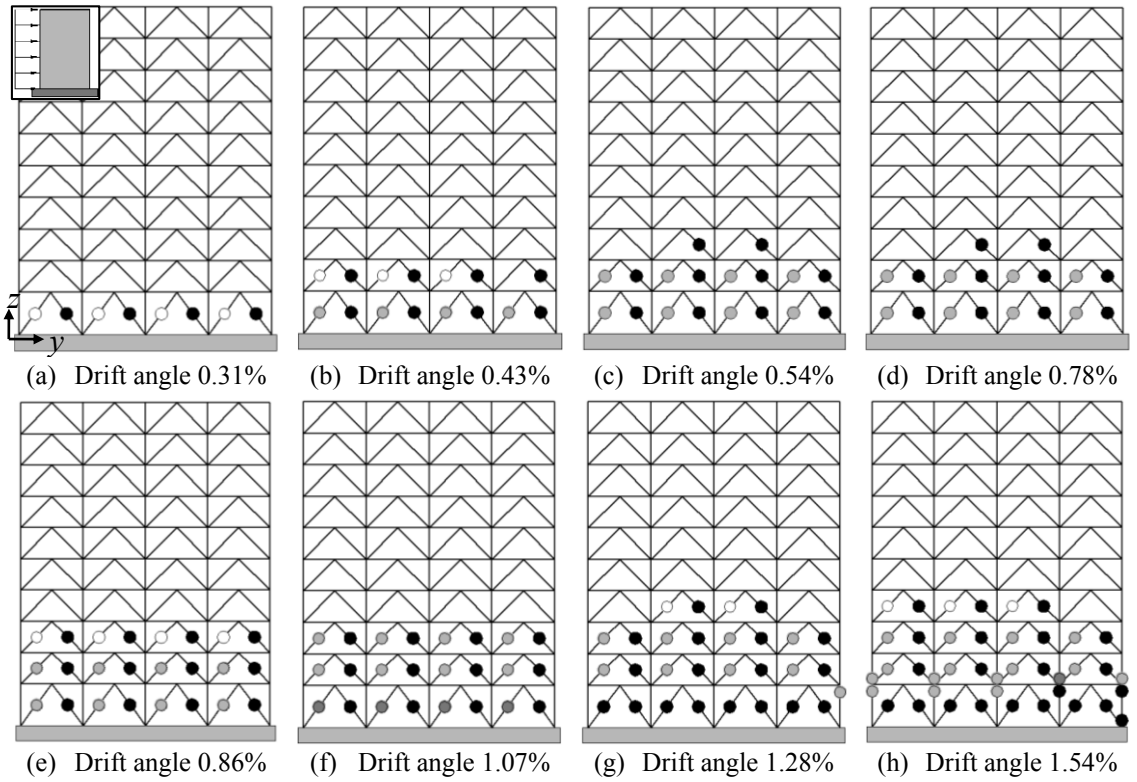

(a) Drift angle 0.31% (b) Drift angle 0.43% (c) Drift angle 0.54% (d) Drift angle 0.78%

(e) Drift angle 0.86% (f) Drift angle 1.07% (g) Drift angle 1.28% (h) Drift angle 1.54%

Figure 5-89. Hinge progression sequence for the 10 – 6 × 6 – CBF building, uniform distribution and *y* direction (right displacement). Zone "Lacustre-500" (new microzonation, Figure 3-7). ○: yielding, ◍: IO, ●: LS, ●: CP [FEMA 356 2000]

Comparison between Figure 5-88 and Figure 5-89 shows that, under modal force distribution (Figure 5-88), the collapse mechanism involves hinges in almost all of the levels of the building; nevertheless, for uniform distribution (Figure 5-89), the hinges concentrate more in the lowest levels, reaching only the fourth one. This difference between modal and uniform pushing forces is consistent with the corresponding distribution laws of shear forces and bending moments along the height of the building (Figure 5-1).

As previously announced, Figure 5-90 displays the capacity curves of the prototype EBF buildings (Table 4-1) designed for the "Lacustre-500" Zone (new microzonation, Figure 3-7).

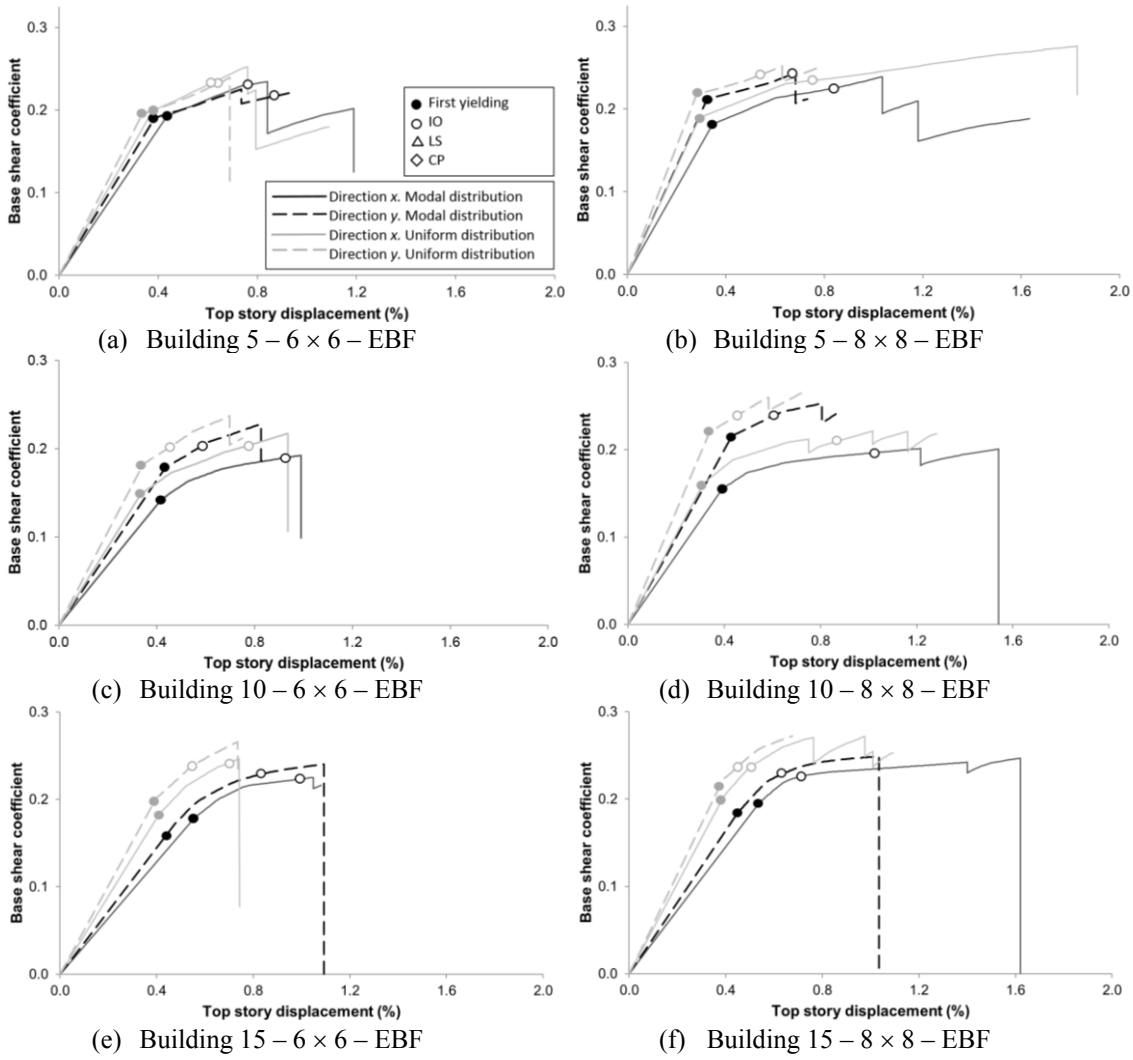

(a) Building 5 – 6 × 6 – EBF (b) Building 5 – 8 × 8 – EBF

(c) Building 10 – 6 × 6 – EBF (d) Building 10 – 8 × 8 – EBF

(e) Building 15 – 6 × 6 – EBF (f) Building 15 – 8 × 8 – EBF

Figure 5-90. Capacity curves and Target Drifts of buildings with Eccentric-Braced Frames. Zone "Lacustre-500" (new microzonation, Figure 3-7)

Most of the results in Figure 5-90 are regular and expected; subsection 5.3.12 holds deeper conclusions issued globally for all the cases. However, Figure 5-90.f shows that, for the 15 – 8 × 8 – EBF prototype building (Table 4-1) in *x* direction, the push-over analysis under modal force distribution predicts less initial stiffness and force strength, whereas that analysis predicts significantly higher displacement ductility than the analysis under constant force distribution. To further investigate this issue, Figure 5-91 and Figure 5-92 display the damage progression of the 15 – 8 × 8 – EBF prototype building in *x* direction designed for the "Lacustre-500" Zone (new microzonation, Figure 3-7). Figure 5-91 and Figure 5-83 correspond to push-over analyses under modal and uniform force distribution, respectively (Figure 5-1).

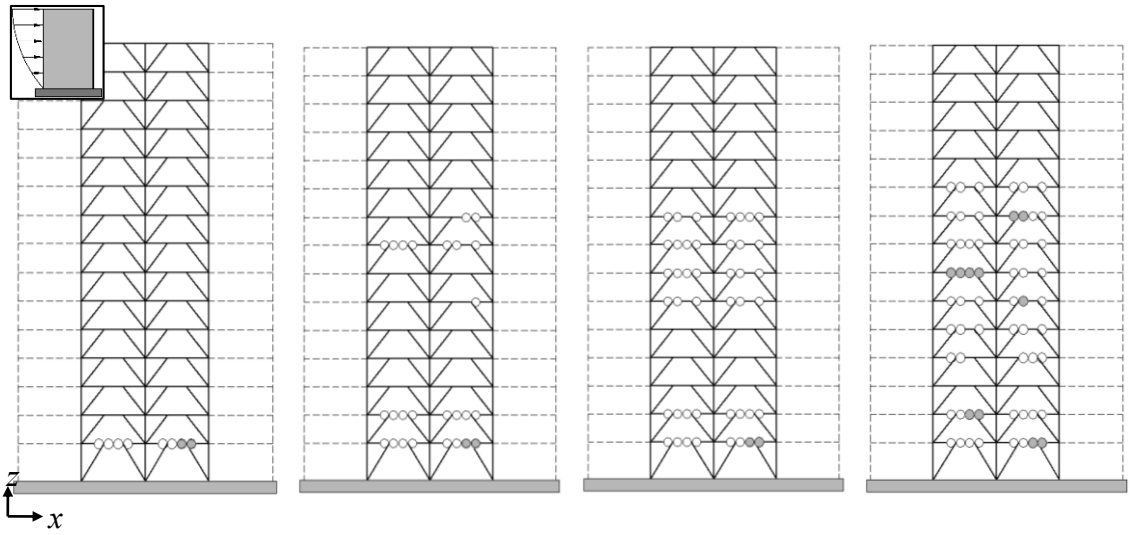

(a) Drift angle 0.60% (b) Drift angle 0.65% (c) Drift angle 0.71% (d) Drift angle 0.78%

(e) Drift angle 0.85% (f) Drift angle 1.14% (g) Drift angle 1.37% (h) Drift angle 1.62%

Figure 5-91. Hinge progression sequence for the 15 – 8 × 8 – EBF building, modal distribution and *x* direction (right displacement). Zone "Lacustre-500" (new microzonation, Figure 3-7). ○: yielding, ◎: IO, ◉: LS, ●: CP [FEMA 356 2000]

Figure 5-91 shows that the plastic hinges appear mainly in the link segments of the beams, as expected. No column experiences any serious damage. This fact can be read again as a fulfillment of the overall principle "strong column-weak beam". As discussed previously, the Colombian seismic design guidelines [NSR-98 1998; NSR-10 2010] do not enforce this verification for medium-seismicity regions, like Bogotá. Noticeably, this type of behavior is also observed for uniform distribution of the pushing forces (Figure 5-92).

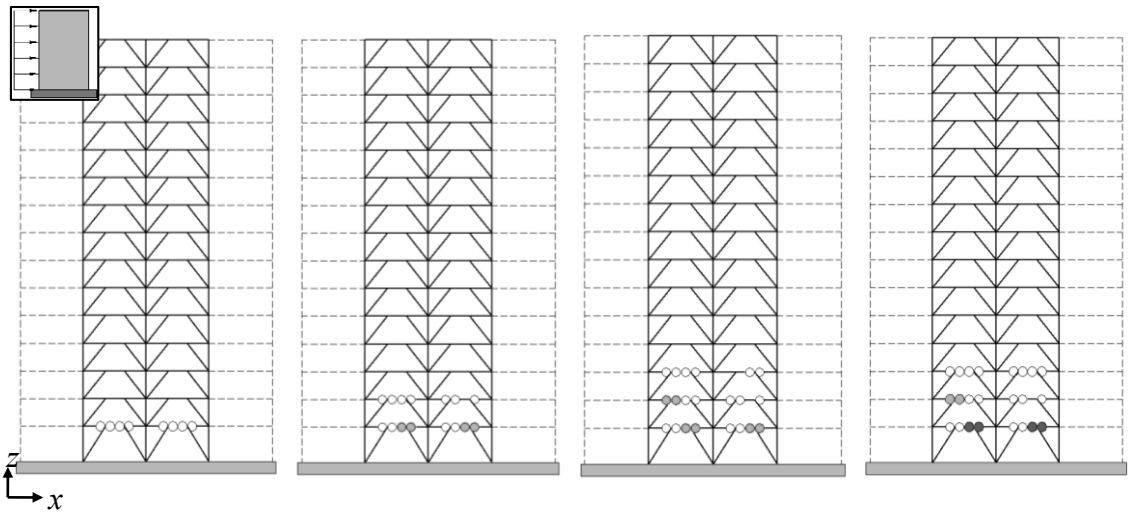

(a) Drift angle 0.40% (b) Drift angle 0.50% (c) Drift angle 0.64% (d) Drift angle 0.65%

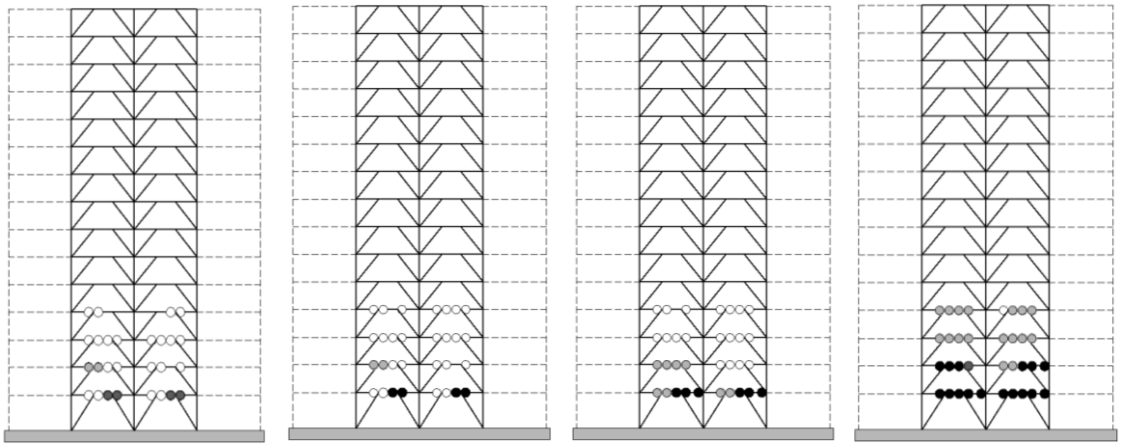

(e) Drift angle 0.73% (f) Drift angle 0.75% (g) Drift angle 0.80% (h) Drift angle 1.09%

Figure 5-92. Hinge progression sequence for the 15 – 8 × 8 – EBF building, uniform distribution and *x* direction (right displacement). Zone "Lacustre-500" (new microzonation, Figure 3-7). ○: yielding, ◎: IO, ◉: LS, ●: CP [FEMA 356 2000]

Comparison between Figure 5-91 and Figure 5-92 shows that under modal force distribution (Figure 5-91), the collapse mechanism involves hinges up to the eleventh level of the building, although for uniform distribution (Figure 5-92), the hinges concentrate only in the four bottom floors. This difference between modal and uniform pushing forces is consistent with the corresponding shear forces and bending moments distribution along the height of the building (Figure 5-1).

Table 5-19 and Table 5-20 display, respectively, the seismic performance and the response reduction factor (R, Ω and R_d) of the prototype buildings (Table 4-1) designed for the "Lacustre-500" Zone (new microzonation, Figure 3-7).

Table 5-19 reveals that 61% of the cases exhibit a satisfactory performance (YES), 12% unsatisfactory (NO) and 27% highly unsatisfactory (-). In the MRF/CBF/EBF buildings, such percentages are 84/100/0%, 1/0/33% and 15/0/67%. In the 5/10/15-story buildings such percentages are 67/60/56%, 11/11/13% and 22/29/31%. For the IO/LS/CP limit states, the percentages are 67/65/51%, 33/1/0% and 0/33/49%. For the Modal/Uniform distributions, the percentages are 60/62%, 12/11% and 28/27%. No relevant differences have been observed for *x*/*y* directions.

Table 5-19. Seismic performance. "Lacustre-500" zone (new microzonation)

Building	Target Drift IO(*)		Target Drift LS(*)		Target Drift CP(*)	
	Direction *x*	Direction *y*	Direction *x*	Direction *y*	Direction *y*	Direction *x*
5 – 6 × 6 – MRF	YES / YES	YES / YES	YES / YES	YES / YES	YES / YES	YES / YES
5 – 8 × 8 – MRF	YES / YES	YES / YES	YES / YES	YES / YES	YES / YES	YES / YES
5 – 6 × 6 – CBF	YES / YES	YES / YES	YES / YES	YES / YES	YES / YES	YES / YES
5 – 8 × 8 – CBF	YES / YES	YES / YES	YES / YES	YES / YES	YES / YES	YES / YES
5 – 6 × 6 – EBF	**NO** / **NO**	**NO** / **NO**	- / -	- / -	- / -	- / -
5 – 8 × 8 – EBF	**NO** / **NO**	**NO** / **NO**	- / -	- / -	- / -	- / -
10 – 6 × 6 – MRF	YES / YES	YES / YES	YES / YES	YES / YES	YES / YES	- / -
10 – 8 × 8 – MRF	YES / YES	YES / YES	YES / YES	YES / YES	- / YES	- / -
10 – 6 × 6 – CBF	YES / YES	YES / YES	YES / YES	YES / YES	YES / YES	YES / YES
10 – 8 × 8 – CBF	YES / YES	YES / YES	YES / YES	YES / YES	YES / YES	YES / YES
10 – 6 × 6 – EBF	**NO** / **NO**	**NO** / **NO**	- / -	- / -	- / -	- / -
10 – 8 × 8 – EBF	**NO** / **NO**	**NO** / **NO**	- / -	- / -	- / -	- / -
15 – 6 × 6 – MRF	YES / YES	YES / YES	YES / YES	**NO** / YES	YES / YES	- / -
15 – 8 × 8 – MRF	YES / YES	YES / YES	YES / YES	YES / YES	- / -	- / -
15 – 6 × 6 – CBF	YES / YES	YES / YES	YES / YES	YES / YES	YES / YES	YES / YES
15 – 8 × 8 – CBF	YES / YES	YES / YES	YES / YES	YES / YES	YES / YES	YES / YES
15 – 6 × 6 – EBF	**NO** / **NO**	**NO** / **NO**	- / -	- / -	- / -	- / -
15 – 8 × 8 – EBF	**NO** / **NO**	**NO** / **NO**	- / -	- / -	- / -	- / -

(*) First / second values correspond to modal and uniform distributions, respectively

Table 5-20**.** Response reduction factor R in the x / y directions. "Lacustre-500" zone (new microzonation)

Building	Over-strength factor (Ω)(*)		Ductility factor R_d(*)		*R* factor ($R = \Omega R_d$) (*)	
	Direction *x*	Direction *y*	Direction *x*	Direction *y*	Direction *x*	Direction *y*
5 – 6 × 6 – MRF	1.50 / 1.53	1.53 / 1.47	4.22 / 4.47	3.59 / 3.50	6.33 / 6.84	5.50 / 5.18
5 – 8 × 8 – MRF	1.39 / 1.34	1.08 / 1.11	4.63 / 4.84	2.60 / 2.78	6.43 / 6.49	2.81 / 3.09
5 – 6 × 6 – CBF	1.55 / 1.55	1.48 / 1.49	4.33 / 4.13	4.09 / 3.85	6.71 / 6.40	6.06 / 6.72
5 – 8 × 8 – CBF	1.51 / 1.65	1.53 / 1.55	4.19 / 4.51	4.39 / 4.54	6.19 / 7.44	6.72 / 7.03
5 – 6 × 6 – EBF	1.59 / 1.26	1.18 / 1.21	1.59 / 1.57	1.64 / 1.72	1.94 / 1.98	1.94 / 2.08
5 – 8 × 8 – EBF	1.33 / 1.63	1.16 / 1.15	2.23 / 3.79	1.82 / 1.97	2.97 / 6.17	2.11 / 2.27
10 – 6 × 6 – MRF	1.31 / 1.38	1.25 / 1.23	2.65 / 1.70	2.45 / 2.62	3.47 / 2.34	3.06 / 2.62
10 – 8 × 8 – MRF	1.29 / 1.25	1.24 / 1.25	1.57 / 2.57	2.16 / 1.88	2.02 / 3.21	2.68 / 2.35
10 – 6 × 6 – CBF	1.44 / 1.55	1.45 / 1.54	3.45 / 3.21	3.65 / 3.26	5.00 / 5.01	5.29 / 5.02
10 – 8 × 8 – CBF	1.63 / 1.84	1.38 / 1.73	2.86 / 2.03	2.94 / 1.93	4.66 / 3.73	4.06 / 3.34
10 – 6 × 6 – EBF	1.37 / 1.46	1.28 / 1.30	1.74 / 1.94	1.48 / 1.58	2.39 / 2.82	1.90 / 2.06
10 – 8 × 8 – EBF	1.33 / 1.39	1.18 / 1.20	2.95 / 2.71	1.58 / 1.78	3.92 / 3.77	1.87 / 2.14
15 – 6 × 6 – MRF	1.43 / 1.36	1.10 / 1.24	2.49 / 1.15	1.11 / 1.94	3.57 / 1.57	1.22 / 2.41
15 – 8 × 8 – MRF	1.39 / 1.26	1.25 / 1.25	3.11 / 1.43	1.15 / 1.32	4.32 / 1.81	1.42 / 1.64
15 – 6 × 6 – CBF	1.59 / 1.60	2.23 / 1.99	2.99 / 3.23	3.96 / 2.85	4.75 / 5.17	8.87 / 5.67
15 – 8 × 8 – CBF	1.46 / 1.65	1.92 / 1.95	4.75 / 2.99	5.40 / 1.96	6.94 / 4.94	2.81 / 3.83
15 – 6 × 6 – EBF	1.27 / 1.35	1.53 / 1.34	1.50 / 1.34	1.61 / 1.41	1.91 / 1.82	2.47 / 1.89
15 – 8 × 8 – EBF	1.26 / 1.37	1.34 / 1.28	2.37 / 1.88	1.72 / 1.44	2.99 / 2.58	2.31 / 1.84

(*) First / second values correspond to modal and uniform distributions, respectively

Comparison among the values of *R* in Table 5-20 with the assumed factors in Table 4-30 shows that, in 65% of the cases, the analyzed buildings do not possess the required ductility. In the MRF/CBF/EBF buildings, such percentage is 75/21/100%. In the 5/10/15-story buildings such percentage is 42/79/75%. For the Modal/Uniform distributions, the percentages are 64/67%. No relevant differences have been observed for *x/y* directions.

5.3.12 Overall conclusions

5.3.12.1 General considerations

The main conclusions concerning the linear behavior of the prototype buildings can be formulated after Table 4-21 through Table 4-30. This subsection presents the conclusions for the nonlinear behavior, after the push-over analyses described in the previous sections of this chapter. Subsections 5.3.2 through 5.3.11 summarize the most relevant results concerning the prototype buildings designed for the 10 seismic zones of the former and new microzonations of Bogotá [Decreto 196 2006; Decreto 523 2010] (Table 4-1 through Table 4-10). The main results that are presented in subsections 5.3.2 through 5.3.11 can be grouped in the following four categories:

- **Capacity curves with performance points** (Figure 5-3, Figure 5-6, Figure 5-9, Figure 5-12, Figure 5-15, Figure 5-18, Figure 5-21, Figure 5-24, Figure 5-27, Figure 5-30, Figure 5-33, Figure 5-36, Figure 5-39, Figure 5-42, Figure 5-45, Figure 5-48, Figure 5-51, Figure 5-54, Figure 5-57, Figure 5-60, Figure 5-63, Figure 5-66, Figure 5-69, Figure 5-72, Figure 5-75, Figure 5-78, Figure 5-81, Figure 5-84, Figure 5-87 and Figure 5-90).
- **Hinge progression and collapse mechanisms** (Figure 5-4, Figure 5-5, Figure 5-7, Figure 5-8, Figure 5-10, Figure 5-11, Figure 5-13, Figure 5-14, Figure 5-16, Figure 5-17, Figure 5-19, Figure 5-20, Figure 5-22, Figure 5-23, Figure 5-25, Figure 5-26, Figure 5-28, Figure 5-29, Figure 5-31, Figure 5-32, Figure 5-34, Figure 5-35, Figure 5-37, Figure 5-38, Figure 5-40, Figure 5-41, Figure 5-43, Figure 5-44, Figure 5-46, Figure 5-47, Figure 5-49, Figure 5-50, Figure 5-52, Figure 5-53, Figure 5-55, Figure 5-56, Figure 5-58, Figure 5-59, Figure 5-61, Figure 5-62, Figure 5-64, Figure 5-65, Figure 5-67, Figure 5-68, Figure 5-70, Figure 5-71, Figure 5-73, Figure 5-74, Figure 5-76, Figure 5-77, Figure 5-79, Figure 5-80, Figure 5-82, Figure 5-83, Figure 5-85, Figure 5-86, Figure 5-88, Figure 5-89, Figure 5-91 and Figure 5-92).
- **Seismic performance** (Table 5-1, Table 5-3, Table 5-5, Table 5-7, Table 5-9, Table 5-11, Table 5-13, Table 5-15, Table 5-17 and Table 5-19).
- **Response reduction factor** (Table 5-2, Table 5-4, Table 5-6, Table 5-8, Table 5-10, Table 5-12, Table 5-14, Table 5-16 ,Table 5-18 and Table 5-20).

The conclusions derived from each of these groups of sources are presented and discussed in the next four subsections, respectively.

5.3.12.2 Conclusions from the capacity curves

The observation of Figure 5-3, Figure 5-6, Figure 5-9, Figure 5-12, Figure 5-15, Figure 5-18, Figure 5-21, Figure 5-24, Figure 5-27, Figure 5-30, Figure 5-33, Figure 5-36, Figure 5-39, Figure 5-42, Figure 5-45, Figure 5-48, Figure 5-51, Figure 5-54, Figure 5-57, Figure 5-60, Figure 5-63, Figure 5-66, Figure 5-69, Figure 5-72, Figure 5-75, Figure 5-78, Figure 5-81, Figure 5-84, Figure 5-87 and Figure 5-90 provides the following conclusions on the influence of the involved parameters:

- **Input direction**. The capacity curves for the x and y directions are rather similar. This resemblance is superior in the linear range than in the nonlinear one; this distinction can be explained by the higher difficulty of reproducing accurately the nonlinear behavior and by its greater sensitivity to the structural parameters. Regarding the structural type, the similarity between the capacity curves in both directions is clearer in MRF buildings.
- **Vertical distribution of the pushing forces**. The capacity curves for the modal distribution exhibit smaller initial stiffness (linear range) and force strength (nonlinear range) than those corresponding to the uniform distribution. Since the vertical ordinate of the capacity curves is proportional to the base shear, this difference can be explained by the bigger bending moments generated by the modal distribution (Figure 5-1). In many cases, in the extreme

segments of the nonlinear range (in the vicinity of the collapse), the abovementioned relation between the capacity curves is partially inverted and the curves for the modal distribution show higher ductility. Since the formation and development of plastic hinges is strongly correlated to the overall shear forces in each floor, this tendency can be explained by the rapider variation of the shear forces in the lowest stories for the uniform distribution (Figure 5-1.e). In that case, the plastic hinges concentrate in the lowest stories, thus generating less ductile collapse mechanisms.

- **Span-length**. Comparison among the left and right pairs of curves (6 × 6 and 8 × 8, respectively) shows that the capacity curves and the performance points of the buildings with span-lengths 6 and 8 m are rather analogous. As expected, the difference is bigger in the nonlinear range.
- **Number of floors**. The performance of the 5, 10 and 15-story buildings is rather similar, although minor differences among the tendencies for the different resisting systems can be observed. In MRF buildings, the strength in terms of base shear coefficient decreases with increasing height, although this trend is not uniform, showing an important dispersion; also, the ductility gives the impression of decreasing as height augments. In CBF buildings, the force strength is not significantly affected by height and the ductility appears to increase as height does. In EBF buildings, the trends are rather opposite: the force strength decreases as height does and the ductility is steady.
- **Earthquake-resisting system**. For all the analyzed buildings, the yielding and collapse displacements for MRF are higher than those of CBF; in their turn, such displacements are greater than those of EBF. The differences among MRF buildings compared to EBF and CBF buildings can be explained by the inherent largest flexibility of MRF buildings; between EBF and CBF, the smaller yielding displacement of EBF is caused by their premature failure in the link segments. In terms of forces, the yielding and collapse forces for CBF are higher than those of MRF; in their turn, such forces are greater than those of EBF. Those differences can be explained by the inherent largest strength of CBF buildings compared to MRF ones; among MRF and EBF, the last have less force strength because of the high relevance of the shear-flexural behavior of the link.
- **Seismic zone**. As expected, the seismic strength in terms of the base shear coefficient is approximately proportional to the design forces (Table 4-21 through Table 4-30). The comparison amongst the displacement ductility has not pointed out any dominating tendency.

5.3.12.3 Conclusions from the plastic hinge sketches

The observation of Figure 5-4, Figure 5-5, Figure 5-7, Figure 5-8, Figure 5-10, Figure 5-11, Figure 5-13, Figure 5-14, Figure 5-16, Figure 5-17, Figure 5-19, Figure 5-20, Figure 5-22, Figure 5-23, Figure 5-25, Figure 5-26, Figure 5-28, Figure 5-29, Figure 5-31, Figure 5-32, Figure 5-34, Figure 5-35, Figure 5-37, Figure 5-38, Figure 5-40, Figure 5-41, Figure 5-43, Figure 5-44, Figure 5-46, Figure 5-47, Figure 5-49, Figure 5-50, Figure 5-52, Figure 5-53, Figure 5-55, Figure 5-56, Figure 5-58, Figure 5-59, Figure 5-61, Figure 5-62, Figure 5-64, Figure 5-65, Figure 5-67, Figure 5-68, Figure 5-70, Figure 5-71, Figure 5-73, Figure 5-74, Figure 5-76, Figure 5-77, Figure 5-79, Figure 5-80, Figure 5-82, Figure 5-83, Figure 5-85, Figure 5-86, Figure 5-88, Figure 5-89, Figure 5-91 and Figure 5-92 provides the following conclusions on the influence of the involved parameters:

- **Input direction**. In *x* direction there are four two-bay seismic frames and in *y* direction there are two four-bay seismic frames (Figure 4-3). This distinction causes that the right side columns are more over-compressed by the pushing forces and, therefore, the early failure of the right bottom column is more common in the *x* direction than in the *y* one. This fact over-demands the left bay and it can lead to brittle collapse mechanisms.
- **Vertical distribution of the pushing forces**. For the modal distribution, the plastic hinges are more spread along the height of the building, while for the uniform distribution, they are more concentrated in the lowest levels, thus generating more fragile collapse mechanisms. This difference between modal and uniform pushing forces is consistent with the

corresponding shear forces and bending moments distribution along the height of the building (Figure 5-1).

- **Span-length**. No relevant influence of the span-length is observed.
- **Number of floors**. The aforementioned early failure of the right bottom column in the *x* direction (Figure 4-3) is more common for 10 and 15-story buildings. This circumstance can be explained by the higher over-compression.
- **Earthquake-resisting system**. In the MRF buildings, the hinges appear and develop both in the columns and in the beams. This circumstance stems from the lack of enforcement of the "strong column-weak beam" requirement by the Colombian design codes [NSR-98 1998; NSR-10 2010]. In the CBF buildings, the hinges start first in the braces; in the 10 and 15-story buildings, later additional hinges emerge and progress in the right columns. In the EBF buildings, the hinges appear and develop in the link segments of the beams; no other locations have been observed.
- **Seismic zone**. Not any dominating tendency has been perceived.

5.3.12.4 Conclusions from the seismic performances

The observation of Table 5-1, Table 5-3, Table 5-5, Table 5-7, Table 5-9, Table 5-11, Table 5-13, Table 5-15, Table 5-17 and Table 5-19 shows that in 56% of the considered cases the performance is satisfactory ("represented as "YES" in the Tables), in 14% of the cases the performance is not satisfactory ("represented as "NO" in the Tables) and in 30% of the cases the performance is highly not satisfactory ("represented as "-" in the Tables). As well, the aforementioned Tables provide the following conclusions on the influence of the involved parameters:

- **Input direction**. The performances for the *x* and *y* directions are rather similar.
- **Vertical distribution of the pushing forces**. For the modal distribution of the pushing forces, in 57% of the considered cases the performance is satisfactory ("represented as "YES" in the Tables), in 14% of the cases the performance is not satisfactory ("represented as "NO" in the Tables) and in 29% of the cases the performance is highly not satisfactory ("represented as "-" in the Tables). For the uniform distribution of the pushing forces, in 56% of the considered cases the performance is satisfactory ("represented as "YES" in the Tables), in 12% of the cases the performance is not satisfactory ("represented as "NO" in the Tables) and in 32% of the cases the performance is highly not satisfactory ("represented as "-" in the Tables).
- **Span-length**. The performances for 6 × 6 and 8 × 8 buildings are rather similar.
- **Earthquake-resisting system**. For the MRF buildings, in 71% of the considered cases the performance is satisfactory ("represented as "YES" in the Tables), in 10% of the cases the performance is not satisfactory ("represented as "NO" in the Tables) and in 19% of the cases the performance is highly not satisfactory ("represented as "-" in the Tables). For the CBF buildings, in 95% of the considered cases the performance is satisfactory ("represented as "YES" in the Tables), in 4% of the cases the performance is not satisfactory ("represented as "NO" in the Tables) and in 1% of the cases the performance is highly not satisfactory ("represented as "-" in the Tables). For the EBF buildings, in 2% of the considered cases the performance is satisfactory ("represented as "YES" in the Tables), in 29% of the cases the performance is not satisfactory ("represented as "NO" in the Tables) and in 69% of the cases the performance is highly not satisfactory ("represented as "-" in the Tables).
- **Number of floors**. For the 5-story buildings, in 66% of the considered cases the performance is satisfactory ("represented as "YES" in the Tables), in 12% of the cases the performance is not satisfactory ("represented as "NO" in the Tables) and in 22% of the cases the performance is highly not satisfactory ("represented as "-" in the Tables). For the 10-story buildings, in 55% of the considered cases the performance is satisfactory ("represented as "YES" in the Tables), in 16% of the cases the performance is not satisfactory ("represented as "NO" in the Tables) and in 29% of the cases the performance is highly not satisfactory ("represented as "-" in the Tables). For the 15-story buildings, in 47% of the considered cases the performance is satisfactory ("represented as "YES" in the Tables), in 15% of the cases the performance is not satisfactory ("represented as "NO" in the Tables) and in 38% of the cases the performance

is highly not satisfactory ("represented as "-" in the Tables).

- **Limit states (Target Drifts)**. For the IO/LS/CP limit states, the percentages of satisfactory/unsatisfactory/highly unsatisfactorily (Y/N/-) performance are 61/59/50%, 32/6/1% and 7/35/49%, respectively.
- **Seismic zone**. In the "Piedemonte" Zone (former microzonation, Figure 3-5) in 54% of the considered cases the performance is satisfactory ("represented as "YES" in the Tables), in 8% of the cases the performance is not satisfactory ("represented as "NO" in the Tables) and in 38% of the cases the performance is highly not satisfactory ("represented as "-" in the Tables). In the "Lacustre A" Zone (former microzonation, Figure 3-5) in 56% of the considered cases the performance is satisfactory ("represented as "YES" in the Tables), in 9% of the cases the performance is not satisfactory ("represented as "NO" in the Tables) and in 35% of the cases the performance is highly not satisfactory ("represented as "-" in the Tables). In the "Piedemonte A" Zone (new microzonation, Figure 3-7) in 53% of the considered cases the performance is satisfactory ("represented as "YES" in the Tables), in 16% of the cases the performance is not satisfactory ("represented as "NO" in the Tables) and in 31% of the cases the performance is highly not satisfactory ("represented as "-" in the Tables). In the "Piedemonte B" Zone (new microzonation, Figure 3-7) in 48% of the considered cases the performance is satisfactory ("represented as "YES" in the Tables), in 31% of the cases the performance is not satisfactory ("represented as "NO" in the Tables) and in 21% of the cases the performance is highly not satisfactory ("represented as "-" in the Tables). In the "Piedemonte C" Zone (new microzonation, Figure 3-7) in 49% of the considered cases the performance is satisfactory ("represented as "YES" in the Tables), in 21% of the cases the performance is not satisfactory ("represented as "NO" in the Tables) and in 30% of the cases the performance is highly not satisfactory ("represented as "-" in the Tables). In the "Lacustre-50" Zone (new microzonation, Figure 3-7) in 56% of the considered cases the performance is satisfactory ("represented as "YES" in the Tables), in 14% of the cases the performance is not satisfactory ("represented as "NO" in the Tables) and in 30% of the cases the performance is highly not satisfactory ("represented as "-" in the Tables). In the "Lacustre-100" Zone (new microzonation, Figure 3-7) in 61% of the considered cases the performance is satisfactory ("represented as "YES" in the Tables), in 12% of the cases the performance is not satisfactory ("represented as "NO" in the Tables) and in 27% of the cases the performance is highly not satisfactory ("represented as "-" in the Tables). In the "Lacustre-200" Zone (new microzonation, Figure 3-7) in 61% of the considered cases the performance is satisfactory ("represented as "YES" in the Tables), in 9% of the cases the performance is not satisfactory ("represented as "NO" in the Tables) and in 30% of the cases the performance is highly not satisfactory ("represented as "-" in the Tables). In the "Lacustre-300" Zone (new microzonation, Figure 3-7) in 60% of the considered cases the performance is satisfactory ("represented as "YES" in the Tables), in 12% of the cases the performance is not satisfactory ("represented as "NO" in the Tables) and in 28% of the cases the performance is highly not satisfactory ("represented as "-" in the Tables). In the "Lacustre-500" Zone (new microzonation, Figure 3-7) in 61% of the considered cases the performance is satisfactory ("represented as "YES" in the Tables), in 12% of the cases the performance is not satisfactory ("represented as "NO" in the Tables) and in 27% of the cases the performance is highly not satisfactory ("represented as "-" in the Tables).

These figures are summarized in Table 5-21 and in Table 5-22. Table 5-21 contains information regarding the influence of the vertical distribution of the pushing forces (Modal/Uniform), the type of earthquake-resisting system (MRF/CBF/EBF) and the number of floors (5/10/15) and Table 5-22 reports on the situation for each seismic zone.

Table 5-21. Percentages of buildings with satisfactory seismic performance (YES), unsatisfactory seismic performance (NO) and highly unsatisfactory seismic performance (-)

Seismic performance	Vertical distribution of the pushing forces		Type of earthquake-resisting system			Limit state			Number of floors			Total
	Modal	Uniform	MRF	CBF	EBF	IO	LS	CP	5	10	15	
YES	57	56	71	95	2	61	59	50	66	55	47	**56**
NO	14	12	10	4	29	32	6	1	12	16	15	**14**
-	29	32	19	1	69	7	35	49	22	29	38	**30**

Table 5-22. Percentages of buildings with satisfactory seismic performance (YES), unsatisfactory seismic performance (NO) and highly unsatisfactory seismic performance (-) for each seismic zone

Seismic performance	Former microzonation	New microzonation							
	Pied.	Lac. A	Pied. A	Pied. B	Pied. C	Lac. 50	Lac. 100	Lac. 200	Lac. 300	Lac. 500
YES	54	56	53	48	49	56	61	61	60	61
NO	8	9	16	31	21	14	12	9	12	12
-	38	35	31	21	30	30	27	30	28	27

5.3.12.1 Conclusions from the response reduction factors

Comparison among the values in Table 5-2, Table 5-4, Table 5-6, Table 5-8, Table 5-10, Table 5-12, Table 5-14, Table 5-16 ,Table 5-18 and Table 5-20 with the assumed response reduction factors listed in Table 4-21 through Table 4-30 shows that, in 66% of the cases, the analyzed buildings do not possess the required ductility.

The observation of Table 5-2, Table 5-4, Table 5-6, Table 5-8, Table 5-10, Table 5-12, Table 5-14, Table 5-16 ,Table 5-18 and Table 5-20 provides the following conclusions on the influence of the involved parameters:

- **Input direction**. The situations for the *x* and *y* directions are rather similar.
- **Vertical distribution of the pushing forces**. For the modal distribution of the pushing forces, in 62% of the cases, the analyzed buildings do not possess the required ductility. For the uniform distribution of the pushing forces, in 69% of the cases, the analyzed buildings do not possess the required ductility.
- **Span-length**. The situations for 6 × 6 and 8 × 8 buildings are rather similar.
- **Earthquake-resisting system**. For the MRF buildings, in 78% of the cases, the analyzed buildings do not possess the required ductility. For the CBF buildings, in 20% of the cases, the analyzed buildings do not possess the required ductility. For the EBF buildings, in 100% of the cases, the analyzed buildings do not possess the required ductility. As discussed in subsection 2.2.6, the Eurocode 8 [EN-1998 2004] states that for MRF and EBF buildings with Ductility Class High (DCH) the behavior factor q (which is equivalent to the R factor) can be obtained as $q = 5\ \alpha_u / \alpha_1$, where factor 5 plays the role of the ductility factor R_d and α_u / α_1 corresponds to the over-strength factor Ω. If none push-over analysis has been carried out, for MRF and EBF buildings like those considered in this work, $\alpha_u / \alpha_1 = 1.3$ and 1.2, respectively. If capacity curves are available, the arising value of α_u / α_1 can be considered, with a top limit equal to 1.6. For CBF with V-bracing (chevron braces) the Eurocode 8 states that $q = 2.5$. Comparison with Table 5-2 , Table 5-4, Table 5-6, Table 5-8, Table 5-10, Table 5-12, Table 5-14, Table 5-16 ,Table 5-18 and Table 5-20 provides the following conclusions: **MRF**.
- **Number of floors**. For the 5-story buildings, in 50% of the cases, the analyzed buildings do not possess the required ductility. For the 10-story buildings, in 80% of the cases, the analyzed buildings do not possess the required ductility. For the 15-story buildings, in 67% of the cases, the analyzed buildings do not possess the required ductility.
- **Seismic zone**. In the "Piedemonte" Zone (former microzonation, Figure 3-5), in 67% of the cases, the analyzed buildings do not possess the required ductility. In the "Lacustre A" Zone,

in 71% of the cases, the analyzed buildings do not possess the required ductility. In the "Piedemonte A" Zone, in 65% of the cases, the analyzed buildings do not possess the required ductility. In the "Piedemonte B" Zone, in 63% of the cases, the analyzed buildings do not possess the required ductility. In the "Piedemonte C" Zone, in 67% of the cases, the analyzed buildings do not possess the required ductility. In the "Lacustre-50" Zone, in 67% of the cases, the analyzed buildings do not possess the required ductility. In the "Lacustre-100" Zone, in 61% of the cases, the analyzed buildings do not possess the required ductility. In the "Lacustre-200" Zone, in 65% of the cases, the analyzed buildings do not possess the required ductility. In the "Lacustre-300" Zone, in 67% of the cases, the analyzed buildings do not possess the required ductility. In the "Lacustre-500" Zone, in 65% of the cases, the analyzed buildings do not possess the required ductility.

These conclusions are summarized in Table 5-23 and in Table 5-24. Table 5-23 contains information regarding the influence of the vertical distribution of the pushing forces (Modal/Uniform), the type of earthquake-resisting system (MRF/CBF/EBF) and the number of floors (5/10/15) and Table 5-24 reports on the situation for each seismic zone.

Table 5-23. Percentages of buildings with insufficient ductility

Vertical distribution of the pushing forces		Type of earthquake-resisting system			Number of floors			Total
Modal	Uniform	MRF	CBF	EBF	5	10	15	
62	69	78	20	100	50	80	67	**66**

Table 5-24. Percentages of buildings with insufficient ductility for each seismic zone

Former microzonation		New microzonation							
Pied.	Lac. A	Pied. A	Pied. B	Pied. C	Lac. 50	Lac. 100	Lac. 200	Lac. 300	Lac. 500
67	71	65	63	67	67	61	65	67	65

The work [Ferraioli et al. 2012] contains a numerical study for steel MRF buildings designed according to the European regulations for high seismicity regions; overall comparison among the obtained values of the response reduction factor (R) from that work and from Table 5-2, Table 5-4, Table 5-6, Table 5-8, Table 5-10, Table 5-12, Table 5-14, Table 5-16 ,Table 5-18 and Table 5-20 show that both are relatively similar. As well, the aforementioned decrease of R with the increased number of floors is also confirmed.

6 SUMMARY, CONCLUSIONS AND FUTURE INVESTIGATIONS

6.1 Summary

This work presents a numerical seismic vulnerability assessment of eighteen 5, 10 and 15-story steel buildings. These buildings have plan-symmetry and vertical uniformity and are selected to represent the vast majority of similar buildings recently erected in Bogotá, Colombia. Two span-lengths (6 m and 8 m) and three lateral resistant systems are considered: moment resisting frames (MRF) and concentrically and eccentrically braced frames (CBF and EBF, respectively); only chevron braces are used. Each building is designed for ten soil conditions; those conditions correspond to two zones of the former seismic microzonation of Bogotá and eight zones of the new microzonation. The vulnerability is estimated by 2D static push-over analyses by assuming two patterns for the vertical variation of the pushing forces: uniform and modal.

Next sections discusses the most important conclusions of this study. The conclusions are organized in four categories: seismic performance of the considered buildings, observed collapse mechanisms, calculated values of the response reduction factor, and other conclusions. Finally, the generalizability of the results of this study is discussed.

6.2 Conclusions

6.2.1 Seismic performance

This subsection discusses the leading conclusions of this research regarding the seismic performance of the considered buildings for each Target Drift (IO/LS/CP). The global conclusions (i.e. those describing the overall tendencies) are presented first and then the influence of the main parameters of the study (Input direction, Vertical distribution of the pushing forces, Span-length, Earthquake-resisting system, Number of floors, Target Drift, Seismic zone) is considered.

- **Global performance**. A relevant number of the analyzed buildings do not exhibit an adequate seismic behavior, at least for one Target Drift. In 56% of the cases the performance is satisfactory, in 14% of the cases the performance is not satisfactory and in 30% of the cases the performance is highly not satisfactory.
- **Input direction**. The seismic performance in both horizontal directions is similar.
- **Vertical distribution of the pushing forces**. The derived seismic performances are basically the same regardless the vertical distribution of the pushing forces of the push-over analyses. By assuming modal variation of the pushing forces, in 57% of the cases the performance is satisfactory, in 14% of the cases the performance is not satisfactory and in 29% of the cases the performance is highly not satisfactory. By assuming uniform variation of the pushing forces, in 56% of the cases the performance is satisfactory, in 12% of the cases the performance is not satisfactory and in 32% of the cases the performance is highly not satisfactory.
- **Span-length**. The seismic performance of the buildings with 6 m and 8 m span-length is similar.

- **Earthquake-resisting system**. The seismic performances of the MRF, CBF and EBF buildings are clearly different. Most of the CBF buildings exhibit an adequate performance, the performance of EBF is unacceptable in most of the cases and the performance of MRF buildings is intermediate. In the MRF buildings, the percentages of cases with satisfactory, not satisfactory and highly not satisfactory performance are 71%, 10% and 19%, respectively. In the CBF buildings, the percentages of cases with satisfactory, not satisfactory and highly not satisfactory performance are 95%, 4% and 1%, respectively. In the EBF buildings, the percentages of cases with satisfactory, not satisfactory and highly not satisfactory performance are 2%, 29% and 69%, respectively. The intermediate performance of the MRF buildings can be principally explained by the non-fulfillment of the "strong column-weak beam" requirement. The highly adequate performance of the CBF buildings can be explained by the over-conservative design of columns and beams. The highly inadequate performance of the EBF buildings can be justified by the early formation of plastic hinges in the link segment of the beam and the subsequent generation of a brittle collapse mechanism.
- **Number of floors**. The tallest considered buildings demonstrate a worse seismic performance. In the 5-story buildings, the percentages of cases with satisfactory, not satisfactory and highly not satisfactory performance are 66%, 12% and 22%, respectively. In the 10-story buildings, the percentages of cases with satisfactory, not satisfactory and highly not satisfactory performance are 55%, 16% and 29%, respectively. In the 15-story buildings, the percentages of cases with satisfactory, not satisfactory and highly not satisfactory performance are 47%, 15% and 38%, respectively.
- **Limit states (Target Drifts)**. The performance deteriorates with the increasing severity of the Target Drift, mainly in terms of the highly unsatisfactorily results. For the IO/LS/CP limit states, the percentages of satisfactory/unsatisfactory/highly unsatisfactorily performance are 61/59/50%, 32/6/1% and 7/35/49%, respectively.
- **Seismic zone**. According to the former microzonation, the seismic performance of the buildings in each of the two seismic zones is basically the same. According to the new microzonation, there are differences in the seismic performances of the buildings in each of the eight seismic zones, but no clear tendencies can be observed. In the "Piedemonte" Zone (former microzonation) in 54% of the considered cases the performance is satisfactory, in 8% of the cases the performance is not satisfactory and in 38% of the cases the performance is highly not satisfactory. In the "Lacustre A" Zone (former microzonation) in 56% of the considered cases the performance is satisfactory, in 9% of the cases the performance is not satisfactory and in 35% of the cases the performance is highly not satisfactory. In the "Piedemonte A" Zone (new microzonation) in 53% of the considered cases the performance is satisfactory, in 16% of the cases the performance is not satisfactory and in 31% of the cases the performance is highly not satisfactory. In the "Piedemonte B" Zone (new microzonation) in 48% of the considered cases the performance is satisfactory, in 31% of the cases the performance is not satisfactory and in 21% of the cases the performance is highly not satisfactory. In the "Piedemonte C" Zone (new microzonation) in 49% of the considered cases the performance is satisfactory, in 21% of the cases the performance is not satisfactory and in 30% of the cases the performance is highly not satisfactory. In the "Lacustre-50" Zone (new microzonation) in 56% of the considered cases the performance is satisfactory, in 14% of the cases the performance is not satisfactory and in 30% of the cases the performance is highly not satisfactory. In the "Lacustre-100" Zone (new microzonation) in 61% of the considered cases the performance is satisfactory, in 12% of the cases the performance is not satisfactory and in 27% of the cases the performance is highly not satisfactory. In the "Lacustre-200" Zone (new microzonation) in 61% of the considered cases the performance is satisfactory, in 9% of the cases the performance is not satisfactory and in 30% of the cases the performance is highly not satisfactory. In the "Lacustre-300" Zone (new microzonation) in 60% of the considered cases the performance is satisfactory, in 12% of the cases the performance is not satisfactory and in 28% of the cases the performance is highly not satisfactory. In the "Lacustre-500" Zone (new microzonation) in 61% of the considered cases the performance is satisfactory, in 12% of the cases the performance is not satisfactory and in 27% of the cases the performance is highly not satisfactory.

6.2.2 Response reduction factor

This subsection discusses the leading conclusions of this research regarding the comparison between the obtained values of the response reduction factor and the values assumed in the design, i.e. those stated by the Colombian codes. The global conclusions (i.e. those describing the overall tendencies) are presented first and then the influence of the main parameters of the study (Input direction, Vertical distribution of the pushing forces, Span-length, Earthquake-resisting system, Number of floors, Seismic zone) is considered.

- **Global performance**. An important number of the analyzed buildings (66%) do not possess the required ductility.
- **Input direction**. The ductility for the *x* and *y* directions is rather similar.
- **Vertical distribution of the pushing forces**. Assuming uniform distribution of the pushing forces, the number of buildings without the required ductility is higher. The percentages are 69% and 62%, respectively.
- **Span-length**. The ductility for 6 × 6 and 8 × 8 buildings is rather similar.
- **Earthquake-resisting system**. The ductility of the MRF, CBF and EBF buildings is clearly different; 78% of the MRF buildings, 20% of the CBF buildings, and 100% of the EBF buildings do not have the required ductility. The low ductility of the MRF buildings can be principally explained by the non-fulfillment of the "strong column-weak beam" requirement. The rather high ductility of the CBF buildings can be explained by the over-conservative design of columns and beams. The extremely low ductility of the EBF buildings can be justified by the early formation of plastic hinges in the link segment of the beam and the subsequent generation of a brittle collapse mechanism.
- **Number of floors**. For the 5/10/15-story buildings, the percentages of buildings without the required ductility are 50/80/67%, respectively.
- **Seismic zone**. In the ten seismic zones, the percentages of buildings without the required ductility are rather similar.

6.2.3 Other conclusions

- **Eurocode 8**. Regarding the response reduction factor, comparison between European and American regulations, shows that Eurocode 8 is over-conservative for MRF and EBF buildings but is under-conservative for CBF buildings.

6.2.4 Scope of this study

The conclusions of this research can be broadly generalized to other cities in Colombia with similar seismicity than Bogotá. Among them, Ibagué, Medellín, Montería, Riohacha, Santa Marta, Sincalejo and Tunja. Approximately 60% of the Colombian population belongs to the intermediate seismicity region, like Bogotá. Noticeably, the wide diversity of soils in such zones can be covered by the ten seismic zones considered in this study.

6.3 Future Investigations

Given the potential professional interest of this research for Bogotá and the rest of Colombia, the next step will consist in spreading these results among the concerned professionals, mainly structural designers. This task cannot be considered research, since no new knowledge is added, but is deemed extremely necessary to complement the usefulness of the carried out research. A full dissemination plan will be developed; the main activities will be: (i) presentations at the national conference "Encuentro Internacional del Acero en Colombia", (ii) lectures, conferences and work-shops at the "Asociación Colombiana de Ingeniería Estructural", (iii) meetings with the "Asociación Colombiana de Ingeniería Sísmica", (iv) conferences at the "Federación Colombiana

de fabricantes de estructuras metálicas" (FEDESTRUCTURAS), (v) several activities at the "Feria de Construcción y Vivienda en Colombia", and (vi) teaching activities at Universities, mainly the "Universidad Nacional de Colombia" and the Universidad de los Andes".

From the obtained results, the following future researches are envisaged:

- This study will be generalized to other cities in Colombia with higher seismicity than Bogotá, namely high seismicity, according the Colombian design code. Among them, Bucaramanga, Cali, Cúcuta, Mocoa, Neiva, Pasto, Popayán, Quidbó, Villavicencio, and Yopal. Approximately 25% of the Colombian population belongs to the high seismicity region. Given the biggest seismicity of this region, the push-over analyses should be complemented with nonlinear time-history analyses for representative sets of seismic inputs characterizing the local seismicity.
- Diagonal braces (x-shaped) for steel buildings are not very frequent and Colombia, perhaps for architectural limitations. The seismic efficiency of this solution will be investigated; if positive conclusions are obtained, this type of braces will be promoted among designers and users.
- In the last few years (after 2010, approximately) a new construction technology is becoming increasingly popular in Bogotá and in Medellín, among other major cities. This technology consists of combining steel columns (made with ordinary hot-rolled sections) with short RC structural walls; the lengths of these walls arranges between 1.5 and 2.5 m. The steel columns and the RC walls are connected by shear studs. The seismic performance of these constructions will be investigated following basically the same approach than in this study.
- The seismic efficiency of the Concentric Braced Frames might be further improved by adding zipper columns (e.g. vertical members linking the connection points between the chevron braces and the beam). This solution could allow designing less stiff beams, thus reducing the mass and the cost of the building.
- The use of energy dissipators as seismic protection of steel building structures will be investigated, compared to the considered approaches. Simple devices (e.g. hysteretic dissipators) will be preferred, since they are well suited for mass use in developing countries, like Colombia. This activity will be linked to other tasks inside the research group, namely proposal of design energy spectra for Colombia and of design criteria for buildings with energy dissipators.

REFERENCES

1. Abolmaali A., Kukreti A., Motahari A., Ghassemieh M. (2009). Energy dissipation characteristics of semi-rigid connections. Journal of Constructional Steel Research. 65(5):1187-1197. DOI:10.1016/j.jcsr.2008.05.014.
2. AISC-327 (2005). Seismic Provisions for Structural Steel Building. American Institute on Steel Construction.
3. AISC (2010). Steel Construction Manual. American Institute on Steel Construction.
4. AISC 360-10 (2010). Specification for Structural Steel Buildings. American Institute on Steel Construction.
5. AISC-327 (2010). Seismic Design Manual. American Institute on Steel Construction.
6. Akiyama H. Earthquake-Resistant Limit-State Design for Buildings, University of Tokyo Press, Tokyo (1985).
7. Akiyama H. (1999). Earthquake-Resistant Design Method for Buildings Based on Energy Balance, Gihodo Shuppan, Tokyo 25-26.
8. ASCE 7-05. (2005). Minimum design loads for buildings and other structures. ASCE/SEI 7-05, American Society of Civil Engineers. Reston, VA.
9. ASTM A36 / A36 M-08. (2008). Standard Specification for Carbon Structural Steel. DOI: 10.1520/A0036_A0036M-08.
10. ASTM A500 / A500 M-09. (2009). Standard Specification for Cold-Formed Welded and Seamless Carbon Steel Structural Tubing in Rounds and Shapes. DOI: 10.1520/A0500_A0500M-09.
11. ASTM A572 / A572 M-12. (2012). Standard Specification for High-Strength Low-Alloy Columbium-Vanadium Structural Steel. DOI: 10.1520/A0572_A0572M-12.
12. ASTM A1008 / A1008 M-13. (2013). Standard Specification for Steel, Sheet, Cold-Rolled/Carbon, Structural, High-Strength, Low-Alloy with Improved Formability Solution, Hardened and Bake Hardenable. DOI: 10.1520/A1008_A1008M.
13. ASTM A6/A6M-13. (2013). Standard Specification for General Requirements for Rolled Structural Steel Bars, Plates, Shapes, and Sheet Piling.
14. ATC-40. (1996). Seismic Evaluation and Retrofit of Concrete Buildings. Applied Technology Council.
15. ATC-58. (2002). Development of Performance-based Earthquake Design Guidelines, Applied Technology Council, Redwood City.
16. Banon H., Veneciano D. (1982). Seismic safety of reinforced concrete members and structures, Earthquake Engineering and Structural Dynamics, 10 179-193.
17. Becker R. (1995). Seismic Design of Special Concentrically Braced Steel Frames. Steel Tips. Structural Steel Educational Council.
18. Becker R., Ishler M. (1996). Seismic Design Practice for Eccentrically Braced Frames. Steel Tips. Structural Steel Educational Council.
19. Benavent-Climent A., Pujades L.G., López-Almansa F. (2001). Espectros de Input de Energía de Aplicación en el Proyecto Sismorresistente de Estructuras en Regiones de Sismicidad Moderada, CIMNE Monografía IS-43.
20. Benavent-Climent A. (2007). An energy-based damage model for seismic response of steel structures, Earthquake Engineering and Structural Dynamics, 36 1049–1064.
21. Berg G.V., Thomaides S.S. (1960). Energy consumption by structures in strong-motion earthquakes, Proceedings of the Second World Conference on Earthquake Engineering, 2 681-697.
22. Bertero R.D., Bertero V.V., Teran-Gilmore A. (1996). Performance-based earthquake-resistant design based on comprehensive design philosophy and energy concepts, Proceedings of the Eleventh World Conference on Earthquake Engineering, Disc 2 611.
23. Bracci J.M., Kunnath S.K., Reinhorn A.M. (1997). Seismic performance and retrofit evaluation for reinforced concrete structures, Journal of Structural Engineering (ASCE), 123(1), 3–10.
24. Brown A.P., Aiken I.D., Jafarzadeh F.J. (2001). Buckling Restrained Braces Provide the Key to the Seismic Retrofit of the Wallace F. Bennett Federal Building. Modern Steel Construction.
25. Bruneau M. Wang N. (1996). Normalized energy-based methods to predict the seismic ductile response of SDOF structures, Engineering Structures 13-28.
26. Carrillo J., Blandón-Valencia J., Rubiano A. (2013). A review of conceptual transparency in US and Colombian seismic design building codes. Ingeniería e investigación Vol. 33 No. 2, 24-29.
27. Chai Y.H. (1995). Energy-based linear damage model for high-intensity seismic loading, Journal of Structural Engineering ASCE, 121(5) 857-863.
28. Chai Y.H. (2004). Incorporating low-cycle fatigue model into duration-dependent inelastic design spectra, Earthquake Engineering and Structural Dynamics, 34 83–96.

29. Chapman M.C. (1999). On the use of elastic input energy for seismic hazard analysis, Earthquake Spectra, 15(4) 607-635.
30. Chintanapakdee C., Chopra A.K. (2003). Evaluation of modal pushover analysis using generic frames, Earthquake Engineering and Structural Dynamics, 32 417–442.
31. Chopra A.K., Goel R.K. (2001). A modal pushover analysis procedure to estimating seismic demands for buildings: theory and preliminary evaluation, PEER Report 2001/03, Pacific Earthquake Engineering Research Center, University of California, Berkeley.
32. Chou C.C., Uang C.M. (2000). Establishing absorbed energy spectra -an attenuation approach, Earthquake Engineering and Structural Dynamics, 29 1441-1455.
33. Clark P., Aiken I., Kasai K., Ko E., Kimura I. (1999). Design Procedures for Buildings Incorporating Hysteretic Damping Devices. Proceedings of the 68th Annual Convention. Structural Engineers Association of California. Sacramento; 355-371.
34. Clough R.W., Penzien J. (1993). Dynamics of Structures, McGraw Hill, New York.
35. Cosenza E., Manfredi G., Ramasco K. (1990). An evaluation of the use of damage functional in earthquake-resistant design, Proc. 9th European Conference on Earthquake Engineering, The Kucherenko Tsniik of the USSR, Gosstroy, Moscow, 9 303-312.
36. CSI Analysis reference manual for SAP2000®, ETABS® and SAFE®. (2010). CSI (Computers and Structures, Inc.).
37. Cuesta I., Aschheim M.A., Fajfar P. (2003). Simplified R-Factor Relationships for Strong Ground Motions. Earthquake Spectra, 19(1) 25-45.
38. Decreto 1400. Código Colombiano de Construcciones Sismo-Resistentes. (1984). Asociación Colombiana de Ingeniería Sísmica, (in Spanish).
39. Decreto 196. Microzonificación sísmica de Bogotá. (2006). Alcaldía mayor de Bogotá, (in Spanish).
40. Decreto 523. Microzonificación sísmica de Bogotá. (2010). Alcaldía mayor de Bogotá, (in Spanish).
41. EERC (1995). Performance-based Seismic Design of Buildings: An Action Plan, The Earthquake Engineering Research Center Library, The Earthquake Image Information System (EqIIS), University of California, Berkeley. http://nisee.ce.berkeley.edu/~eqiis/eqiis.html.
42. Elghazouli A.Y. Editor. (2009). Seismic Design of Buildings to Eurocode 8. Taylor and Francis.
43. EN-10025-2. (2004). Technical delivery conditions for non-alloy steels. European Committee for Standarization.
44. EN-10034. (1993). Tolerances on shape and dimensions. European Committee for Standarization.
45. EN-1993 (EC-3). (2005). Design of steel structures, European Committee of Standarization.
46. EN-1998. (2004). Eurocode 8: Design of structures for earthquake resistance. European Committee for Standarization.
47. EN-1998-2. (2005). Eurocode 8: Design of structures for earthquake resistance. Part 2: Bridges. European Committee for Standarization.
48. Erberik A., Sucuoğlu H. (2004). Seismic energy dissipation in deteriorating systems through low cycle fatigue, Earthquake Engineering and Structural Dynamics, 33 49–67.
49. Fajfar P., Fischinger M. (1988). N2. A method for nonlinear seismic analysis of regular structures, Proceedings of the 9th World Conference on Earthquake Engineering, Tokyo-Kyoto, Japan, 5 111–116.
50. Fajfar P. (1992). Equivalent ductility factors taking into account low-cycle fatigue, Earthquake Engineering & Structural Dynamics, 21 837-848.
51. Fajfar P., Vidic T. (1992). Fischinger M. On energy demand and supply in SDOF systems, In: Nonlinear Seismic Analysis and Design of Reinforced Concrete Buildings, Elsevier, Amsterdam 41-61.
52. FEMA 349. (2000). Action Plan for Performance-Based Seismic Design, FEMA/EERI, Washington DC, (2000).
53. FEMA 350. (2000). Recommended Seismic Design Criteria for New Steel Moment-Frame Buildings, FEMA/SEAOC/ATC/CUREe (2000).
54. FEMA-355D. (2000). State of the Art Report on Connection Performance, prepared by the SAC Joint Venture for the Federal Emergency Management Agency, Washington, DC.
55. FEMA 356. (2000). Prestandard and commentary for the seismic rehabilitation of buildings. Federal Emergency Management Agency.
56. FEMA 440. (2005). Improvement of Nonlinear Static Seismic Analysis Procedures. Federal Emergency Management Agency.
57. FEMA 450. (2003). NEHRP Recommended Provisions and Commentary for Seismic Regulations for New Buildings and Other Structures. Federal Emergency Management Agency.
58. Ferraioli M., Lavino A., Mandara A. (2012). Behaviour Factor for seismic design of moment-resisting steel frames. 15th World Conference on Earthquake Engineering. Lisbon, Portugal.

59. García Reyes L.E. (1998). Dinámica estructural aplicada al diseño sísmico, Universidad de Los Andes, Bogotá, Colombia.
60. Goel S., Hani A. (1994). Seismic-Resistant Special Truss-Moment Frame. Journal of Structural Engineering, 120:6 1781-1797.
61. Gunturi S.K. (1992). Building specific earthquake damage estimation, Ph.D. Thesis, Stanford University, Stanford, California.
62. Gupta B, Kunnath S.K. (2000). Adaptive spectra-based pushover procedure for seismic evaluation of structures, Earthquake Spectra, 16(2) 367–392.
63. Guyader A.C., Iwan, W.D. (2006). Determining Equivalent Linear Parameters for Use in a Capacity Spectrum Method. Journal of Structural Engineering, 132(1): 59-67.
64. Hamburger R.O. (1998). Performance-Based Analysis and Design Procedure for Moment Resisting Steel Frames, Background Document, SAC Steel Project.
65. Hashemi S.H. (2011). Ductility and Ultimate Strength of Eccentric Braced Frame. 2011 International Conference on Advanced Materials Engineering IPCSIT, Singapore.
66. Higashino M., Okamoto S. (2006). Response Control and Seismic Isolation of Buildings. Taylor & Francis.
67. Housner G.W. (1956). Limit design of structures to resist earthquakes, Proceedings of First World Conference on Earthquake Engineering, 5 1-12.
68. Housner G.W., Jennings P.C. (1977). The capacity of extreme earthquake motions to damage structures, Structural and Geotechnical Mechanics, A volume honoring Nathan M. Newmark 102-116.
69. Housner G.W. (1990). Historical Review of Earthquake Engineering, In: Selected Earthquake Engineering Papers of George W. Housner, American Society of Civil Engineers, New York 764–777.
70. Housner G.W., Bergman L.A., Caughey T.K., Chassiakos A.G., Claus R.O., Masri S.F., Skelton R.E., Soong T.T., Spencer B.F., Yao J.T.P. (1997). Structural Control: Past, Present, and Future. Journal of Engineering Mechanics ASCE; 123:897−971.
71. IBC (International Building Code). (2000). International Code Council.
72. Ingeominas: Instituto Colombiano de Geología y Minería. (2005). http://www.ingeominas.gov.co/. (In Spanish).
73. Iwata M. (2004). Applications-Design of Buckling-Restrained Braces in Japan. 13th World Conference on Earthquake Engineering. Paper No. 3208. Vancouver Canada.
74. Kang C.K., Choi B.J. (2011). New approach to evaluate the response modification factors for steel moment resisting frames. International Journal of Steel Structures. 11:3 275-286.
75. Kato B., Akiyama H. (1975). Energy input and damages in structures subjected to severe earthquakes, Journal of Structural and Construction Engineering Trans. AIJ, 235 9-18 (in Japanese).
76. Kelly J.M. (1993). Earthquake-resistant Design with Rubber. Springer-Verlag.
77. Kelly J.M., Konstantinidis D. (2011). Mechanics of Rubber Bearings for Seismic and Vibration Isolation. John Wiley.
78. Kircher C., Nassar A., Kustu O., Holmes, W. (1997). Development of building damage functions for earthquake loss estimation, Earthquake Spectra, 13(4) 663-682.
79. Krawinkler H. (1998). Pros and cons of a pushover analysis of seismic performance evaluation. Engineering Structures, 20:4-6 452-464.
80. Kumar S., Rao P. (2004). Seismic Qualification of Semi-Rigid Connections in Steel Frames. 13th World Conference on Earthquake Engineering. Paper No. 2149. Vancouver, B.C., Canada.
81. Kunnath S.K., Gupta B. (2000). Validity of deformation demand estimates using nonlinear static procedures, Proceedings of U.S.–Japan Workshop on Performance-Based Earthquake Engineering Methodology for Reinforced Concrete Building Structures, Sapporo, Hokkaido, Japan 117–128.
82. Lybas J., Sozen M. (1977). Effect of beam strength and stiffness on dynamic behavior of reinforced concrete coupled walls, Civil Engineering Studies, Structural Research Series, N.444, University of Illinois, Urbana.
83. Mahmoudi M., Zaree M. (2011). Evaluating the overstrength of concentrically braced steel frame systems considering members post-buckling strength. International Journal of Civil Engineering. Vol. 9(1) 59-62.
84. Malhotra P.K. (2006). Return Period of Recorded Ground Motions, Journal of Structural Engineering, 132(6) 833-839.
85. Matsumori T., Otani S., Shiohara H., Kabeyasawa T. (2000). Earthquake member deformation demands in reinforced concrete frame structures, Proceedings of U.S.–Japan Workshop on Performance-Based Earthquake Engineering Methodology for Reinforced Concrete Building Structures, Maui, Hawaii, 79–94.
86. McCabe S.L., Hall W.J. (1989). Assessment of Seismic Structural Damage, J. Struct. Engrg. 115(9) 2166-2183.

87. Milutinovic Z.V., Trendafiloski G.S. (2003).Vulnerability of current buildings, Work-Package 4 of RISK_UE Project, European Commission, EVK4-CT-2000-00014.
88. Miranda E., Bertero V.V. (1994). Evaluation of strength reduction factors for earthquake-resistant design. Earthquake Spectra, 10:2, 357-379.
89. Miranda E. (1997). Strength Reduction Factors in Performance-Based Design. EERC Berkeley.
90. Montaña M.A., López Almansa F. (2012). Seismic vulnerability analysis of steel buildings in Bogotá, Colombia. 15th World Conference on Earthquake Engineering (15WCEE). Lisbon, Portugal. Art. 529 (publication in CD).
91. Naeim F., Kelly J.M. (1999). Design of Seismic Isolated Structures. John Wiley.
92. Nassar A.A., Krawinkler H. (1991). Seismic Demands for SDOF and MDOF Systems. Stanford University, (The John A. Blume Earthquake Engineering Center) Report No. 95.
93. NBCC. (2005). National Building Code of Canada. Institute for Research in Construction, National Research Council of Canada, Ottawa Ont.
94. NCSE-02. (2002). Norma de Construcción Sismorresistente: Parte General y Edificación. Ministerio de Fomento.
95. Newmark N.M., Hall W.J. (1973). Seismic design criteria for nuclear reactor facilities. Buildings practices for disaster mitigation. Rep. Nº 45. National Bureau of Standards. U. S. Dept. of commerce, 209-236.
96. NSR-10. (2010). Normas Colombianas de Diseño y Construcción Sismo Resistente. Asociación Colombiana de Ingeniería Sísmica, (in Spanish).
97. NSR-98. (1998). Normas Colombianas de Diseño y Construcción Sismo Resistente. Asociación Colombiana de Ingeniería Sísmica, (in Spanish).
98. Ohashi U. (1993). History of Structural Standards for Buildings in Japan, Japan Building Center (in japanese).
99. Ordaz M., Pérez-Rocha L.E. (1998). Estimation of strength-reduction factors for elastoplastic systems: a new approach, Earthquake Engineering and Structural Dynamics, Vol. 27, 889-901.
100. Palazzo G., López-Almansa F., Cahís X., Crisafulli F. (2009). A low-tech dissipative buckling-restrained brace. Design, analysis, production and testing. Engineering Structures; 31:2152-2161.
101. Paret T.F., Sasaki K.K., Eilbeck D.H., Freeman S.A. (1996). Approximate inelastic procedures to identify failure mechanisms from higher mode effects, Proceedings of the 11th World Conference on Earthquake Engineering, Acapulco, Mexico, 966.
102. Park Y.J., Ang A. (1985). Mechanistic seismic damage model for reinforced concrete, Journal of Structural Engineering, ASCE 111 722-739.
103. Park Y.J., Reinhorn A.M., Kunnath S.K. (1987). IDARC: Inelastic Damage Analysis of Reinforced Concrete Frame-Shear Wall Structures, Technical Report NCEER-87-0008, National Center for Earthquake Engineering Research, State University of New York at Buffalo.
104. Powell G. (2007). Performance based design using nonlinear analysis, Computers and Structures, Inc., (CSI). Berkeley.
105. Priestley M.J.N., Calvi G.M., Kowalsky M.J. (2007). Displacement-Based Seismic Design of Structures, IUSS Press.
106. Pujades L.G., Barbat A.H., González-Drigo R., Avila J., Lagomarsino S. (2012). Seismic performance of a block of buildings representative of the typical construction in the Eixample district in Barcelona (Spain). Bulletin of Earthquake Engineering 10:1.331–349.
107. Sasaki K.K., Freeman S.A., Parent T.F. (1998). Multimode pushover procedure (MMP)—a method to identify the effects of higher modes in a pushover analysis, Proceedings of the 6th U.S. National Conference on Earthquake Engineering, Seattle, Washington.
108. SEAOC. (1995). Vision 2000: Performance Based Seismic Engineering of Buildings, San Francisco.
109. Seek M.W., Murray T.M. (2009). Seismic strength of moment end-plate connections with attached concrete slab. AISC Report No. 3279.
110. Skinner R.I., Robinson W.H., McVerry G.H. (1993). An Introduction to Seismic Isolation. John Wiley.
111. Smith B.S., Coull A. (1997). Tall Building Structures: Analysis and Design. John Wiley.
112. Soo Y., Meyer C., Shizuoka M. (1989). Modeling of concrete damage, ACI Structural Journal, 86 259-271.
113. Soong T., Dargush G. (1997). Passive energy Dissipation Systems in Structural Engineering, John Wiley.
114. STAAD.Pro V8i Technical Reference manual. (2010). Bentley Sustaining Infrastructure.
115. Stone W.C., Taylor A.W. (1994). ISDP: Integrated approach to seismic design of reinforced concrete structures, Journal of Structural Engineering, ASCE, 120(12) 3548-3566.
116. Sucuoğlu H., Erberik A. (2004). Energy-based hysteresis and damage for deteriorating systems, Earthquake Engineering and Structural Dynamics, 33 69–88.

117. Tanahashi R. (1956). Studies on the nonlinear vibrations of structures subjected to destructive earthquakes, Proceedings of first World Conference on Earthquake Engineering.
118. Tapia-Hernández E., Tena-Colunga A. (2008). Behavior of regular steel moment resisting concentrically braced frames (MRCBFs) in seismic zones. 14th World Conference on Earthquake Engineering. Beijing, China.
119. Teran-Gilmore A., Jirsa J.O. (2005). A simple damage model for practical seismic design that accounts for low cycle fatigue, Earthquake Spectra, 21(3) 803-832.
120. Teran-Gilmore A., Jirsa J.O. (2007). Energy demands for seismic design against low-cycle fatigue, Earthquake Engineering and Structural Dynamics, 36 383-404.
121. The spectrus group. Tru-frame ® design guide. Wireframe Modeling of the Special Truss Moment Frame. Downloadable from http://thespectrusgroup.com/pdfs/STMF_White_Paper.pdf (last accessed August 2013).
122. Tsai K.C., Lai J.W., Hwang Y.C., Lin S.L., Weng C.H. (2004). Research and application of double-core buckling-restrained braces in Taiwan. 13th World Conference on Earthquake Engineering. Paper No. 2179 Vancouver Canada.
123. Uang C.M., Bertero V.V. (1988). Use of energy as a design criterion in earthquake–resistant design, Report No. UBC/EERC-88/18, Earthquake Engineering Research Center, University of California.
124. Uang C.M., Bertero V.V. (1990). Evaluation of seismic energy in structures, Earthquake Engineering and Structural Dynamics 77-90.
125. Vamvatsikos D., Cornell C.A. (2001). Tracing and post-processing of IDA curves: Theory and software implementation, Report No. RMS-44, RMS Program, Stanford University, Stanford.
126. Vamvatsikos D., Cornell C.A. (2002). Incremental dynamic analysis, Earthquake Engineering & Structural Dynamics, 31 491–514.
127. Vamvatsikos D. (2002). Seismic performance, capacity and reliability of structures as seen through incremental dynamic analysis, Doctoral dissertation, Stanford University.
128. Vega del Rey J.I., Alarcón E. (2009). Pounding force assessment in performance-based design of bridges, Earthquake Engineering & Structural Dynamics, 38 1525-1544.
129. Veletsos A., Newmark N.M. (1960). Effect of inelastic behavior on response of simply systems to earthquake motions, Proceedings of the Second World Conference on Earthquake Engineering 895-912.
130. Watanabe A., Hitomi Y., Saeki E., Wada A., Fujimoto M. (1988). Properties of Brace Encased in Buckling-Restraining Concrete and Steel Tube. Proceedings of the Ninth World Conference on Earthquake Engineering. Vol. IV. 719-724. Japan Association for Earthquake Disaster Prevention. Tokyo-Kyoto. Japan.
131. Zhu T.J., Tso W.K. (1992). Design of torsionally unbalanced structural systems based on code provisions II: strength distribution, Earthquake Engineering & Structural Dynamics, 21 629-644.

Appendix A PUBLICATIONS GENERATED DURING THIS RESEARCH

This appendix lists the main publications generated during this research.

Publications in Proceedings of Conferences:

- M.A. Montaña, F. López Almansa. Seismic vulnerability analysis of steel buildings in Bogotá, Colombia. 15th World Conference on Earthquake Engineering (15WCEE). Lisbon, Portugal. Art. 529 (publication in CD).
- M.A. Montaña, F. López Almansa. Cost comparison of MRF, CBF and EBF mid-height steel buildings in Bogotá. 8th STESSA Conference on Behaviour of Steel Structures in Seismic Areas. Shanghai (China) (2015).

Publications in Journals indexed by the Journal of Citation Reports (Web of Knowledge, former ISI):

- F. López Almansa, M.A. Montaña. Numerical seismic vulnerability analysis of steel buildings in Bogotá, Colombia. Journal of Constructional Steel Research. Vol. 92, No. 1 1–14 (2014). 2012/5-years Impact Factor of the Journal: 1.327/1.565. DOI 10.1016/j.jcsr.2013.09.002.